



Memorandum

U.S. Department
of Transportation

**National Highway
Traffic Safety
Administration**

52790

Subject: Submittal of Final Report, Advanced Integrated
Structural Seat, by EASi Engineering and Johnson
Controls, Inc., to Docket No. NHTSA-1998-4064

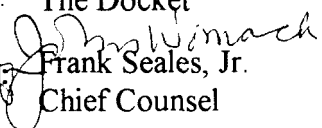
Date: MAR 24 1999

-27

From: Raymond P. Owings, Ph.D.
Associate Administrator for
Research and Development

Reply to
Attn. of:

To: The Docket

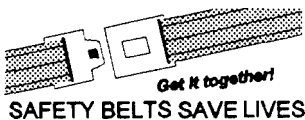
Through: 
Frank Seales, Jr.
Chief Counsel

The attached report, Advanced Integrated Structural Seat, is the final report of the work accomplished under Task Ordering Agreement Contract No. DTNH 22-92-D-07323, Task 11, and prepared by EASi Engineering and Johnson Controls, Inc. This report summarizes the advanced integrated structural seat criteria used, the design concepts evolved and adapted, the evaluation of the design concepts using various computer aided engineering methodologies, and the resulting changes in occupant crash protection. The design concepts studied include rollover-sensing seat belt pretensioners and extended headrest frames for improved rollover protection, belt load limiter for improved frontal crash protection, energy absorbing dual recliners and inflatable headrest for rear impact protection, and seat back wing structures for improved side impact protection and side intrusion resistance.

The work reported and continuation of this contract into the planned subsequent phases in which seat prototypes will be fabricated and tested will supply technical support in considerations for upgrading FMVSS No. 207, Seating Systems, and FMVSS No. 202, Head Restraints.

Research and Development recommends that the final report, Advanced Integrated Structural Seat, be placed in the public docket.

Attachment
(2 Copies)



TRAFALGAR SQUARE STATION
99 MAR 25 AM 10:16
LOCKER SECTION

52790
Advanced Integrated Structural Seat

Contract Number **DTNH22-92-D-07323**, Task-11

Final Report

February, 1997

by

EASi Engineering
Vikas Gupta, Rajiv Menon, Sanjeev Gupta, A.Mani
&
Johnson Controls, Inc.
Rango Shanmugavelu

NOTICE

This document is disseminated under the sponsorship of the Department of **Transportation** in the interest of information exchange. The United States Government assumes no liability for its contents or use thereof

NOTICE

The United States Government does not endorse products or manufactures. Trade or manufacturers' names appear herein solely because they are considered essential to the object of this report.

TABLE OF CONTENTS

	Page
BACKGROUND	6
1. INTRODUCTION	6
2. FRONTAL CRASH PROTECTION	8
2.1 Load Limiter..	8
2.2 Pretensioner	20
3. REAR IMPACT PROTECTION..	22
3.1 Effect of Increasing Distance Available for Torso Acceleration..	25
3.2 Seat Back Structure..	27
3.3 Recliner With Energy Absorber..	28
3.3.1 Design for Energy Absorber..	33
3.3.2 Design Verification for Rear Impact.	33
3.4 Inflatable Head Rest.	38
4. ROLLOVER..	58
4.1 MADYMO Simulations..	58
4.2 Extended Headrest	61
5. SIDE IMPACT PROTECTION..	67
FUTURE WORK	76
SUMMARY	76
REFERENCES.....	77

LIST OF FIGURES

	Page
Figure 2.1 Load limiter and airbag interaction.	9
Figure 2.2 MADYMO model and simulation.....	10
Figure 2.3 Load limiter force and belt payout for 30 mph frontal crash.	12
Figure 2.4 Comparison of Head Injury Criteria with and without load limiters (30 mph).....	13
Figure 2.5 Comparison of chest compression with and without load limiters (30 mph).	13
Figure 2.6 Load limiter force and belt payout for 40 mph frontal crash.	14
Figure 2.7 Comparison of Head Injury Criteria with and without load limiters (40 mph).	15
Figure 2.8 Comparison of chest compression with and without load limiters (40 mph).	15
Figure 2.9 Shoulder belt load vs. time for 30 mph.	20
Figure 2.10 Effect of pretensioner on injury parameters (50th percentile dummy at 30 mph).....	21
Figure 3.1 Body region injuries attributed to frontal components in rear crash.....	23
Figure 3.2 Source of injury for outboard, belted occupant.	24
Figure 3.3 Design concepts for increasing torso travel.....	26
Figure 3.4 Crash sequence in rear impact. Figure 3.5 Acceleration pulse.	28
Figure 3.6 Torque vs. rotation curve for the seat back.....	29
Figure 3.7 Energy absorption of a typical seat back and low rebound seat.	30
Figure 3.8 Head excursion due to seat back rebound.	32
Figure 3.9 Layout of modified recliner.	34
Figure 3.10 Torque-theta curve with the metal element.	35
Figure 3.11 Model setup for the coupled simulation.	36
Figure 3.12 Headrest positions from blueprint (courtesy JCI).	39
Figure 3.13 MADYMO model setup with headrest.	40
Figure 3.14 Types of inflatable headrest studied.	41
Figure 3.15 Occupant response using Type 2 inflatable headrest.....	42
Figure 3.16 Occupant neck response using Type 2 inflatable headrest.	43
Figure 3.17 Occupant response using Type 3 inflatable headrest.....	44
Figure 3.18 Occupant neck response using Type 3 inflatable headrest.	45
Figure 3.19 Comparison of occupant response using different types of inflatable headrest.	46
Figure 3.20 Comparison of accelerations using different types of inflatable headrest.	47
Figure 3.2.1 Occupant neck response using different types of inflatable headrests.....	48
Figure 3.22 Comparison of injury numbers using different inflatable headrests.....	49
Figure 3.23 Baseline case (without inflatable headrest) simulation.	50
Figure 3.24 Simulation with inflatable headrest Type 1.....	51
Figure 3.25 Simulation with inflatable headrest Type 2.....	52
Figure 3.26 Simulation with inflatable headrest Type 3.....	53

Figure 3.27 Comparison of occupant response at 30 and 5 mph.	54
Figure 3.28 Comparison of occupant neck response at 30 and 5 mph.	55
Figure 3.29. Trajectories of the upper and lower neck with inflatable headrest	56
Figure 3.30 Trajectories of the upper and lower neck with standard headrest.	57
Figure 4. I Model setup for MADYMO rollover simulations	59
Figure 4.2 Vehicle rollover simulation.	59
Figure 4.3 Characteristics of the pretensioner.	60
Figure 4.4 Model setup of the inverted simulation.	61
Figure 4.5 Full car rollover drop test.	62
Figure 4.6 Comparison of standard and extended headrest in inverted drop test.....	64
Figure 4.7 Vertical travel of seat bottom hinge.	65
Figure 4.8 Vertical travel of shoulder point.	66
Figure 5.1 Model setup for side impact test with wing and shield.	68
Figure 5.2 Simulation for side impact test with wing and shield.	69
Figure 5.3 Comparison of displacement of the top right pillar with standard and enhanced seat.	71
Figure 5.4 Comparison of lower torso velocity with standard and enhanced seat.	72
Figure 5.5 Comparison of lower torso movement with standard and enhanced seat.	73
Figure 5.6 Comparison of the pelvic acceleration with standard and enhanced seat.	74
Figure 5.7 Comparison of the T12 acceleration with standard and enhanced seat.....	75

LIST OF TABLES

	Page
Table 1.1 Criteria Matrix	7
Table 2.1 Simulation results without load limiter at 30 mph.....	16
Table 2.2 Simulation results with load limiter at 30 mph.....	17
Table 2.3 Simulation results without load limiter at 40 mph.....	18
Table 2.4 Simulation results with load limiter at 40 mph.....	19
Table 2.2 Specifications for the Belt Pretensioner.....	21
Table 3.1 Participation of the proposed design features in addressing various rear impact performance criteria.:	25
Table 3.2 Effect of lowered pivot seat and sliding seat	27
Table 3.3 Maximum seat back angle with respect to the seat bottom (Initial seat back angle = 23°)	28
Table 3.4 Effect of seat back rebound.....	31
Table 3.5 Injury numbers for 5th, 50th and 95th percentile dummy models.....	37
Table 4.1 Simulation results.....	60
Table 4.2 Simulation results of the inverted tests.	61

BACKGROUND

Through a contract from National Highway Traffic Safety Administration (NHTSA), EASi Engineering in conjunction with Johnson Controls Inc. (JCI) worked to conceive and develop an advanced integrated structural seat that meets the current FMVSS requirements, significantly improve occupant protection for frontal, rear, side and rollover accidents and contributes to passenger compartment intrusion resistance. This work is a cooperative effort between the government and industry, bringing together the strengths of impact biomechanics, computer aided engineering and seat systems engineering and manufacturing.

This report summarizes the advanced integrated structural seat criteria used, the design concepts evolved and adapted, the evaluation of the design concepts using various computer aided engineering (CAE) methodologies, and the resulting changes in occupant crash protection. Concept level models were created primarily through use of the MADYMO software to establish potential benefits. Further design evolution and evaluation were achieved via detailed finite element models and coupled models using LS-DYNA3D and LS-DYNA3D/MADYMO coupling. The design concepts studied include rollover-sensing seat belt pretensioners and extended head rest frames for improved rollover protection, belt load limiter for improved frontal crash protection, 'energy absorbing dual recliners and inflatable headrest for rear impact protection, seat back wing structures for improved side impact protection and side intrusion resistance. This study does not include seat mounted side airbags as they have been explored already (Pihall et al., 1994) and are in production.

1. INTRODUCTION

The advanced integrated structural seat (AISS) is aimed at enhancing occupant protection in all of the four basic crash modes (frontal, rear, rollover and side crashes) primarily by modifications of the seat structure and by addition of seat mounted safety/restraint features. By focusing on the seat structure modifications, it is hoped the resulting designs will be simple and cost-efficient. Also, the seat system is designed to function with the body structure to resist passenger compartment intrusion in side and rollover crashes. This seat system design is being developed starting from an existing integrated structural seat design. Integrated seats have all the belt anchorages on the seat itself as opposed to conventional seats where the shoulder belt upper anchorage is located on the car upper body structure. The belt fit is considerably improved regardless of the seating position. Also, the assembly of the seat in the car becomes much easier with this design as the belts are an integral part of the seat. An integrated structural seat was chosen as the baseline seat since it is expected to enhance occupant protection.

The criteria matrix shown in Table 1.1, lists the loading conditions and evaluation criteria for the seat in various crash modes. This matrix was established based on current

Table 1.1 Criteria Matrix

	Criteria	Loading		Characteristics of Interest	Dummy	Back Position	Remarks
		Speed/ Location	Load				
C O M P L I A N C E	Rollover	30 mph	Drop from rollover dolly (FMVSS 208)	Head excursion; Neck injury, Shoulder belt loads on occupant; Failure mode	50th & 95th %ile male Hybrid III belted	Design	Consideration for 5th %ile female head excursion relative to torso
	Rear impact	35 mph	301 crash pulse extrapolated	Shoulder belt loading; Neck injury; Ramp up; Back collapse; Rebound	50th & 95th %ile male Hybrid III belted	Design	Hybrid III may not be adequate; Check for 5th %ile
	Side impact	33.5 mph	MDB	TTI; Pelvic injury, Head injury; Head Excursion	SID belted	Design	Head excursion relative to torso
	Frontal impact	30 mph	30 mph pulse	Head injury, Chest g; Anti submarining Rebound	50th & 95th %ile male Hybrid III belted	Design	Airbag interaction to be considered; Check for 5th %ile female; Submarining
P R A C T I C E	Torsional Rigidity	Seat back corner	2260 in-lb. about H-point	Permanent set		Design	
	Abuse load	Seat back crossbar	6400 in-lb. rearward about H-point	seat Integrity		Design	
	Submarine loads	Cushion Game	Simulated	Seat Integrity			
3 F E E R	Cost estimate	NA	NA	Market acceptable range			
	Ingress/Egress	NA	NA	Ease			
	Styling	NA	NA	Acceptable practices			
	Manufacturing	NA	NA	Mass production feasible			
	Vibrational characteristic	NA	NA	Away from discomfort range			
	Weight	NA	NA	Within market range			

regulations and a sample of industry design practice. The matrix should not be considered a statement of NHTSA's future regulatory intentions.

The concepts evolved, their evaluation procedure and detailed design are described in the following sections.

2. FRONTAL CRASH PROTECTION

2.1 Load Limiter

Recent work done in evaluating *injury* reduction in frontal crashes suggests that belt restraints and **airbag** restraints may not interact in a way which achieves optimal occupant protection (Mertz et al., 1995). Ideally, at frontal collision speeds below the threshold of air bag deployment, torso belt forces should be limited to those levels required to prevent occupant impact against compartment interior surfaces such as steering wheels and instrument panels. Additionally, for the **AISS** (Advanced Integrated Structural Seat) design, the torso belt should sustain loads capable of retaining the occupant within the compartment during rollovers and side crashes. Such reduced torso belt load limits are far below current practice (Figure 2.1). The upper anchorage of the torso belt on the seat back structure of current integrated seats is the source of the greatest seat **back** bending moment and shear load on the seat structure. As a result, limiting the torso belt loads allows weight reduction of the seat back structure and reduced floor pan shear while reducing occupant injuries at higher crash severities. At present, significant re-designing of the vehicle floor pan is required to adapt it for an integrated structural seat. Introduction of load limiter may reduce the extent of redesign required to replace a conventional seat (shoulder belt upper anchorage on the vehicle structure, mostly the **b-pillar**) with an integrated structural seat.

Mertz et al. (1995), have shown vast improvement in occupant injury parameters for the 50th percentile occupant by limiting the seat belt loads to 2000 N. They have shown a 27 percent reduction in chest acceleration and 67 percent reduction in chest compression. The risk of **AISS** ≥ 4 was reduced from 14.5 percent to 0.4 percent, and the risk of **AISS** ≥ 3 was reduced from 94 percent to 19 percent. The 95th percentile occupants although, were studied only at low speeds (15 mph) in non-deploy situations.

In the current study, a rigid body MADYMO model validated using a front impact sled test, is used for evaluating the torso belt load limit. The model is set up for a Ford Taurus environment with an existing integrated structural seat design (Figure 2.2). The seat model includes the seat back joint stiffness, seat cushion stiffness, anti-submarining plane and a 3-point seat belt. Eight percent nominal belt stiffness is used. Three different impact velocities of 12, 30 and 40 mph were studied, with and without the presence of a

load limiter. The airbag and the inflator model are assigned characteristics taken from a production airbag. A small (40 liter) and a large (80 liter) airbag were used for the study.

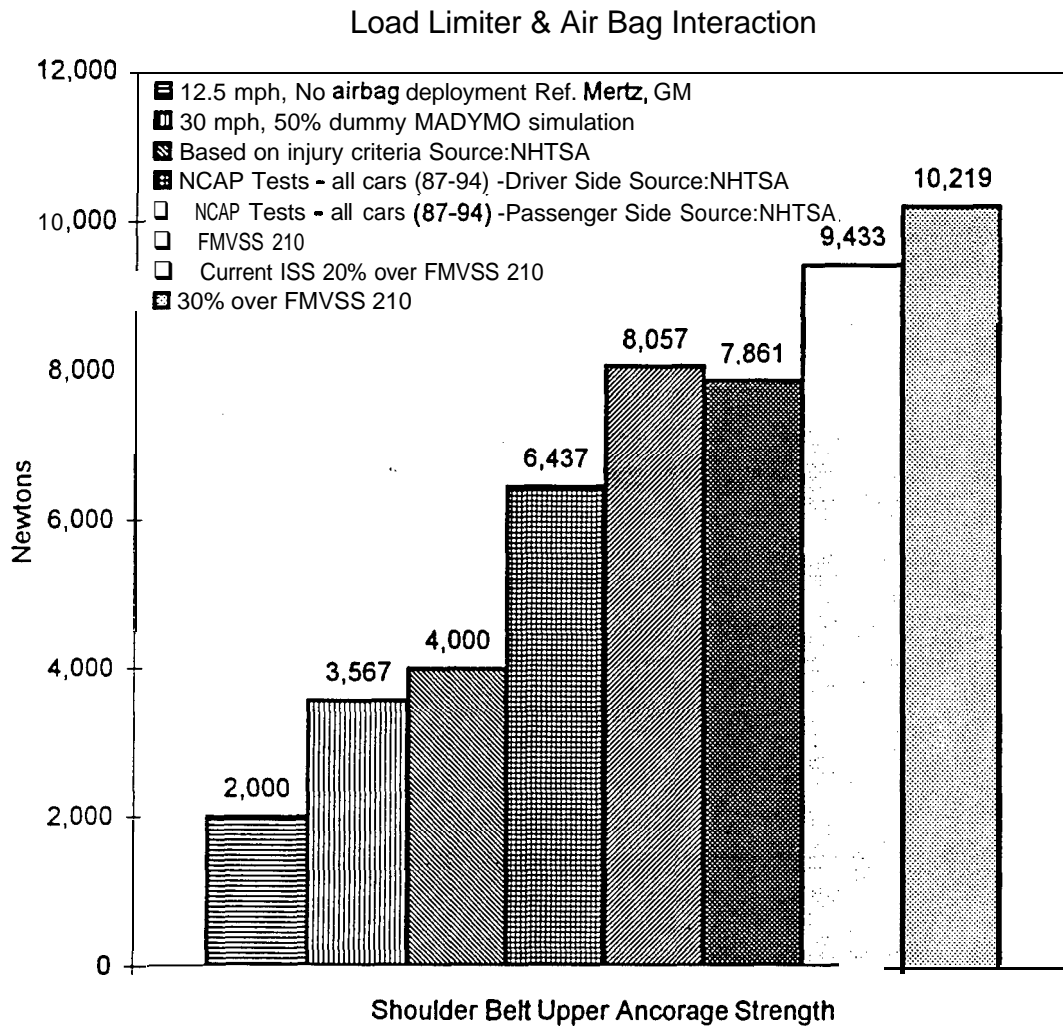


Figure 2.1 Load limiter and airbag interaction.

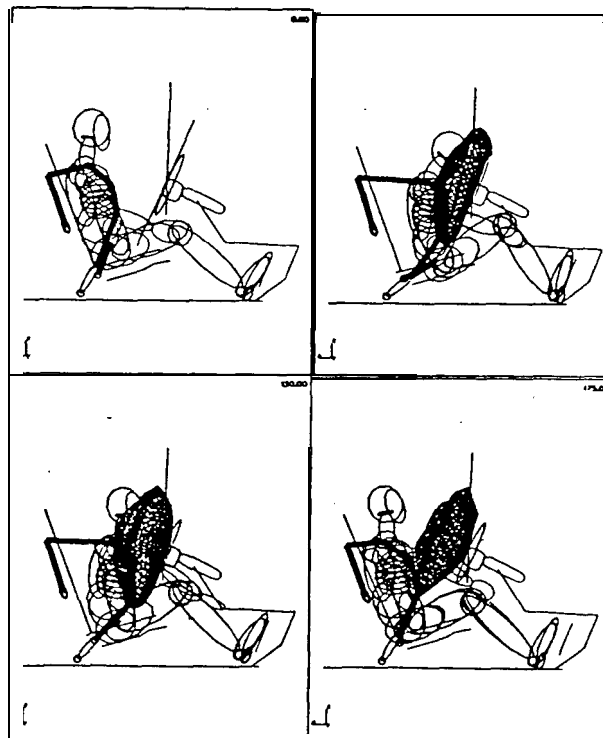
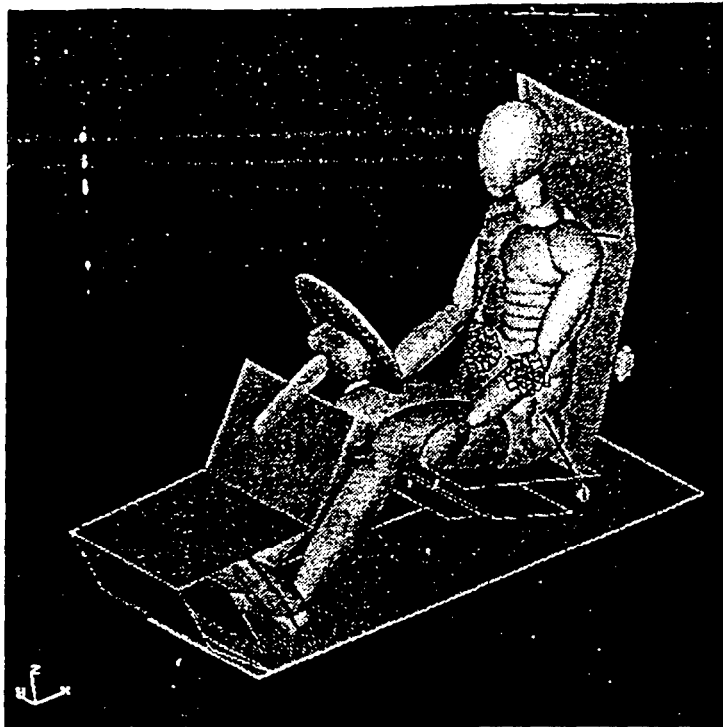


Figure 2.2 MADYMO model and simulation.

A load limit of 4000 Newton was found to be ideal based on a new research on rib fracture by Kallieris et al (1995). In the current study, no head to wheel contact was seen for a 50th percentile Hybrid III dummy, at a 30 mph frontal impact with a 4000 N load limit. Figure 2.3 shows the belt payout for a range of load limits for 30 mph impact pulse. The load limit for a 95th percentile male, that produces no wheel to head contact was found to be 4500 Newtons.

Figure 2.4 and 2.5 show the bar charts for the HIC and chest compression for the 5th, 50th and the 95th percentile occupants respectively, for a 30 mph frontal impact. With the 4000 N load limit substantial reduction in HIC values and neck loads are seen. HIC is reduced by 51%, neck loads by 15% and chest compression by 14% for a 50th percentile occupant with a 40 liter airbag. This translates to a 30 percent reduction in the risk for AIS ≥ 3 thoracic injury. Figure 2.6 shows the belt payout for a range of load limits for 40 mph impact pulse. Payout of the belt is higher for the 30 mph frontal impact (140 mm for 50th percentile large airbag) than the 40 mph (90 mm for 50th percentile large airbag) because the load limits used are 3500 N for 30 mph and 4500 N for 40 mph for the same body mass to travel forward. Figures 2.7 and 2.8 show the HIC and chest compression results for 40 mph impact. Tables 2.1 through 2.4 show the injury numbers for 30 and 40 mph frontal impacts, with small and large airbags, with and without the load limiters. The injury parameters reported are HIC, head excursion, peak head acceleration, maximum linear chest acceleration sustained over a period of 3 msec. or more and referred to as 3MS, neck load which are joint loads recorded at the lower neck, left and right femur load, chest compression and shoulder belt loads. All the results are reported for the 5th, 50th and the 95th percentile dummies.

Vast reduction in belt loads due to the introduction of load limiter (Figure 2.9), would make one expect significant reduction in chest compression values. But, from Figure 2.5 it is clear that chest compression reductions are only moderate. This is explained by the influence of airbag in frontal impact. Limiting of the belt loads causes the airbag to pick up the loads. Optimum design to minimize injury indices would involve concurrent tuning of the seat belts, the load limiter and the airbag. This is further illustrated by the vast differences in injury parameters between the three sizes of occupants, for the two sizes of airbags.

If a load limiter, that causes increased belt payout, is activated in an impact mode other than frontal, e.g. rollover, the risk of injury to the occupant could increase. However, rollover simulation performed by EASi as part of this research show shoulder belt loads much below 4000 N. Lap belt with retractor and pretensioner significantly limits the motion of the occupant in a rollover and hence lower loads on the shoulder belt are seen.

Several load limiters based on different concepts such as, stitch tearing, torsion rod, shearing/extrusion etc. are available in the market. Most of them are capable of limiting the load at 4000 N.

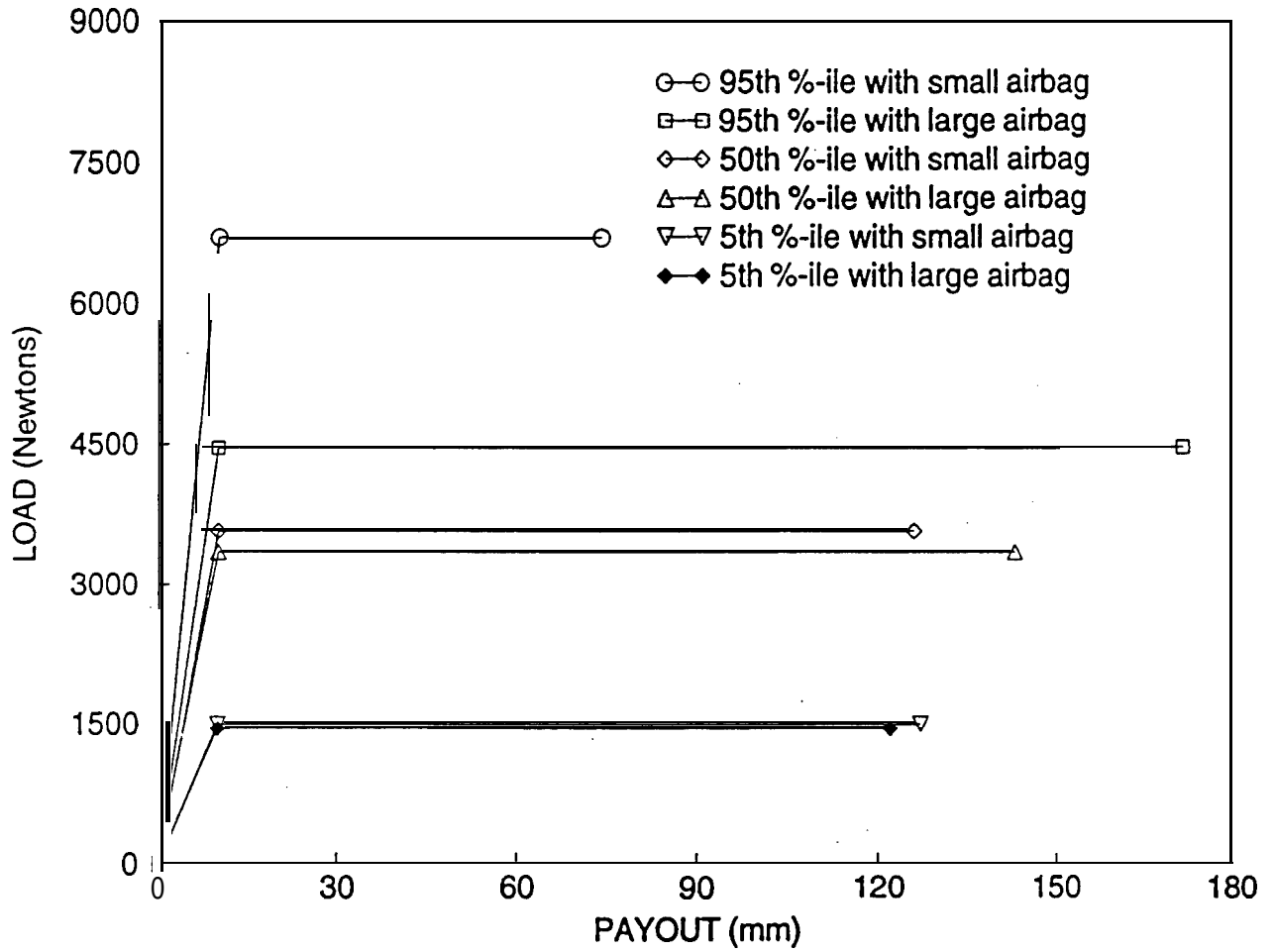


Figure 2.3 Load limiter force and belt payout for 30 mph frontal crash.

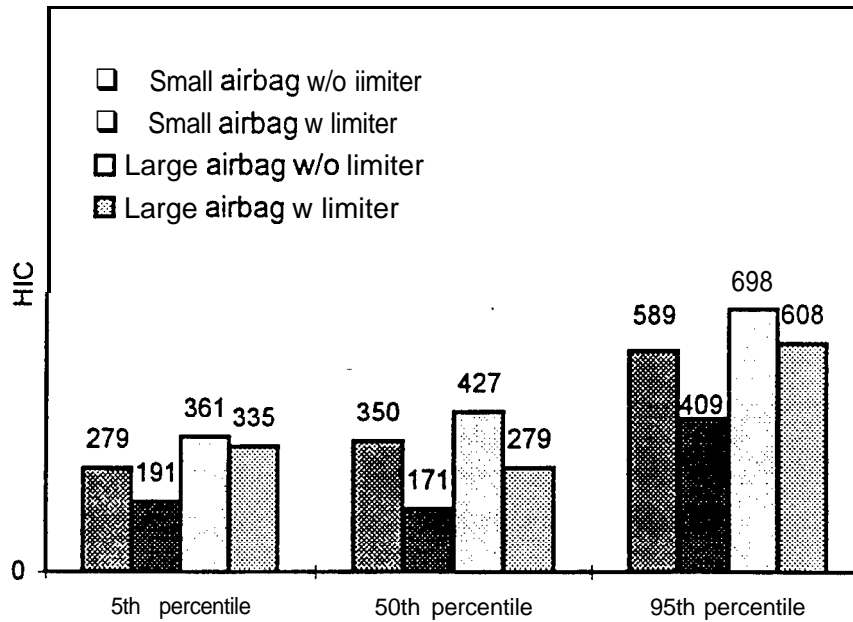


Figure 2.4 Comparison of Head Injury Criteria with and without load limiters (30 mph).

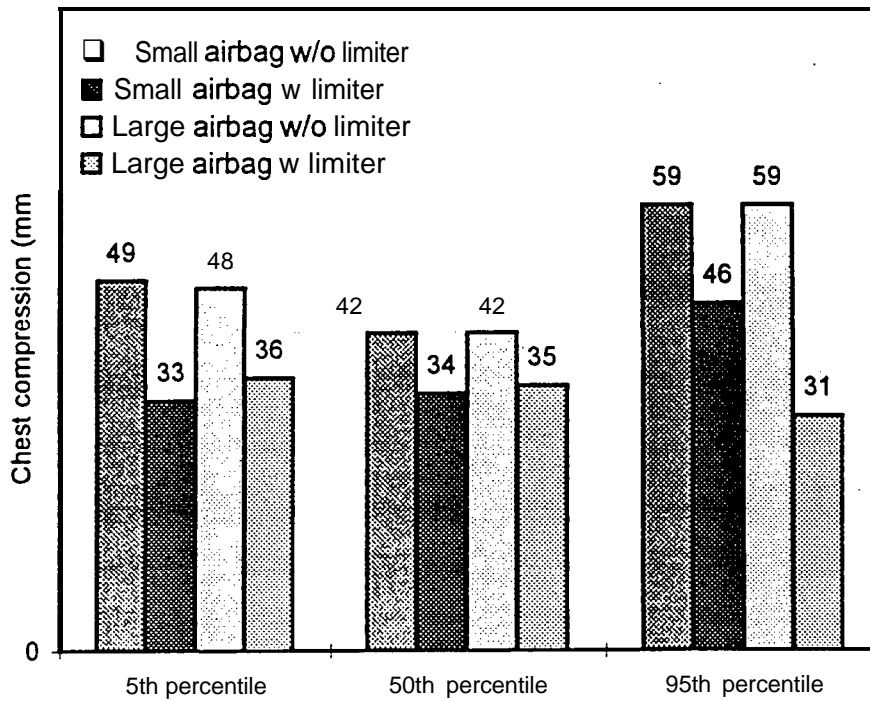


Figure 2.5 Comparison of chest compression with and without load limiters (30 mph).

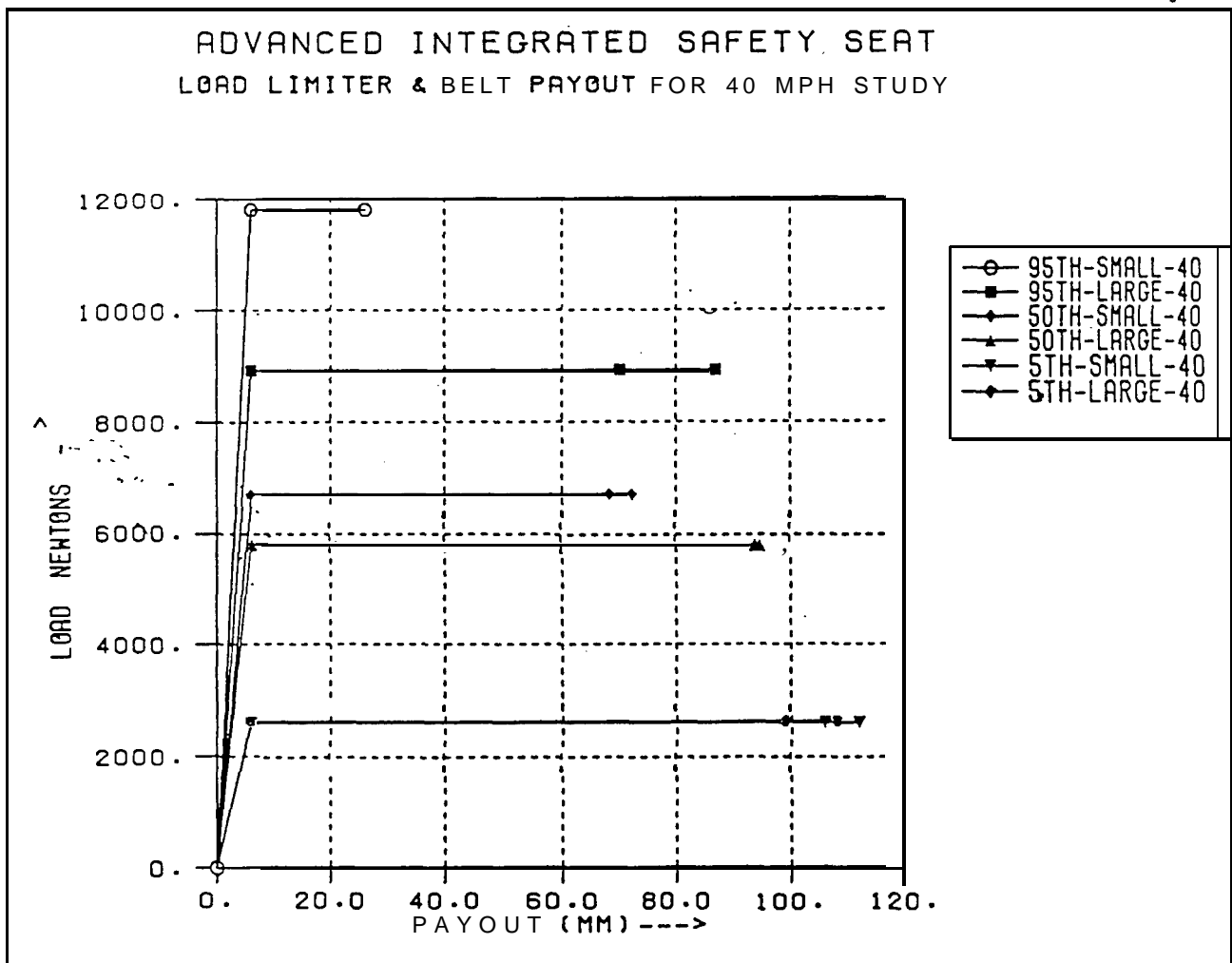


Figure 2.6 Load limiter force and belt payout for 40 mph frontal crash.

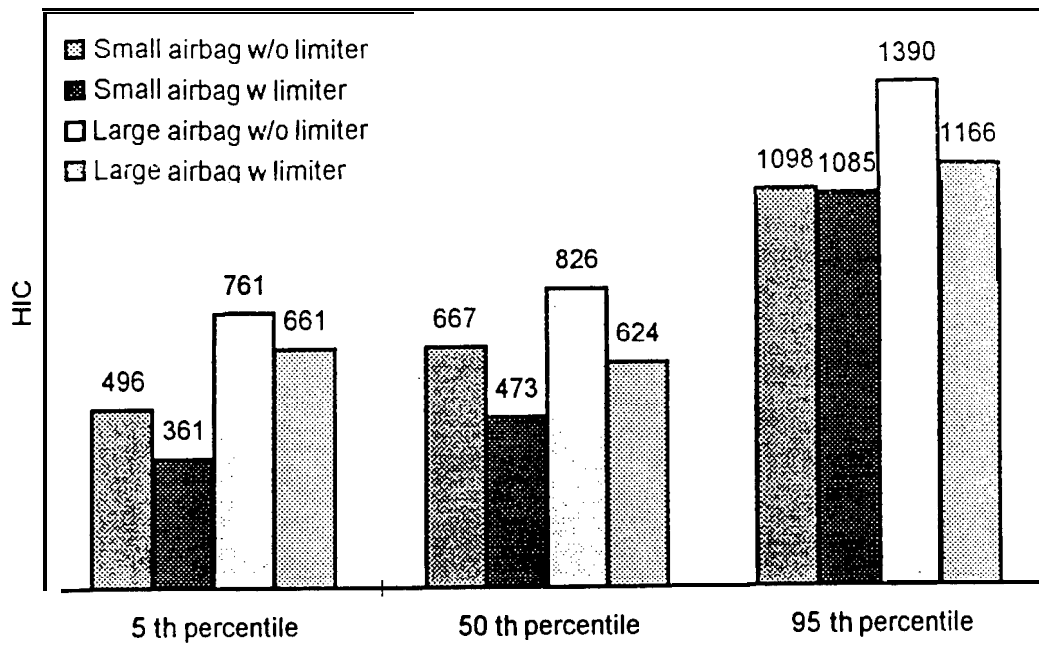


Figure 2.7 Comparison of Head Injury Criteria with and without load limiters (40 mph).

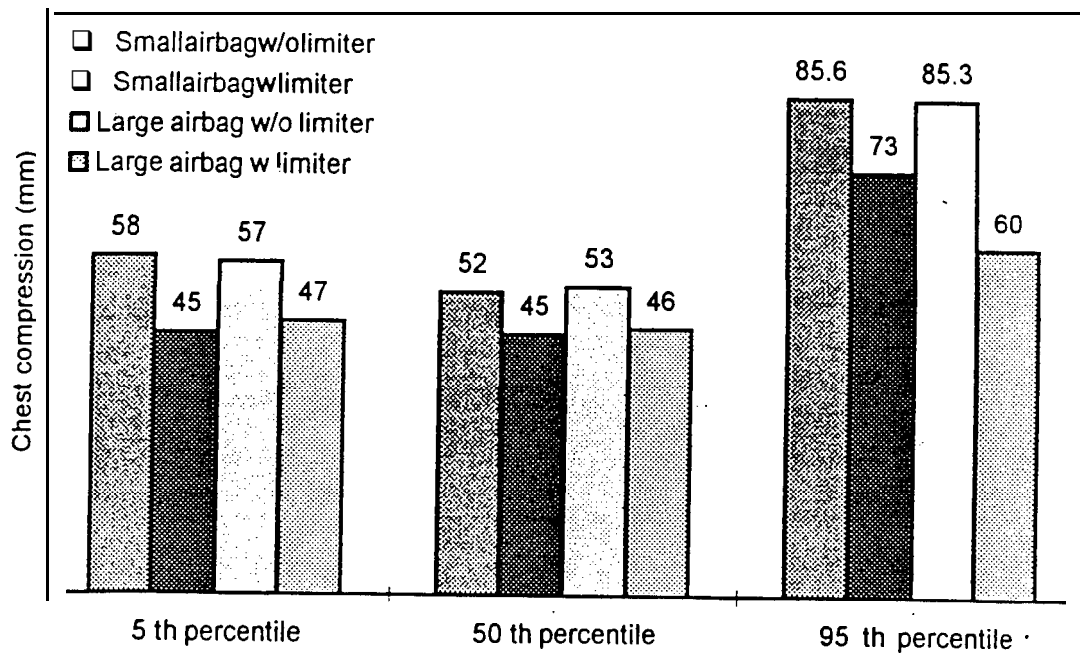


Figure 2.8 Comparison of chest compression with and without load limiters (40 mph).

Table 2.1 Simulation results without load limiter at 30 mph

With Small Airbag @ 30 mph									
	HIC	Head Excursion (mm)	Peak Head Acc. (m/s ²)	3MS (m/s ²)	Neck Load (N)	Left Femur Load (N)	Right Femur Load (N)	Chest Compression (mm)	Shoulder Belt Load (N)
5 th %-ile	279	187	487	448	905	1450	1210	49	4236
50 th %-ile	350	299	477	460	1150	1966	2163	42	7524
95 th %-ile	589	442	634	1142	2679	2019	2401	59	9371

With Large Airbag @ 30 mph									
	HIC	Head Excursion (mm)	Peak Head Acc. (m/s ²)	3MS (m/s ²)	Neck Load (N)	Left Femur Load (N)	Right Femur Load (N)	Chest Compression (mm)	Shoulder Belt Load (N)
5 th %-ile	361	209	559	437	1093	1521	1259	48	4086
50 th %-ile	427	300	538	465	1134	2004	2141	42	7562
95 th %-ile	698	419	650	1136	2555	2006	2 4 2 2	59	9205

Table 2.2 Simulation results with load limiter at 30 mph

With Small Airbag @ 30 mph with load limiter									
	HIC	Head Excursion (mm)	Peak Head Acc. (m/s ²)	3MS (m/s ²)	Neck Load (N)	Left Femur Load (N)	Right Femur Load (N)	Chest Compression (mm)	Shoulder Belt Load (N)
5 th %-ile	191	251	446	433	599	1117	1127	33	1500
50 th %-ile	171	378	410	494	986	1947	2043	34	3567
95 th %-ile	409	470	570	1185	2218	1923	2231	46	6688

With Large Airbag @ 30 mph with load limiter									
	HIC	Head Excursion (mm)	Peak Head Acc. (m/s ²)	3MS (m/s ²)	Neck Load (N)	Left Femur Load (N)	Right Femur Load (N)	Chest Compression (mm)	Shoulder Belt Load (N)
5 th %-ile	335	235	619	421	758	1131	1127	36	1450
50 th %-ile	279	368	478	500	892	1936	2047	35	3344
95 th %-ile	608	499	596	1245	1766	1863	1972	31	3567

Table 2.3 Simulation results without load limiter at 40 mph

With Small Airbag @ 40 mph									
	HIC	Head Excursion (mm)	Peak Head Acc. (m/s ²)	3MS (m/s ²)	Neck Load (N)	Left Femur Load (N)	Right Femur Load (N)	Chest Compression (mm)	Shoulder Belt Load (N)
5 th %-ile	498	236	598	580	1254	1441	1969	58	5410
50 th %-ile	667	335	690	652	1814	2170	2477	52	9786
95 th %-ile	1098	491	845	1627	3504	3285	3219	73	11867

With Large Airbag @ 40 mph									
	HIC	Head Excursion (mm)	Peak Head Acc. (m/s ²)	3MS (m/s ²)	Neck Load (N)	Left Femur Load (N)	Right Femur Load (N)	Chest Compression (mm)	Shoulder Belt Load (N)
5 th %-ile	761	248	657	572	1528	1398	2001	57	5428
50 th %-ile	826	338	789	658	1855	2170	2479	53	9773
95 th %-ile	1390	478	883	1590	3491	3256	3197	73	11722

Table 2.4 Simulation results with load limiter at 40 mph

With Small Ah-bag @ 40 mph with load limiter									
	HIC	Head Excursion (mm)	Peak Head Acc. (m/s ²)	3MS (m/s ²)	Neck Load (N)	Left Femur Load (N)	Right Femur Load (N)	Chest Compression (mm)	Shoulder & Belt Load (N)
5 th %-ile	361	275	575	562	889	504	1506	45	2600
50 th %-ile	473	373	605	608	1434	2089	2475	45	6688
95 th %-ile	1085	493	842	1634	3523	3035	3031	73	11808

With Large Airbag @ 40 mph with load limiter									
	HIC	Head Excursion (mm)	Peak Head Acc. (m/s ²)	3MS (m/s ²)	Neck Load (N)	Left Femur Load (N)	Right Femur Load (N)	Chest Compression (mm)	Shoulder Belt Load (N)
5 th %-ile	661	266	645	550	1075	1494	1398	47	2625
50 th %-ile	624	385	608	594	1338	1968	2477	46	5796
95 th %-ile	1166	498	794	1618	2932	3103	3005	60	8918

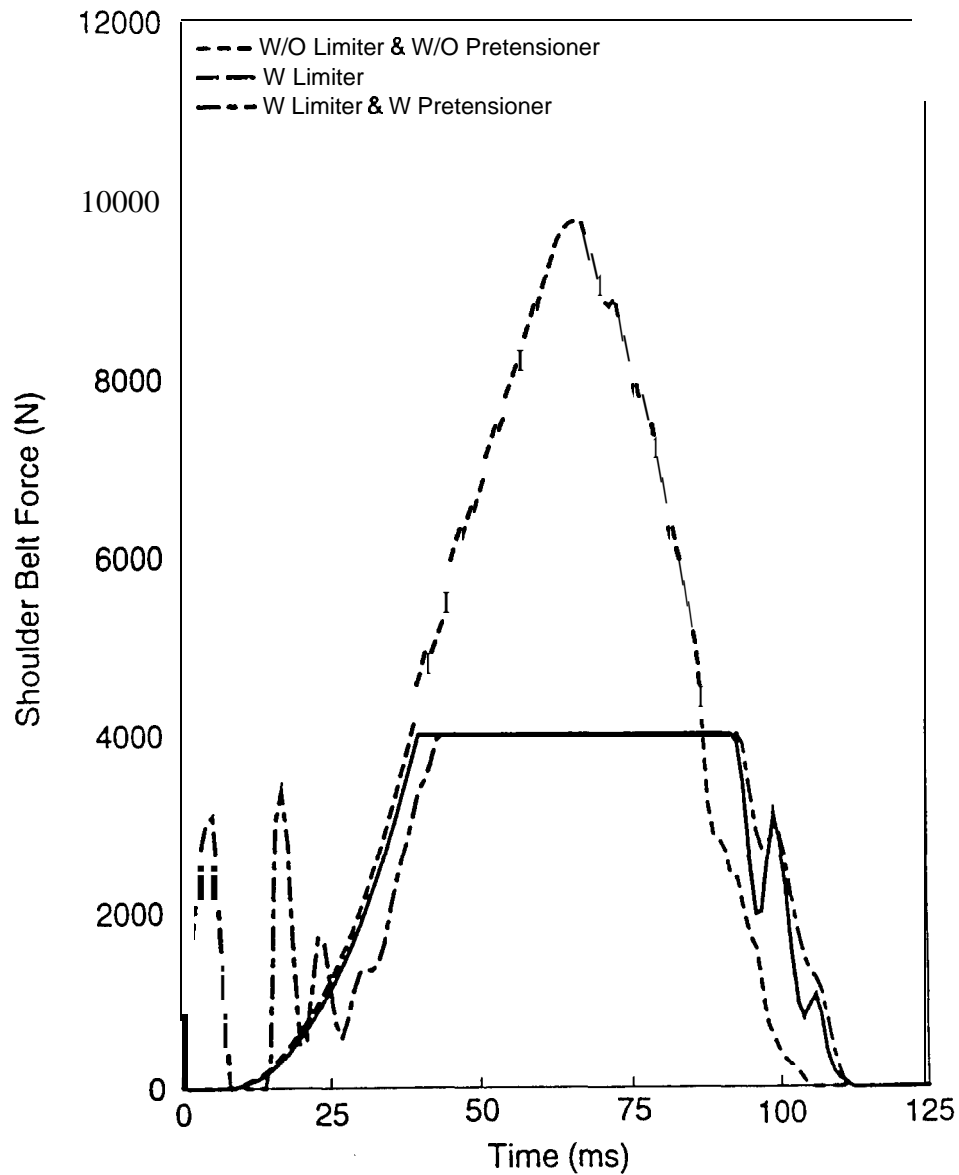


Figure 2.9 Shoulder belt load vs. time for 30 mph.

2.2 Pretensioner

To realize the effectiveness of shoulder belt load limit, belt slack and loose webbing wrap should be minimized. This can be achieved with the device called pretensioner, which takes 'up belt slack early in the collision by pulling on the belt at the buckle or the retractor location. This induces energy absorption during the early forward travel of the occupant in a frontal impact. This is illustrated in Figure 2.9 which compares the shoulder

belt loads vs. time for the cases of : (1) no load limiter, (2) with load limiter and (3) load limiter with pretensioner in 30 mph frontal impact. In this figure the initial spikes are seen at the shoulder level of the belt which may be induced due to the pretensioner effect at the buckle end, friction between the dummy and belt and initial kinematics of the dummy. Figure 2.10 shows the bar chart for injury numbers with and without the pretensioner in the presence of a 4000 N load limiter and a large airbag for a 50th percentile dummy at 30 mph.. More than 10 percent reduction is seen for all the injury parameters, with the resultant chest acceleration (3MS) reducing by 50%.

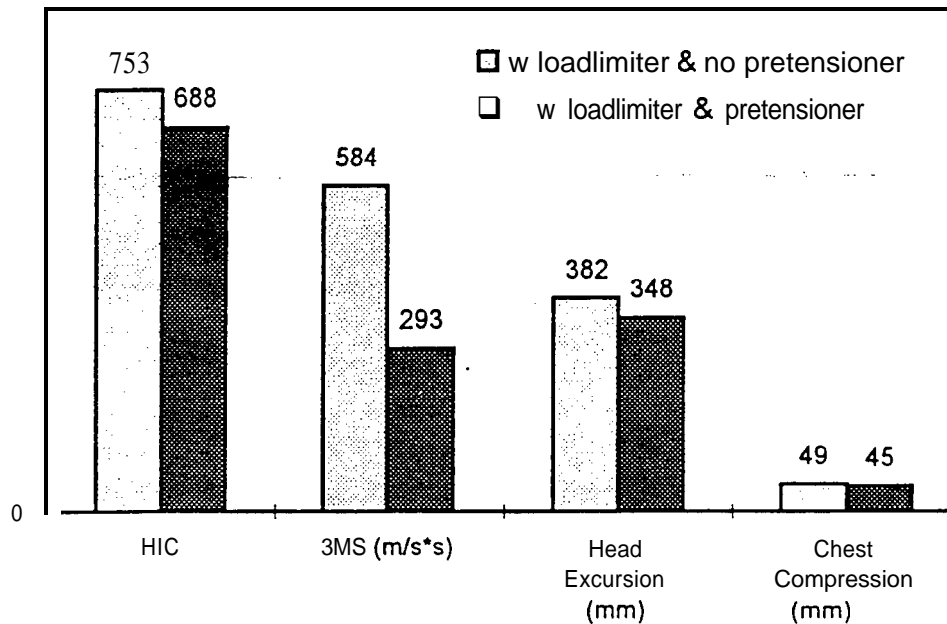


Figure 2.10 Effect of pretensioner on injury parameters (50th percentile dummy at 30 mph).

Work done as part of this study has shown improved occupant protection by the use of pretensioner in rollover crashes. Introduction of belt pretensioner has also been shown to significantly reduce the risk of submarining (Halund et al., 1993). The pretensioner (buckle mounted) helps prevent submarining by reducing the slack (Leung et al., 1982) and by pulling the buckle downwards, which narrows the opening for pelvis to slide through. A buckle mounted seat belt pretensioner with specifications as shown in Table 2.2 is used in this study.

Table 2.2 Specifications for the Belt Pretensioner

Pulling Distance	80 mm
Pulling Time	9.5 msec.
Pulling Force	<1000 N (Depending on Test Set-up)
Operating Temperature	-40°C to 100°C
Weight	450 grams
Type	Pyrotechnic, Buckle Mounted

3. REAR IMPACT PROTECTION

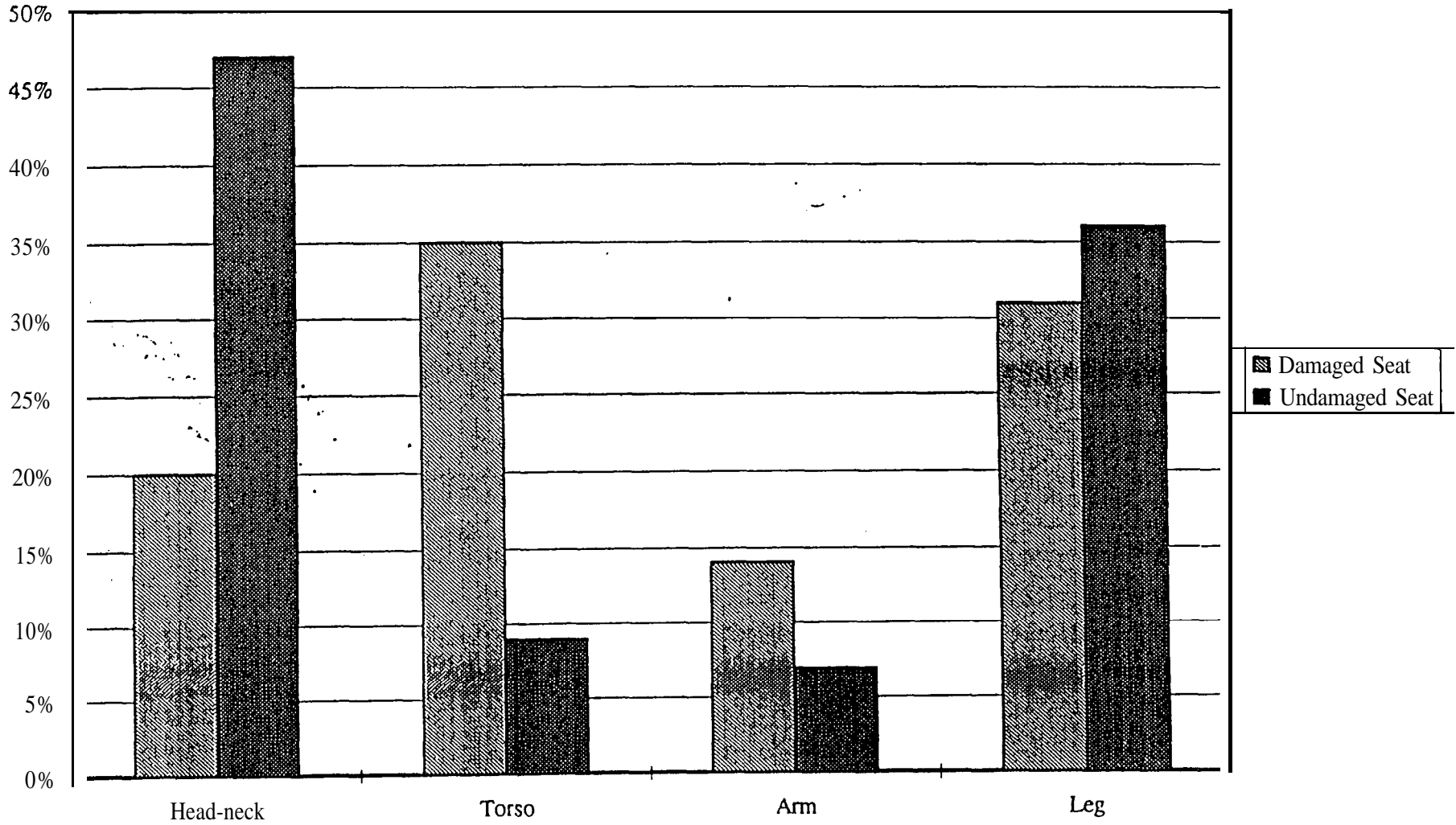
Neck injuries with risk of permanent disability are frequent in low severity rear-end collisions (Carlsson et al., 1985). Studies by Langweider (1981) and Kahane (1982) suggest that of those occupants injured in rear impact accidents 80 to 90 percent suffer neck injury. Figure 3.1 illustrates the nature of body injuries attributed to frontal components in rear crashes and Figure 3.2 addresses sources of injuries based on seat conditions for different crash modes. Because such accidents are common, they cause significant human suffering and high societal costs, despite the fact that the injuries are usually classified as “minor” (AIS 1) in the Abbreviated Injury Scale (AIS) (Nygren, 1984 and Nygren et al., 1985). Analysis of Cooperative Crash Injury Study (CCIS) database (Renouf, 1991) has indicated that 95 percent of neck injuries to front seat occupants are recorded as AIS 1. The importance of certain seat. (particularly seat back) characteristics on rear impact and criteria relevant to minimize the related injuries are discussed below. Seat back bending stiffness strongly influences occupant response in rear impact. Seat back rotation can be beneficial from an energy absorption standpoint. A seat back that collapses without absorbing energy is not desirable. A study on protection against rear end accidents (Thomas et al., 1982) suggests that failure of the seat back or mountings has a greater effect on cervical spine injury than the head restraint. A small number of cases exist where rear seat occupants have been killed by the front seat collapsing on to them (Lowne et al., 1987). In an integrated structural seat, large rotation angles will cause greater demands on the shoulder belt in restraining the occupant from sliding backwards. At the same time, excessive rotation will encroach on rear seat occupant space. Therefore a 30 degrees seat back rotation from the design position is selected as the maximum allowable for the 95th percentile dummy under a 30 mph rear impact crash pulse. This seat back rotation angle is consistent with the current industry practice.

In contrast to a seat back that deforms too easily, a rigid seat back may cause occupant rebound (Partyka et al.). The elastic springback energy stored in the seat is sufficient to throw the occupant far enough to hit the steering wheel or the dash. A rigid seat back may also cause the occupant to ramp up, which may lead to partial or complete ejection. Due to ramp up of the occupant, the head may rise above the headrest leaving no support to stop the head from tilting rearward thereby increasing head to neck torque. This leads to “whiplash” related injuries. Seat back design should aim at minimizing occupant ramp up and rebound, and at the same time contain seat back rotation. In this study the maximum seat back rotation was restricted to 30” from the design position. Effect of the various seat characteristics described above, on the occupant, is reflected in the occupant injury numbers, such as HIC, neck extension and flexion torque, etc. While a seat needs to address the management of energy transfer to the occupant in severe rear crashes, biomechanical responses need to be below tolerance levels and proportionately lower with decreasing crash severity for overall injury prevention.

Body Region Injuries Attributed to Frontal Components in Rear Crash

Source: S. C. Partyka; Seat Damage & Occupant Injury in Passenger Car Towaway Crashes (1988-1990 NASS Data)

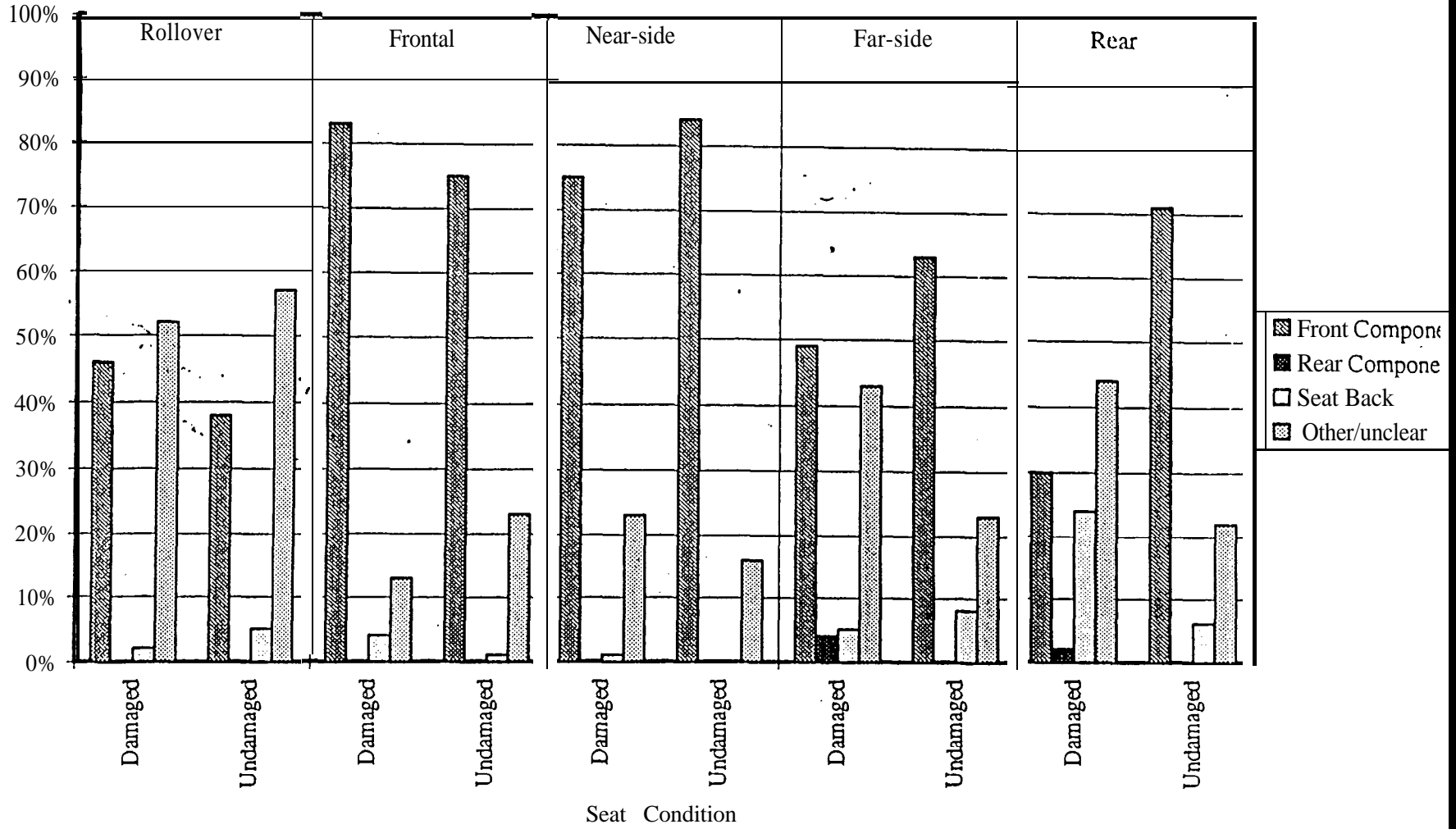
Figure 3.1 Body region injuries attributed to frontal components in rear crash.



Source of Injury For Outboard, Belted Occupant

Source: S. C. Partyka; Seat Damage & Occupant Injury in Passenger Car Towaway Crashes (1988-1990 NASS Data)

Figure 3.2 Source of injury for outboard, belted occupant.



Some form of limited and controlled deformation of the front seats is therefore desirable. In this way energy could be absorbed by the seat, reducing the risk of injury to the front seat occupants, without endangering rear seat occupants. In this study several design features are explored to address the above injuries and to reduce them below the human threshold limit. Table 3.1 relates the design features to the different requirements. The evaluation methodology and the results for various design features are described below.

Table 3.1 Participation of the proposed design features in addressing various rear impact performance criteria

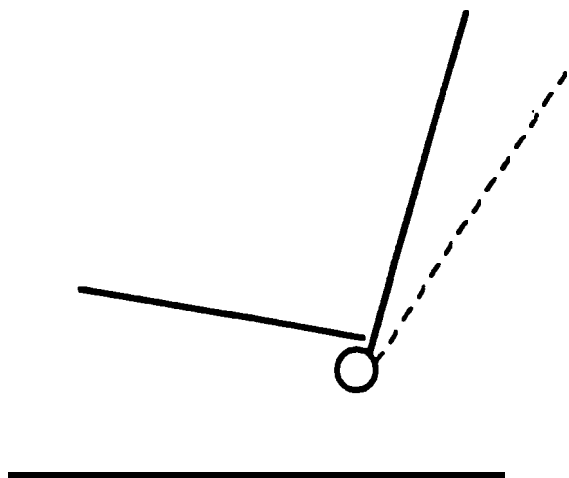
	Dual Recliner	Modified Seat Back	Energy Absorber	Inflatable Headrest	Integrated Seat Belts
Whiplash			X	X	
Excessive Seat Back Deformation	X	X			
Ramp Up			X		X
Rearward Ejection	X	X			X
Excessive Rebound			X	X	

3.1 Effect of Increasing Distance Available for Torso Acceleration

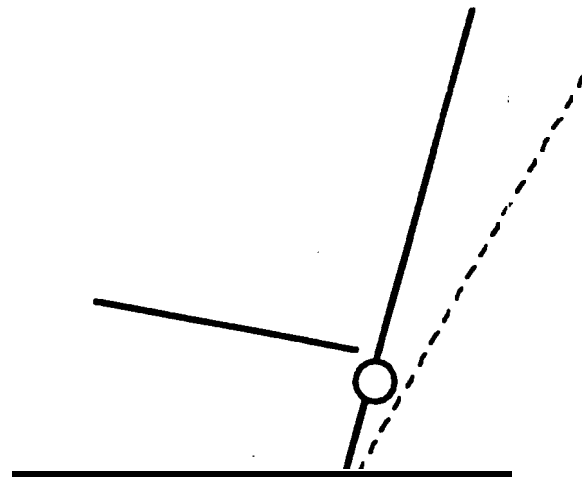
The effect of a crash pulse on an occupant can be mitigated by increasing the available “ride down” distance, i.e. to decelerate the body in the case of frontal crash, or accelerate the body in the case of side impact or rear impact. Two different design concepts are developed in order. to accelerate the torso over a larger distance under rear impact conditions. These two concepts are illustrated in Figure 3.3.

The first concept involves lowering the effective center of rotation of the seat back. This may be effected by designing a “plastic hinge” for the seat back close to the floor. This hinge essentially lowers the effective center or rotation of the seat back. It may be designed to occur below the existing recliner as shown in the figure, or at a lowered recliner location. The lowered hinge increases the available distance for the lower torso to accelerate, thereby reducing peak forces and accelerations. An added benefit of a lowered recliner is that, according to recent research at Johnson Controls, it is more comfortable for an occupant while adjusting the reclining angle of the seat because the effective center of rotation of the upper torso has been found to be well below the seat plane.

The second concept involves a sliding seat. This design would also increase the distance available for the torso to accelerate forward. The seat would be restrained by an appropriate mechanical device. Possible options would be honeycomb, crushable foam, or a metal draw bead. Thus the seat motion itself would dissipate energy.

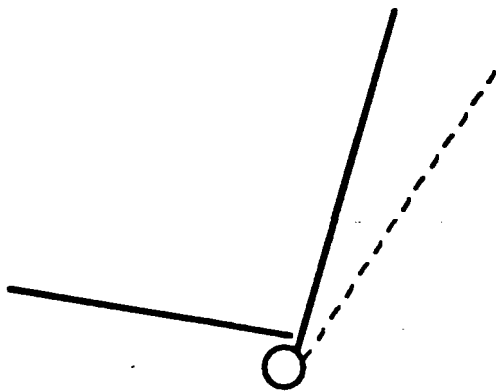


Standard seat

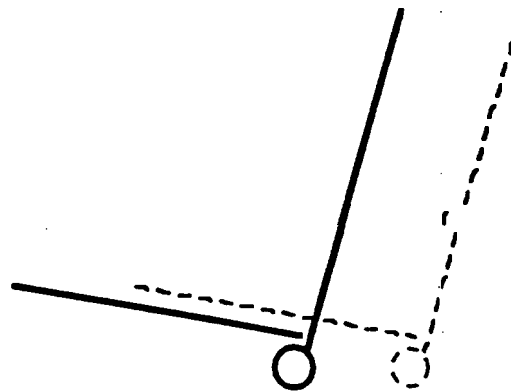


Lowered plastic hinge

Lowered effective center of rotation of seatback increases lower torso travel for a given amount of seat back excursion. Lower torso and shoulder loads are reduced.



Standard seat



Sliding seat

Sliding seat increases deceleration distance for lower torso. Seat loads are reduced.

Figure 3.3 Design concepts for increasing torso travel.

Both these concepts were analyzed using MADYMO simulation. The results are summarized in Table 3.2. Both concepts do lead to a reduction in peak force values. However one serious objection that might be raised with these seats is that the moving seat back may injure the lower extremities of rear seat occupants. Another is that it would be difficult to lower the pivot due to space restrictions imposed by the seat track. Therefore these two concepts are not considered to be universally adaptable.

Table 3.2 Effect of lowered pivot seat and sliding seat

Seat Type	HIC	3MS (m/s ²)	Lower torso contact force (N)	Shoulder contact force (N)
Standard	116	192	9692	4932
Low Pivot	133	210	6760	4418
Sliding seat	40 -	144	7905	3662

3.2 Seat Back Structure

Torsional resistance of the seat back was considered as part of this project. A second recliner was added to the inboard side of the existing seat to consider the effect of that configuration on torsional rigidity. The existing baseline seat design has a single linear recliner on the outboard side and shows twisting in 30 mph rear crash. The analytical models used to evaluate the existing seat with and without dual recliners are described below.

To study the performance of the existing seat in rear impact, a nominal static design load that the seat must withstand is first estimated from a series of MADYMO simulations. The seat back is modeled in MADYMO as a pivoted structure which is restrained by a resistive torque function. The pivot is located at the recliner position. The torque function at the pivot defines the elasto-plastic bending stiffness characteristic of the seat back. Figure 3.4 shows the MADYMO model and crash sequence in rear crash for a 50th percentile occupant. Similar models were developed incorporating the 95th percentile and 5th percentile Hybrid-III dummy models. A 30 mph rear impact crash pulse is used in the model. This pulse (Figure 3.5) is obtained from a FMVSS 301 (fuel integrity) moving barrier crash test at 30 mph. The resulting change in velocity of the struck vehicle is 20 mph.

A series of MADYMO simulations with different seat back stiffness characteristics were performed until satisfactory response, meeting the criterion of a maximum seat back rotation of 30 degrees for the 95th percentile dummy is achieved. Figure 3.6 shows the torque vs. seat back rotation characteristic for the seat back that produces the desired maximum seat back rotations shown in Table 3.3.

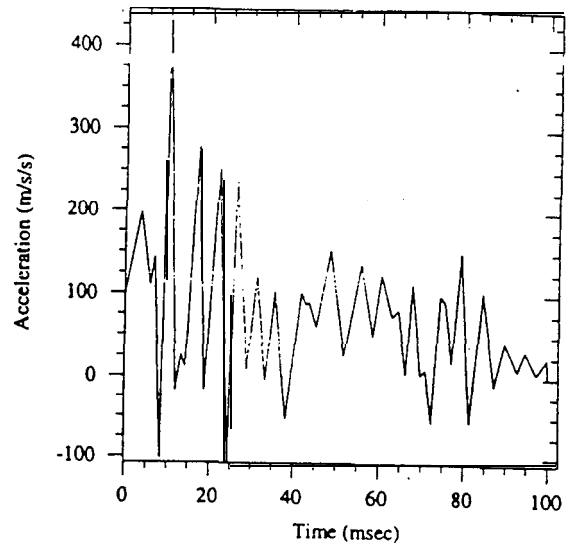
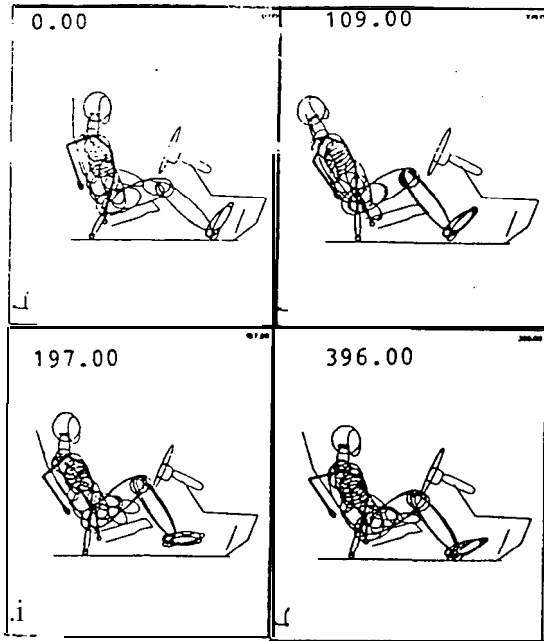


Figure 3.4 Crash sequence in rear impact. Figure 3.5 Acceleration pulse.

Table 3.3 Maximum seat back angle with respect to the seat bottom
(Initial seat back angle = 23°)

	5 th percentile	50 th percentile	95 th percentile
Rotation of the seat back	10°	22°	29°
Peak seat back angle (wrt. vertical)	33°	45°	52°

Equivalent torque applied to a finite element model of the existing seat produces a seat back twist of approximately 15°. A 17° rotation is seen using a LSDYNA/MADYMO coupled model for a 95th percentile dummy in 30 mph rear crash. This rotation is decreased to 3 degrees for the modified seat with a second recliner added on the inboard side

3.3 Recliner With Energy Absorber

Occupant rebound and ramp up can be minimized by designing a seat back that deforms plastically in a controlled manner. Rebound is caused primarily by the elastic energy stored in the seat back during rearward deformation, which is imparted to the

occupant during the forward travel. In order to obtain the necessary compliance in the rearward direction a mechanical energy absorbing element was added in series to both the recliners on either side of the seat.

The design of this device (described later) is such so as to modify the torque vs. angle function of the seat back to approximate the desired curve originally obtained from the MADYMO model (Figure 3.6). It should be noted that the torque-theta curve has a very sharp rise followed by a relatively flat region. Upon unloading at any point along the curve, the drop in force is also very sharp. This implies that the amount of elastic energy stored in the seat back is very small compared to the amount of energy absorbed by the energy absorber. A typical existing seat back would have a torque-theta curve which has a much lower initial slope. This translates to a higher proportion of stored spring back energy compared to the dissipated energy. The difference between these two cases is illustrated in Figure 3.7.

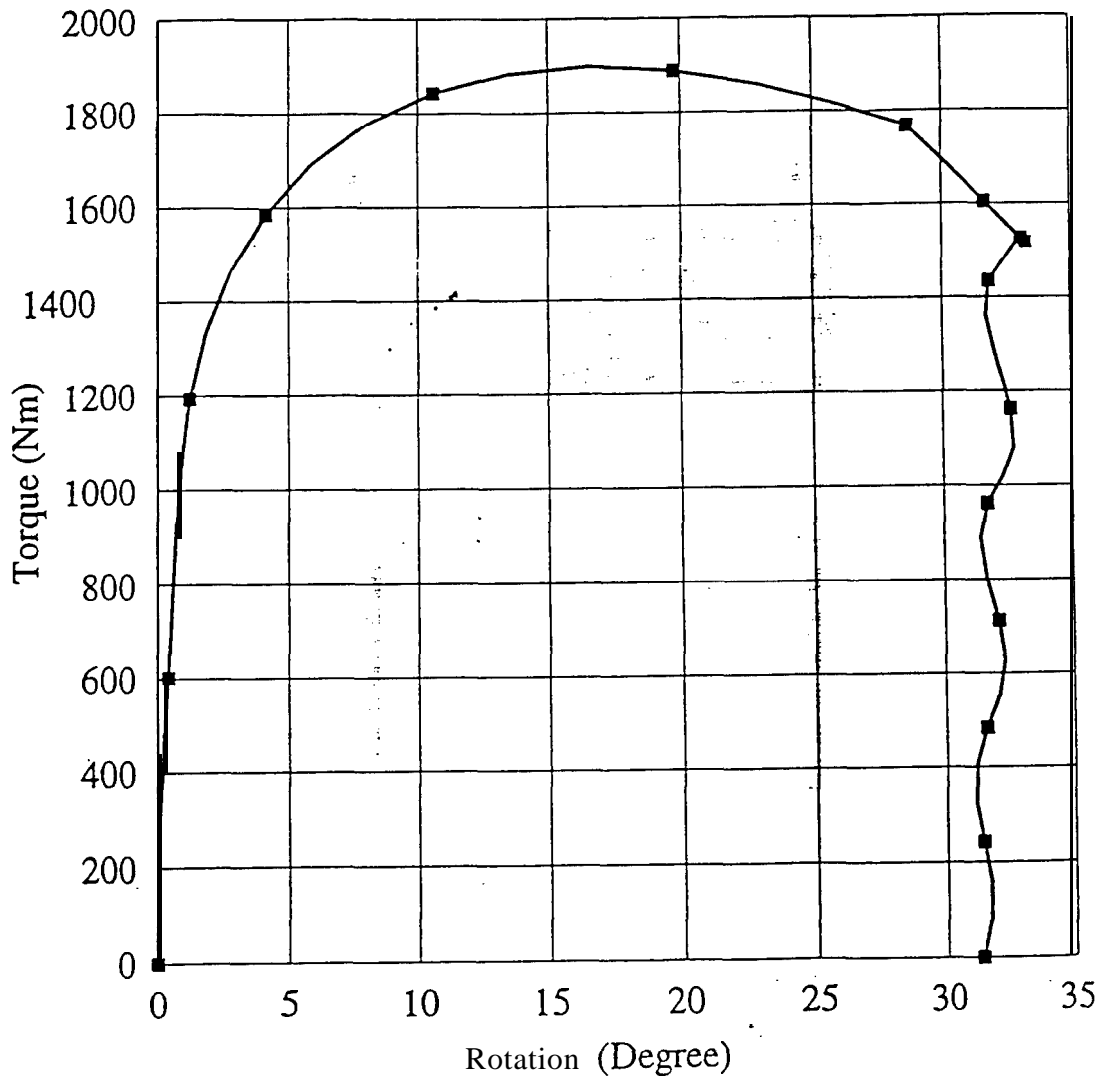


Figure 3.6 Torque vs. rotation curve for the seat back.

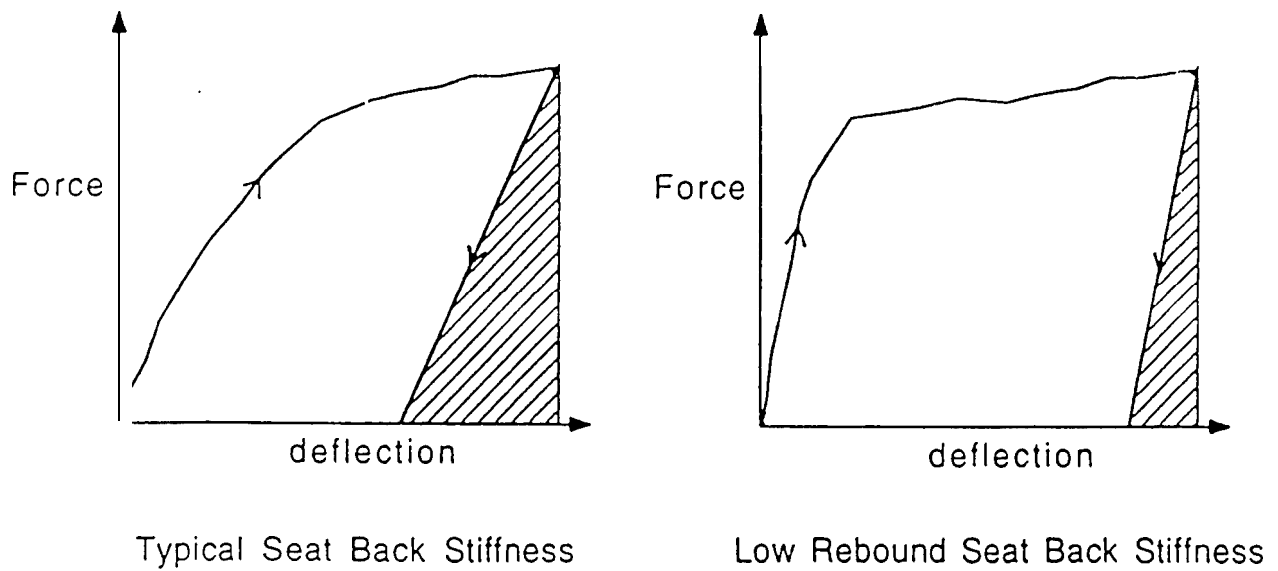


Figure 3.7 Energy absorption of a typical seat back and low rebound seat.

In order to quantify the amount of forward excursion due to seat rebound, a series of MADYMO simulations were performed with and without seat back rebound. This was implemented in the MADYMO model by changing the hysteresis slope of the torque-theta curve of the seat back joint stiffness. The scaled seat back **stiffness** curve was used. Table 3.4 shows a comprehensive table of results for all three dummies with and without seat back rebound. In Table 3.4 it can be seen that the force on the shoulder belt is the same for the cases with and without rebound of the seat back for the 50th percentile occupant. This is due to the “ramp up” effect of the occupant in the rigid no rebound seat.

Figure 3.8 summarizes some of the results, and graphically illustrates how the forward excursion of the 50th percentile dummy is affected by rebound as a **function** of rear impact velocity. Head excursion is defined as the distance of the head **from** the initial pre-impact position to the forward most rebound position. Shoulder belt loads were also recorded to see the effect of any ramp up of the occupant with and without the rebound.

To check the performance of the modified design in frontal impact, a non-linear finite element analysis **is performed** to simulate a 4,000 N load limited shoulder belt load for a **frontal** crash. The seat withstands this loading condition very well. The seat back rotation is less than 5°.

Table 3.4 Effect of seat back rebound.

	5 %-ile (w rebound)	5 %-ile (w/o rebound)	50 %-ile (w rebound)	50 %-ile (w/o rebound)	95 %-ile (w rebound)	95 %-ile (w/o rebound)
DISPLACEMENT (M)						
Chest compression	.0047	.0022	.0110	.0113	.0129	.0063
Head excursion	.1534	.0061	.1432	-.0580	.1059	-.1661
Left shoulder	.1955	.1760	.2440	.2440	.3203	.3197
Left seat corner	.1080	.1088	.1750	.1754	.2283	.2273
ACCELERATION (M/s²)						
Lower Torso	280	273	228	228	227	228
Chest	670	672	324	324	825	823
Head	364	372	485	485	457	462
FORCE (N)						
St. back-lower torso	5325	5184	5621	5621	8633	8615
St. back-left shoulder	458	440	205	161	577	584
St. back-right shoulder	444	424	194	167	521	528
Shoulder belt	2559	1774	1939	1939	1785	1203
FLEXION TORQUE (N.M)						
Head-neck	25	23	33	26	34	34
CONSTRAINT FORCE (N)						
On head from neck	769	797	1075	1075	1239	1153
On neck from upper torso	722	738	1340	1340	1300	1213
INJURY						
BMS (m/s ²)	563	562	200	200	663	670
HIC	91	82	152	149	98	99
ANGLE (DEGREES)						
Seat back angle w.r.t. vertical (initial=23°)	33	33	40	40	45	45

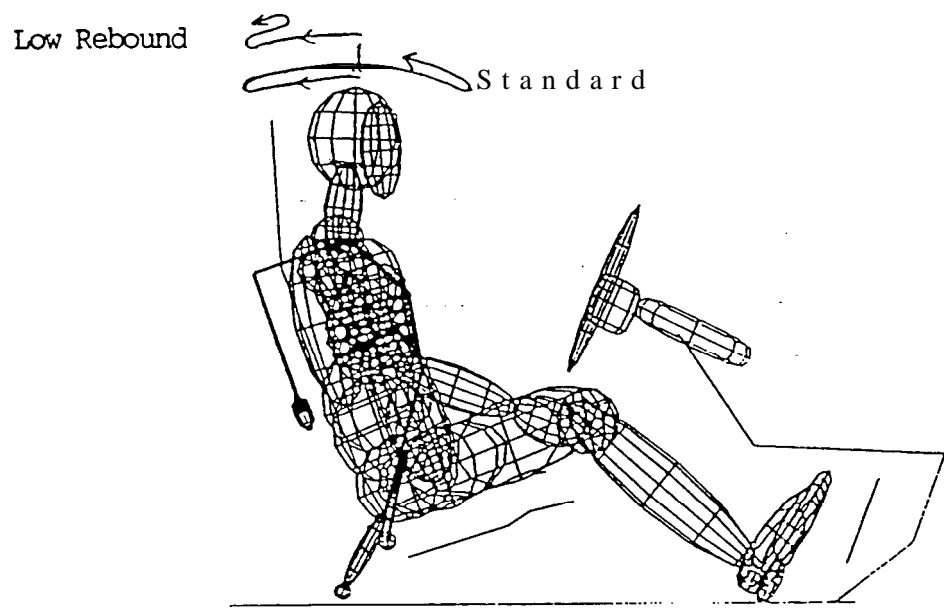
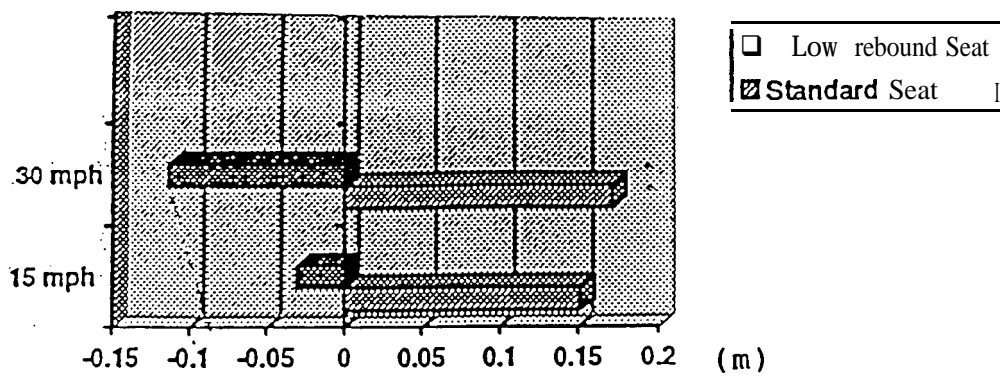


Figure 3.8 Head excursion due to seat back rebound.

3.3.1 Design for Energy Absorber (EA)

This section describes the development of an energy absorbing recliner which serves the purpose of deforming the seat back in a controlled manner. The energy absorber is expected to deform by about 50 mm to produce the desired amount of rotation (maximum of 30°) of the seat back. Design evolved in this study utilizes the support plates of the existing recliner with appropriate modifications. The energy absorption is primarily achieved by the deformation of metal as the recliner pin traverses down a tapered slot created in the supporting metal plates.

For modeling purposes, a portion of the seat is cut to isolate the recliner and the surrounding area. Tapering slots are created in the recliner support plates. The recliner diameter is 15 mm and it drives down the metal slots which decrease in width from 90% of recliner diameter (at the top) to 40% (at the bottom). About 50 mm of crush space is made available. Since slot width is smaller than the diameter of recliner, resistance is offered by the slot as recliner tries to drive down through it. Metal deformation occurs in the process and energy is absorbed. The recliner is assumed rigid for this purpose. The basic layout of the modified recliner and the existing recliner is shown in Figure 3.9.

A mechanical device is added to the energy absorber to (1) avoid activation of shearing mechanism for low speed crashes and (2) to avoid rattling which would occur if there were no firm support to the recliner. The force-displacement curve for this metal element 1 mm thick is shown in Figure 3.10. A sharp increase in the strength can be noticed during the initial part of the simulation. This would prevent the activation of the energy absorber at low speed crashes.

The energy absorber design is developed and tested using a very refined finite element model of the recliner support plates and the surrounding areas. Due to a very small time step of this refined model, analyzing a full seat model is computationally very expensive. Hence, the seat structure represented by beam elements and the dummy by lumped masses, is attached to the refined recliner model. Once the design for the energy absorber was finalized, it was further tested using a LS-DYNA3D/MADYMO coupling method described below.

3.3.2 Design Verification for Rear Impact

The various design features for rear impact protection were finally tested using a detailed model. A detailed finite element seat model, incorporating the Dual Recliner, Modified Seat Back and the Energy Absorber, is coupled with the MADYMO model of the 50th percentile Hybrid III dummy. The dummy model used had been enhanced by EASi for greater biofidelity. The hip joint had been released. The neck to upper torso joint stiffness had been modified to represent the rearward extension of the neck (Kolita et

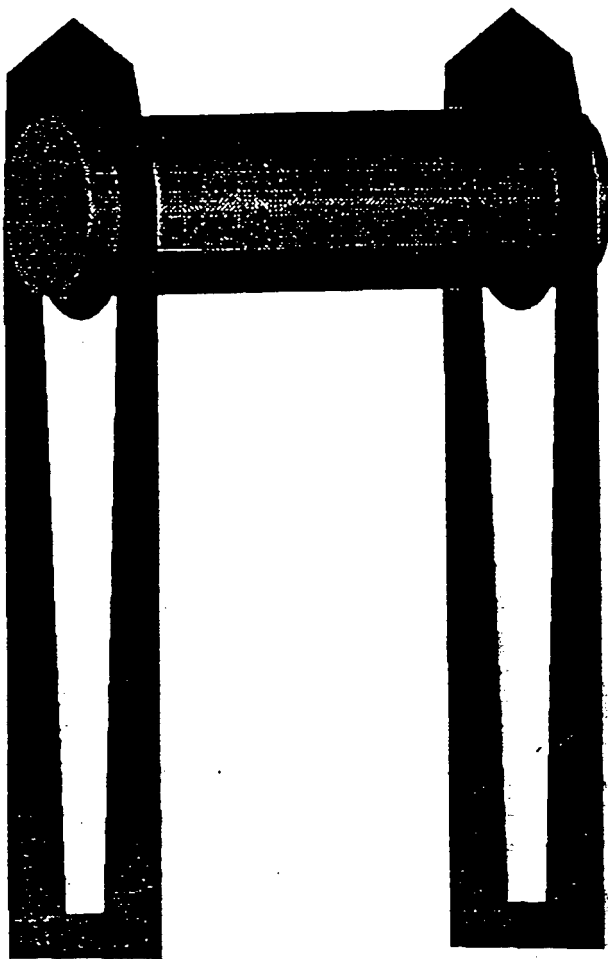
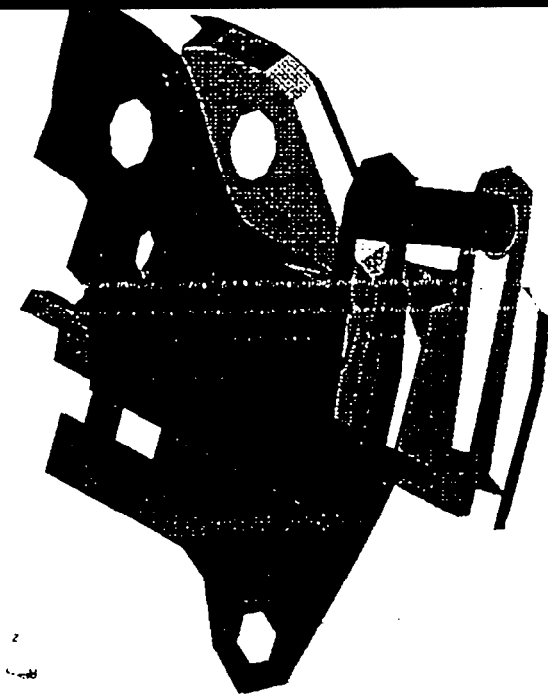


Figure 3.9 Layout of modified recliner.

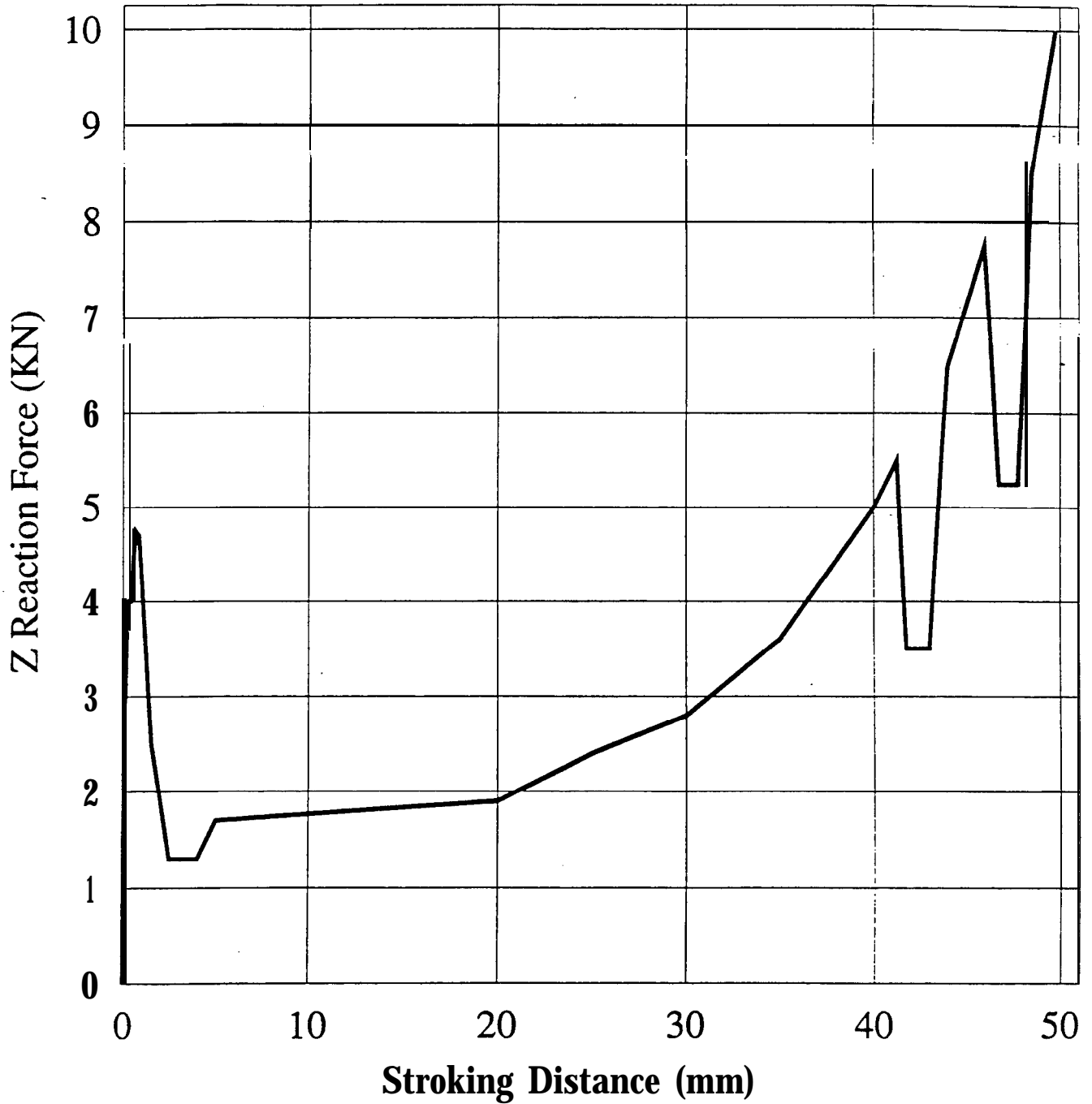


Figure 3.10 Force-displacement curve with the metal element.

al.). The characteristics for the EA are obtained from the detailed EA model and represented in the full seat model as a spring element, in series with the recliner.

The coupled simulation was carried out for 200 msec. with the same rear impact crash pulse as used in the MADYMO study (Figure 3.5). Figure 3.11 shows the set up for the coupled simulation. The results are presented in Table 3.5. Table 3.5 lists the results for the 5th, 50th and 95th percentile dummy obtained from the MADYMO models. The table also lists the results for the 50th percentile dummy obtained using the LSDYNA/MADYMO coupled model. The coupled model has a finite element representation of the seat structure, which is more accurate compared to the rigid body assumptions of the MADYMO model. Table 3.5 also lists the human tolerance values for some of the injury parameters. The injury numbers for the AISS design are well below the human tolerance levels. The injury parameters are compared with the human tolerance values. The final design was also tested for the 5th and the 95th percentile dummies using a MADYMO simulation. These results are reported in Table 3.5 and compared with the human tolerance values.

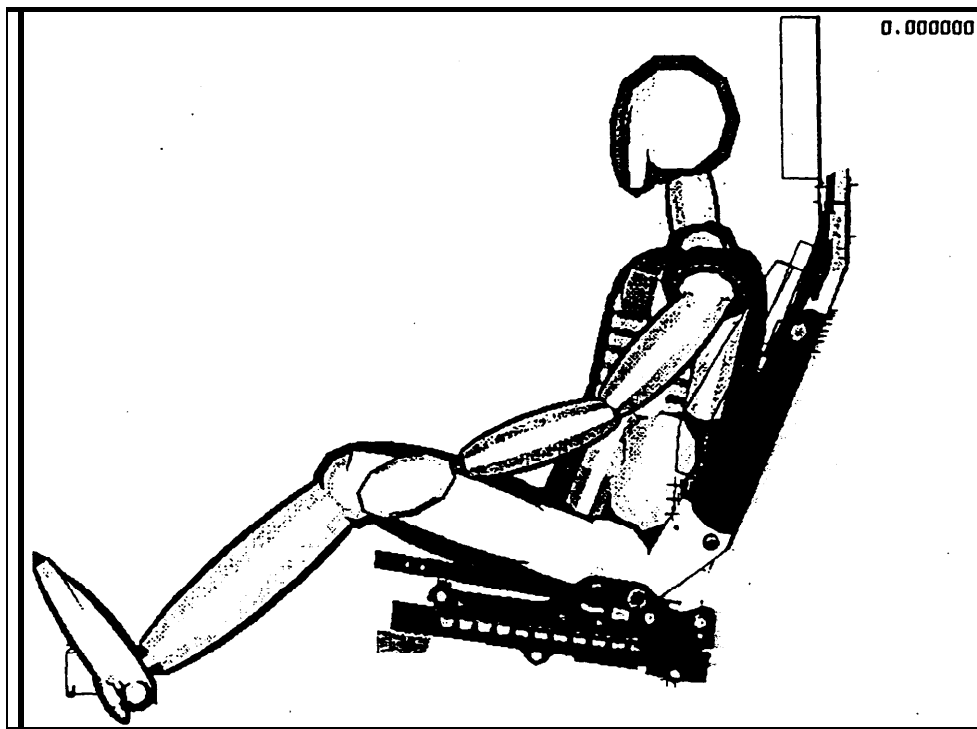


Figure 3.11 Model setup for the coupled simulation.

Table 3.5 Injury numbers for 5th, 50th and 95th percentile dummy models.

	50th %-ile Coupled LSDYNA- MADYMO	To lerance Levels	5 %-ile MADYMO	50 %-ile MADYMO	9.5 %-ile MADYMO
DISPLACEMENT (M)					
Chest compression	0.0016	0.0760*	0.0011	0.0087	0.0074
Head excursion			-0.0858	-0.1531	-0.2299
Left shoulder			0.2143	0.2908	0.3409
Left seat corner			0.1506	0.2156	0.2377
ACCELERATION (M/S²)					
Lower Torso	173		289	210	275
Chest	155		175	242	261
Head	248		343	612	620
FORCE (N)					
St. back-lower torso			5648	5863	10824
St. back-left shoulder			444	110	543
St. back-right shoulder			426	115	554
Shoulder belt			891	1352	1330
FLEXION TORQUE (N.M)					
Head-neck	10	60*	27	24	17
CONSTRAINT FORCE (N)					
On head from neck	258		791	1071	1179
On neck from upper torso	338		736	1159	1228
INJURY					
3 MS (m/s ²)	94	588	167	220	223
HIC		1000	43	259	240
ANGLE (DEGREES)					
Seat back angle w.r.t. vertical (initial=23°)	43		37.6	44	46

* Armenia-Cope at al., 1993.

3.4 Inflatable Head Rest

Proper support to the head and neck region during a rear impact can minimize the severity of injury to these regions (Status Report, 1995). Also to be taken into account is the comfort and visibility issues that go with the head-neck support. One of the headrest concepts which helps reduce the severity of injury to the head-neck region is the Catcher's Mitt, which is a reactive system that operates on the pressure **from** the occupants back to force the headrest forward. This system may indeed reduce the whiplash effects by keeping the headrest close to the head, but if the force of the forward motion of the headrest is not substantially controlled, the possibility of an impact to the head is very high. Another concept which was looked at during the course of this project is the use of a non pyrotechnic (compressed gas) inflatable headrest. The idea **is** to inflate a small bag during the heads forward motion, so as to give a pillow effect to the head on its return towards the headrest.

A MADYMO model was used to study the inflatable headrest concept. A baseline model was developed based on a Ford Taurus and a JCI seat from the blue prints. The position of the headrest was modeled in accordance with the blueprints provided by JCI, the headrest section of the blueprint and the MADYMO headrest section of the model are shown in Figures 3.12 and 3.13. For this study three types of FE **airbags** were used with varying inflator parameters and bag shapes. The three types of bags are shown in Figure 3.14. The response of the occupant with the use of these bags were studied by' varying different characteristics of the bag, namely the shape, inflator jet angle, inflator jet diameter and the trigger time of inflation.

Simulations were first performed using a 50th percentile Hybrid III dummy for a 30 mph rear impact. Optimum time of triggering was found to be 25 milliseconds for the cushioning effect of the head. Figures 3.15 through 3.18 show the response of the occupant with the different parametric changes made to the three types of bags. It can be observed that the shape of the bag the gas jet direction and inflator size helps reduce or increase the aggressivity of the bag. From these figures it can be seen that the best inflatable headrest was the type 3 with an inflator jet angle of 45 degrees and a jet diameter of 5 mm. Figures 3.19 through 3.22 show the response of the occupant and the injury numbers with the best parameter for the three types of bags and compared with the baseline case where there was no inflatable headrest. It can be observed that inflatable headrest helps reduce the head excursion and acceleration and reduces the extension torque, which is one of the influencing factors of the whiplash syndrome. Simulation results of the occupant kinematics are shown in Figures 3.23 through 3.26.

Simulations were then performed with the same 50th percentile Hybrid III dummy for a 5 mph rear impact. For this set of simulations based on the 30 mph case, the optimum trigger time was set at 25 ms and the type 3 bag was used. Figures 3.27 and 3.28 show the occupant response, for the baseline and with inflatable headrest simulations, from both the 30 mph and 5 mph rear impact simulations. Figures 3.29 and 3.30 show the trajectory

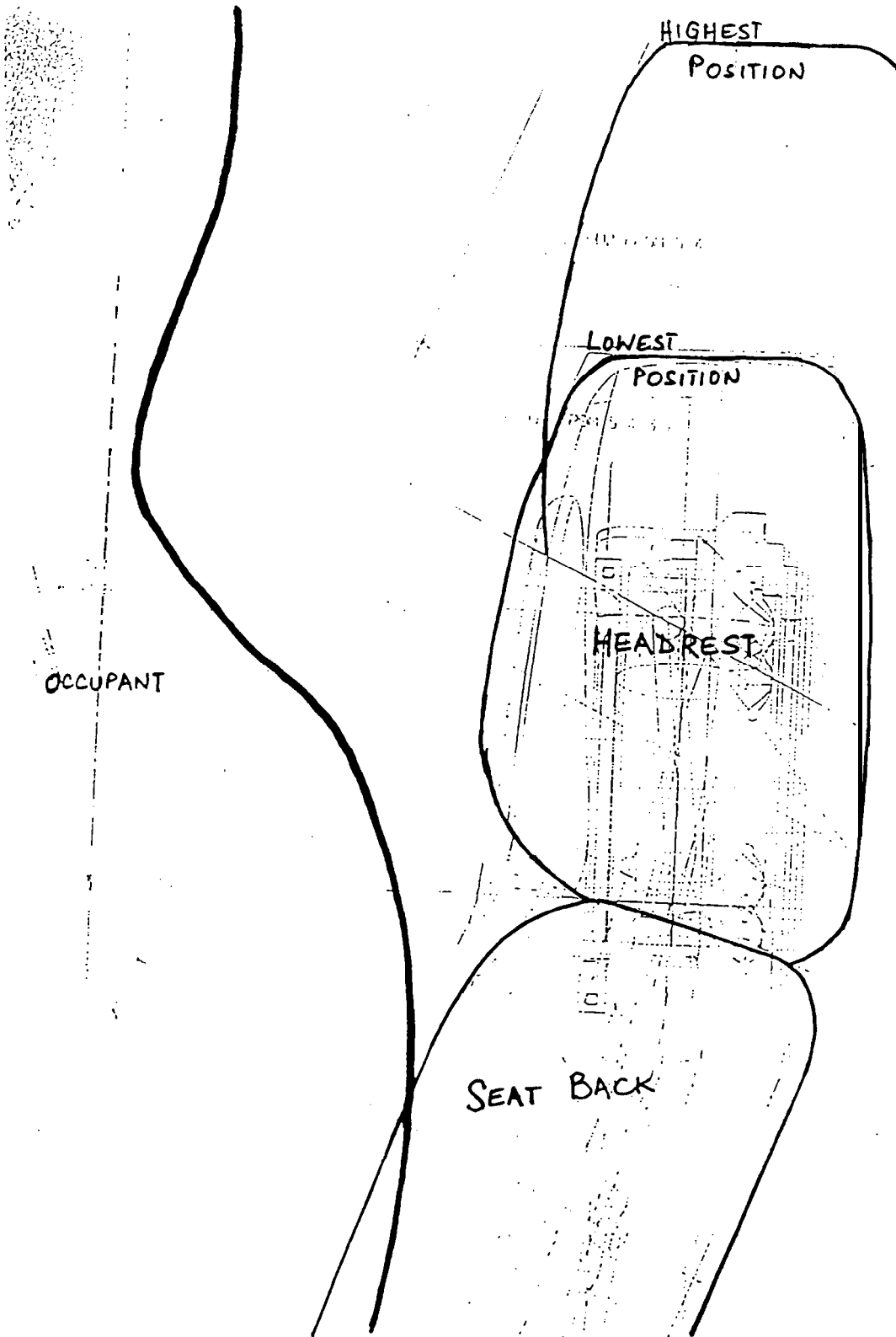


Figure 3.12 Headrest positions from blueprint (courtesy JCI).

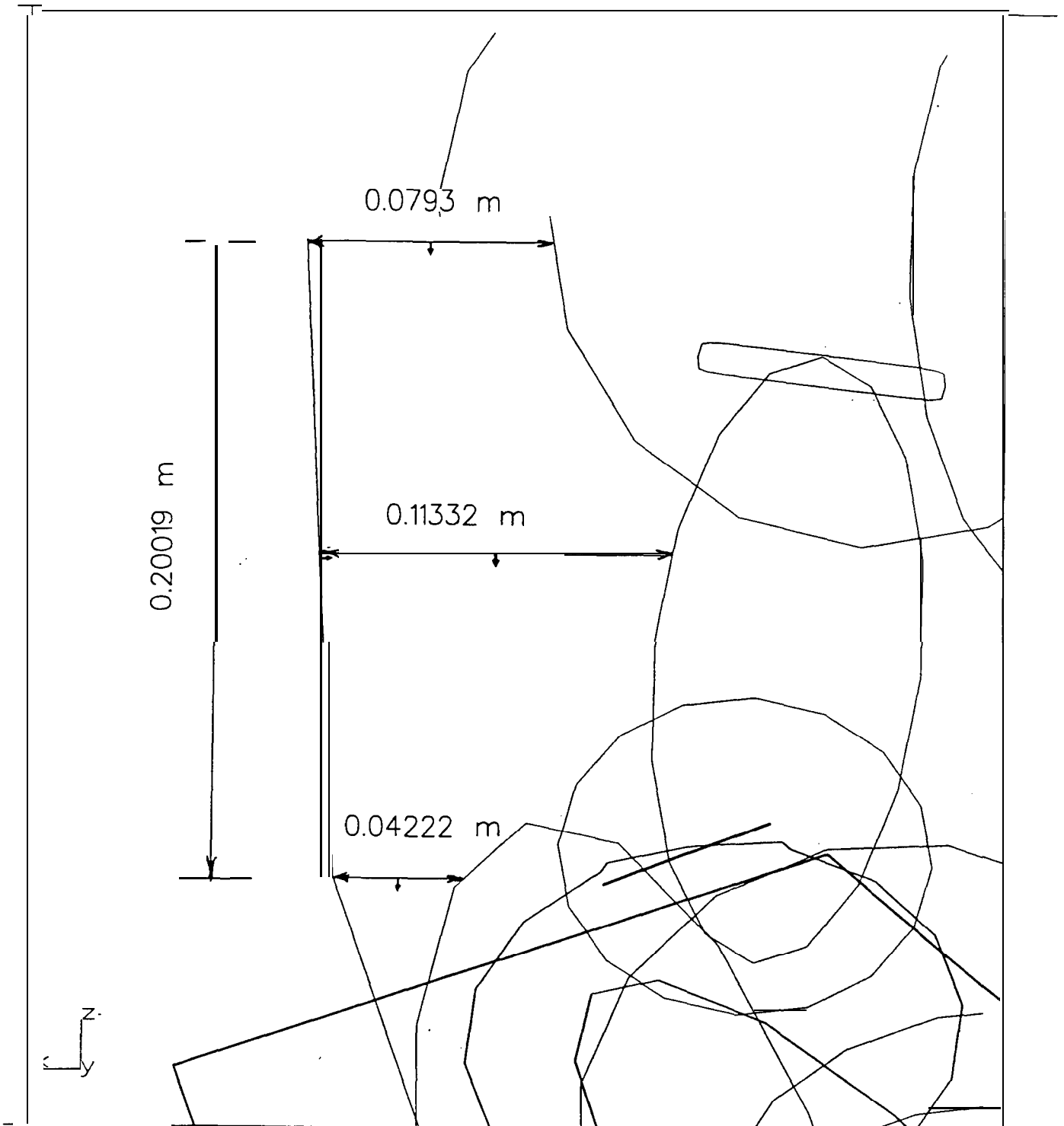


Figure 3.13 MADYMO model setup with headrest.

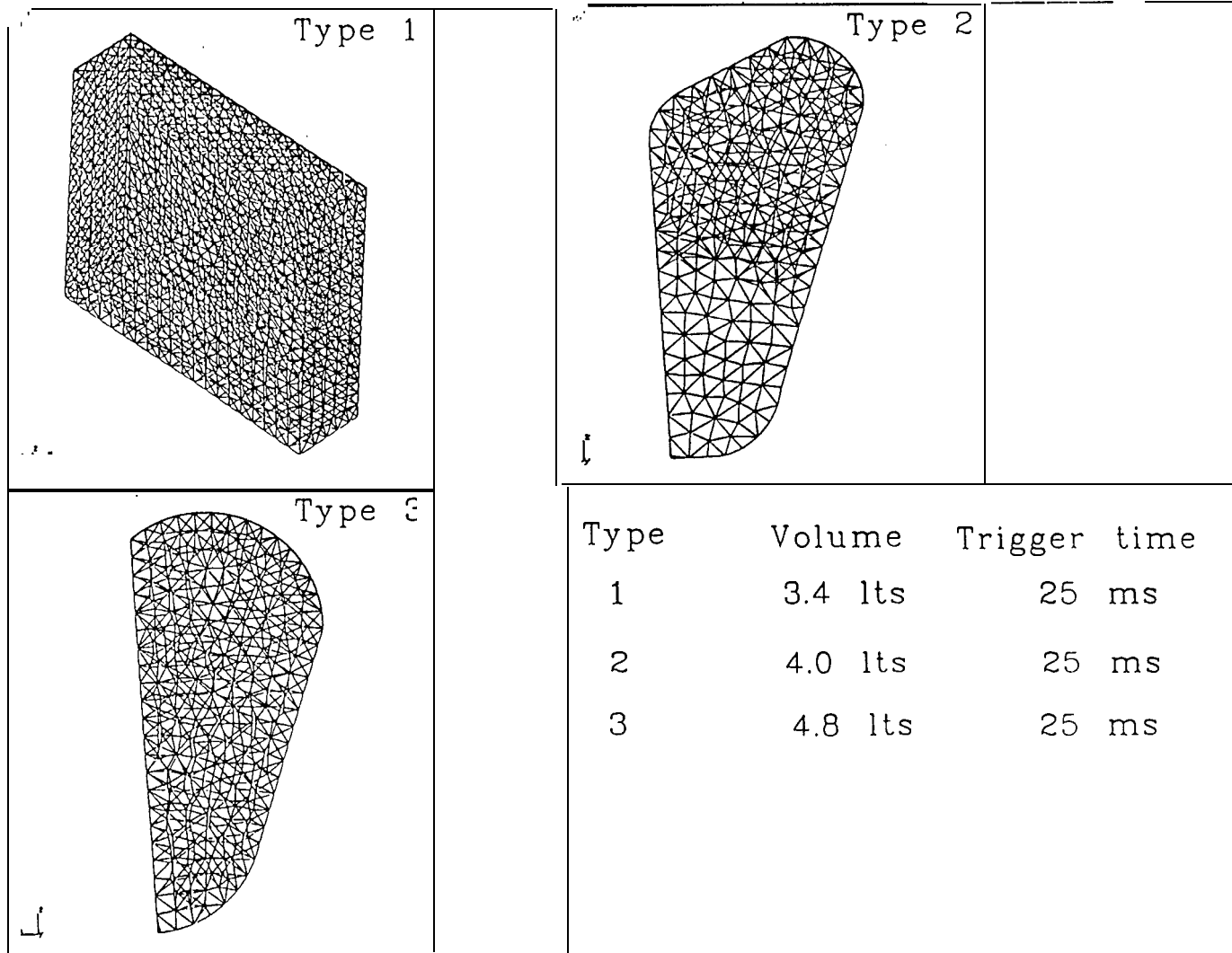


Figure 3.14 Types of inflatable headrest studied.

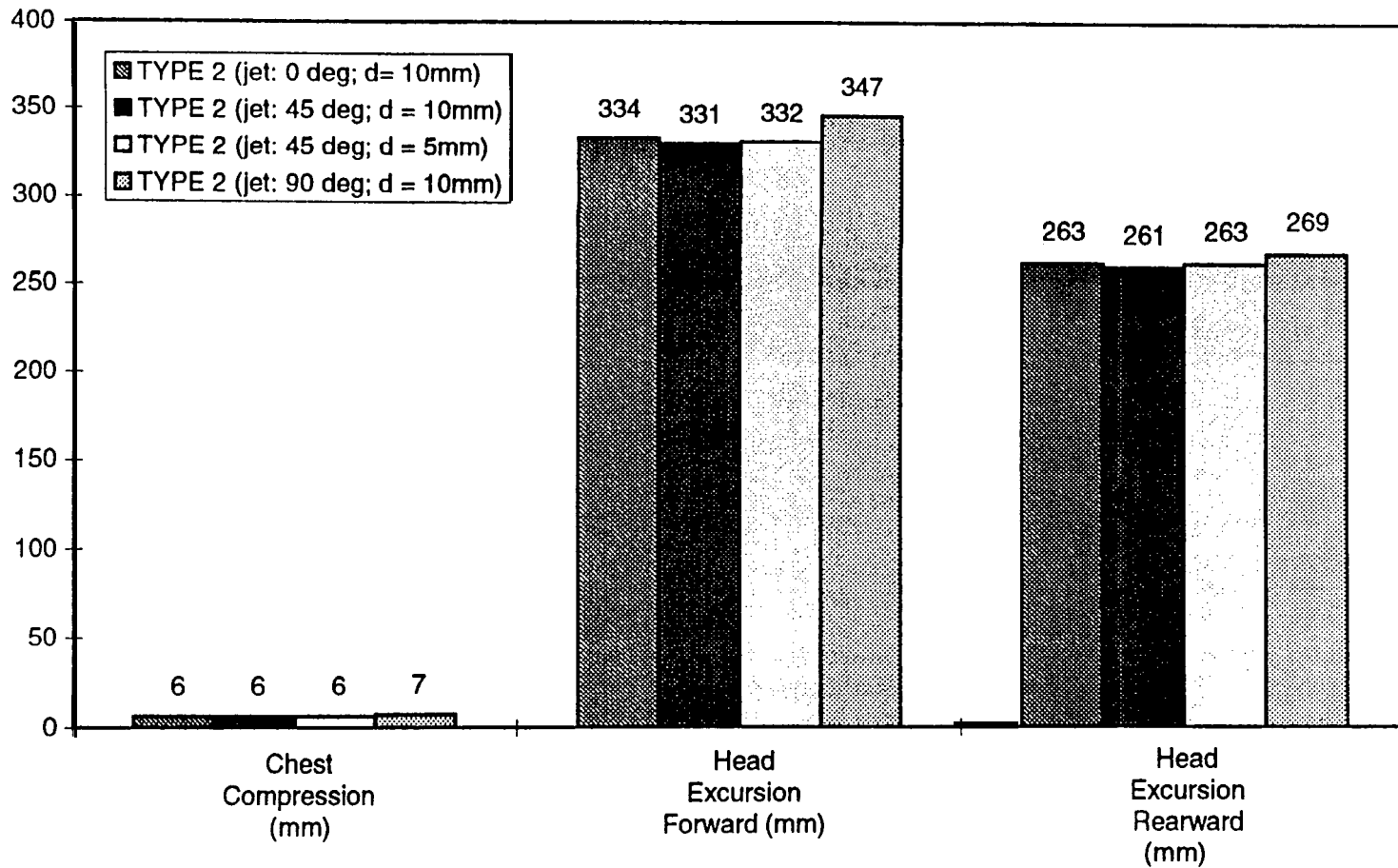


Figure 3.15 Occupant response using Type 2 inflatable headrest (30 mph rear impact).

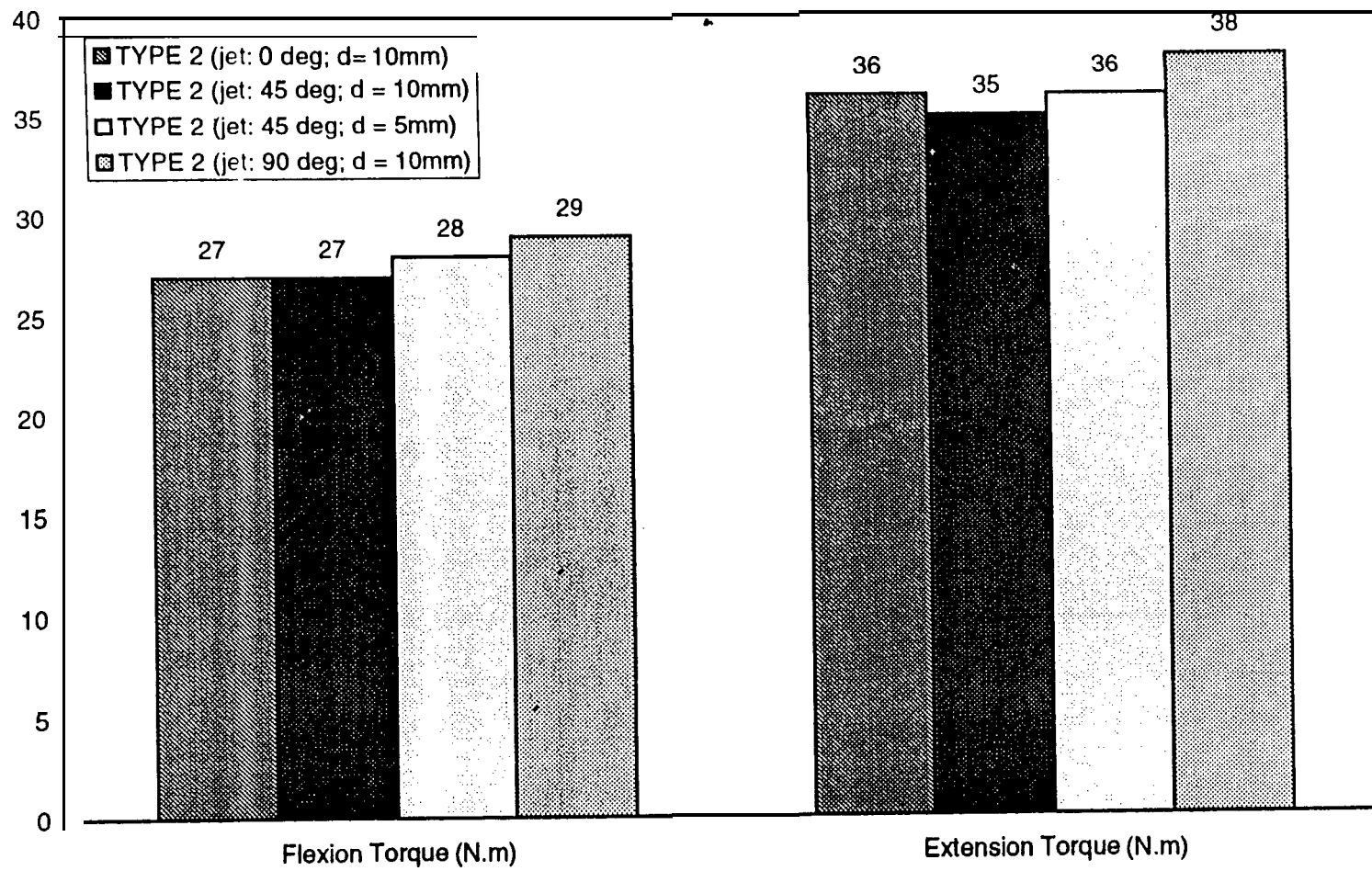


Figure 3.16 Occupant neck response using Type 2 inflatable headrest (30 mph rear impact).

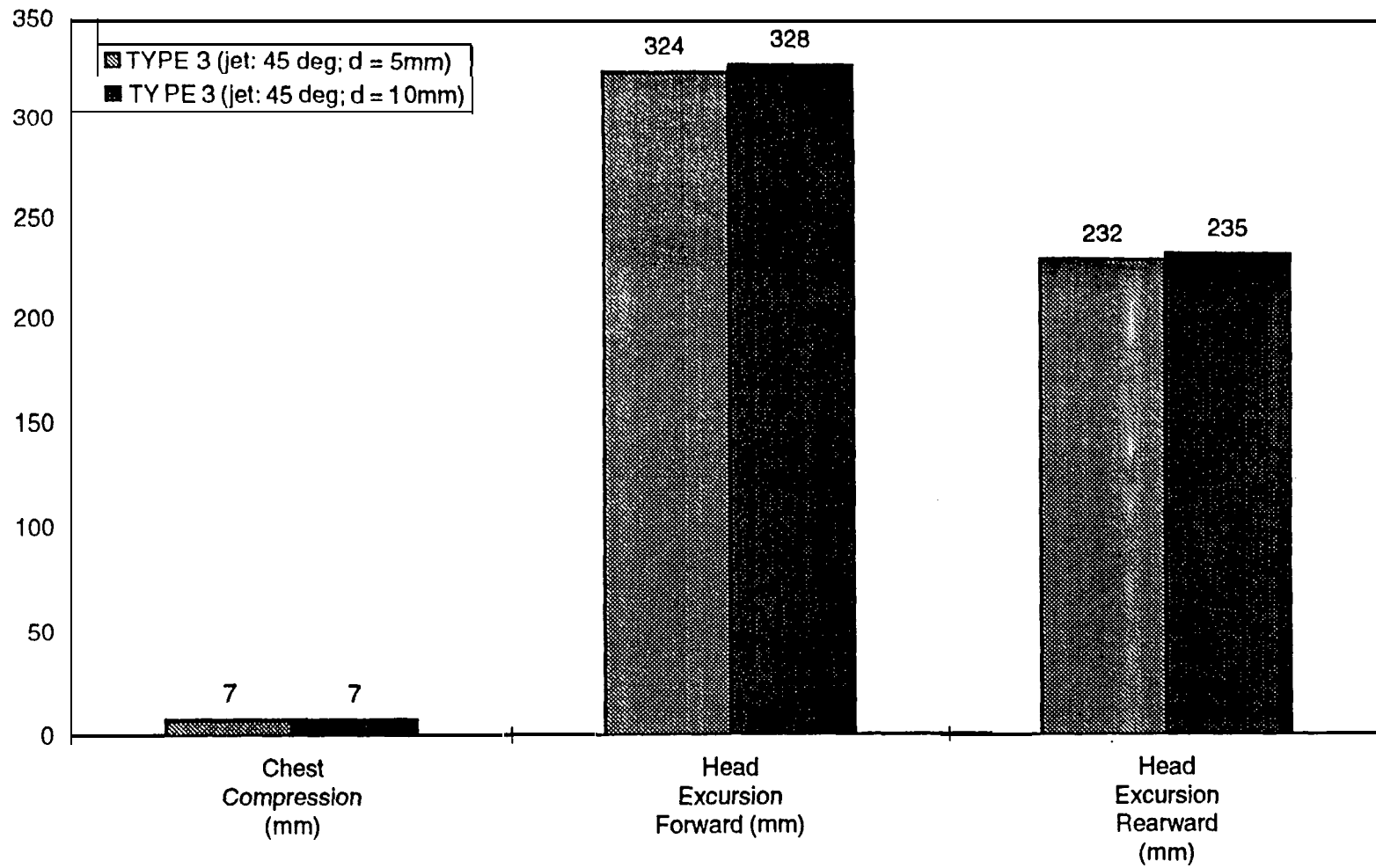


Figure 3.17 Occupant response using Type 3 inflatable headrest (30 mph rear impact).

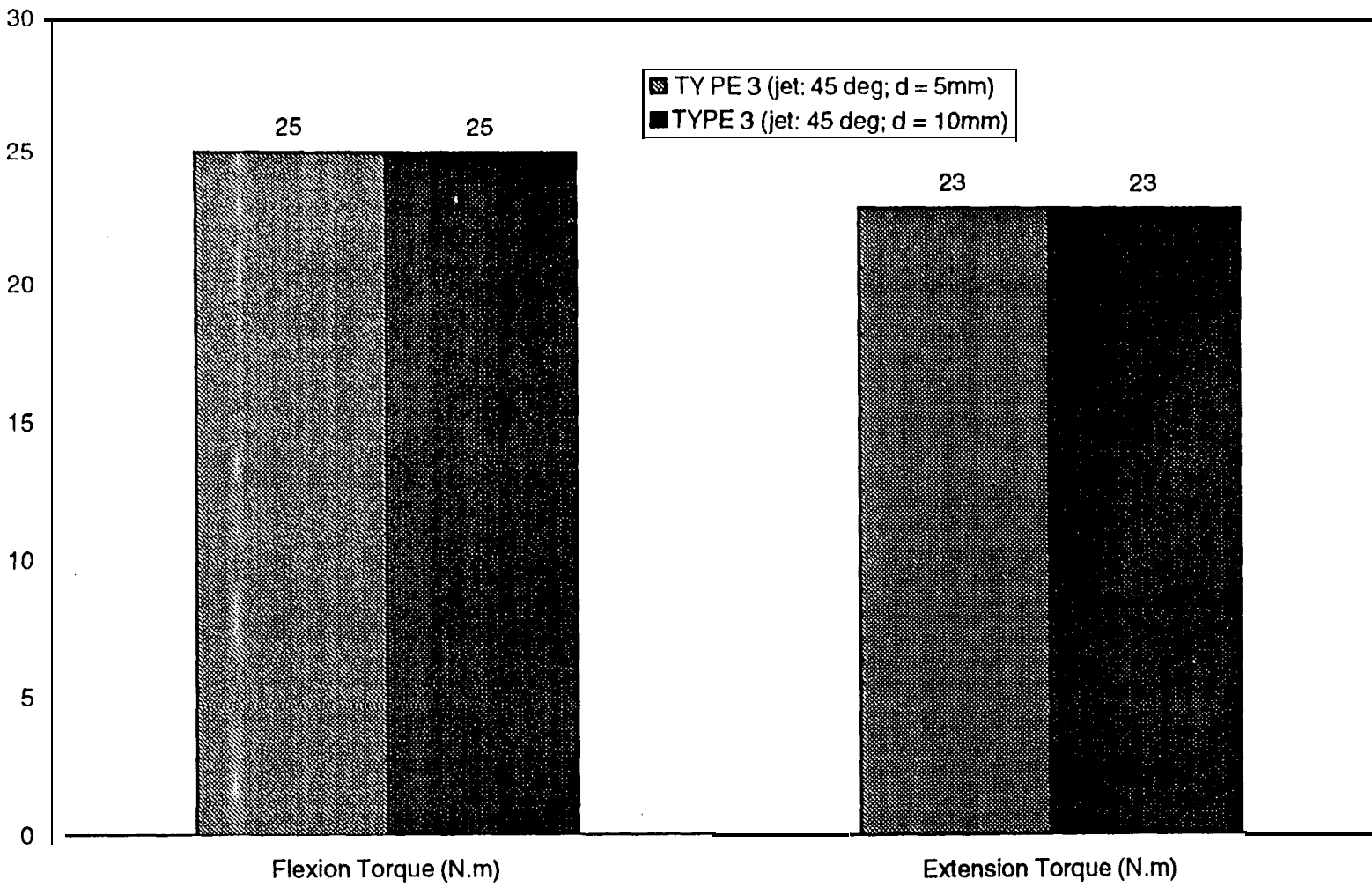


Figure 3.18 Occupant neck response using Type 3 inflatable headrest (30 mph rear impact).

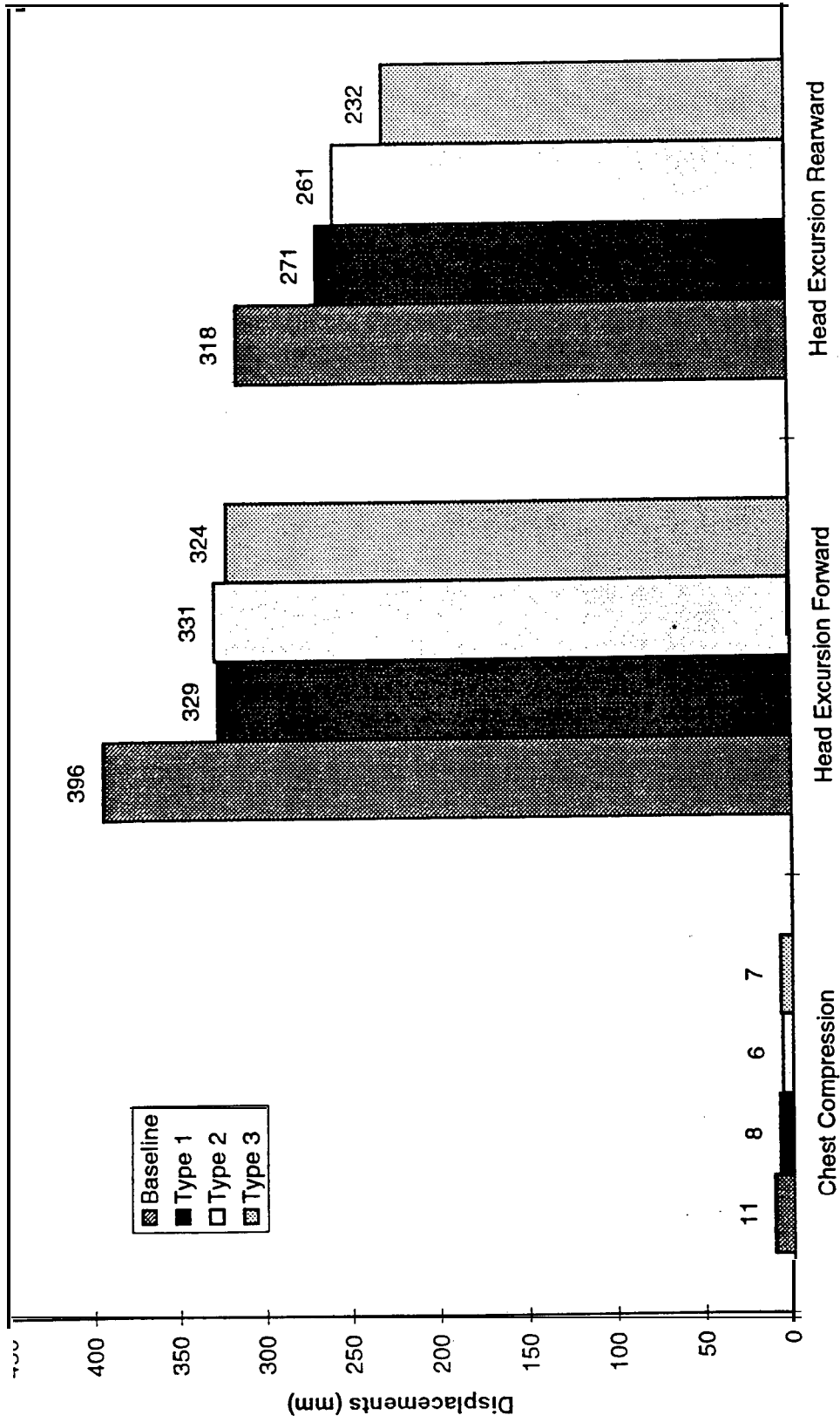


Figure 3.19 Comparison of occupant response using different types of inflatable headrest (30 mph rear impact).

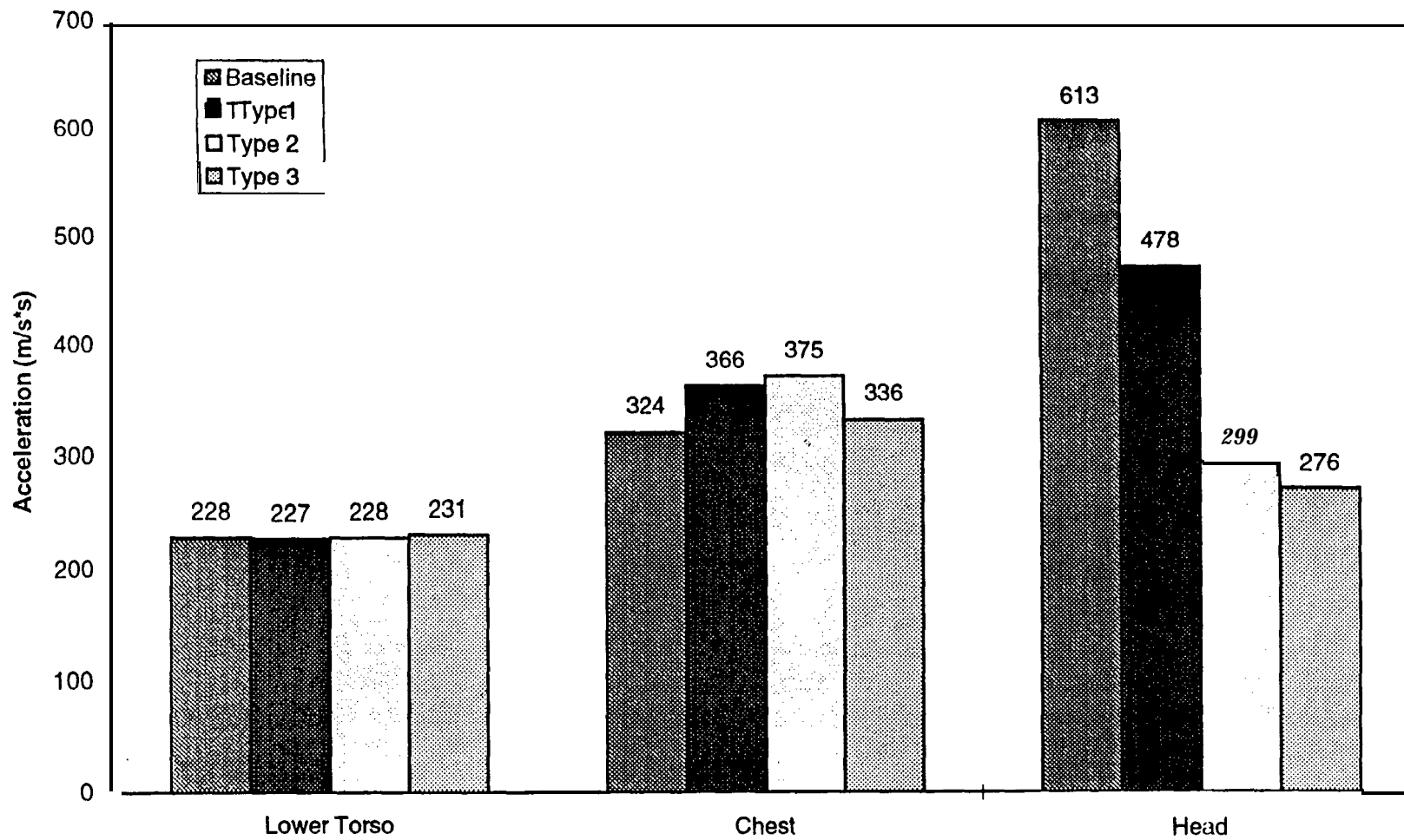


Figure 3.20 Comparison of accelerations using different types of inflatable headrests (30 mph rear impact).

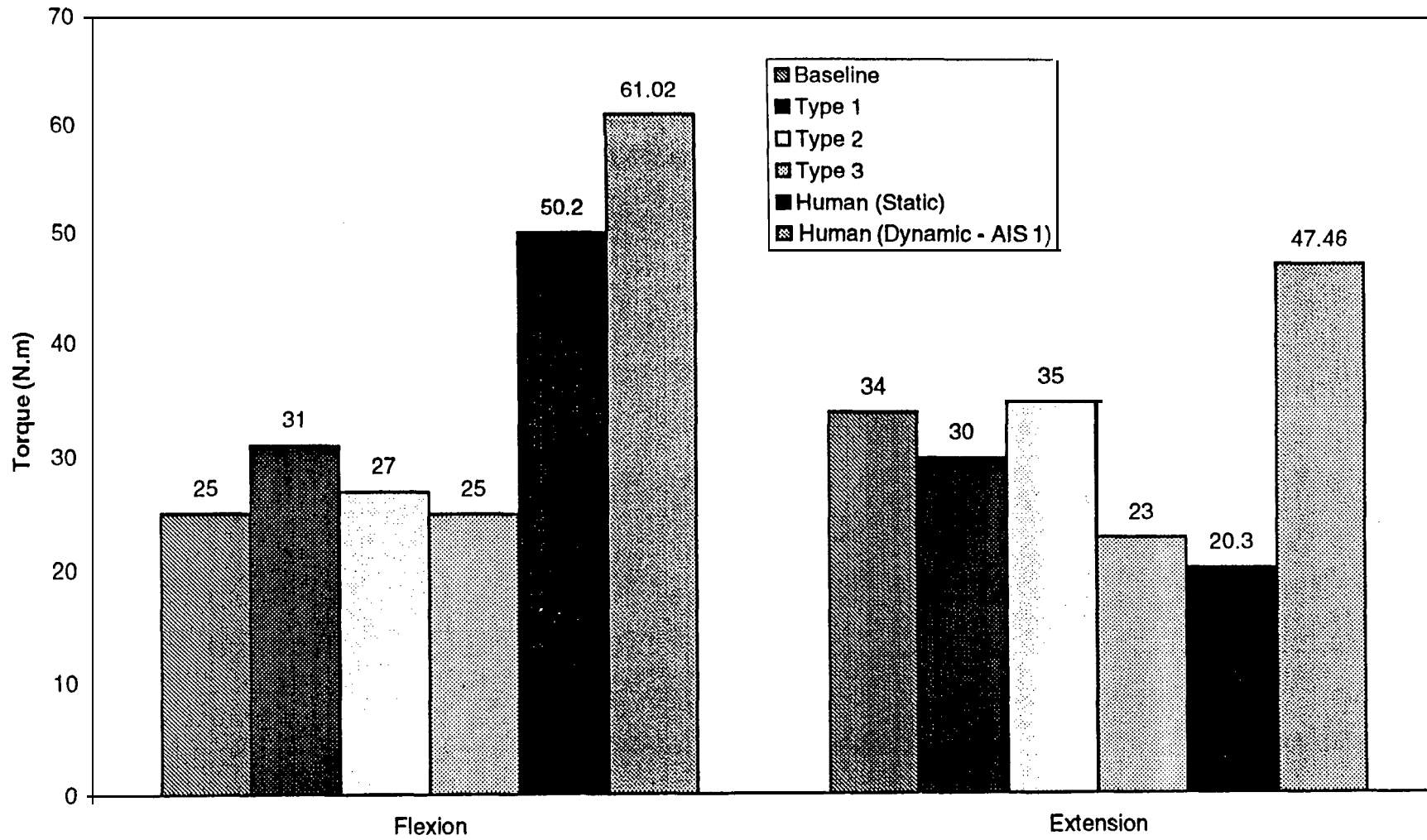


Figure 3.21 Occupant neck response using different types of inflatable headrests (30 mph rear impact).

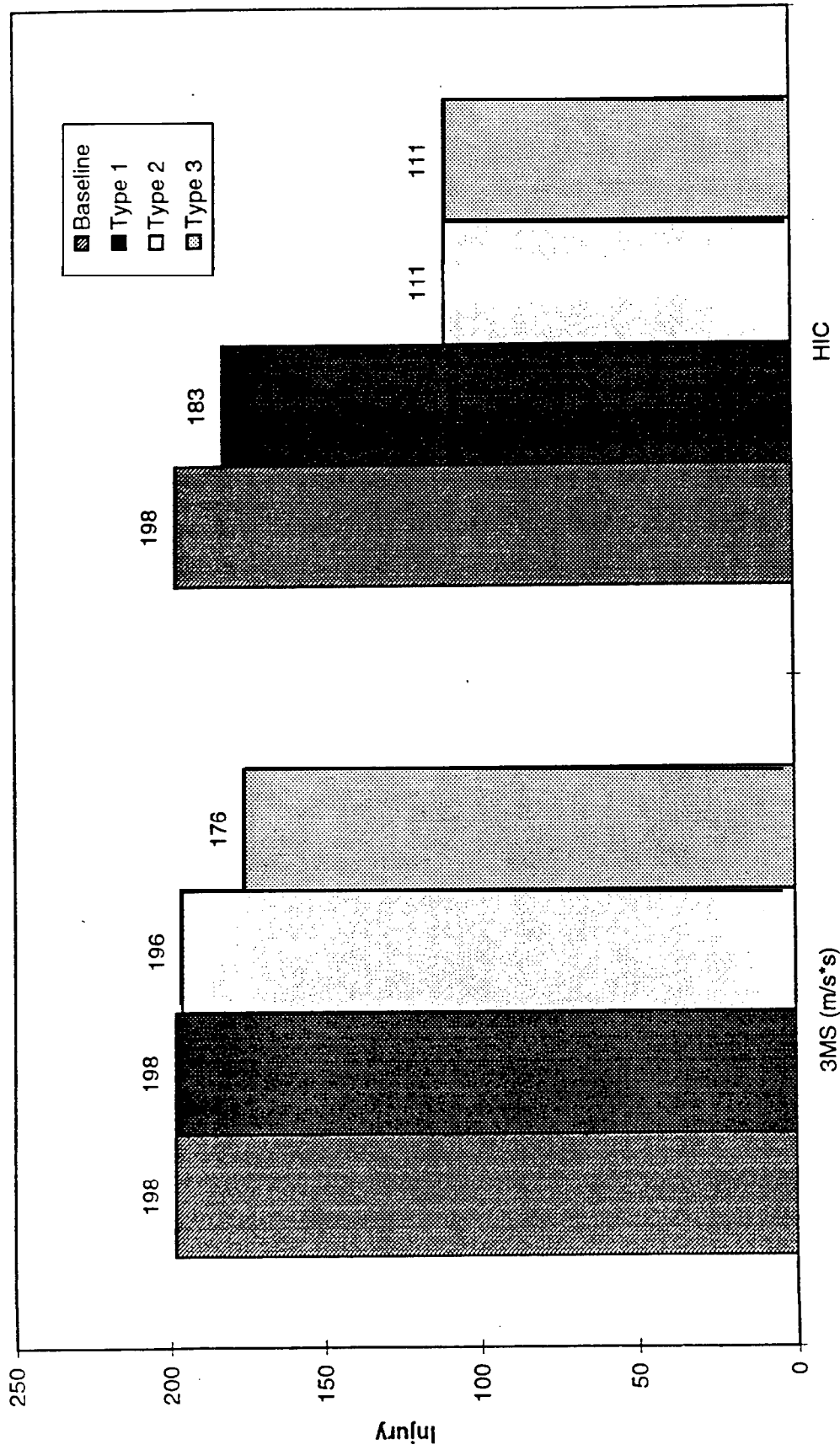


Figure 3.22 Comparison of injury numbers using different inflatable headrests (30 mph rear impact).

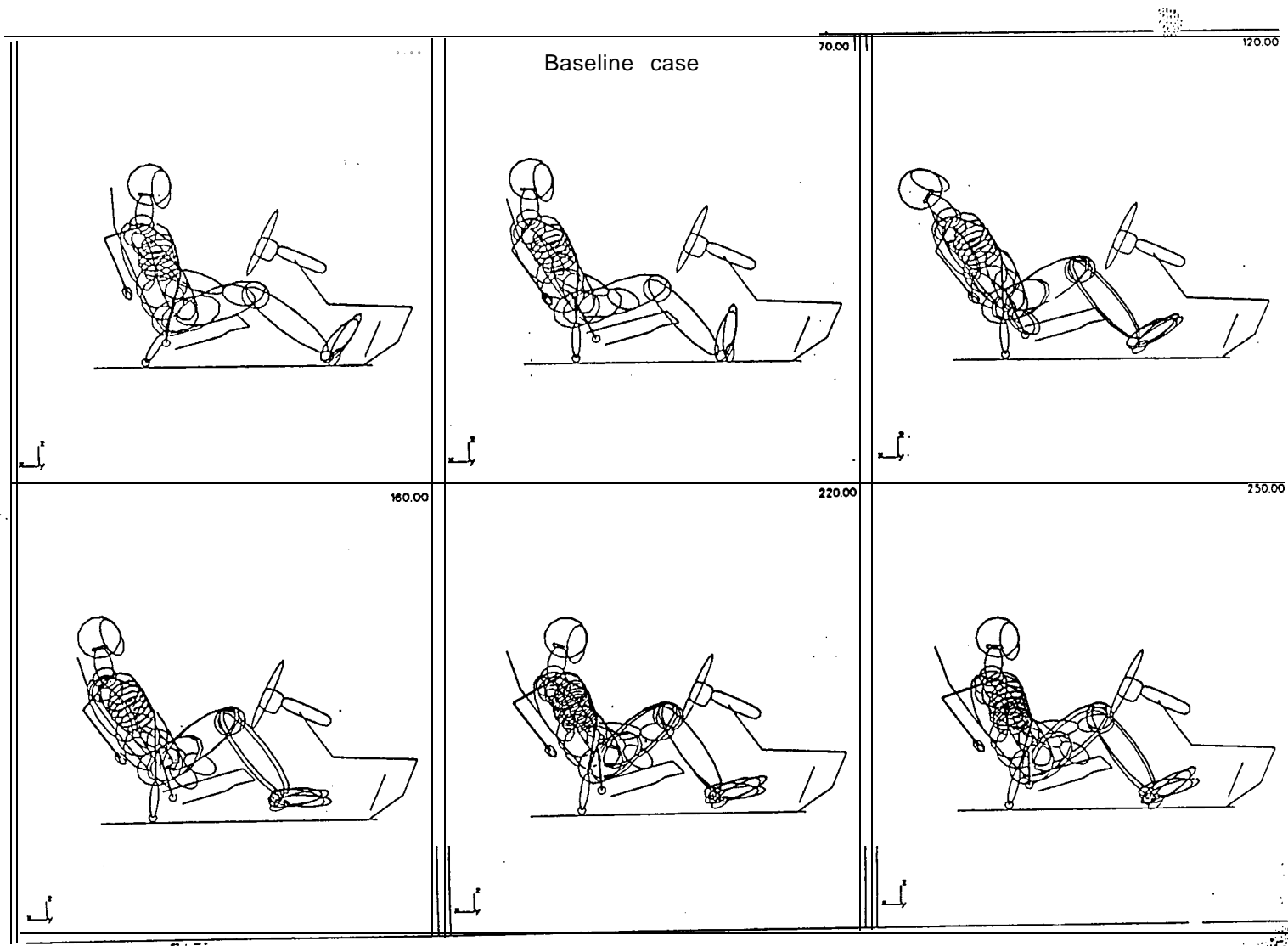


Figure 3.23 Baseline case (without inflatable headrest) simulation (30 mph rear impact).

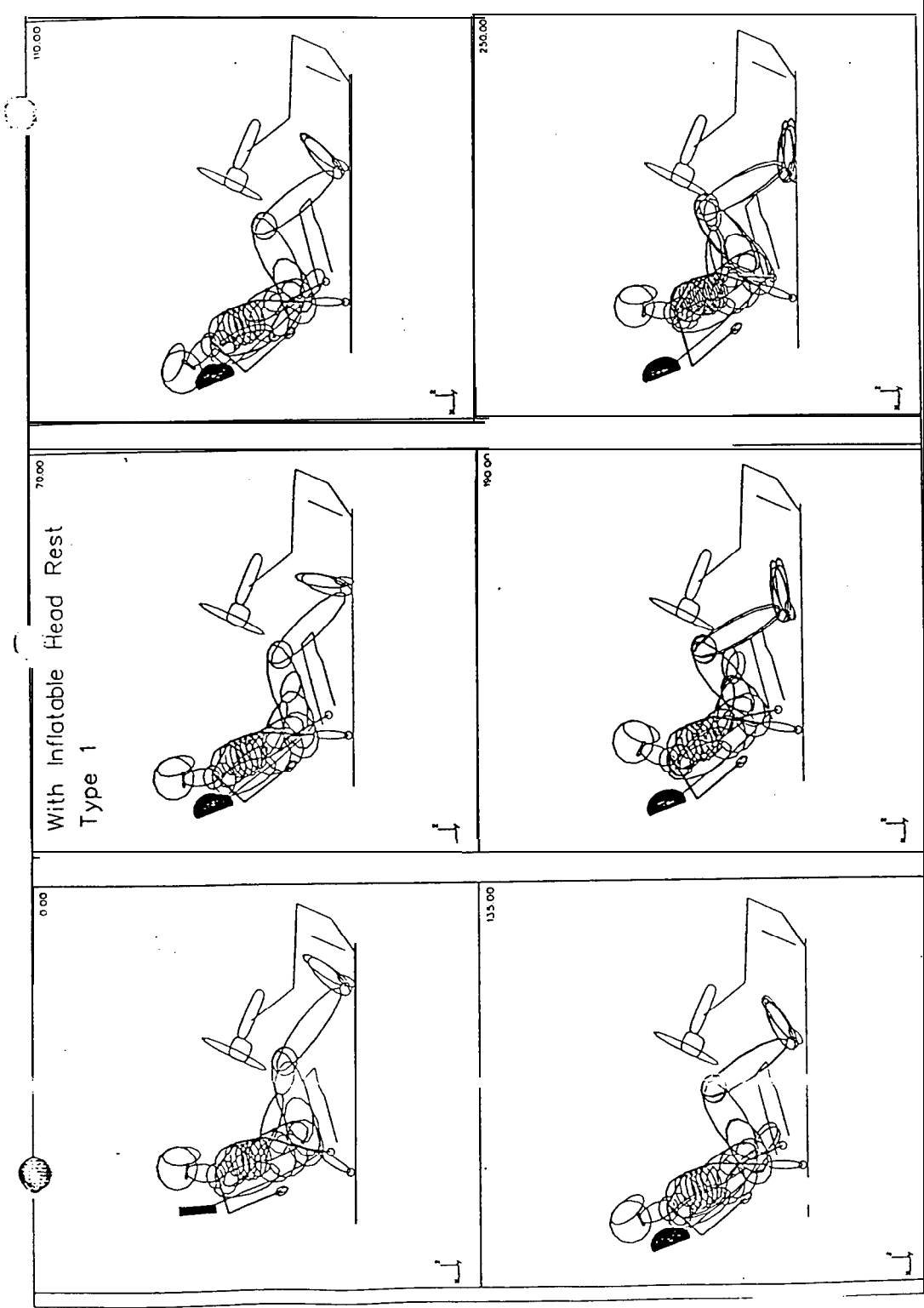


Figure 3.24 Simulation with inflatable headrest Type 1 (30 mph rear impact).

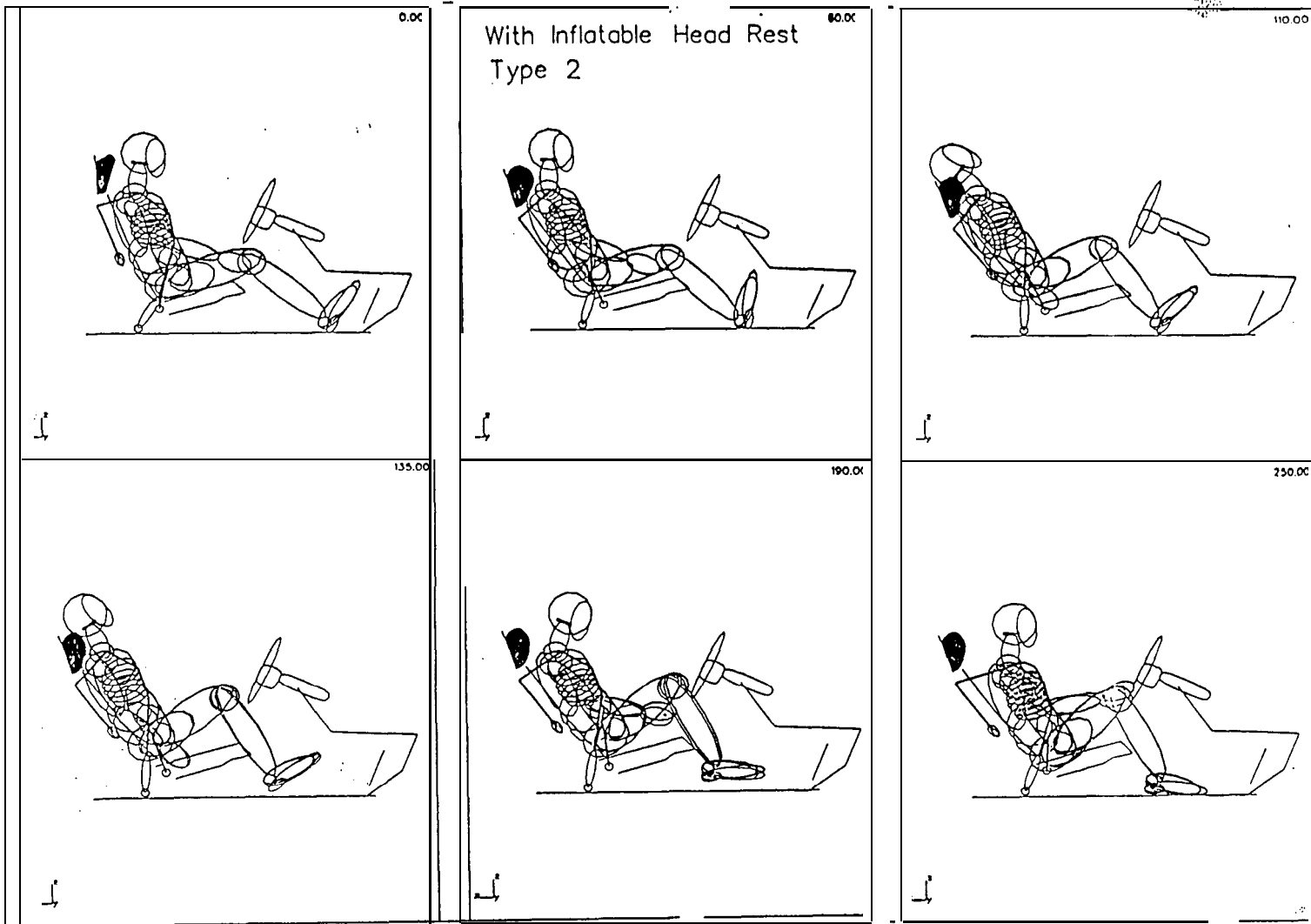


Figure 3.25 Simulation with inflatable headrest Type 2 (30 mph rear impact).

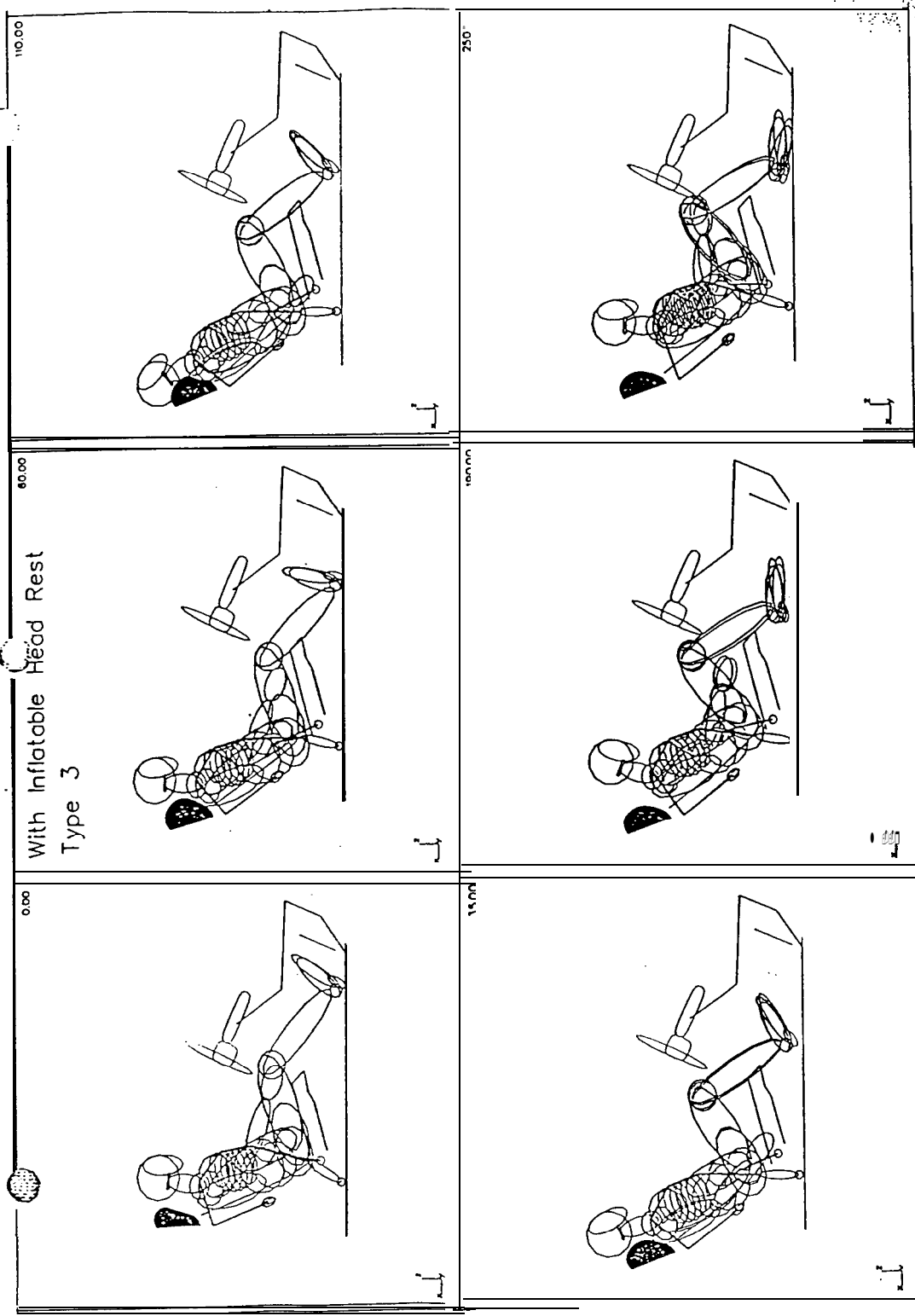


Figure 3.26 Simulation with inflatable headrest Type 3 (30 mph rear impact).

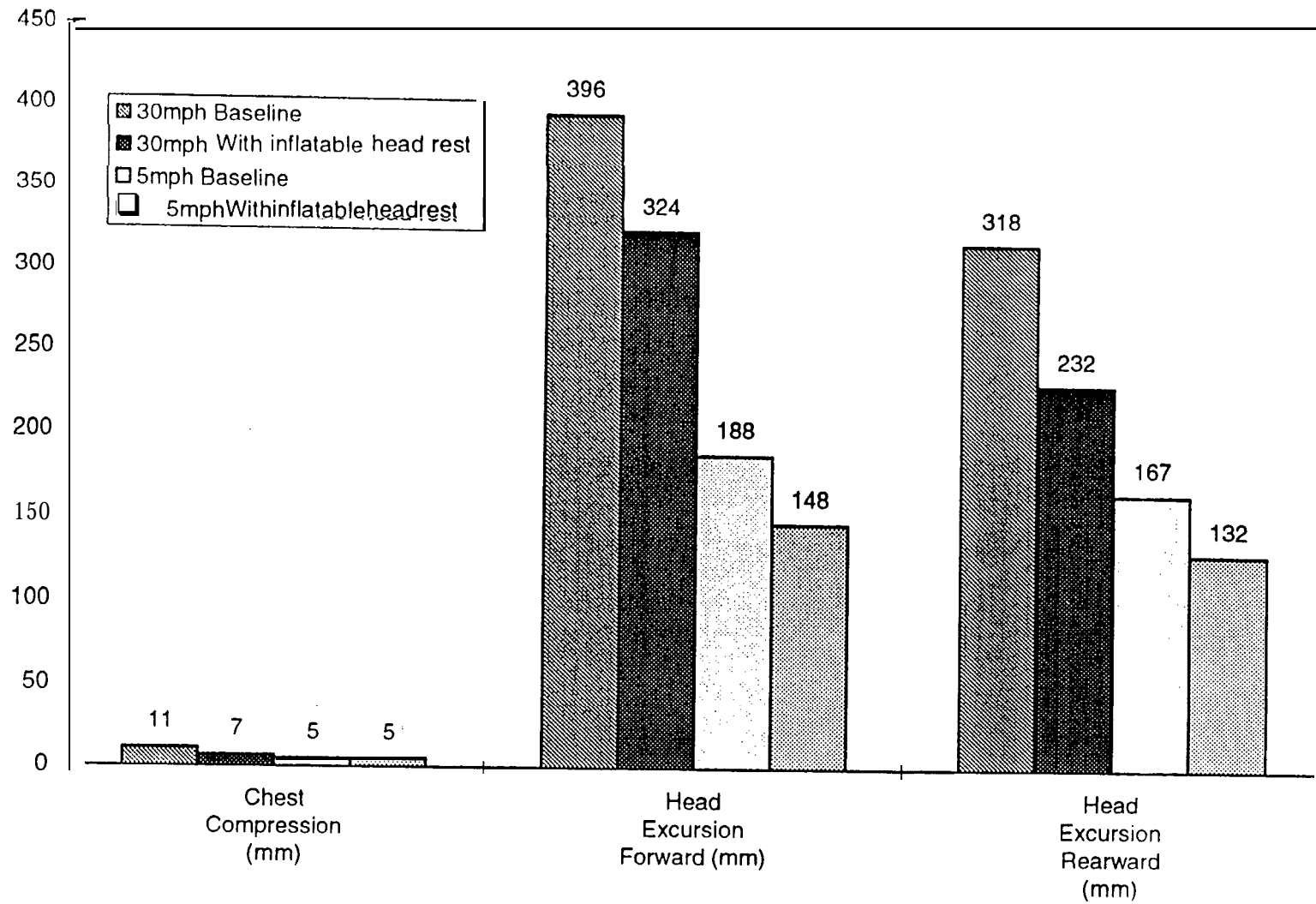


Figure 3.27 Comparison of occupant response at 30 and 5 mph rear impacts.

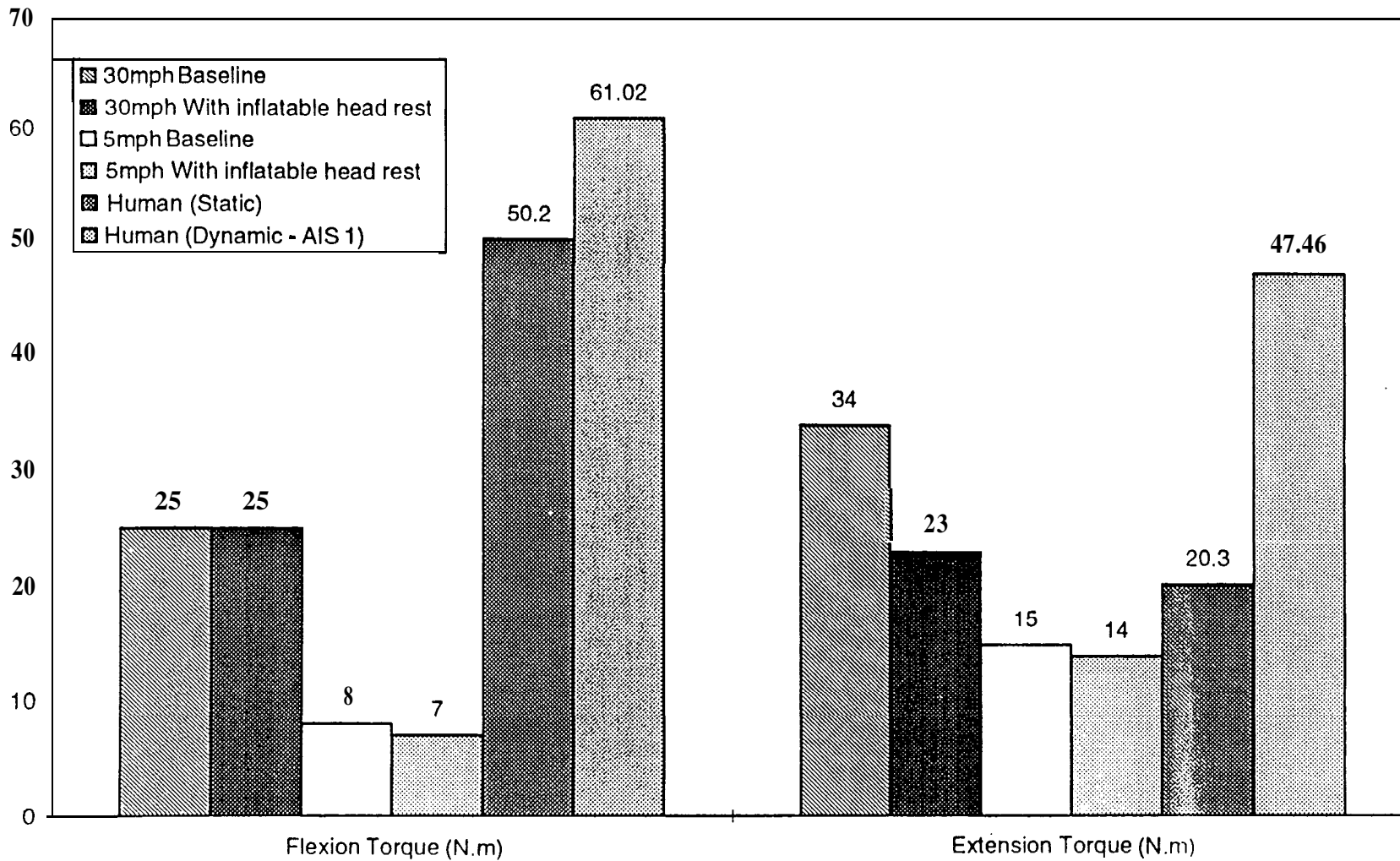


Figure 3.28 Comparison of occupant neck response at 30 and 5 mph rear impacts.

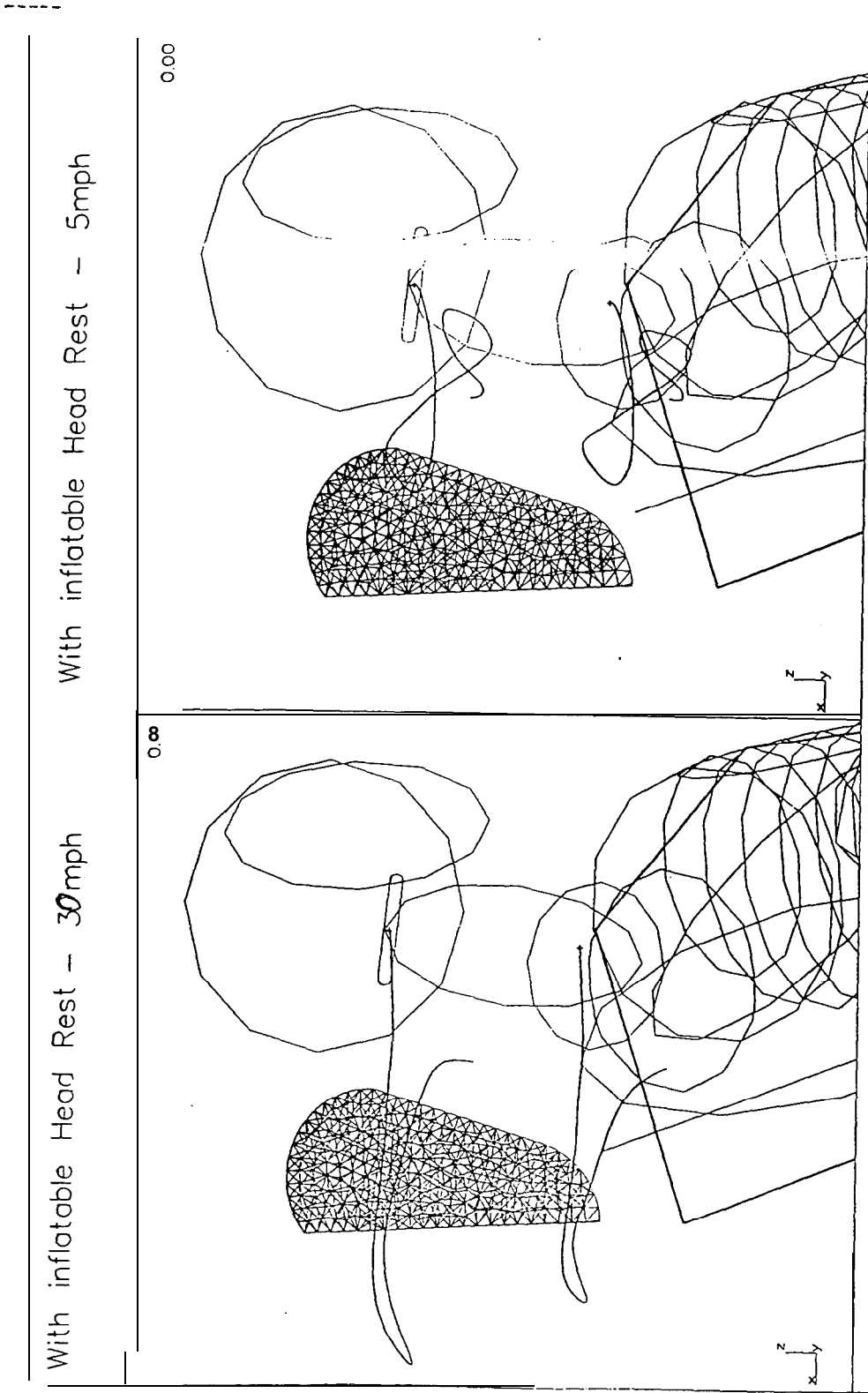


Figure 3.29 Trajectories of the upper and lower neck with inflatable headrest for 30 and 5 mph rear impacts.

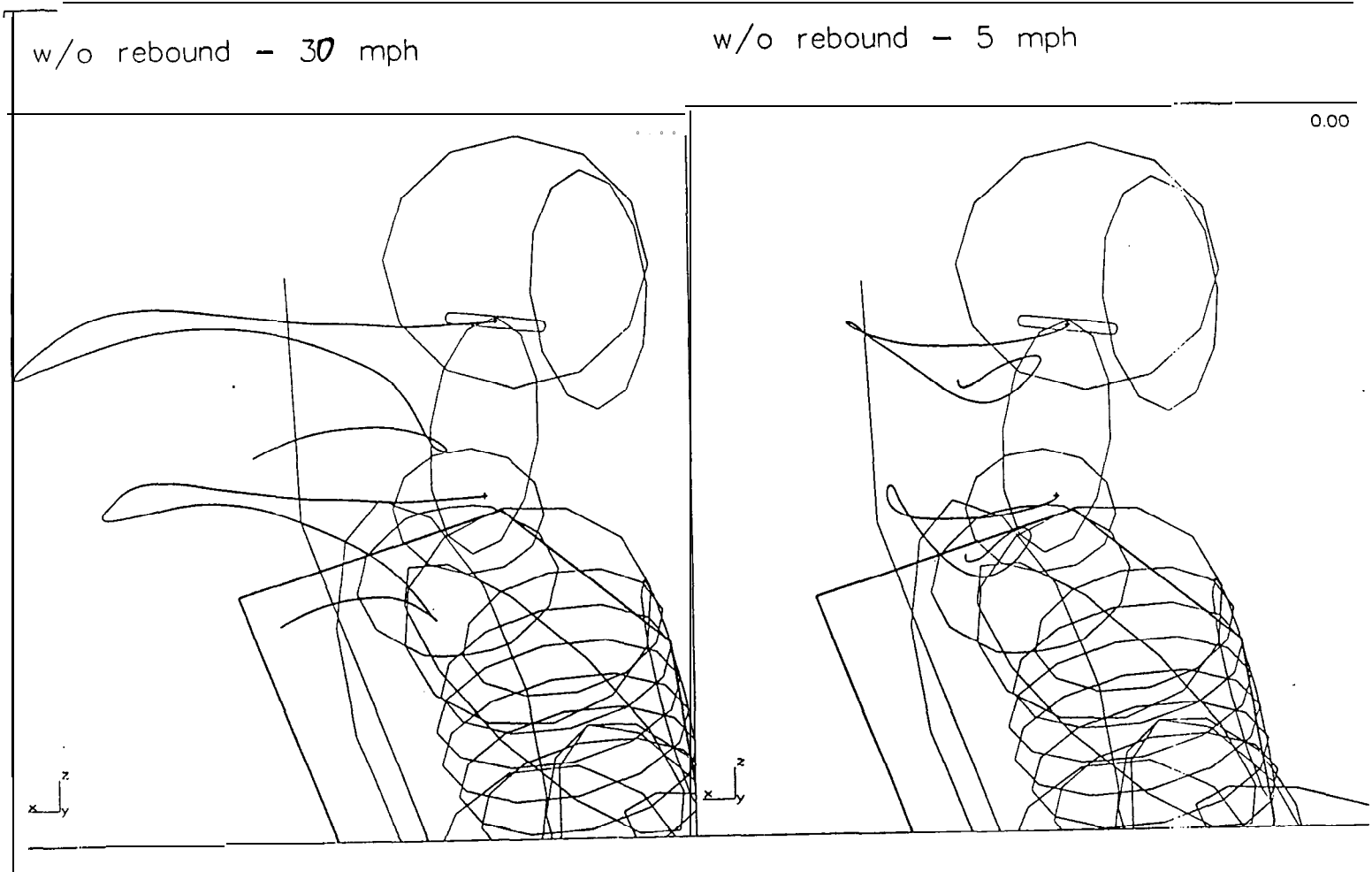


Figure 3.30 Trajectories of the upper and lower neck with standard headrest with a non rebound seat for a 30 and 5 mph rear impact.

of the upper and lower parts of the neck with and without the inflatable headrest for both 30 and 5 mph cases.

Observations:

- High and low speed rear impact (30 mph and 5 mph)
- Helps reduce the head acceleration and head excursion.
- Reduces the extension torque - one of the factors influencing the *whiplash* syndrome.
- Triggering time is very important - optimal trigger observed : 25 msec.
- Shape of the bag, the gas jet direction and inflator size helps reduce or increase the aggressivity of the bag.
- Energy absorbing seat back also reduces the whiplash effect considerably.

4. ROLLOVER

4.1 MADYMO Simulations

Simulations were performed using MADYMO to depict rollover test conditions as per the FMVSS 208 criteria to study the retention of an occupant in the vehicle compartment. A MADYMO model of a Ford Taurus was used (Figure 4.1.). The sled on which the vehicle rests is braked to a stop from 30 mph. The vehicle roll and translation accelerations at the center of gravity were extracted. These were used as inputs in a separate occupant simulation model of the driver (Figure 4.2.). Simulations were conducted using 50th and 95th percentile Hybrid III dummies which were belted down with both the shoulder and lap belts. Two sets of simulations were run with and without a pretensioner. The accelerations from the vehicle rollover model was applied to the occupant model. Rolling was simulated about a roll point coincident with the test vehicle center of gravity. Simulations were run for 5 seconds.

The first set of simulations were performed without the use of a belt pretensioner. It was observed that for both dummies the shoulder belt slipped off the occupant shoulder and only the lap belt retained the occupant. In this case the possibility of an ejection was quite high.

The second set of simulations were conducted under very similar conditions as the first except that a belt pretensioner with a pulling distance of 80 mm and pulling time of 9.5 msec, characteristics which are shown in Figure 4.3, was used. The occupant remained restrained through the simulation and there was no head contact with the roof of the vehicle. Results from these simulations are compared in Table 4.1. In this table values for the shoulder belt loads in the case without a pretensioner are not available because the shoulder belt slipped off the dummy shoulder.

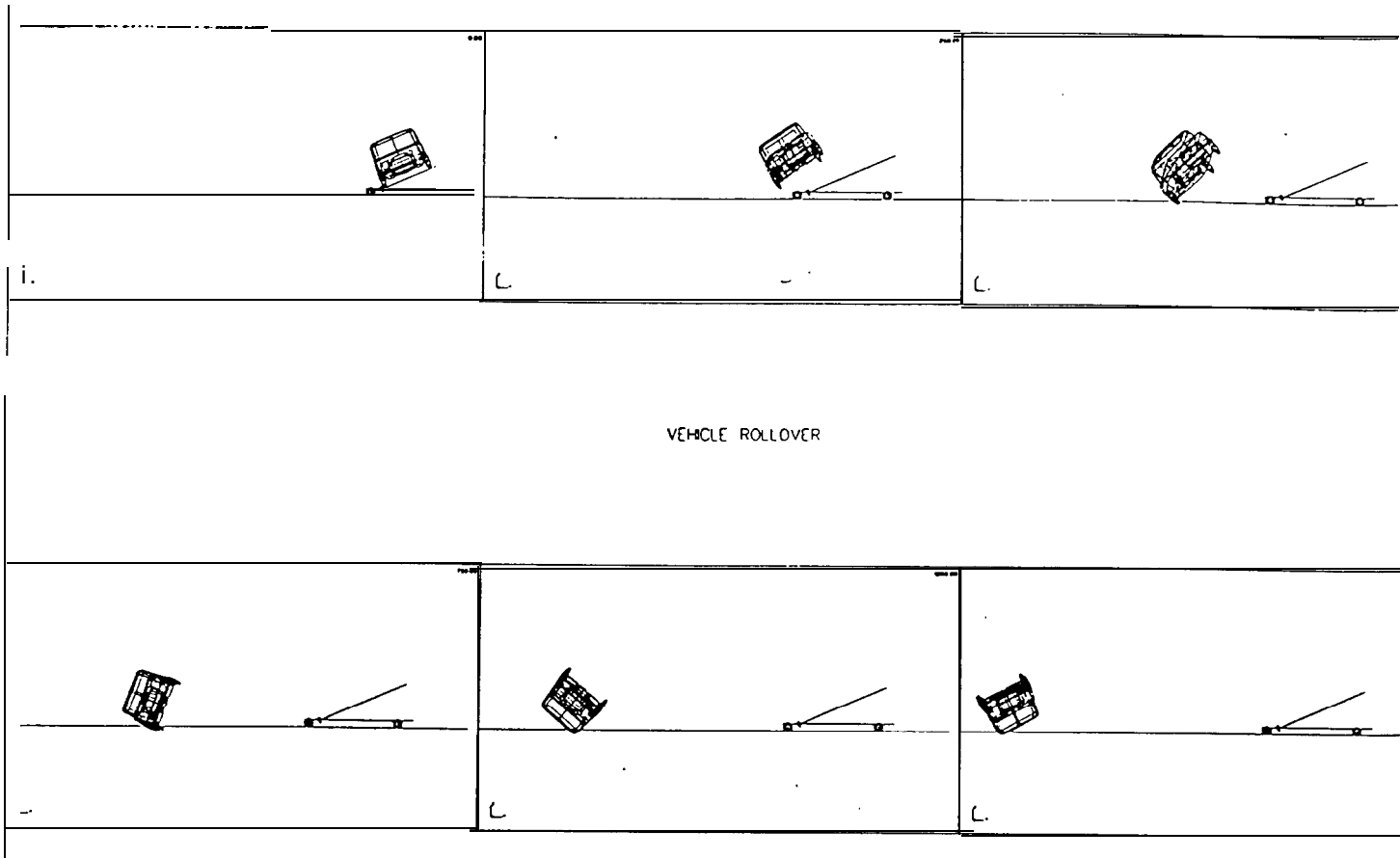


Figure 4.1 Vehicle rollover simulation.

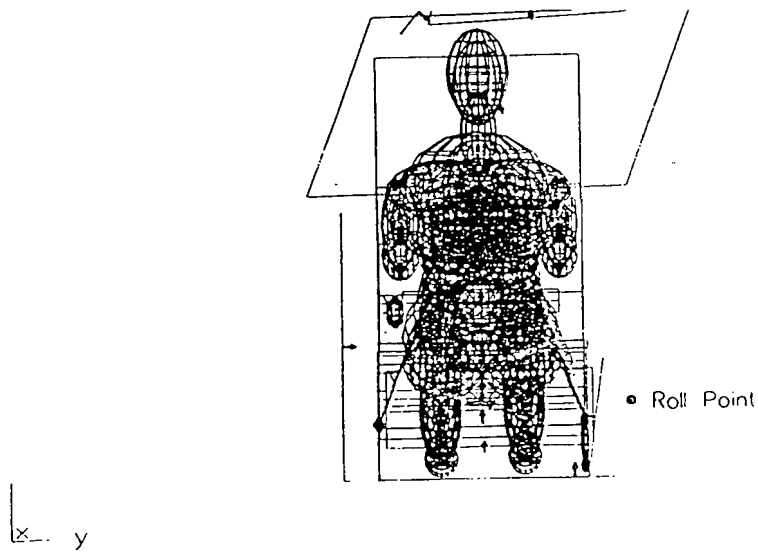


Figure 4.2 Model setup for MADYMO rollover simulations.

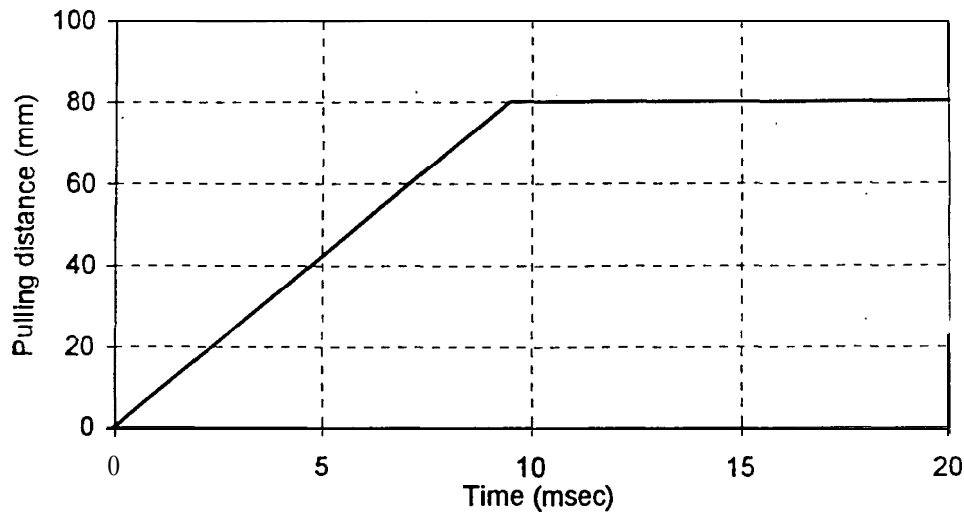


Figure 4.3 Characteristics of the pretensioner.

Table 4.1 Simulation results

		HIC	3MS (m/s ²)	Neck Axial Load, N		Belt Force, N	
				Upper	Lower	Shoulder	Lap
50 th percentile	Without pretensioner	28	34	281	38	-	568
	With pretensioner	27	34.8	118	118	1905.4	516
95 th percentile	Without pretensioner	17	31	318	318	-	792
	With pretensioner	15	43.6	238	332	1383.7	694

Finally a third set of simulations were conducted by inverting the whole vehicle and the occupant as shown in Figure 4.4, to study the head excursion relative to the head rest and roof of the vehicle. For this simulation the occupant was restrained using both belts with and without a pretensioner, and an acceleration field of 1g was applied on the occupant. Results show that both belts held the occupant and there was no contact of the head with the roof of the vehicle.

The layout of the shoulder belt in an integrated restraint seat helps to reduce the vertical drop of the occupant because it loops around the shoulder as seen in Figure 4.4. The shoulder belt would not be able to “catch” the occupant in this manner if it were attached to the B-pillar.

Results of this set of simulations are given in Table 4.2. The head drop of the 95th percentile dummy with a pretensioner was 5.3 cm. This Value can be used as guideline to establish the head rest height. Neck loads were small as their was no head contact with the roof and the applied acceleration field was only 1g.

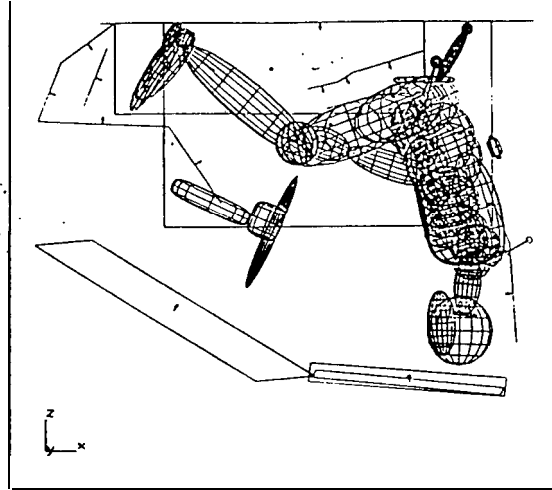


Figure 4.4 Model setup of the inverted simulation.

Table 4.2 Simulation results of the inverted tests.

		HIC	3MS (m/s ²)	Belt Force, N		Head Excursion m
				Shoulder	Lap	
50 th percentile	no pretensioner	1.0	9.8	712	133	0.045
	with pretensioner	0.2	3.4	615	52	0.011
95 th percentile	no pretensioner	0.4	22.1	607	177	0.062
	with pretensioner	0.2	28.5	600	118	0.053

Simulations were also performed with the passenger side shoulder belt anchor position being changed from the right to the left. This change in position was found to be very beneficial for a rollover situation because it reduces the risk of interior body contact. This change in position may hinder visibility and may be of concern from a styling point of view

4.2 Extended Headrest

To study the behavior of AISS seat in a rollover crash, a full car 20 degree drop test was performed (Bahling et al., 1990). FORD Taurus car model was used for this purpose (Figure 4.5). The objective was to see if an extended head rest could be used to reduce head excursion of the dummy and the potential roof contact due to roof crush. The seat was modeled using beams and springs. Two simulations were made. In the first baseline simulation, the height of the headrest was equivalent to the height of headrest in the current ISS seat. In the second enhanced simulation, the headrest has an additional height. It extends beyond the top of the head of the 95th percentile dummy. This extension equals

the head excursion of a belted dummy which is 62 mm under -1 G. This result was obtained through a simulation in MADYMO.

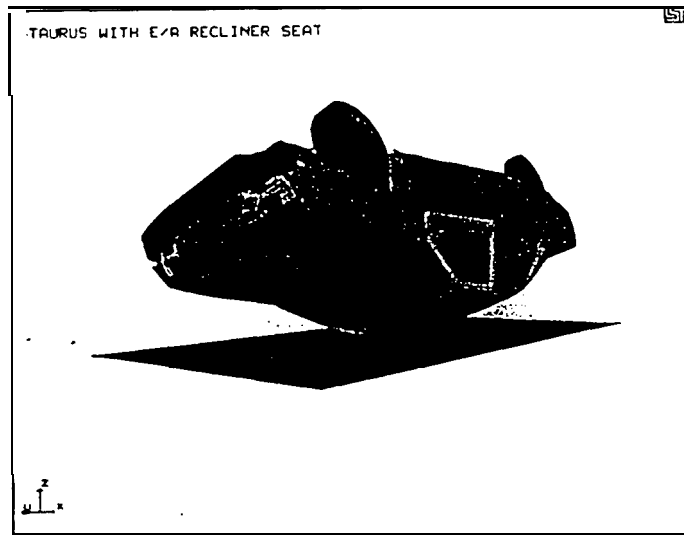


Figure 4.5 Full car rollover drop test.

The deformed shapes for the baseline and enhanced simulations are shown in Figure 4.6. Overall, longer headrest has little effect on the deformed shape of the B-pillar. In addition, the headrest does not decrease the roof crush as inertial forces due to the mass of the car are very high. The headrest and seat structure under either simulation does not provide occupant protection functionality similar to an energy absorbing roll bar.

In the Baseline case, head rest remains clear **from** the roof. When the contact between headrest and roof occurs, the structure of the car simply pushes the headrest aside and continues to deform. However, in the enhanced case, the headrest is long enough that during roof crush, it strikes the roof. This causes the seat-back to deform laterally and rear-wards by few inches.

The vertical travel of the seat bottom hinge is plotted for these two simulations in Figure 4.7. Very little change in the vertical displacement can be seen between these two cases. This confirms that the seat bottom or the floor pan vertical travel is not reduced by the longer headrest.

If we compare the vertical travel of the shoulder point for these two simulations (Figure 4.8), a significant reduction is noticed. For the enhanced case, the displacement reduces from 82 mm to 40 mm. Hence, due to lateral shift in the seat-back, vertical drop in the shoulder point is reduced by almost 50%. When seat-back deflects laterally, the belted dummy is assumed to move with the seat back. With this assumption, a longer headrest can significantly help in reducing injuries due to head excursion in rollover crashes.

Features relevant to AISS for rollover protection:

1. **Pretensioner**

- The results of these simulations show that the primary function of the **AISS** under rollover conditions is to retain the occupant in the seat.
- To this end the firing of the pretensioner is imperative.
- The belt loads under rollover conditions are seen to be only a small **fraction** of the values anticipated under **frontal** crash conditions.

2. **Extended Headrest**

- The “inverted dummy” simulations have provided an estimate of the height of the headrest which would prevent head to roof contact from occurring. For this seat design this distance is 0.98 m from the recliner pivot point to the top of the headrest.
- Extended headrest also prevents head to roof contact by altering the trajectory of the head and carrying it away from the intruding roof

3. **Load Carrying Capacity of Seat under Roof Crush Loads**

- It is also possible to invoke the seat as a load carrying compression/bending member to reduce roof intrusion in a rollover. This is because the **AISS** seat-back has been designed to take rear impact loads.
- It was found that the extended headrest does not help in decreasing roof crush.
- Extended headrest **after** contact with the intruding roof modifies the trajectory of the occupant head and moves the head away **from** the roof, subsequently avoiding any head to roof contact.

4. **Belt Anchor Position**

- Change the position of the passenger side shoulder anchor from right to left
- Helps reduce the interior contact of bodies.

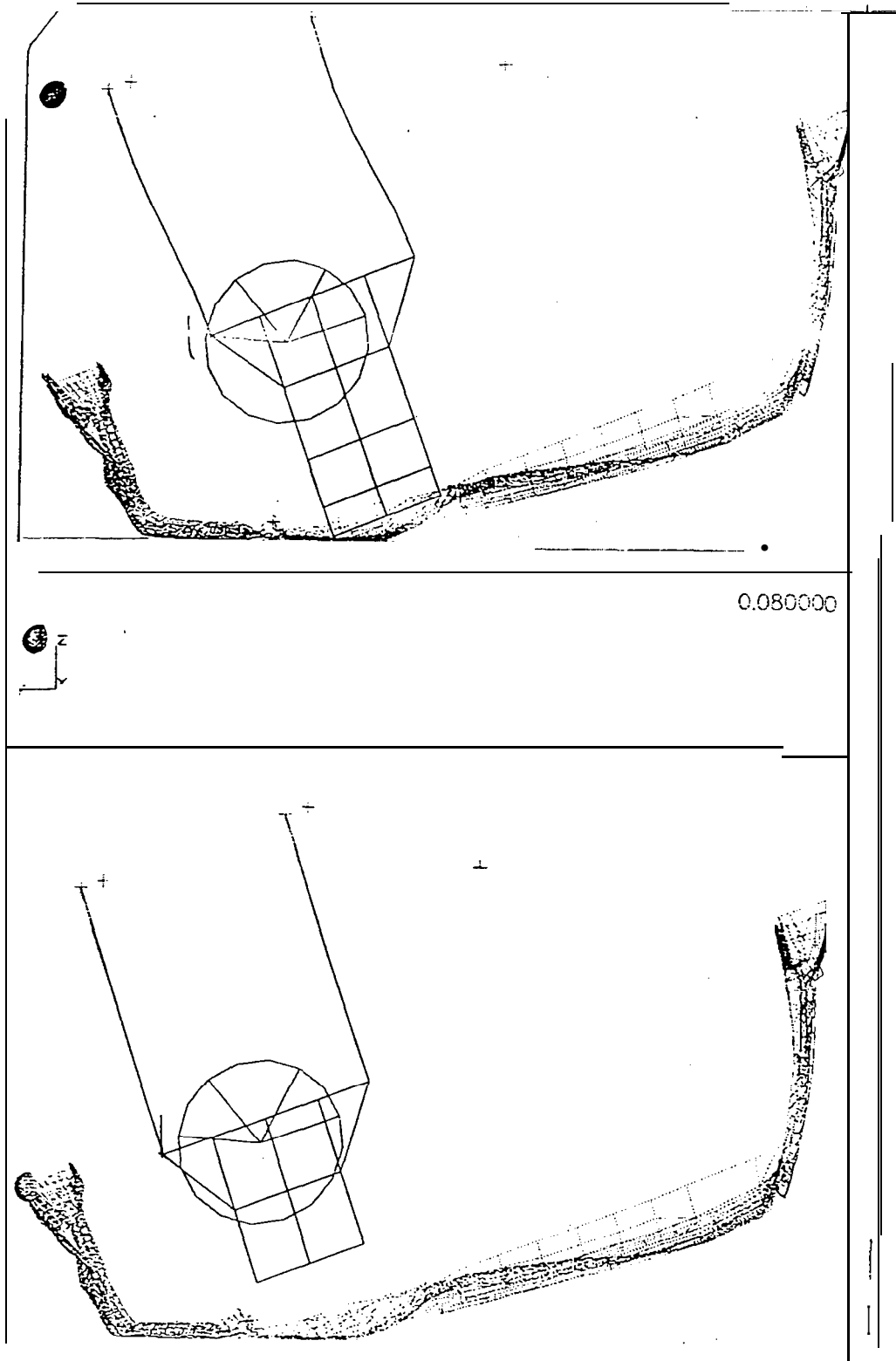


Figure 4.6 Comparison of standard and extended headrest in inverted drop test.

Vertical Travel of Seat Bottom Hinge

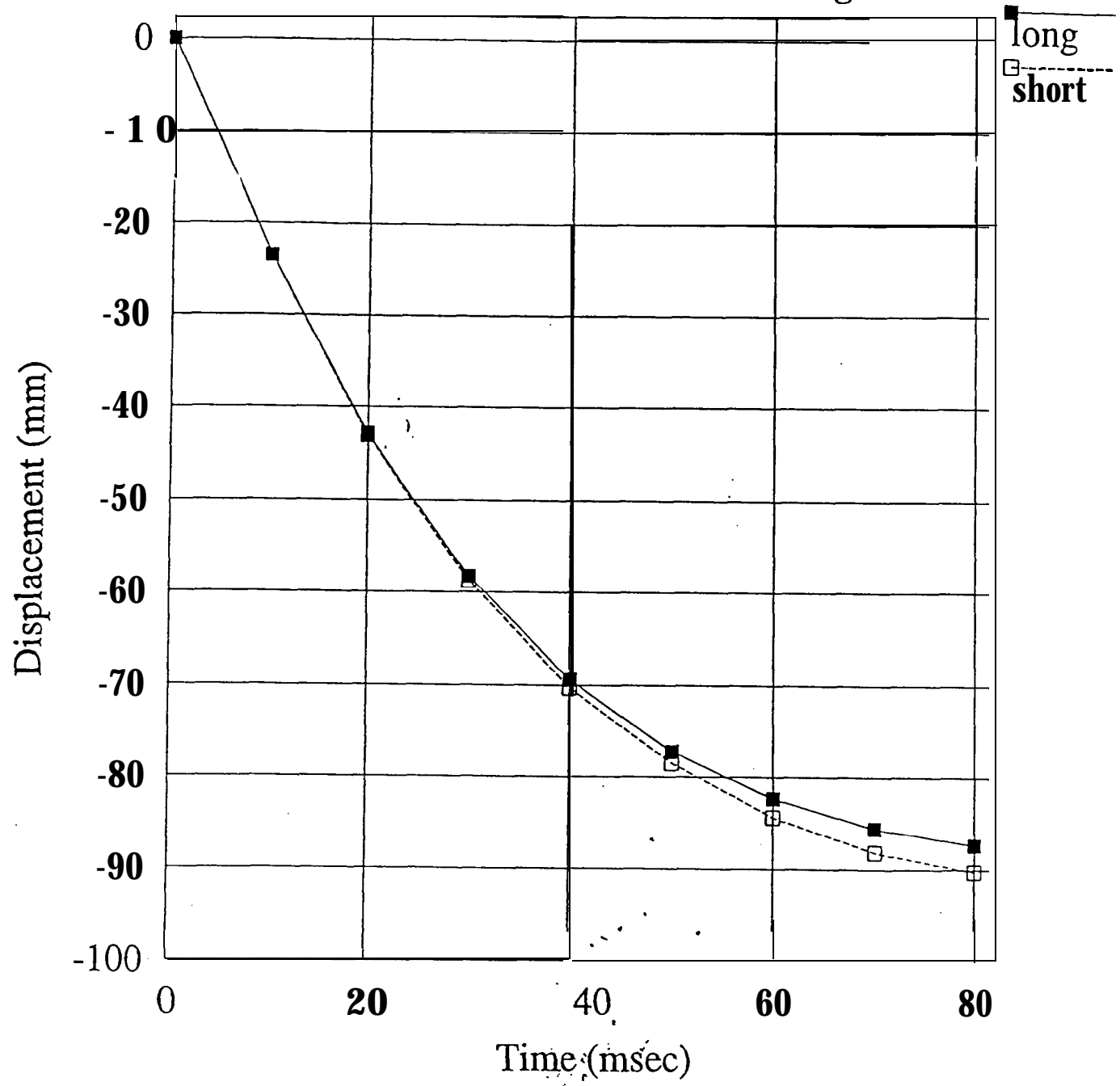


Figure 4.7 Vertical travel of seat bottom hinge.

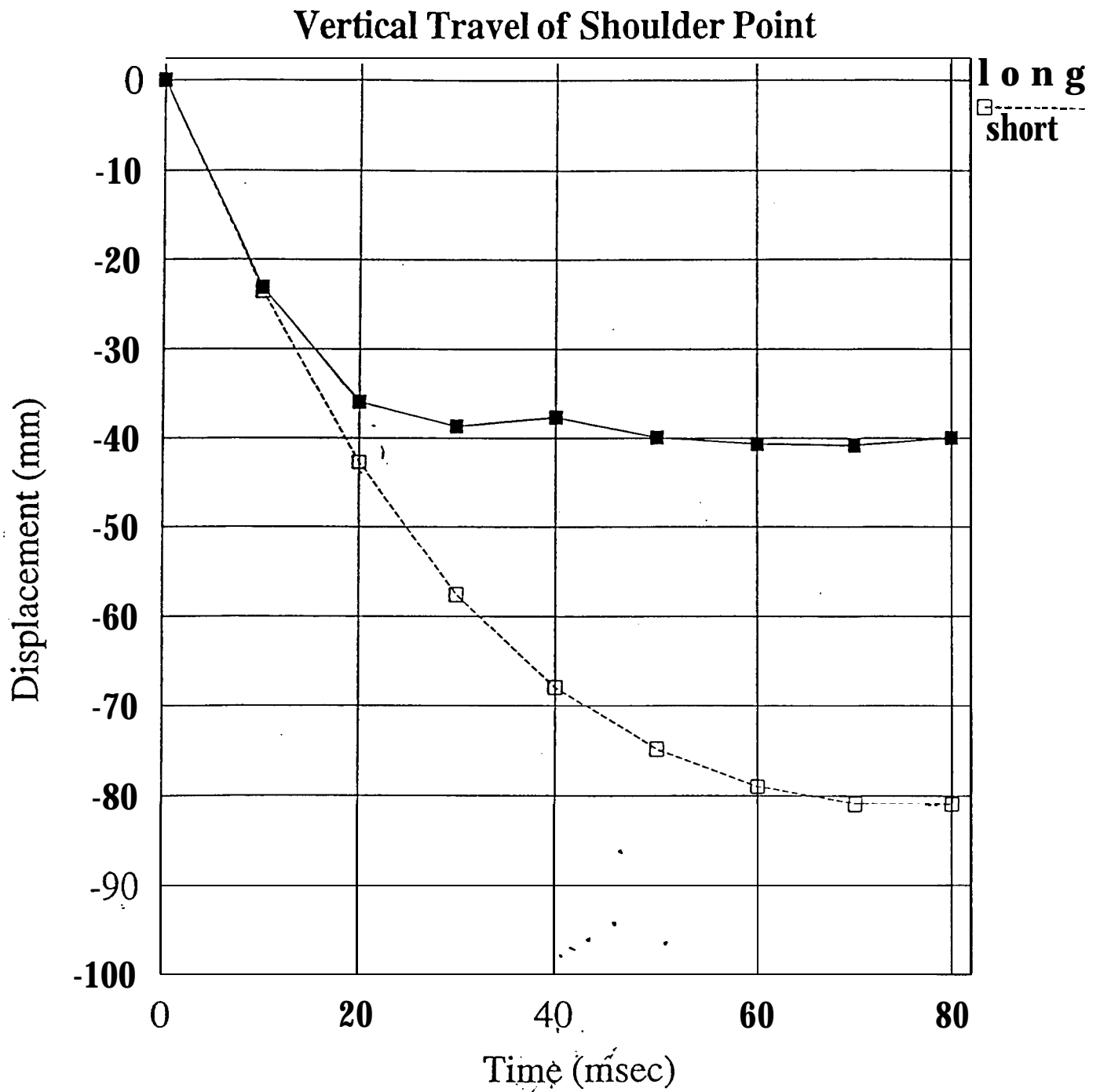


Figure 4.8 Vertical travel of shoulder point.

5. Side Impact Protection

Injuries in side impact collision constitute one fourth of the serious-to-fatal (AIS 3+) injuries sustained by occupants in ordinary passenger cars (Stig **Pilhall** et al., 1994). On the basis of the review of the accident data during the late 1980's it has been found that head injuries are the most frequent sources of side impact fatalities followed by chest and abdominal injuries.

Even though researchers have differences of opinion on the mechanisms that produce injury in side crashes, the commonly held belief is that as the striking vehicle or the barrier momentum is transferred to the target vehicle door, the door structure collapses inward with the inner panel striking the stationary occupant. If the occupant comes in contact with the collapsing door as door decelerates, one would expect the door-chest contact velocity to be lower. On the other hand, if the door strikes the occupant as its velocity ramps up, and at or near the peak door velocity, the severity of the impact would be higher. The lower contact velocity can be achieved either by locating the occupant as far away **from** the door as possible, or by ensuring that the door offers enough resistance to sudden collapse so that the barrier does not "punch" the occupant. This could also be achieved if the seat can be used to move the occupant away from the intruding door. The side impact wing concept evaluated in this study does just that.

To evaluate the concept of improved side impact protection, Ford Taurus **full** car model is used with AISS seat placed in the car. The model is coupled with a **MADYMO** 50th percentile side impact dummy in the seat. This dummy model, called **EASi-SID** was developed and calibrated at **EASi** Engineering.

A shield is provided for the dummy using a 1 mm thick plate near the shoulder. A wing is also provided near the bottom of the seat-back so that it gets the hit **from** the door and starts deforming the seat-back (Figure 5.1). The wing is provided slightly above the pivot point of the seat-back such that maximum deformation can be achieved near shoulder point. The concept explored in this model is that when the almost rigid wing near the pivot point takes the hit, it will move the shoulder point laterally at an even higher rate. This will cause the dummy's upper body to move due to the shield. The shield is placed at 45 degrees with respect to the seat-back plane. If the seat-back starts slipping behind the dummy, then the shield will catch the dummy and impart velocity to the upper body. A deformable shield is modeled because a rigid shield would have the same effect as if the impact occurs right next to the dummy. As the shield gets loaded, it will start deforming, thereby passing less force or acceleration to the upper body. This will of course bring the door profile closer to the upper body. Deformed shape of the door and seat is shown in Figure 5.2. Although, there is contact between the door and the wing, lateral displacement of the wing causes local buckling in the seat pillar and does not induce significant movement in the seat-back.

Since placement of wing at the bottom of the pillar does not produce desired lateral movement in the seat-back, in the next iteration the wing was placed at the middle of the

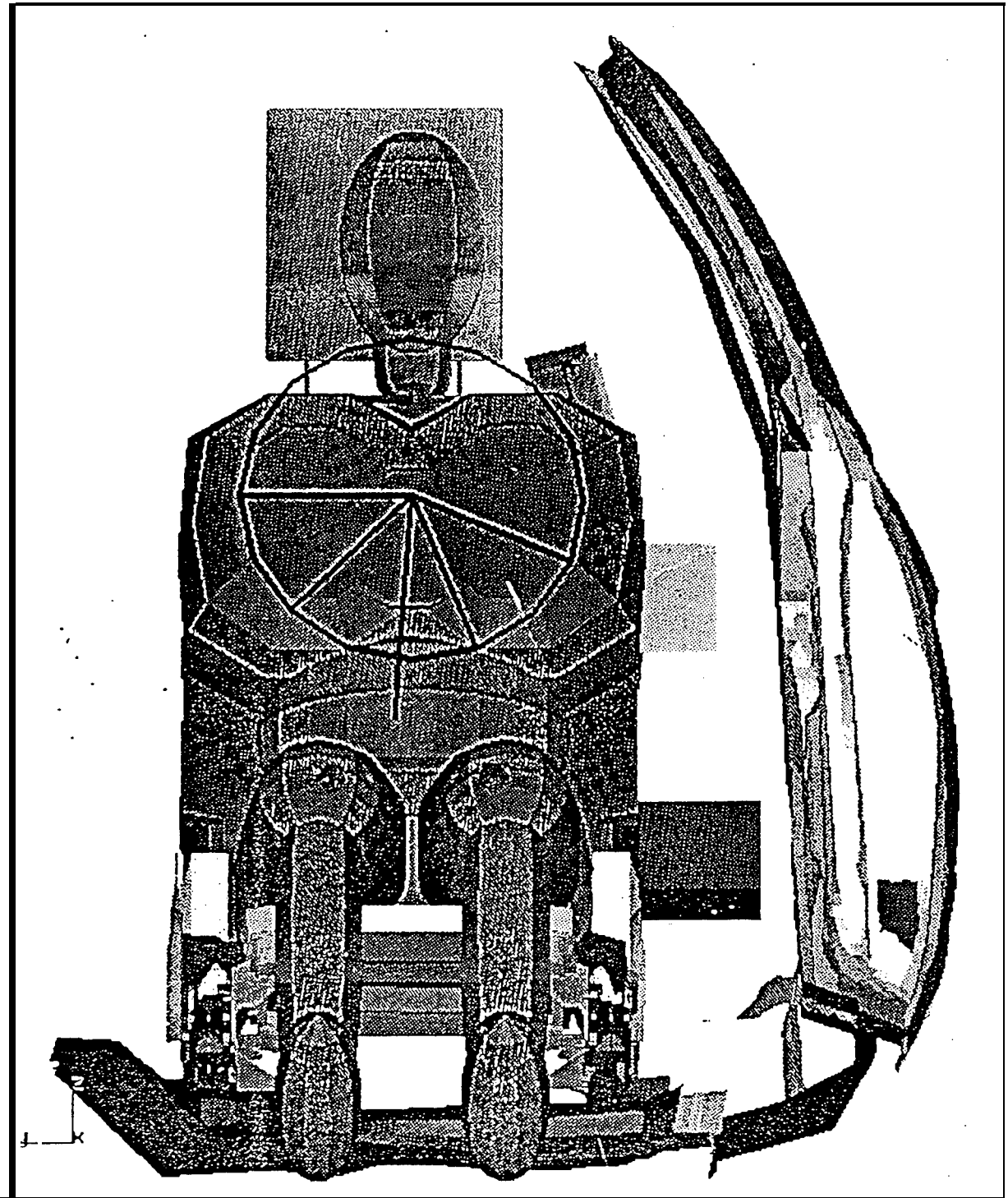


Figure 5.1 Model setup for side impact test with wing and shield.

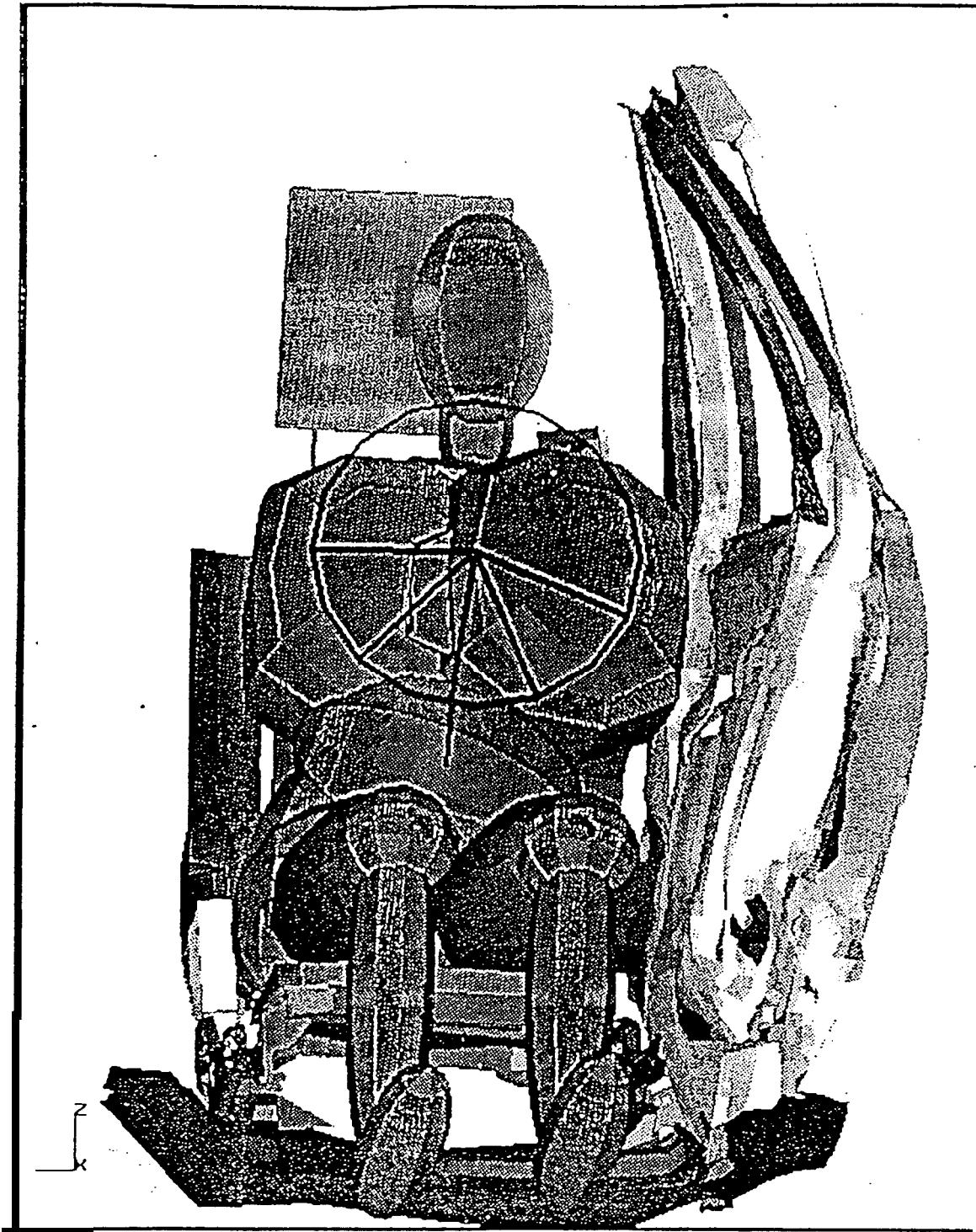


Figure 5.2 Simulation for side impact test with wing and shield.

left pillar. For faster turn-around time the model was simplified, where only the seat was modeled in detail and the door was modeled by a rigid wall. The seat was constrained by rigidly fixing the mounting brackets. Although, in a full car simulation, seat mounting brackets move with the floor pan, not very significant movement occurs in such simulation: Hence, we believed this assumption to be quite **reasonable** at least for the first few milliseconds. Velocity of the rigid wall was approximated by the velocity of the face of the wing in the above simulation. It increased from 0 to 10 m/sec in the first 12 msec and then remained constant. However, in this case excessive bending of the **left** pillar also occurs without significant movement of the seat-back as a whole. Hence, in the next iteration, the wing was placed at the top of the left pillar. This iteration showed that by placing the wing at the top, local buckling of the **left** pillar was avoided. When the door comes in contact with the wing, it starts pushing the seat back laterally. As the seat moves, the shield attached to the **left** pillar comes in contact with the dummy's upper body. The upper body of dummy starts picking up the velocity and moving away **from** the door. However, in this simulation it was noticed that hard contact between the metal of the shield and upper body of dummy caused some numerical problems. To get around this problem and also to enhance the effectiveness of the shield, a foam padding is provided in the front of the shield. Foam is provided such that, the outside angle of shield is maintained at 45 degrees while the inside angle of the front face of the foam is increased to 60 degrees with respect to the seat-back.

Further, in order to **quantify** the improvements, if any, due to the introduction of wing and shield concept, a baseline simulation was also made. The **AISS** seat without wing or shield was simulated under the same conditions as the seat with these improvements. The rigid wall comes in contact with the seat at 17 msec.

For the enhanced case, a point at the top of right pillar had a displacement of 139.8 mm at 22.33 msec (Figure 5.3). The same point in the baseline case covered the same distance in 33.95 msec. Since, the seat is fixed at the brackets, going beyond this point started causing distortion problems. Hence, we restricted ourselves to this range. As the rigid wall or door hit the seat, because of the seat-back foam and shield, the lower torso starts attaining velocity. Comparison of the lower torso velocity is shown in Figure 5.4. In the baseline case, its velocity increased to about 10 m/s at 28 msec. Since the hit occurred at 17 msec, this increase happened in 11 msec only causing high acceleration in the lower torso. On the other hand, in the enhanced case, maximum velocity attained by lower torso was only about 5 m/s and the increase occurred over a period of 22 msec. This significantly reduced the accelerations seen by the lower torso. At about 20 msec when the lower torso started picking up velocity in the baseline run, it had already moved away from the door by 42 mm (Figure 5.5) in the enhanced run while in the baseline run it had hardly moved at all. This places the lower torso very much closer to the rigid wall and so more vulnerable to a stronger hit. In the enhanced case, the lower torso starts going away early in the simulation when rigid wall is at a distance. While in the baseline case, the lower torso moves when rigid wall is much closer and imparts a much higher force.

Movement of Top of Right Pillar

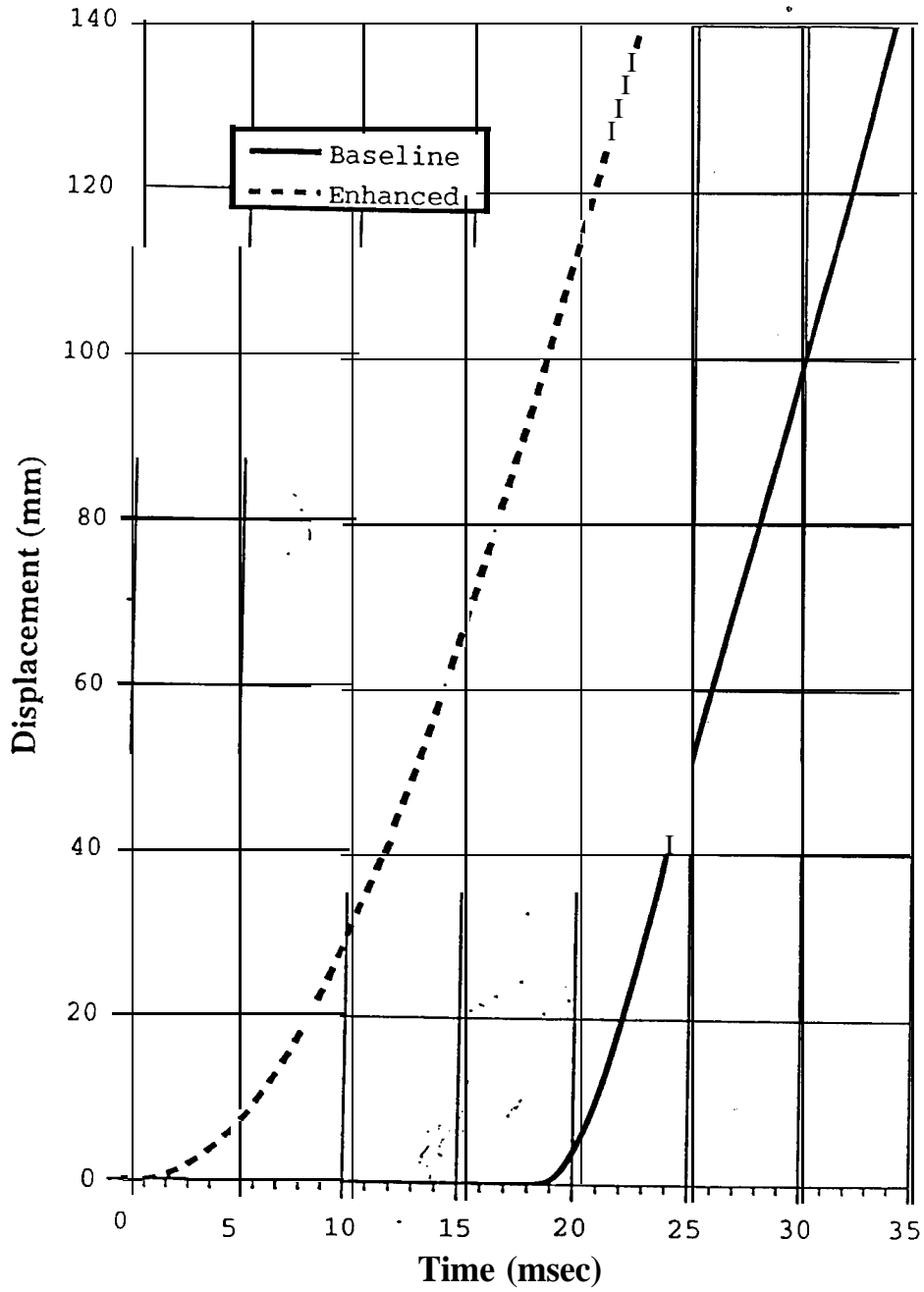


Figure 5.3 Comparison of displacement of the top right pillar with standard and enhanced seat.

Velocity of Lower Torso

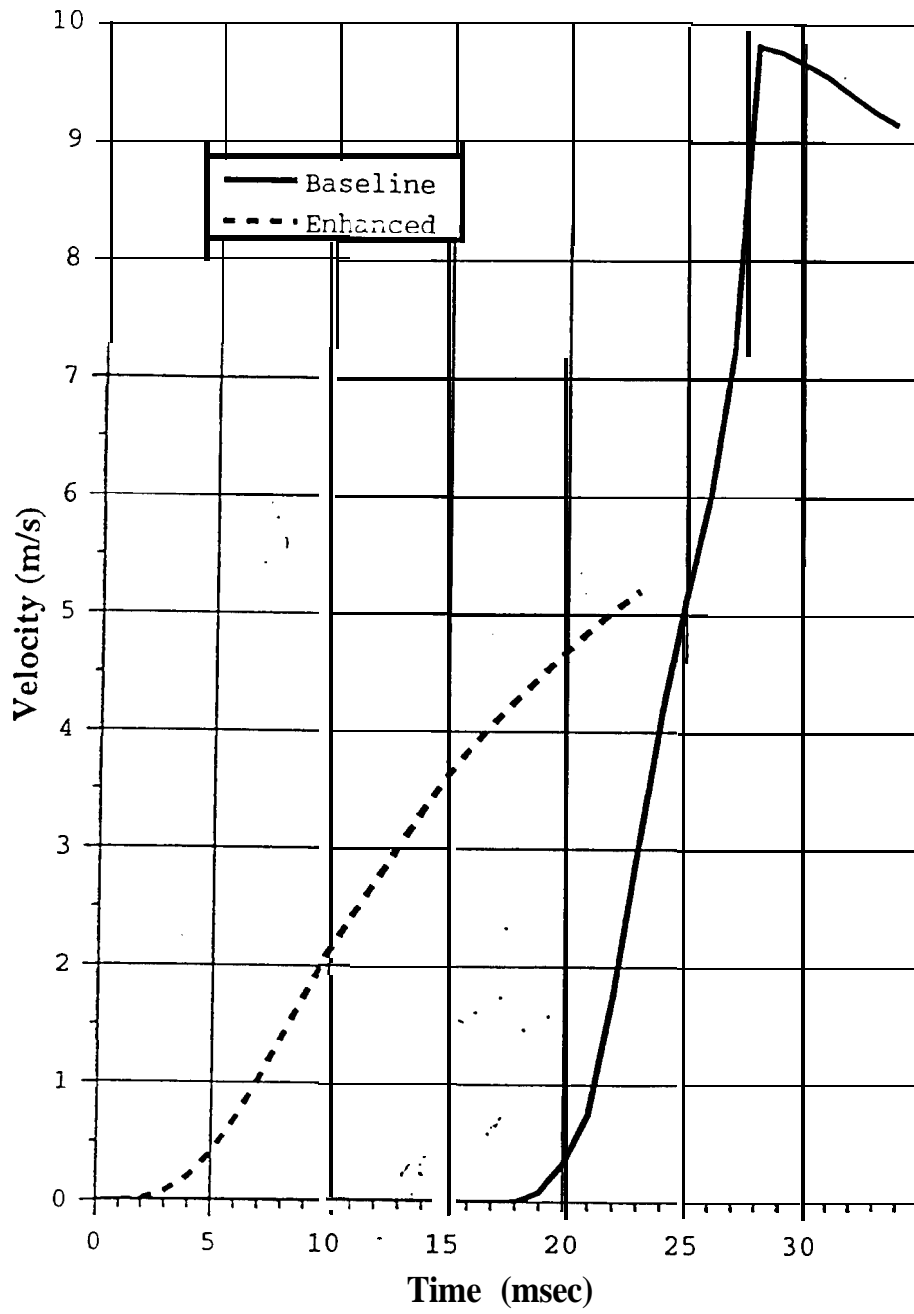


Figure 5.4 Comparison of lower torso velocity with standard and enhanced seat.

Movement of Lower Torso

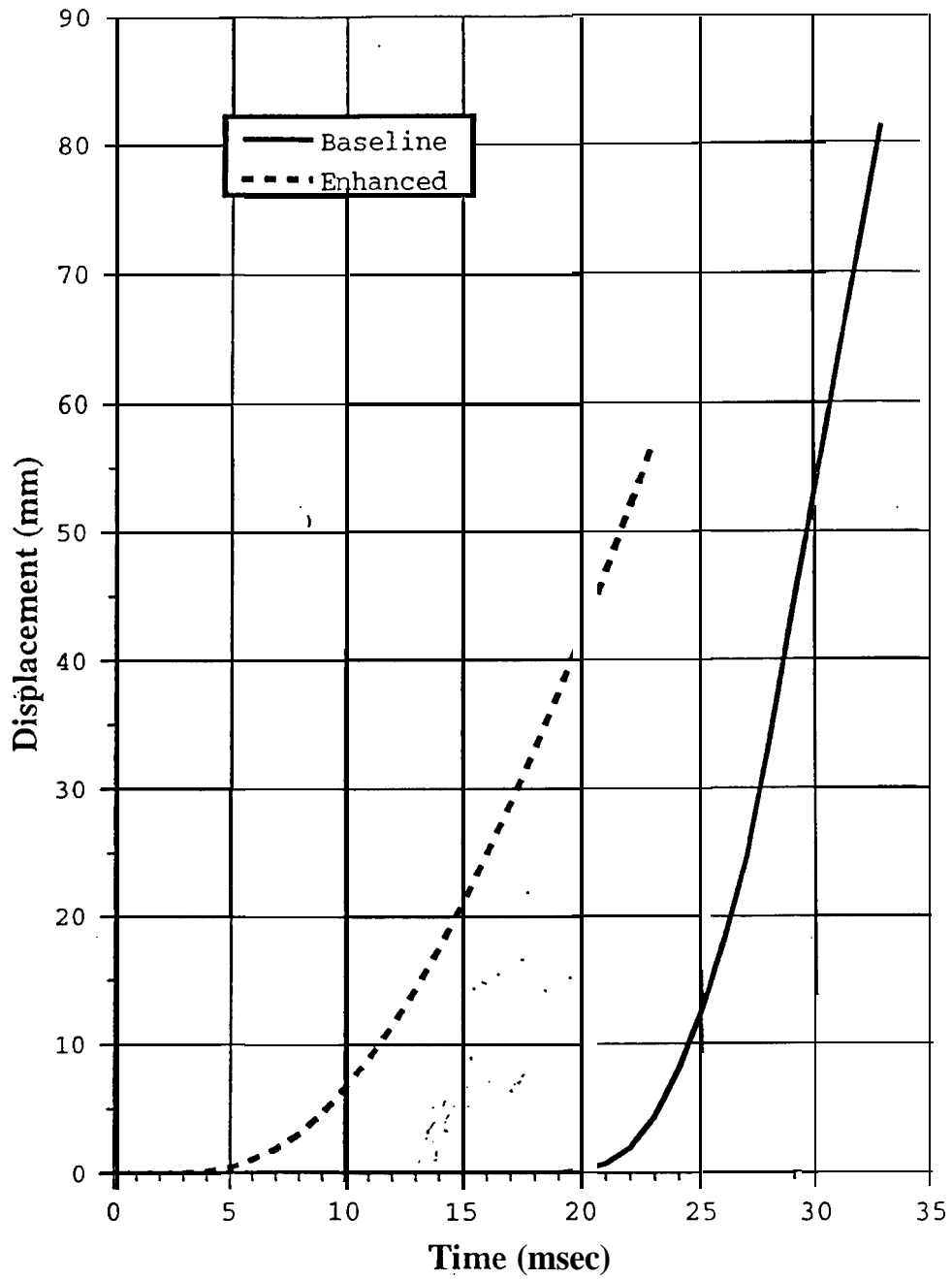


Figure 5.5 Comparison of lower torso movement with standard and enhanced seat.

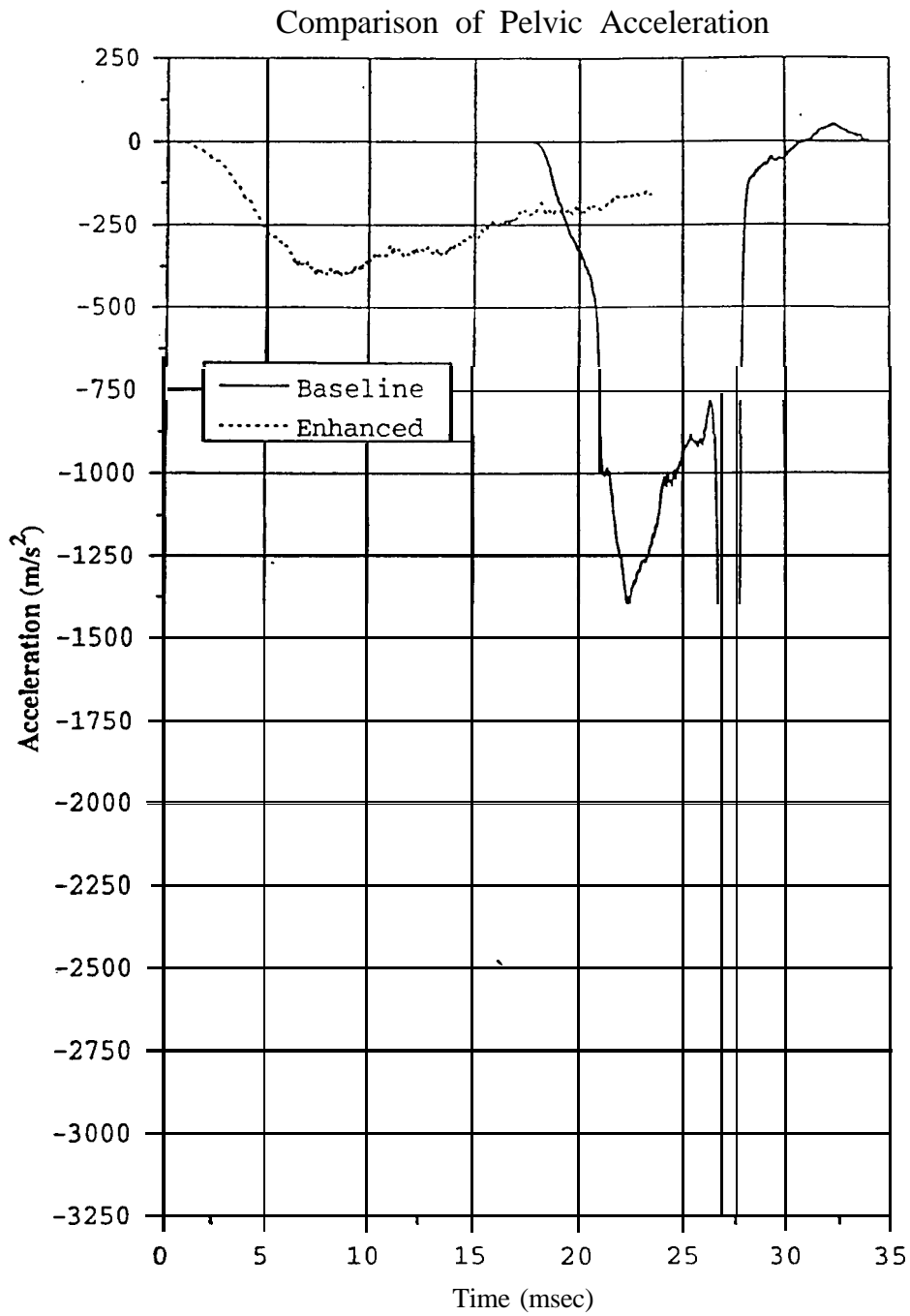


Figure 5.6 Comparison of the pelvic acceleration with standard and enhanced seat.

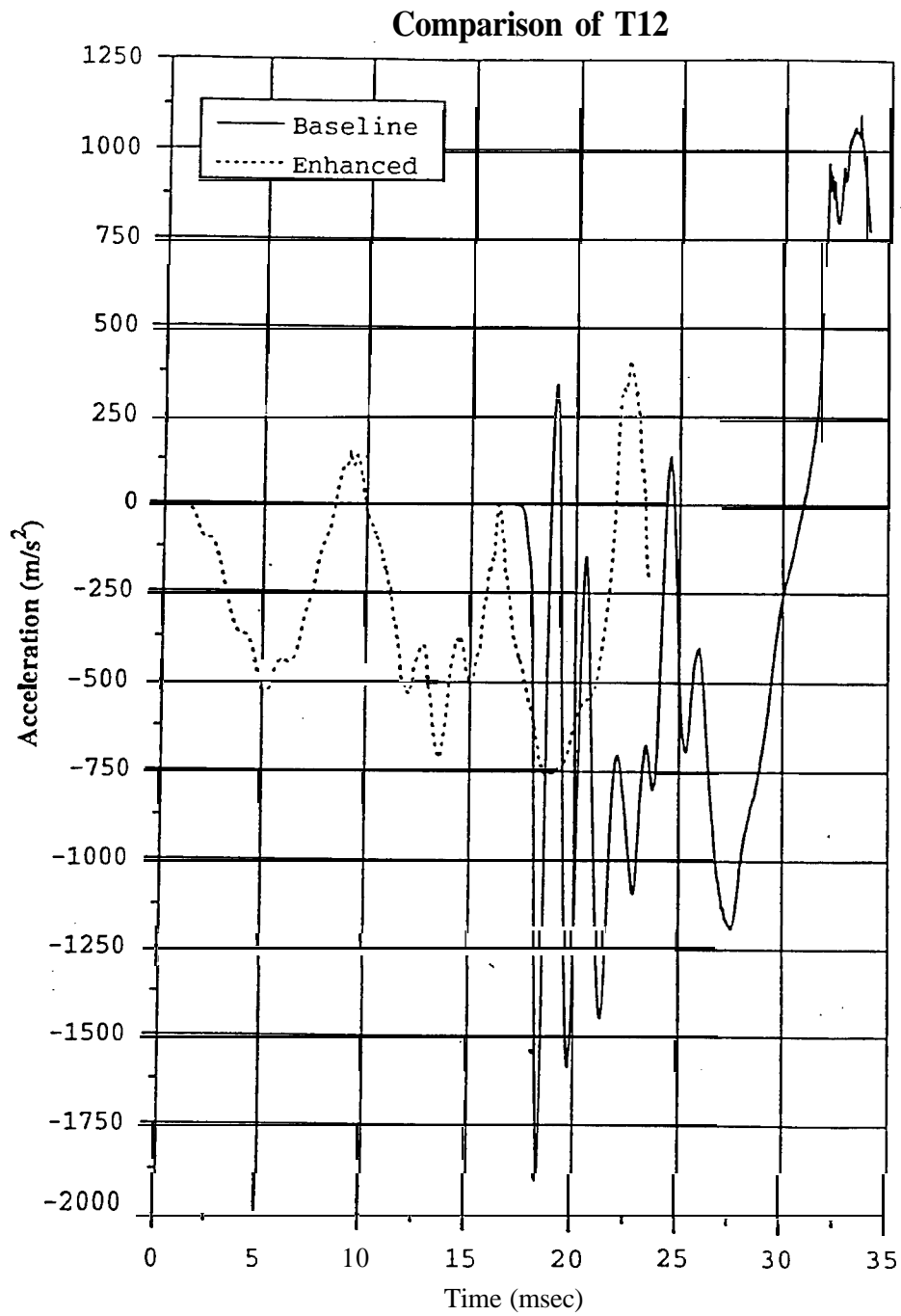


Figure 5.7 Comparison of the T12 acceleration with standard and enhanced seat.

In Figure 5.6 the pelvic acceleration is compared for the two cases. Pelvic acceleration was obtained from the MADYMO database. As expected, a significant reduction can be noted in the pelvic acceleration for the enhanced run. For the baseline case, maximum pelvic acceleration is about 320 G while for the enhanced case, it is only about 40 G. Similar reduction can be noted for T12 also (Figure 5.7). T12 is about 190 G for the baseline case and is reduced to about 75 G for the enhanced case. Overall TTI injury criterion is reduced from a significantly high value for the baseline case to 88 for the enhanced case.

FUTURE WORK

- The analytical results presented here are to be verified with prototyping and testing in the future.
- Incorporating the design concepts proposed here into production will be based on cost versus benefit analysis.
- Investigate the inflatable tubular (ITC) for side impact protection.

SUMMARY

- 4000 N load limit is found to be favorable for 30 mph frontal impact for a 50th percentile Hybrid III dummy. A 30 percent reduction in the risk of AIS \geq 4 thoracic injury is seen.
- Belt pretensioner increases the effectiveness of shoulder belt load limiter in frontal impact. 50 percent reduction in linear chest acceleration 3MS is seen with the use of a pretensioner. Belt pretensioner is also found to be very effective in rollover crashes by reducing head excursion.
- A design concept for an energy absorber in series with a linear recliner has been explored and shows promise as a basis for further development.
- The energy absorber meets the maximum seat back rotation guideline for the 5th, 50th and the 95th percentile dummies.
- The occupant kinematics and injury parameters are very favorable for the 50th percentile dummy, calculated using a LS-DYNA/MADYMO coupled simulation.

REFERENCES

Bahling, G. S., Bundorf, R. T., Kaspzyk, G. S., Moffatt, E. A., Orłowski, K. F. and Stocke, J. E., "Rollover and Drop Tests - The Influence of Roof Strength on Injury Mechanics Using Belted Dummies", SAE Paper # 9023 14, 1990.

Haland, Y., Nilson, G., "Seat Belt Pretensioners to Avoid the Risk of Submarining - A Study of Lap-Belt Slippage Factors", 13 th International Technical Conference on Experimental Safety Vehicles", 1993, pp. 1060- 1068.

Kallieris, D., Rizzetti, A., Mattem, R., Morgan, R., Eppinger, R., Keenan, L., "On the Synergism of the Driver Air Bag and the 3-Point Belt in Frontal Collisions", 39th Stapp Car Crash Conference Proceedings, 1995.

Langweider K., Hummel T., Sagerer F., "Characteristics of Neck Injuries of Car Occupants", Proc. International IRCOBI Conference on the Biomechanics of Impacts, 1981, pp. 78-79.

Lowne R., Gloyns P., Roy P., "Fatal Injuries to Restrained Children Aged 0-4 Years in Great Britain 1972-1 986", Eleventh International Conference on Experimental Safety Vehicles, 1987.

Mendis, K., Ridella, A, and Mani, A., "Dummy Neck Design Support," Contract No DTNI-I-22-92-D-07323, Project No. NRD-01-3-07227, EASi Engineering, Dec, 1994.

Mertz, H.J., Williamson, J.E., Vander Lugt, D., "The Effect of Limiting Shoulder Belt Load with Air Bag Restraint", SAE paper # 950886.

Partyka, S., "Office of Vehicle Safety Standards, Rulemaking, NHTSA, 1992.

Pillhall, S., Komer, J., Ouchterlony, B., "SIPSBAG - A New, Seat-Mounted Side Impact Airbag System", Volvo Car Corporation, 14th ESV Conference paper # 94-S6-O-13, 1994.

Pilkey W.D. and Sieveka, E., "Analytical Modeling of Occupant Seating/Restraint Systems", NHTSA Report for DTRS-57-90-C-00092, 1994.

Renouf, M.A., "A Car Accident Injury Database: Overview and Analyses of Entrapment and Ejection. TRRL Research Report 320. Transport and Road Research Laboratory, Crawthorne, 199 1.

Status Report, Insurance Institute for Highway Safety, Vol. 30, No. 8, September 16, 1995.

Svensson, M.Y., Lovsund, P., Haland, Y., and Larsson, S., "Rear End Collisions - A Study of the Influence of Backrest Properties on Head-Neck Motion using a new Dummy Neck, SAE Paper # 930343, 1993.

Thomas C. et al., "Protection Against Rear-End Accidents", Proc. International IRCOBI Conference on the Biomechanics of Impacts, 1982, pp. 17-29.

Viano, D.C., "Influence of Seat Back Angle on Occupant Dynamics in Simulated Rear End Impacts", SAE Paper # 922521, 1992.

DEPARTMENT OF TRANSPORTATION

99 MAR 25 AM 10:16

DOCKET SECTION

Advanced Integrated Structural Seat

Contract Number **DTNH22-92-D-07323**, Task-11

Final Report

February, 1997

by

EASi Engineering

Vikas Gupta, Rajiv Menon, Sanjeev Gupta, A.Mani

&

Johnson Controls, Inc.

Ilango Shanmugavelu

NOTICE

This document% disseminated under the sponsorship of the Department of **Transportation** in the interest of information exchange. The United states Government assumes no liability for its contents or use thereof

NOTICE

The United States Government does not endorse products or **manufactures**. Trade or : manufacturers' names appear herein solely because they are considered essential to the object of this report.

TABLE OF CONTENTS

	Page
BACKGROUND.....	6
1. INTRODUCTION..	6
2. FRONTAL CRASH PROTECTION.. .. .	8
2.1 Load Limiter	8
2.2 Pretensioner	20
3. REAR IMPACT PROTECTION	22
3.1 Effect of Increasing Distance Available for Torso Acceleration.. .. .	25
3.2 Seat Back Structure	27
3.3 Recliner With Energy Absorber.. .. .	28
3.3.1 Design for Energy Absorber.. .. .	33
3.3.2 Design Verification for Rear Impact	33
3.4 Inflatable Head Rest	38
4. ROLLOVER.. .. .	58
4.1 MADYMO Simulations.. .. .	58
4.2 Extended Headrest	61
5. SIDE IMPACT PROTECTION.. .. .	67
FUTURE WORK.	76
SUMMARY	76
REFERENCES.....	77

LIST OF FIGURES

	Page
Figure 2.1 Load limiter and airbag interaction.	9
Figure 2.2 MADYMO model and simulation.....	10
Figure 2.3 Load limiter force and belt payout for 30 mph frontal crash.	12
Figure 2.4 Comparison of Head Injury Criteria with and without load limiters (30 mph).	13
Figure 2.5 Comparison of chest compression with and without load limiters (30 mph).	13
Figure 2.6 Load limiter force and belt payout for 40 mph frontal crash.	14
Figure 2.7 Comparison of Head Injury Criteria with and without load limiters (40 mph).	15
Figure 2.8 Comparison of chest compression with and without load limiters (40 mph).	15
Figure 2.9 Shoulder belt load vs. time for 30 mph.	20
Figure 2.10 Effect of pretensioner on injury parameters (50th percentile dummy at 30 mph).	21
Figure 3.1 Body region injuries attributed to frontal components in rear crash.	23
Figure 3.2 Source of injury for outboard, belted occupant.	24
Figure 3.3 Design concepts for increasing torso travel.	26
Figure 3.4 Crash sequence in rear impact. Figure 3.5 Acceleration pulse.	28
Figure 3.6 Torque vs. rotation curve for the seat back.	29
Figure 3.7 Energy absorption of a typical seat back and low rebound seat.	30
Figure 3.8 Head excursion due to seat back rebound.	32
Figure 3.9 Layout of modified recliner.	34
Figure 3.10 Torque-theta curve with the metal element.	35
Figure 3.11 Model setup for the coupled simulation.	36
Figure 3.12 Headrest positions from blueprint (courtesy JCI).	39
Figure 3.13 MADYMO model setup with headrest.	40
Figure 3.14 Types of inflatable headrest studied.	41
Figure 3.15 Occupant response using Type 2 inflatable headrest.	42
Figure 3.16 Occupant neck response using Type 2 inflatable headrest.	43
Figure 3.17 Occupant response using Type 3 inflatable headrest.	44
Figure 3.18 Occupant neck response using Type 3 inflatable headrest.	45
Figure 3.19 Comparison of occupant response using different types of inflatable headrest.	46
Figure 3.20 Comparison of accelerations using different types of inflatable headrest	47
Figure 3.2.1 Occupant neck response using different types of inflatable headrests.	48
Figure 3.22 Comparison of injury numbers using different inflatable headrests.	49
Figure 3.23 Baseline case (without inflatable headrest) simulation.	50
Figure 3.24 Simulation with inflatable headrest Type 1.	51
Figure 3.25 Simulation with inflatable headrest Type 2.	52
Figure 3.26 Simulation with inflatable headrest Type 3.	53

Figure 3.27 Comparison of occupant response at 30 and 5 mph.	54
Figure 3.28 Comparison of occupant neck response at 30 and 5 mph.	55
Figure 3.29 Trajectories of the upper and lower neck with inflatable headrest.	56
Figure 3.30 Trajectories of the upper and lower neck with standard headrest.	57
Figure 4.1 Model setup for MADYMO rollover simulations	59
Figure 4.2 Vehicle rollover simulation.	59
Figure 4.3 Characteristics of the pretensioner.	60
Figure 4.4 Model setup of the inverted simulation.	61
Figure 4.5 Full car rollover drop test.	62
Figure 4.6 Comparison of standard and extended headrest in inverted drop test.....	64
Figure 4.7 Vertical travel of seat bottom hinge.....	65
Figure 4.8 Vertical travel of shoulder point.	66
Figure 5.1 Model setup for side impact test with wing and shield.	68
Figure 5.2 Simulation for side impact test with wing and shield.	69
Figure 5.3 Comparison of displacement of the top right pillar with standard and enhanced seat.	71
Figure 5.4 Comparison of lower torso velocity with standard and enhanced seat.	72
Figure 5.5 Comparison of lower torso movement with standard and enhanced seat.	73
Figure 5.6 Comparison of the pelvic acceleration with standard and enhanced seat. ..	74
Figure 5.7 Comparison of the T12 acceleration with standard and enhanced seat.....	75

LIST OF TABLES

	Page
Table 1.1 Criteria Matrix	7
Table 2.1 Simulation results without load limiter at 30 mph.	16
Table 2.2 Simulation results with load limiter at 30 mph.	17
Table 2.3 Simulation results without load limiter at 40 mph	18
Table 2.4 Simulation results with load limiter at 40 mph.....	19
Table 2.2 Specifications for the Belt Pretensioner.....	21
Table 3.1 Participation of the proposed design features in addressing various rear impact performance criteria.....	25
Table 3.2 Effect of lowered pivot seat and slid&seat	27
Table 3.3 Maximum seat back angle with respect to the seat bottom (Initial seat back angle = 23°)	28
Table 3.4 Effect of seat back rebound.	31
Table 3.5 Injury numbers for 5th, 50th and 95th percentile dummy models	37
Table 4.1 Simulation results	60
Table 4.2 Simulation results of the inverted tests.....	61

BACKGROUND

Through a contract from National Highway Traffic Safety Administration (NHTSA), EASi Engineering in conjunction with Johnson Controls Inc. (JCI) worked to conceive and develop an advanced integrated structural seat that meets the current FMVSS requirements, significantly improve occupant protection for frontal, rear, side and rollover accidents and contributes to passenger compartment intrusion resistance. This work is a cooperative effort between the government and industry, bringing together the strengths of impact biomechanics, computer aided engineering and seat systems engineering and manufacturing.

This report summarizes the advanced integrated structural seat criteria used, the design concepts evolved and adapted, the evaluation of the design concepts using various computer aided engineering (CAE) methodologies, and the resulting changes in occupant crash protection. Concept level models were created primarily through use of the MADYMO software to establish potential benefits. Further design evolution and evaluation were achieved via detailed finite element models and coupled models using LS-DYNA3D and LS-DYNA3D/MADYMO coupling. The design concepts studied include rollover-sensing seat belt pretensioners and extended head rest frames for improved rollover protection, belt load limiter for improved frontal crash protection, 'energy absorbing dual recliners and inflatable headrest for rear impact protection, seat back wing structures for improved side impact protection and side intrusion resistance. This study does not include seat mounted side airbags as they have been explored already (Pillhall et al., 1994) and are in production.

1. INTRODUCTION

The advanced integrated structural seat (AISS) is aimed at enhancing occupant protection in all of the four basic crash modes (frontal, rear, rollover and side crashes) primarily by modifications of the seat structure and by addition of seat mounted safety/restraint features. By focusing on the seat structure modifications, it is hoped the resulting designs will be simple and cost-efficient. Also, the seat system is designed to function with the body structure to resist passenger compartment intrusion in side and rollover crashes. This seat system design is being developed starting from an existing integrated structural seat design. Integrated seats have all the belt anchorages on the seat itself as opposed to conventional seats where the shoulder belt upper anchorage is located on the car upper body structure. The belt fit is considerably improved regardless of the seating position. Also, the assembly of the seat in the car becomes much easier with this design as the belts are an integral part of the seat. An integrated structural seat was chosen as the baseline seat since it is expected to enhance occupant protection.

The criteria matrix shown in Table 1.1, lists the loading conditions and evaluation criteria for the seat in various crash modes. This matrix was established based on current

Table 1.1 Criteria Matrix

	Criteria	Loading		Characteristics of Interest	Dummy	Back Position	Remarks
		Speed/ Location	Load				
C O M P L I A N C E	Rollover	30 mph	Drop from rollover dolly (FMVSS 208)	Head excursion; Neck injury ; Shoulder belt loads on occupant ; Failure mode	50th & 95th %ile male Hybrid III belted	Design	Consideration for 5th %ile female head excursion relative to torso
	Rear impact	35 mph	301 crash pulse extrapolated	Shoulder belt loading; Neck injury ; Ramp up ; Back collapse; Rebound	50th & 95th %ile male Hybrid III belted	Design	Hybrid III may not be adequate; Check for 5th %ile
	Side impact	33.5 mph	MDB	TTI; Pelvic injury, Head injury. Head Excursion	SID belted	Design	Head excursion relative to torso
	Frontal impact	30 mph	30 mph pulse	Head injury, Chest g ; Anti submarining Rebound	50th & 95th %ile male Hybrid III belted	Design	Airbag interaction to be considered; Check for 5th %ile female; Submarining
P R A C T I C E	Torsional Rigidity	Seat back corner	2260 m-lb. about H-point	Permanent set		Design	
	Abuse load	Seat back crossbar	6400 m-lb. rearward about H-point	seat Integrity		Design	
	Submarine loads	Cushion Game	Simulated	Seat Integrity			
D I S T R I B U T I O N	Cost estimate	NA	NA	Market acceptable range			
	Ingress/Egress	NA	NA	Ease			
	Styling	NA	NA	Acceptable practices			
	Manufacturing	NA	NA	Mass production feasible			
	Vibrational characteristic	NA	NA	Away from discomfort range			
	Weight	NA	NA	Within market range			

regulations and a sample of industry design practice. The matrix should not be considered a statement of NHTSA's future regulatory intentions.

The concepts evolved, their evaluation procedure and detailed design are described in the following sections.

2. FRONTAL CRASH PROTECTION

2.1 Load Limiter

Recent work done in evaluating injury reduction in **frontal** crashes suggests that belt restraints and **airbag** restraints may not interact in a way which achieves optimal occupant protection (Mertz et al, 1995). Ideally, at frontal collision speeds below the threshold of air bag deployment, torso belt forces should be limited to those levels required to prevent occupant impact against compartment interior surfaces such as steering wheels and instrument panels. Additionally, for the AISS (Advanced Integrated Structural Seat) design, the torso belt should sustain loads capable of retaining the occupant within the compartment during rollovers and side crashes. Such reduced torso belt load limits are far below current practice (Figure 2.1). The upper anchorage of the torso belt on the seat back structure of current integrated seats is the source of the greatest seat back bending moment and shear load on the seat structure. As a result, limiting the torso belt loads allows weight reduction of the seat back structure and reduced floor pan shear while reducing occupant injuries at higher crash severities. At present, significant re-designing of the vehicle floor pan is required to adapt it for an integrated structural seat. Introduction of load limiter may reduce the extent of redesign required to replace a conventional seat (shoulder belt upper anchorage on the vehicle structure, mostly the b-pillar) with an integrated structural seat.

Mertz et al. (1995), have shown vast improvement in occupant injury parameters for the 50th percentile occupant by limiting the seat belt loads to 2000 N. They have shown a 27 percent reduction in chest acceleration and 67 percent reduction in chest compression. The risk of $\text{AIS} \geq 4$ was reduced from 14.5 percent to 0.4 percent, and the risk of $\text{AIS} \geq 3$ was reduced from 94 percent to 19 percent. The 95th percentile occupants although, were studied only at low speeds (15 mph) in non-deploy situations.

In the current study, a rigid body MADYMO model validated using a front impact sled test, is used for evaluating the torso belt load limit. The model is set up for a Ford Taurus environment with an existing integrated structural seat design (Figure 2.2). The seat model includes the seat back joint stiffness, seat cushion stiffness, **anti-submarining** plane and a 3-point seat belt. Eight percent nominal belt **stiffness** is used. Three different impact velocities of 12, 30 and 40 mph were studied, with and without the presence of a

load limiter. The airbag and the inflator model are assigned characteristics taken from a production airbag. A small (40 liter) and a large (80 liter) airbag were used for the study.

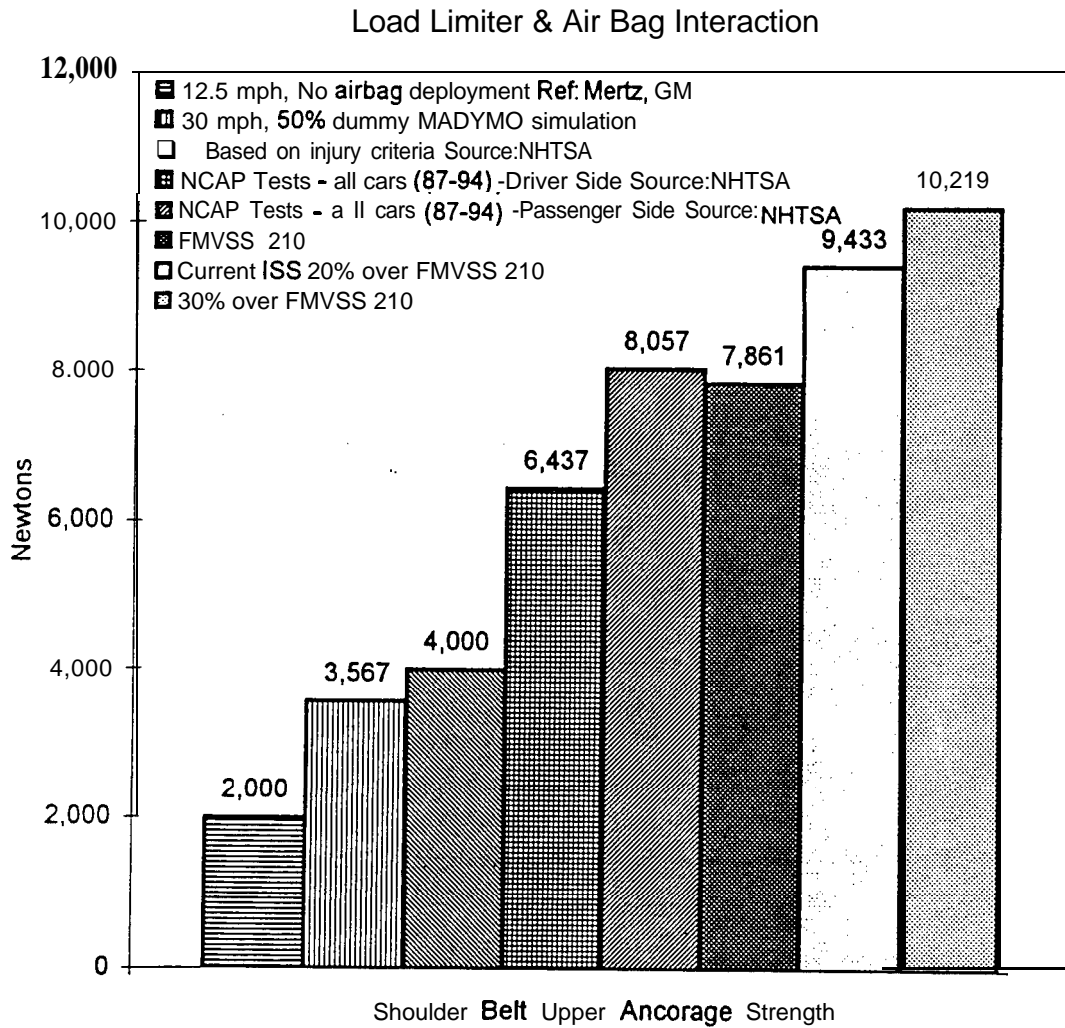


Figure 2.1 Load limiter and airbag interaction.

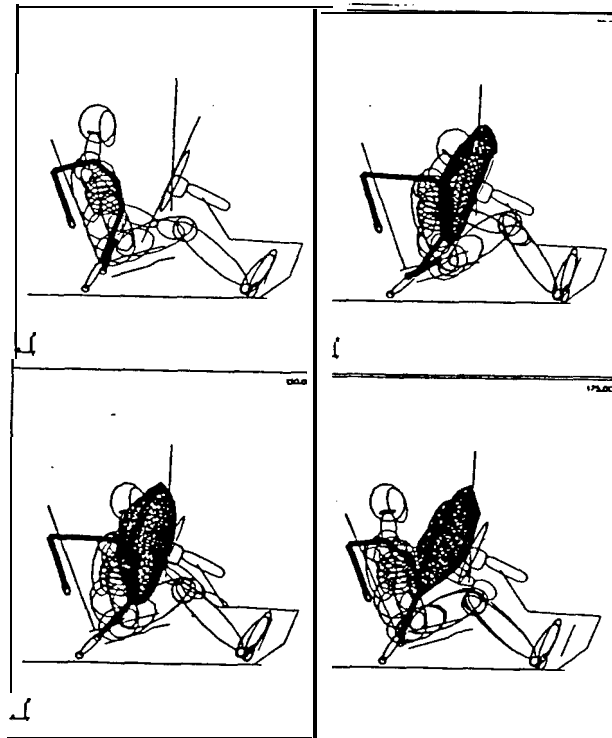
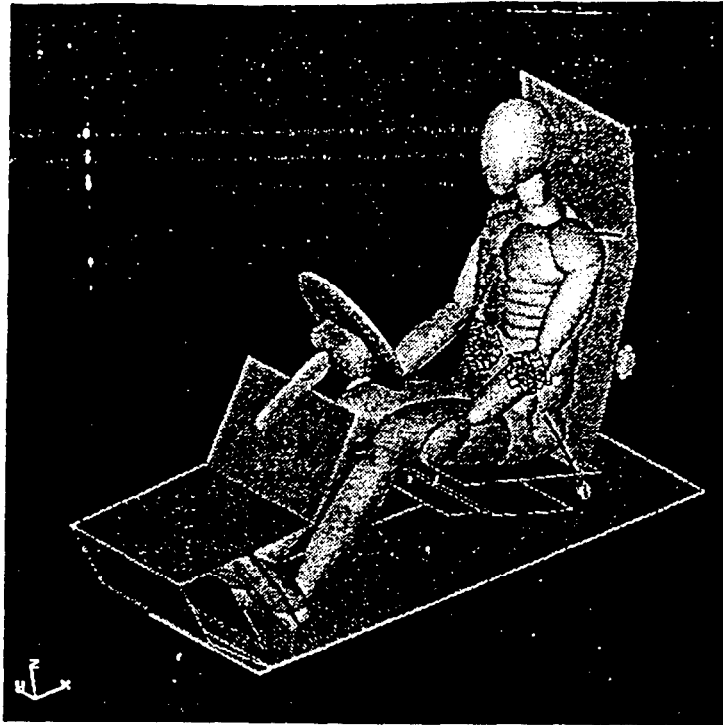


Figure 2.2 MADYMO model and simulation.

A load limit of 4000 Newton was found to be ideal based on a new research on rib fracture by Kallieris et al (1995). In the current study, no head to wheel contact was seen for a 50th percentile Hybrid III dummy, at a 30 mph frontal impact with a 4000 N load limit. Figure 2.3 shows the belt payout for a range of load limits for 30 mph impact pulse. The load limit for a 95th percentile male, that produces no wheel to head contact was found to be 4500 Newtons.

Figure 2.4 and 2.5 show the bar charts for the HIC and chest compression for the 5th, 50th and the 95th percentile occupants respectively, for a 30 mph frontal impact. With the 4000 N load limit substantial reduction in HIC values and neck loads are seen. HIC is reduced by 51%, neck loads by 15% and chest compression by 14% for a 50th percentile occupant with a 40 liter airbag. This translates to a 30 percent reduction in the risk for AIS ≥ 3 thoracic injury. Figure 2.6 shows the belt payout for a range of load limits for 40 mph impact pulse. Payout of the belt is higher for the 30 mph frontal impact (140 mm for 50th percentile large airbag) than the 40 mph (90 mm for 50th percentile large air-bag) because the load limits used are 3500 N for 30 mph and 4500 N for 40 mph for the same body mass to travel forward. Figures 2.7 and 2.8 show the HIC and chest compression results for 40 mph impact. Tables 2.1 through 2.4 show the injury numbers for 30 and 40 mph frontal impacts, with small and large airbags, with and without the load limiters. The injury parameters reported are HIC, head excursion, peak head acceleration, maximum linear chest acceleration sustained over a period of 3 msec. or more and referred to as 3MS, neck load which are joint loads recorded at the lower neck, left and right femur load, chest compression and shoulder belt loads. All the results are reported for the 5th, 50th and the 95th percentile dummies.

Vast reduction in belt loads due to the introduction of load limiter (Figure 2.9), would make one expect significant reduction in chest compression values. But, from Figure 2.5 it is clear that chest compression reductions are only moderate. This is explained by the influence of airbag in frontal impact. Limiting of the belt loads causes the airbag to pick up the loads. Optimum design to minimize injury indices would involve concurrent tuning of the seat belts, the load limiter and the airbag. This is further illustrated by the vast differences in injury parameters between the three sizes of occupants, for the two sizes of airbags.

If a load limiter, that causes increased belt payout, is activated in an impact mode other than frontal, e.g. rollover, the risk of injury to the occupant could increase. However, rollover simulation performed by EASi as part of this research show shoulder belt loads much below 4000 N. Lap belt with retractor and pretensioner significantly limits the motion of the occupant in a rollover and hence lower loads on the shoulder belt are seen.

Several load limiters based on different concepts such as, stitch tearing, torsion rod, shearing/extrusion etc. are available in the market. Most of them are capable of limiting the load at 4000 N.

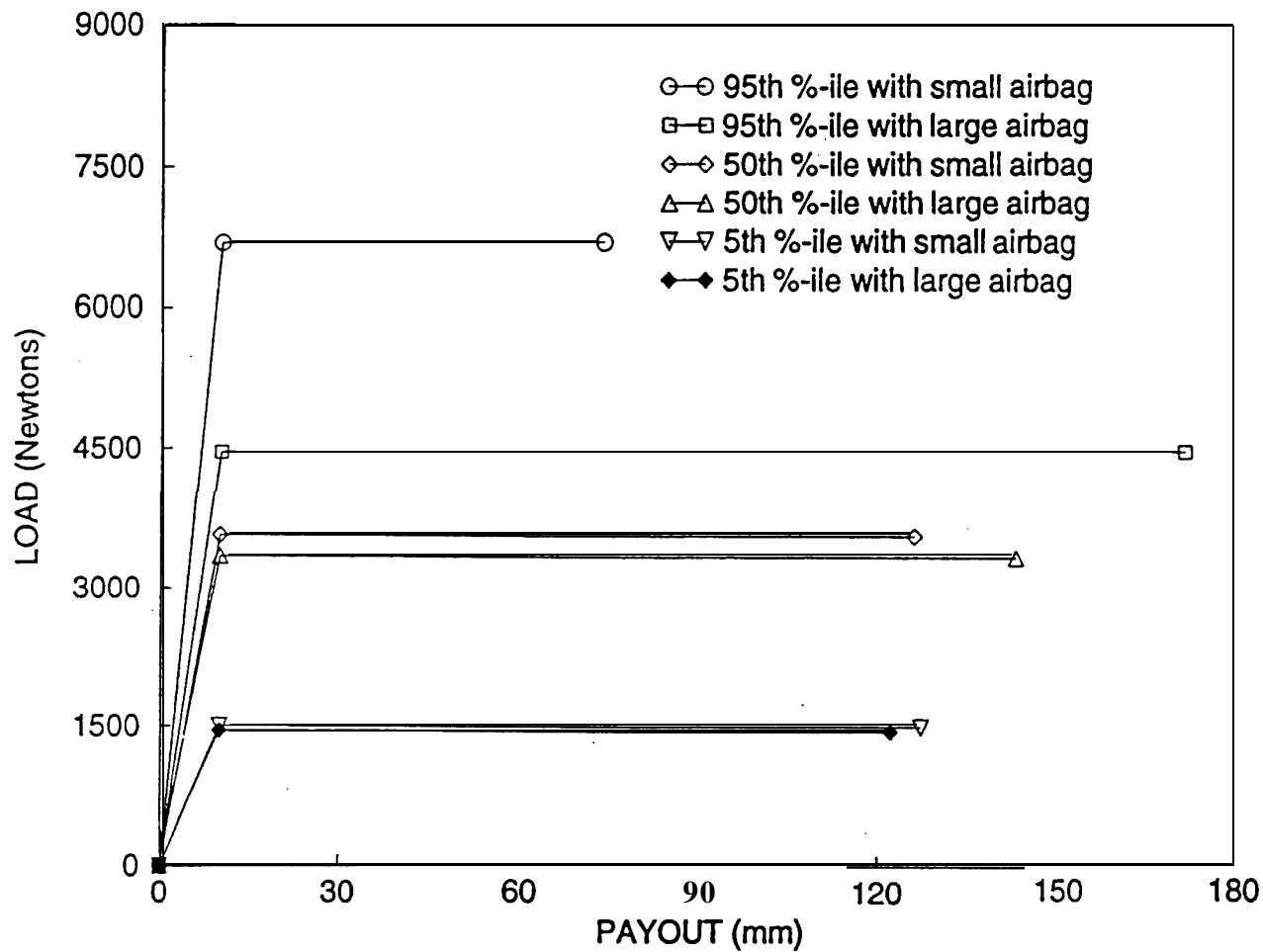


Figure 2.3 Load limiter force and belt payout for 30 mph frontal crash.

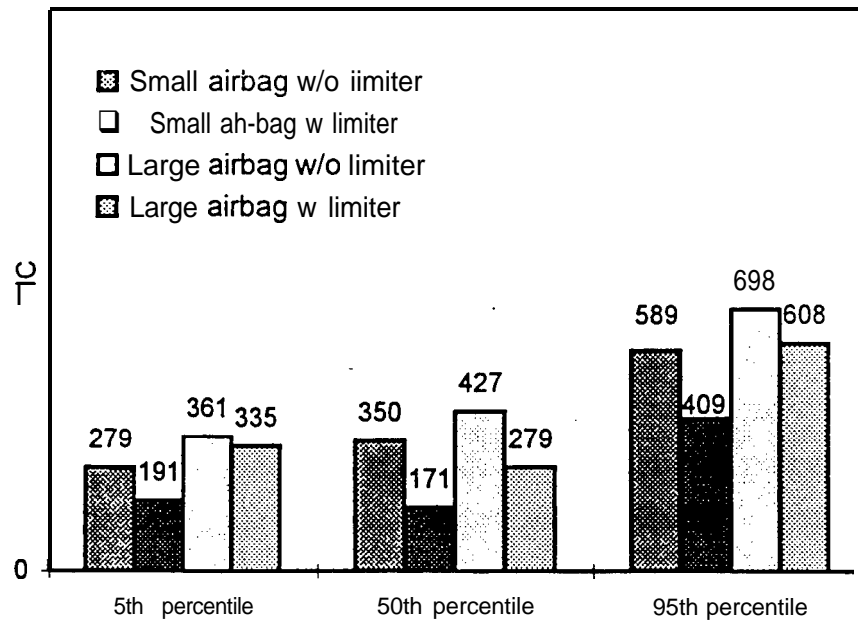


Figure 2.4 Comparison of Head Injury Criteria with and without load limiters (30 mph).

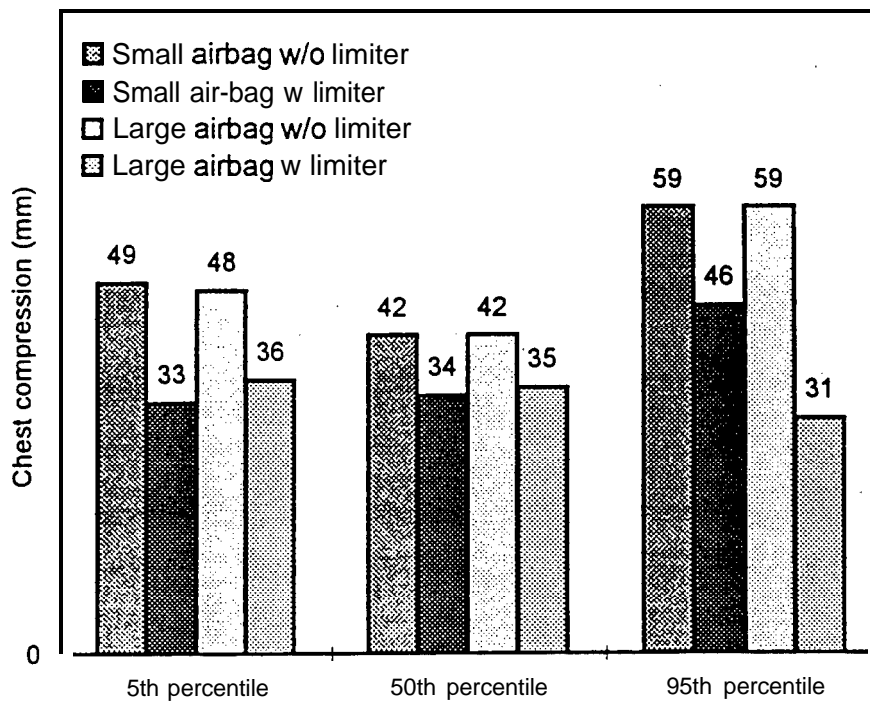


Figure 2.5 Comparison of chest compression with and without load limiters (30 mph).

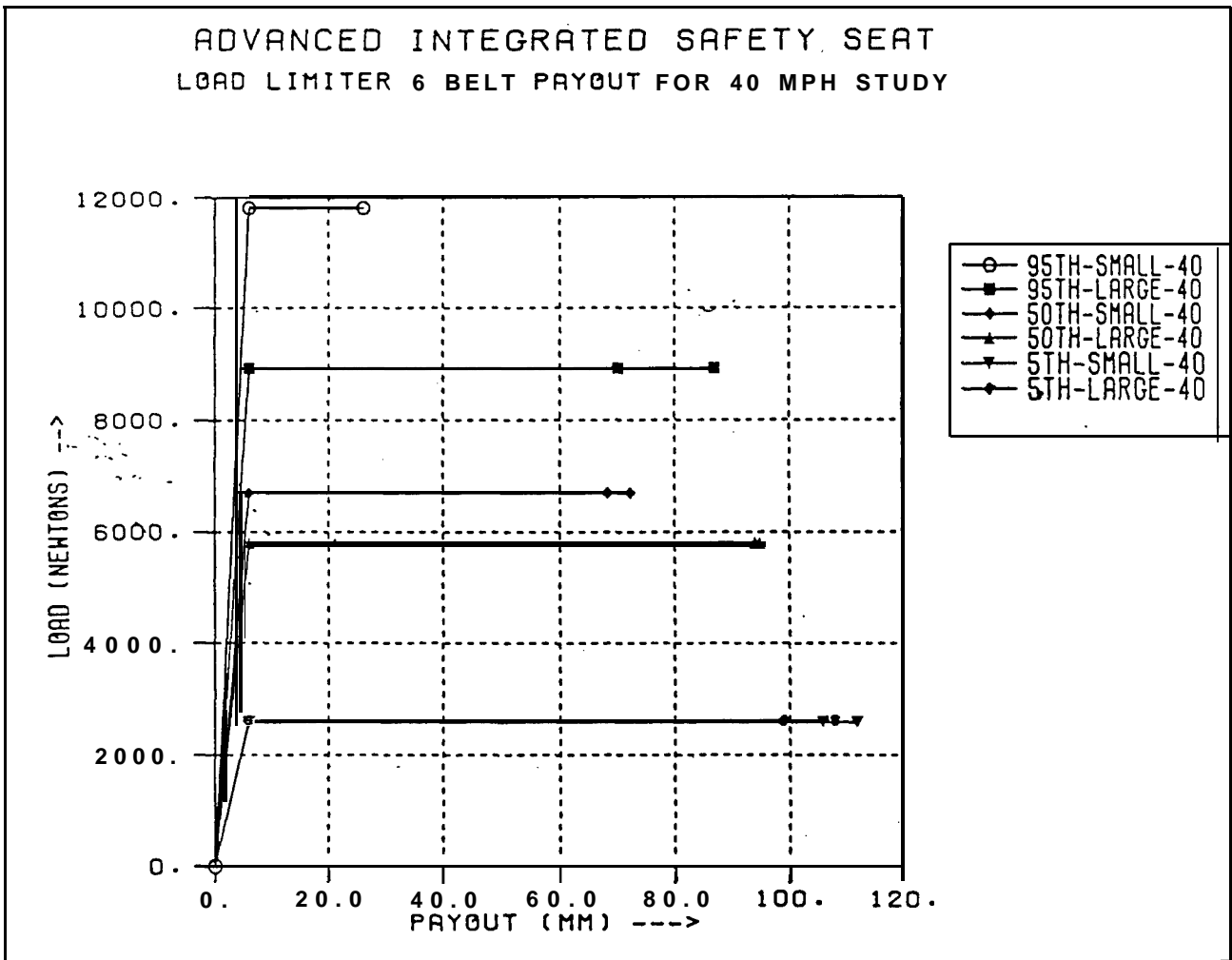


Figure 2.6 Load limiter force and belt payout for 40 mph frontal crash.

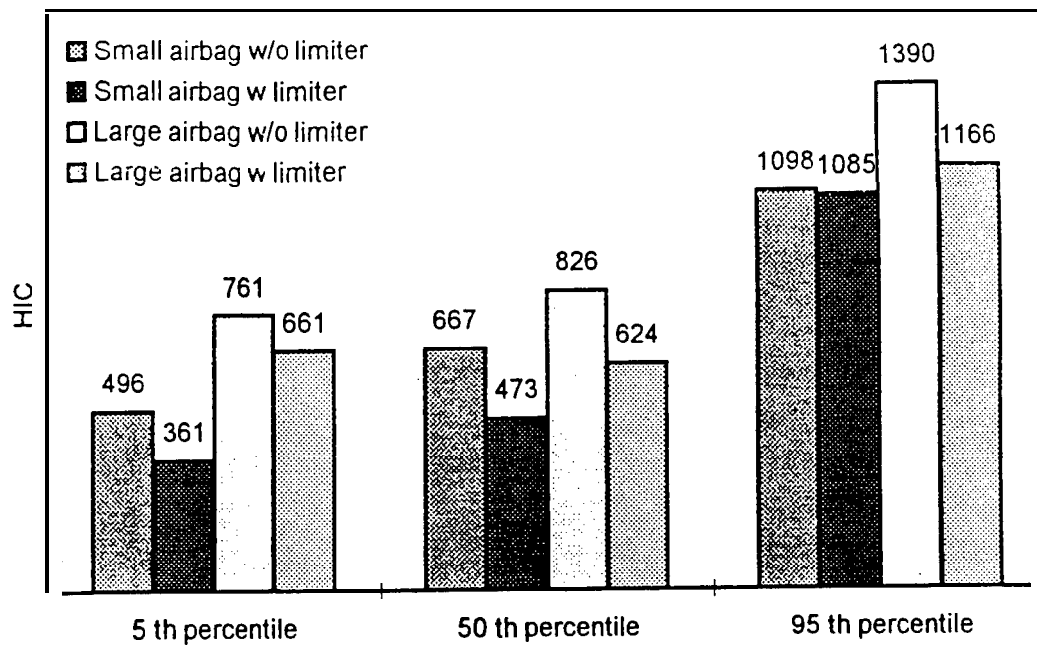


Figure 2.7 Comparison of Head Injury Criteria with and without load limiters (40 mph).

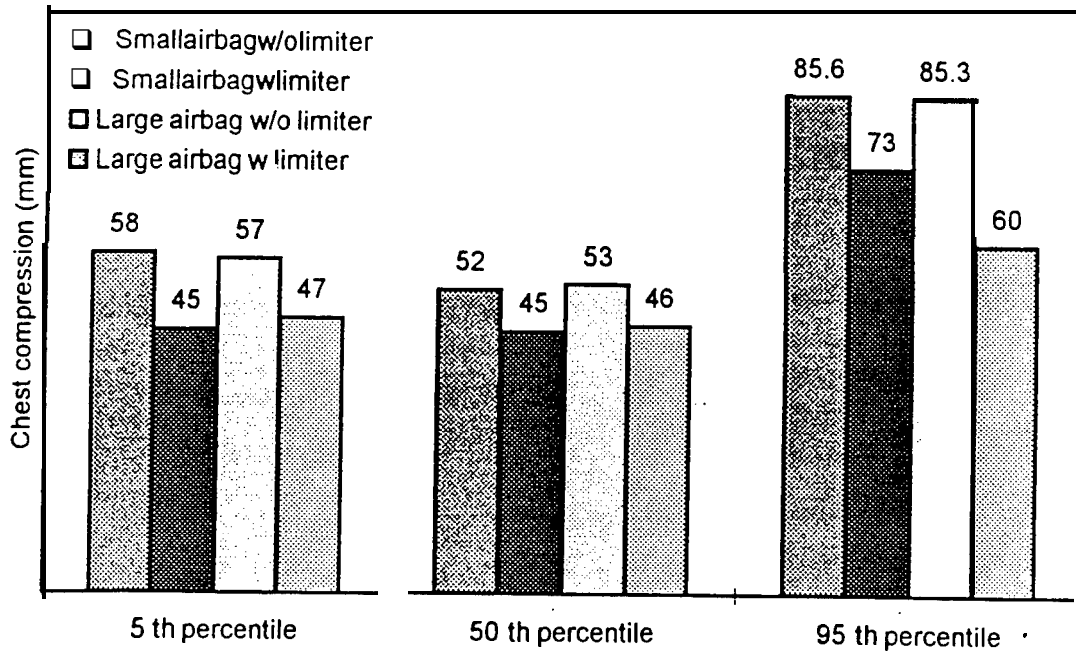


Figure 2.8 Comparison of chest compression with and without load limiters (40 mph).

Table 2.1 Simulation results without load limiter at 30 mph

With Small Airbag @ 30 mph									
	HIC	Head Excursion (mm)	Peak Head Acc. (m/s ²)	3MS (m/s ²)	Neck Load (N)	Left Femur Load (N)	Right Femur Load (N)	Chest Compression (mm)	Shoulder Belt Load (N)
5 th %-ile	279	187	487	448	905	1450	1210	49	4236
50 th %-ile	350	299	477	460	1150	1966	2163	42	7524
95 th %-ile	589	442	634	1142	2679	2019	2401	59	9371

With Large Airbag @ 30 mph									
	HIC	Head Excursion (mm)	Peak Head Acc. (m/s ²)	3MS (m/s ²)	Neck Load (N)	Left Femur Load (N)	Right Femur Load (N)	Chest Compression (mm)	Shoulder Belt Load (N)
5 th %-ile	361	209	559	437	1093	1521	1259	48	4086
50 th %-ile	427	300	538	465	1134	2004	2141	42	7562
95 th %-ile	698	419	650	1136	2555	2006	2422	59	9205

Table 2.2 Simulation results with load limiter at 30 mph

With Small Airbag @ 30 mph with load limiter									
	HIC	Head Excursion (mm)	Peak Head Acc. (m/s ²)	3MS (m/s ²)	Neck Load (N)	Left Femur Load (N)	Right Femur Load (N)	Chest Compression (mm)	Shoulder Belt Load (N)
5 th %-ile	191	251	446	433	599	1117	1127	33	1500
50 th %-ile	171	378	410	494	986	1947	2043	34	3567
95 th %-ile	409	470	570	1185	2218	1923	2231	46	6688

With Large Airbag @ 30 mph with load limiter									
	HIC	Head Excursion (mm)	Peak Head Acc. (m/s ²)	3MS (m/s ²)	Neck Load (N)	Left Femur Load (N)	Right Femur Load (N)	Chest Compression (mm)	Shoulder Belt Load (N)
5 th %-ile	335	235	619	421	758	1131	1127	36	1450
50 th %-ile	279	368	478	500	892	1936	2047	35	3344
95 th %-ile	608	499	596	1245	1766	1863	1972	31	3567

Table 2.3 Simulation results without load limiter at 40 mph

With Small Airbag @ 40 mph									
	HIC	Head Excursion (mm)	Peak Head Acc. (m/s ²)	3MS (m/s ²)	Neck Load (N)	Left Femur Load (N)	Right Femur Load (N)	Chest Compression (mm)	Shoulder Belt Load (N)
5 th %-ile	498	236	598	580	1254	1441	1969	58	5410
50 th %-ile	667	335	690	652	1814	2170	2477	52	9786
95 th %-ile	1098	491	845	1627	3504	3285	3219	73	11867

With Large Airbag @ 40 mph									
	HIC	Head Excursion (mm)	Peak Head Acc. (m/s ²)	3MS (m/s ²)	Neck Load (N)	Left Femur Load (N)	Right Femur Load (N)	Chest Compression (mm)	Shoulder Belt Load (N)
5 th %-ile	761	248	657	572	1528	1398	2001	57	5428
50 th %-ile	826	338	789	658	1855	2170	2479	53	9773
95 th %-ile	1390	478	883	1590	3491	3256	3197	73	11722

Table 2.4 Simulation results with load limiter at 40 mph

With Small Airbag @ 40 mph with load limiter									
	HIC	Head Excursion (mm)	Peak Head Acc. (m/s ²)	3MS (m/s ²)	Neck Load (N)	Left Femur Load (N)	Right Femur Load (N)	Chest Compression (mm)	Shoulder Belt Load (N)
5 th %-ile	361	275	575	562	889	1504	1506	45	2600
50 th %-ile	473	373	605	608	1434	2089	2475	45	6688
95 th %-ile	1085	493	842	1634	3523	3035	3031	73	11808

With Large Airbag @ 40 mph with load limiter									
	HIC	Head Excursion, (mm)	Peak Head Acc. (m/s ²)	3MS (m/s ²)	Neck Load (N)	Left Femur Load(N)	Right Femur Load(N)	Chest Compression (mm)	Shoulder Belt Load (N)
5 th %-ile	661	266	645	550	1075	1494	1398	47	2625
50 th %-ile	624	385	608	594	1338	1968	2477	46	5796
95 th %-ile	1166	498	794	1618	2932	3103	3005	60	8918

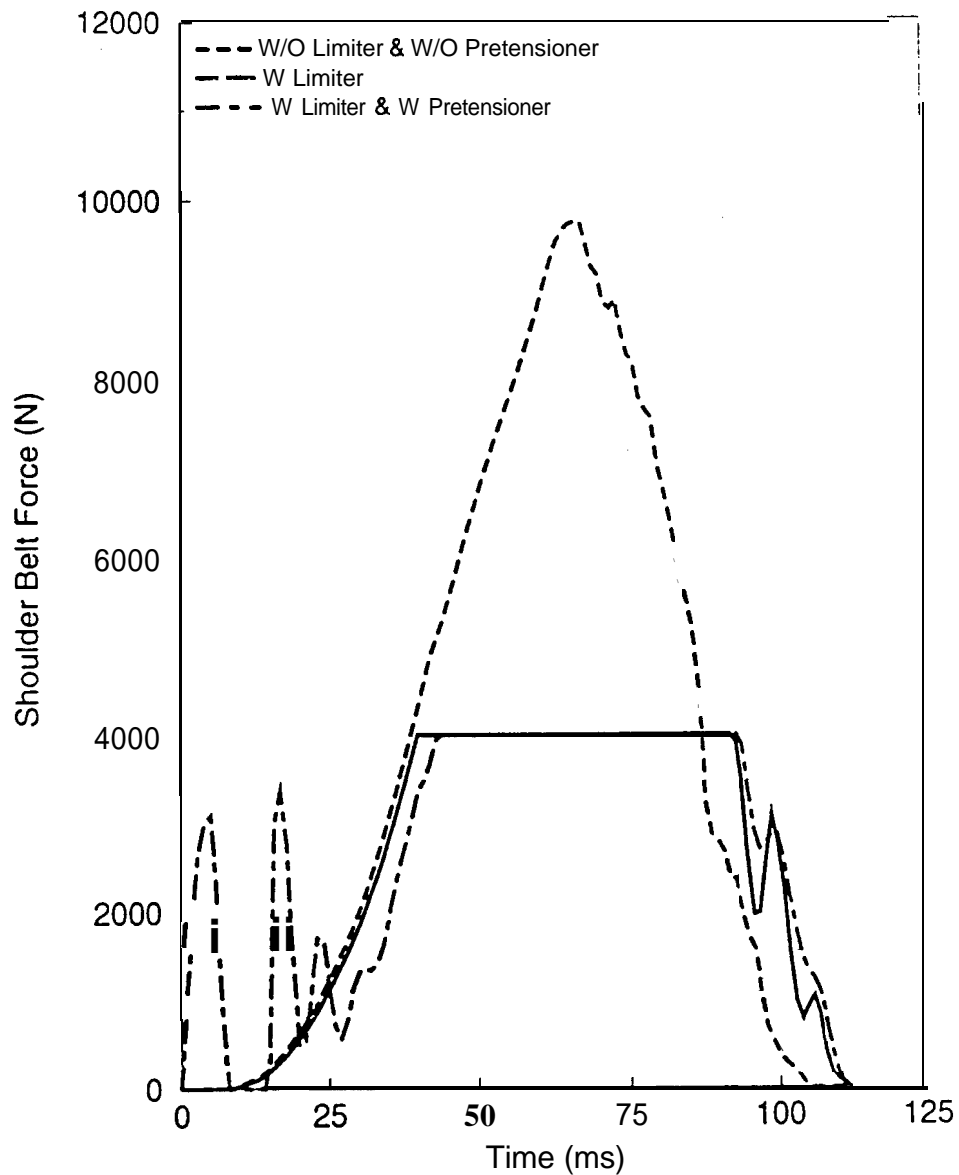


Figure 2.9 Shoulder belt load vs. time for 30 mph.

2.2 Pretensioner

To realize the effectiveness of shoulder belt load limit, belt slack and loose webbing wrap should be minimized. This can be achieved with the device called pretensioner, which takes 'up belt slack early in the collision by pulling on the belt at the buckle or the retractor location. This induces energy absorption during the early forward travel of the occupant in a frontal impact. This is illustrated in Figure 2.9 which compares the shoulder

belt loads vs. time for the cases of : (1) no load limiter, (2) with load limiter and (3) load limiter with pretensioner in 30 mph frontal impact. In this figure the initial spikes are seen at the shoulder level of the belt which may be induced due to the pretensioner effect at the buckle end, friction between the dummy and belt and initial kinematics of the dummy. Figure 2.10 shows the bar chart for injury numbers with and without the pretensioner in the presence of a 4000 N load limiter and a large airbag for a 50th percentile dummy at 30 mph.. More than 10 percent reduction is seen for all the injury parameters, with the resultant chest acceleration (3MS) reducing by 50%.

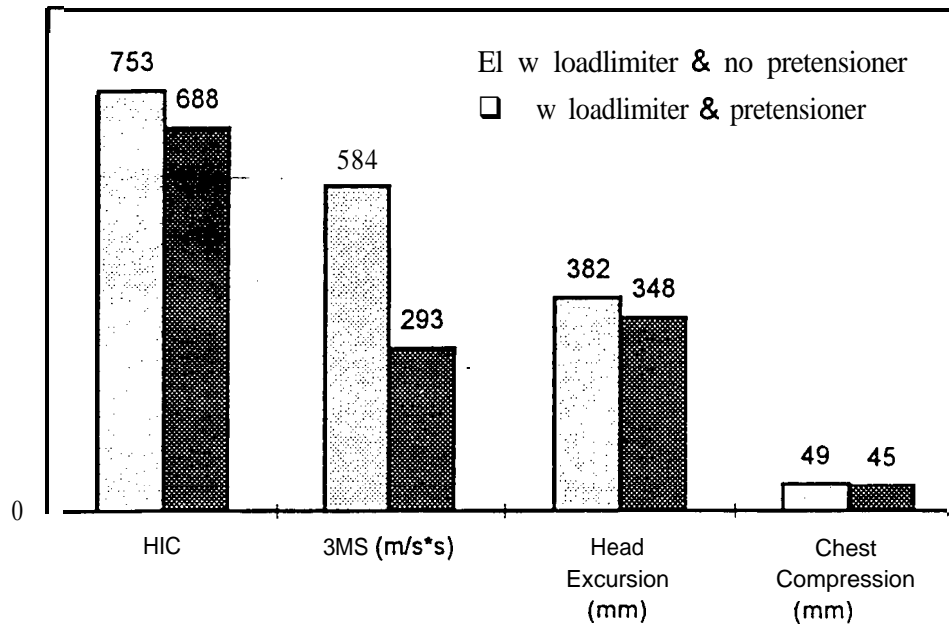


Figure 2.10 Effect of pretensioner on injury parameters (50th percentile dummy at 30 mph).

Work done as part of this study has shown improved occupant protection by the use of pretensioner in rollover crashes. Introduction of belt pretensioner has also been shown to significantly reduce the risk of submarining (Haland et al., 1993). The pretensioner (buckle mounted) helps prevent submarining by reducing the slack (Leung et al., 1982) and by pulling the buckle downwards, which narrows the opening for pelvis to slide through. A buckle mounted seat belt pretensioner with specifications as shown in Table 2.2 is used in this study.

Table 2.2 Specifications for the Belt Pretensioner

Pulling Distance	80 mm
Pulling Time	9.5 msec.
Fulling Force	<1000 N (Depending on Test Set-up)
Operating Temperature	-40°C to 100°C
Weight	450 grams
Type	Pyrotechnic, Buckle Mounted

3. REAR IMPACT PROTECTION

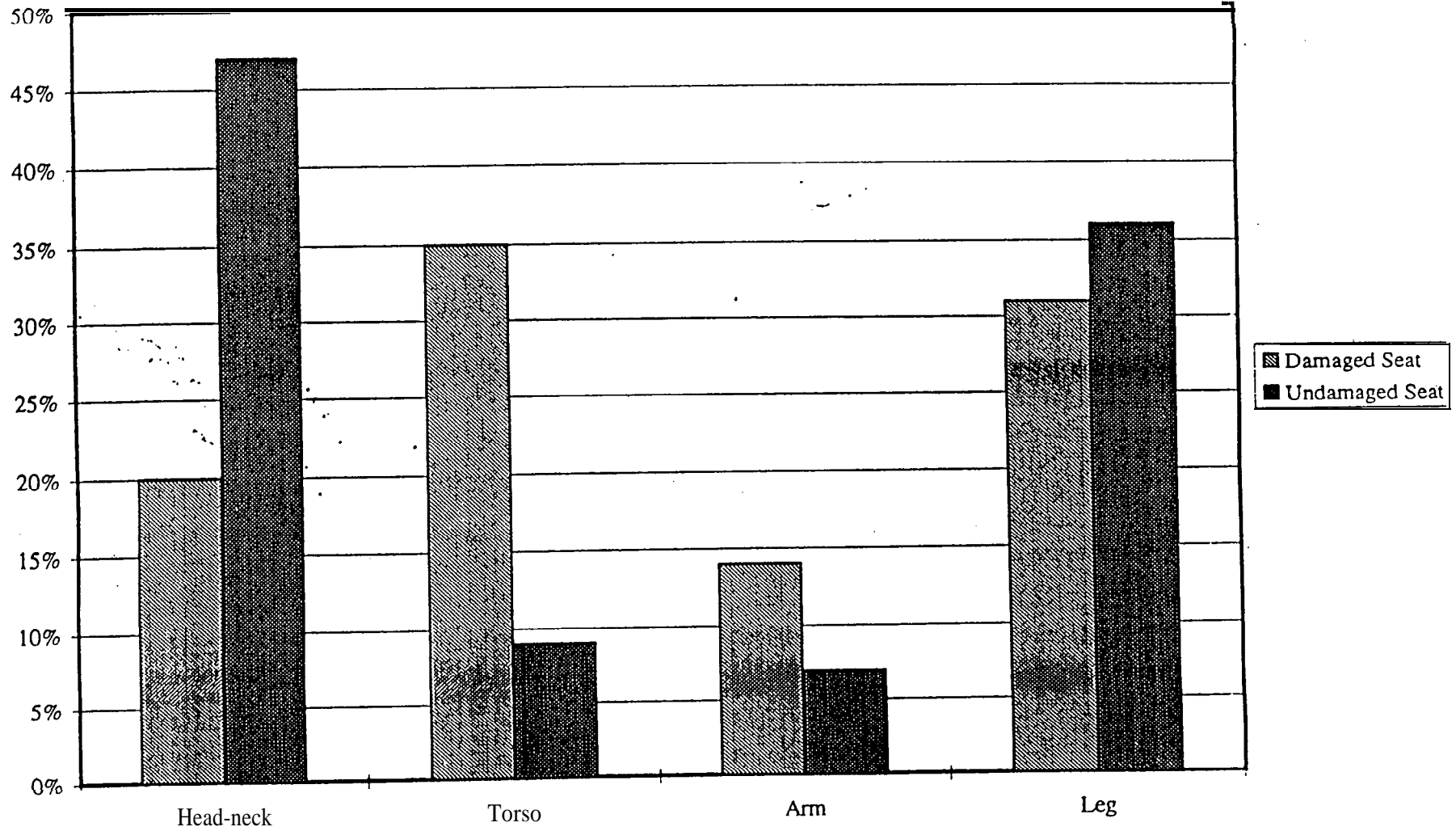
Neck injuries with risk of permanent disability are frequent in low severity rear-end collisions (Carlsson et al., 1985). Studies by Langweider (1981) and Kahane (1982) suggest that of those occupants injured in rear impact accidents 80 to 90 percent suffer neck injury. Figure 3.1 illustrates the nature of body injuries attributed to **frontal** components in rear crashes and Figure 3.2 addresses sources of injuries based on seat conditions for different crash modes. Because such accidents are common, they cause significant human suffering and high societal costs, despite the fact that the injuries are usually classified as “minor” (**AIS 1**) in the Abbreviated Injury Scale (**AIS**) (Nygren, 1984 and Nygren et al., 1985). Analysis of Cooperative Crash Injury Study (CCIS) database (Renouf, 1991) has indicated that 95 percent of neck injuries to **front** seat occupants are recorded as **AIS 1**. The importance of certain seat (particularly seat back) characteristics on rear impact and criteria relevant to minimize the related injuries are discussed below. Seat back bending **stiffness** strongly **influences** occupant response in rear impact. Seat back rotation can be beneficial **from** an energy absorption standpoint. A seat back that collapses without absorbing energy is not desirable. A study on protection against rear end accidents (Thomas et al., 1982) suggests that failure of the seat back or mountings has a greater effect on cervical spine injury than the head restraint. A small number of cases exist where rear seat occupants have been killed by the **front** seat collapsing on to them (Lowne et al., 1987). In an integrated structural seat, large rotation angles will cause greater demands on the shoulder belt in restraining the occupant from sliding backwards. At the same time, excessive rotation will encroach on rear seat occupant space. Therefore a 30 degrees seat back rotation from the design position is selected as the maximum allowable for the 95th percentile dummy under a 30 mph rear impact crash pulse. This seat back rotation angle is consistent with the current industry practice.

In contrast to a seat back that deforms too easily, a rigid seat back may cause occupant rebound (Partyka et al.). The elastic springback energy stored in the seat is sufficient to throw the occupant far enough to hit the steering wheel or the dash. A rigid seat back may also cause the occupant to ramp up, which may lead to partial or complete ejection. Due to ramp up of the occupant, the head may rise above the headrest leaving no support to stop the head from tilting rearward thereby increasing head to neck torque. This leads to “whiplash” related injuries. Seat back design should aim at minimizing occupant ramp up and rebound, and at the same time contain seat back rotation. In this study the maximum seat back rotation was restricted to **30° from** the design position. **Effect** of the various seat characteristics described above, on the occupant, is reflected in the occupant injury numbers, such as HIC, neck extension and **flexion** torque, etc. While a seat needs to address the management of energy transfer to the occupant in severe rear crashes, biomechanical responses need to be below tolerance levels and proportionately lower with decreasing crash severity for overall injury prevention.

Body Region Injuries Attributed to Frontal Components in Rear Crash

Source: S. C. Partyka; Seat Damage & Occupant Injury in Passenger Car Towaway Crashes (1988-1990 NASS Data)

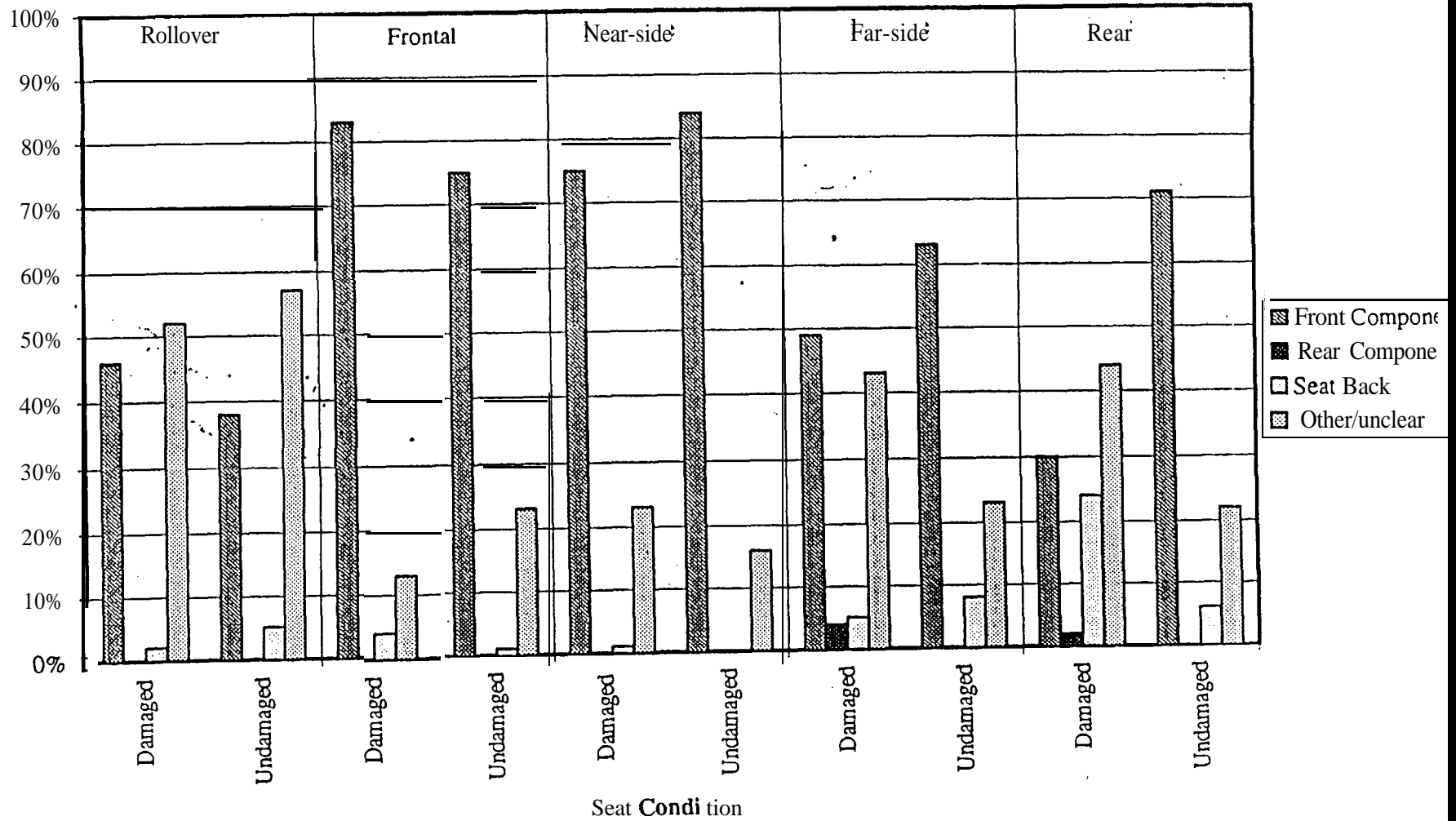
Figure 3.1 Body region injuries attributed to frontal components in rear crash.



Source of Injury For Outboard, Belted Occupant

Source: S. C. Partyka; Seat Damage & Occupant Injury in Passenger Car Towaway Crashes (1988-1990 NASS Data)

Figure 3.2 Source of injury for outboard, belted occupant.



Some form of limited and controlled deformation of the front seats is therefore desirable. In this way energy could be absorbed by the seat, reducing the risk of injury to the front seat occupants, without endangering rear seat occupants. In this study several design features are explored to address the above injuries and to reduce them below the human threshold limit. Table 3.1 relates the design features to the different requirements. The evaluation methodology and the results for various design features are described below.

Table 3.1 Participation of the proposed design features in addressing various rear impact performance criteria

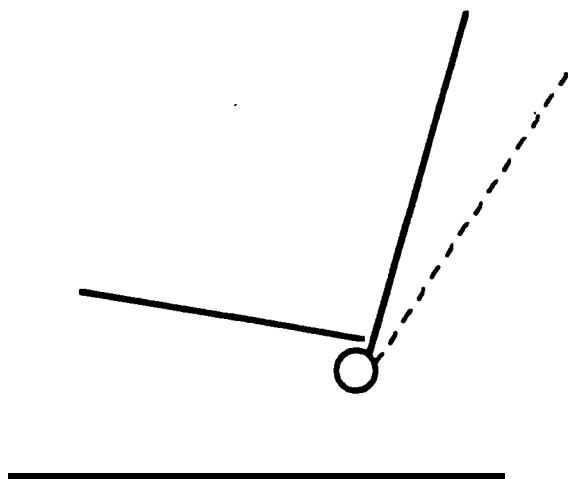
	Dual Recliner	Modified Seat Back	Energy Absorber	Inflatable Headrest	Integrated Seat Belts
Whiplash			X	X	
Excessive Seat Back Deformation	X	X			
Ramp Up			X		X
Rearward Ejection	X	X			X
Excessive Rebound			X	X	

3.1 Effect of Increasing Distance Available for Torso Acceleration

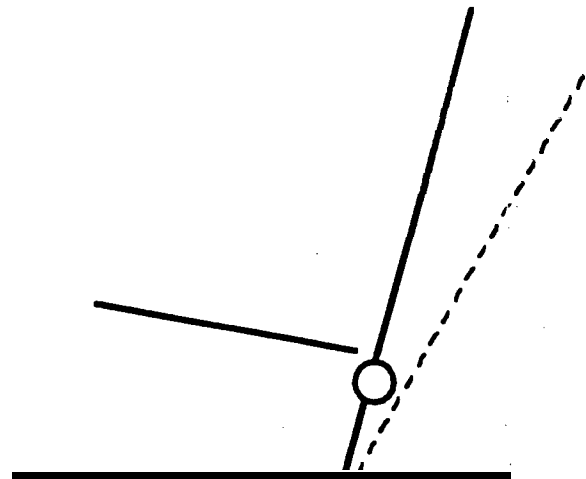
The effect of a crash pulse on an occupant can be mitigated by increasing the available “ride down” distance, i.e. to decelerate the body in the case of frontal crash, or accelerate the body in the case of side impact or rear impact. Two different design concepts are developed in order to accelerate the torso over a larger distance under rear impact conditions. These two concepts are illustrated in Figure 3.3.

The first concept involves lowering the effective center of rotation of the seat back. This may be effected by designing a “plastic hinge” for the seat back close to the floor. This hinge essentially lowers the effective center of rotation of the seat back. It may be designed to occur below the existing recliner as shown in the figure, or at a lowered recliner position. The lowered hinge increases the available distance for the lower torso to accelerate, thereby reducing peak forces and accelerations. An added benefit of a lowered recliner is that, according to recent research at Johnson Controls, it is more comfortable for an occupant while adjusting the reclining angle of the seat because the effective center of rotation of the upper torso has been found to be well below the seat plane.

The second concept involves a sliding seat. This design would also increase the distance available for the torso to accelerate forward. The seat would be restrained by an appropriate mechanical device. Possible options would be honeycomb, crushable foam, or a metal draw bead. Thus the seat motion itself would dissipate energy.

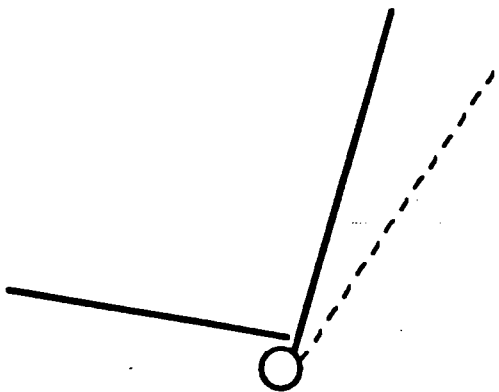


Standard seat

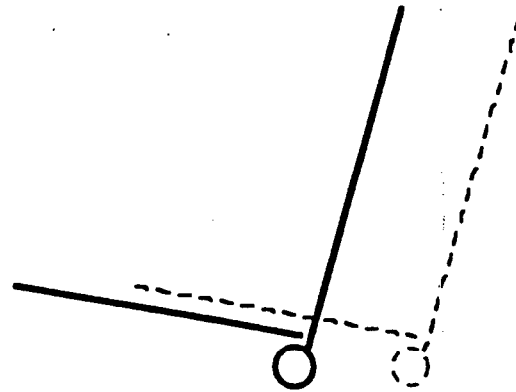


Lowered plastic hinge

Lowered effective center of rotation of seatback increases lower torso travel for a given amount of seat back excursion. Lower torso and shoulder loads are reduced.



Standard seat



Sliding seat

Sliding seat increases deceleration distance for lower torso. Seat loads are reduced.

Figure 3.3 Design concepts for increasing torso travel.

Both these concepts were analyzed using MADYMO simulation. The results are summarized in Table 3.2. Both concepts do lead to a reduction in peak force values. However one serious objection that might be raised with these seats is that the moving seat back may injure the lower extremities of rear seat occupants. Another is that it would be difficult to lower the pivot due to space restrictions imposed by the seat track. Therefore these two concepts are not considered to be universally adaptable.

Table 3.2 Effect of lowered pivot seat and sliding seat

Seat Type	MC	3MS (m/s ²)	Lower torso contact force (N)	Shoulder contact force (N)
Standard	116	192	9692	4932
Low Pivot	133	210	6760	4418
Sliding seat	40 -	144	7905	3662

3.2 Seat Back Structure

Torsional resistance of the seat back was considered as part of this project. A second recliner was added to the inboard side of the existing seat to consider the effect of that configuration on torsional rigidity. The existing baseline seat design has a single linear recliner on the outboard side and shows twisting in 30 mph rear crash. The analytical models used to evaluate the existing seat with and without dual recliners are described below.

To study the performance of the existing seat in rear impact, a nominal static design load that the seat must withstand is first estimated from a series of MADYMO simulations. The seat back is modeled in MADYMO as a pivoted structure which is restrained by a resistive torque function. The pivot is located at the recliner position. The torque function at the pivot defines the elasto-plastic bending **stiffness** characteristic of the seat back. Figure 3.4 shows the MADYMO model and crash sequence in rear crash for a 50th percentile occupant. Similar models were developed incorporating the 95th percentile and 5th percentile Hybrid-III dummy models. A 30 mph rear impact crash pulse is used in the model. This pulse (Figure 3.5) is obtained from a FMVSS 301 (fuel integrity) moving barrier crash test at 30 mph. The resulting change in velocity of the struck vehicle is 20 mph.

A series of MADYMO simulations with different seat back **stiffness** characteristics were performed until satisfactory response, meeting the criterion of a **maximum seat back** rotation of 30 degrees for the 95th percentile dummy is achieved. Figure 3.6 shows the torque vs. seat back rotation characteristic for the seat back that produces the desired maximum seat back rotations shown in Table 3.3.

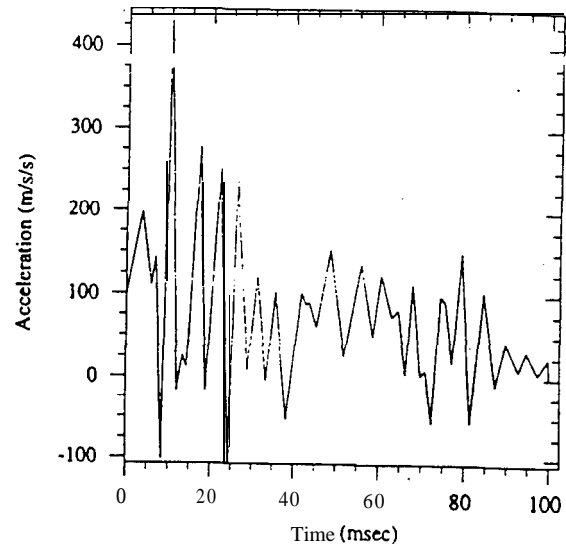
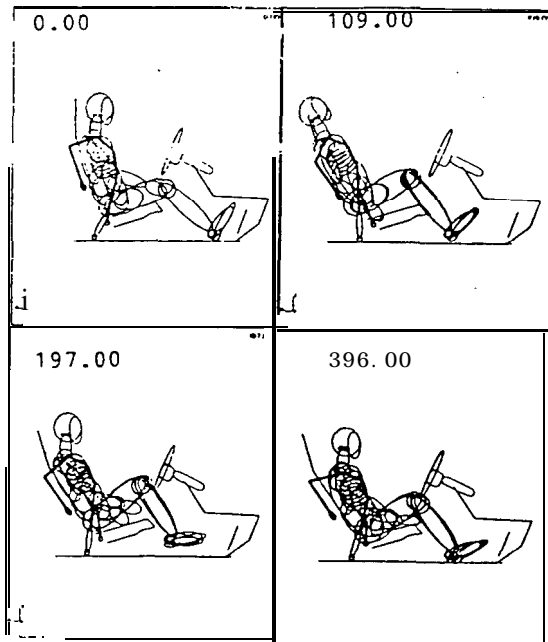


Figure 3.4 Crash sequence in rear impact. **Figure 3.5** Acceleration pulse.

Table 3.3 Maximum seat back angle with respect to the seat bottom
(Initial seat back angle = 23°)

	5 th percentile	50 th percentile	95 th percentile
Rotation of the seat back	10°	22°	29°
Peak seat back angle (wrt. vertical)	33°	45°	52°

Equivalent torque applied to a finite element model of the existing seat produces a seat back twist of approximately 15". A 17" rotation is seen using a LSDYNA/MADYMO coupled model for a 95th percentile dummy in 30 mph rear crash. This rotation is decreased to 3 degrees for the modified seat with a second recliner added on the inboard side

3.3 Recliner With Energy Absorber

Occupant rebound and ramp up can be minimized by designing a seat back that deforms plastically in a controlled manner. Rebound is caused primarily by the elastic energy stored in the seat back during rearward deformation, which is imparted to the

occupant during the forward travel. In order to obtain the necessary compliance in the rearward direction a mechanical energy absorbing element was added in series to both the recliners on either side of the seat.

The design of this device (described later) is such so as to **modify** the torque vs. angle function of the seat back to approximate the desired curve originally obtained from the MADYMO model (Figure 3.6). It should be noted that the torque-theta curve has a very sharp rise followed by a relatively flat region. Upon unloading at any point along the curve, the drop in force is also very sharp. This implies that the amount of elastic energy stored in the seat back is very small compared to the amount of energy absorbed by the energy absorber. A typical existing seat back would have a torque-theta curve which has a much lower initial slope. This translates to a higher proportion of stored spring back energy compared to the dissipated energy. The difference between these two cases is illustrated in Figure 3.7.

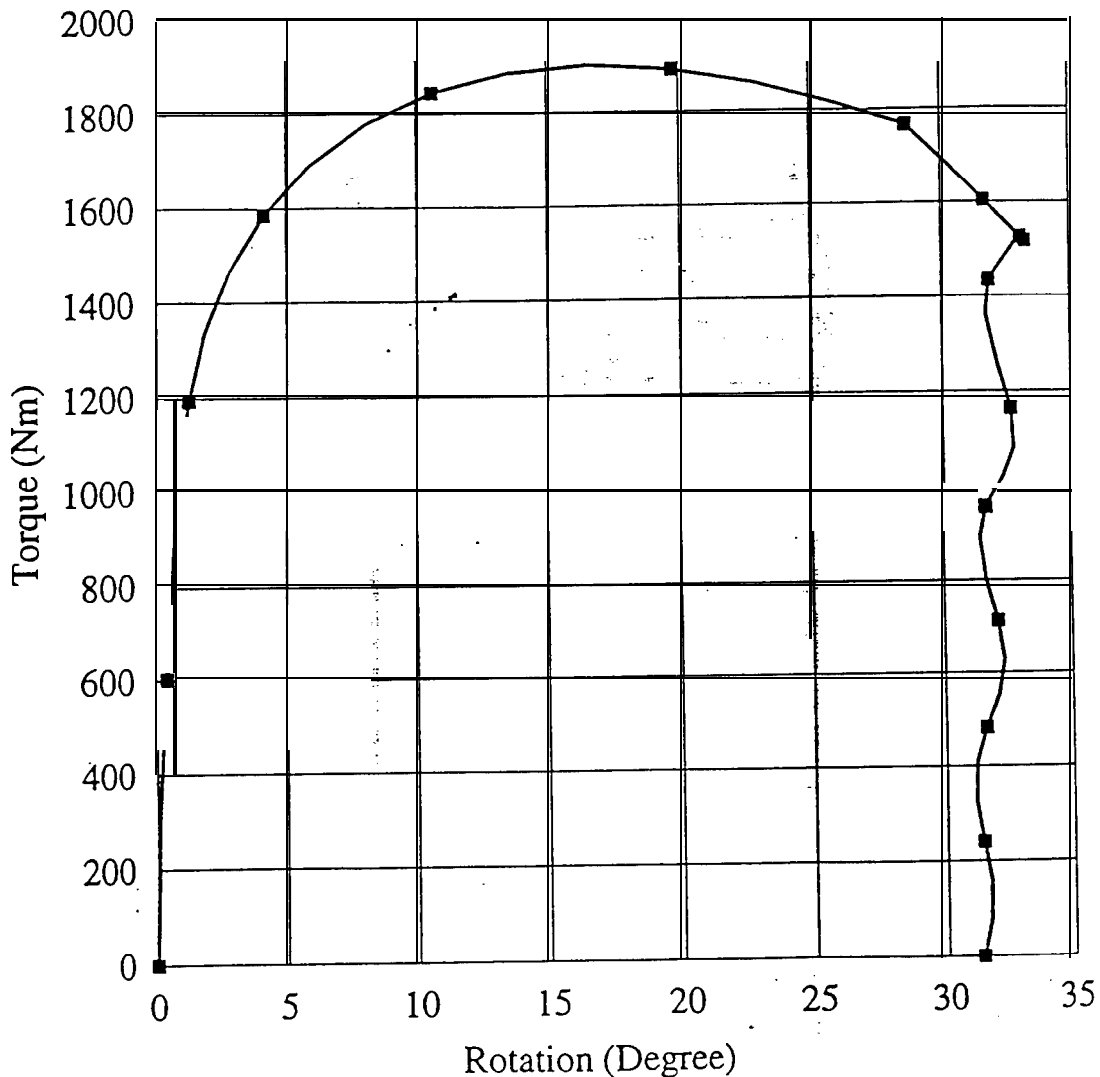


Figure 3.6 Torque vs. rotation curve for the seat back

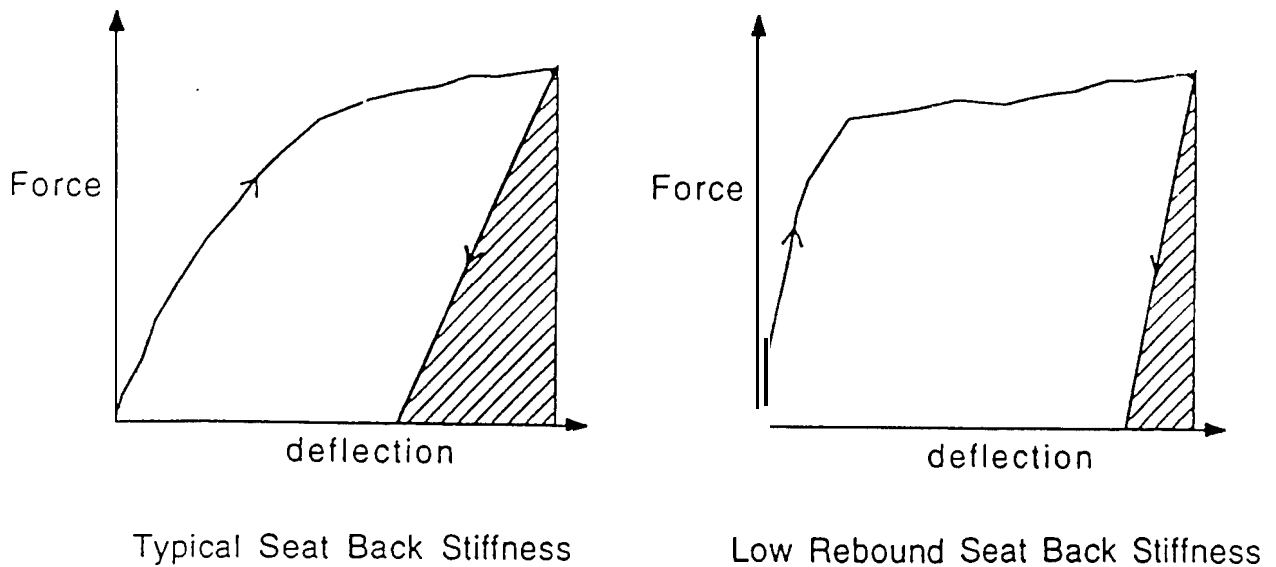


Figure 3.7 Energy absorption of a typical seat back and low rebound seat.

In order to quantify the amount of forward excursion due to seat rebound, a series of MADYMO simulations were performed with and without seat back rebound. This was implemented in the MADYMO model by changing the hysteresis slope of the torque-theta curve of the seat back joint stiffness. The scaled seat back stiffness curve was used. Table 3.4 shows a comprehensive table of results for all three dummies with and without seat back rebound. In Table 3.4 it can be seen that the force on the shoulder belt is the same for the cases with and without rebound of the seat back for the 50th percentile occupant. This is due to the “ramp up” effect of the occupant in the rigid no rebound seat.

Figure 3.8 summarizes some of the results, and graphically illustrates how the forward excursion of the 50th percentile dummy is affected by rebound as a function of rear impact velocity. Head excursion is defined as the distance of the head from the initial pre-impact position to the forward most rebound position. Shoulder belt loads were also recorded to see the effect of any ramp up of the occupant with and without the rebound.

To check the performance of the modified design in frontal impact, a non-linear finite element analysis is performed to simulate a 4,000 N load limited shoulder belt load for a frontal crash. The seat withstands this loading condition very well. The seat back rotation than is less than 5”.

Table 3.4 Effect of seat back rebound.

	5%-ile (w rebound)	5 %-ile (w/o rebound)	50 %-ile (w rebound)	50 %-ile (w/o rebound)	95 %-ile (w rebound)	95 %-ile (w/o rebound)
DISPLACEMENT (M)						
Chest compression	.0047	.0022	.0110	.0113	.0129	.0063
Head excursion	.1534	.0061	.1432	-.0580	.1059	-.1661
Left shoulder	.1955	.1760	.2440	.2440	.3203	.3197
Left seat corner	.1080	.1088	.1750	.1754	.2283	.2273
ACCELERATION (M/S²)						
Lower Torso	280	273	228	228	227	228
Chest	670	672	324	324	825	823
Head	364	372	485	485	457	462
FORCE (N)						
St. back-lower torso	5325	5184	5621	5621	8633	8615
St. back-left shoulder	458	440	205	161	577	584
St.back-right shoulder	444	424	194	167	521	528
Shoulder belt	2559	1774	1939	1939	1785	1203
FLEXION TORQUE (N.M)						
Head-neck	25	23	33	26	3	4 3 4
CONSTRAINT FORCE (N)						
On head from neck	769	797	1075	1075	1239	1153
On neck from upper torso	722	738	1340	1340	1300	1213
INJURY						
GMS (m/s ²)	563	562	200	200	663	670
HIC	91	82	152	149	98	99
ANGLE (DEGREES)						
Seat back angle w.r.t. vertical (initial=23°)	33	33	40	40	45	45

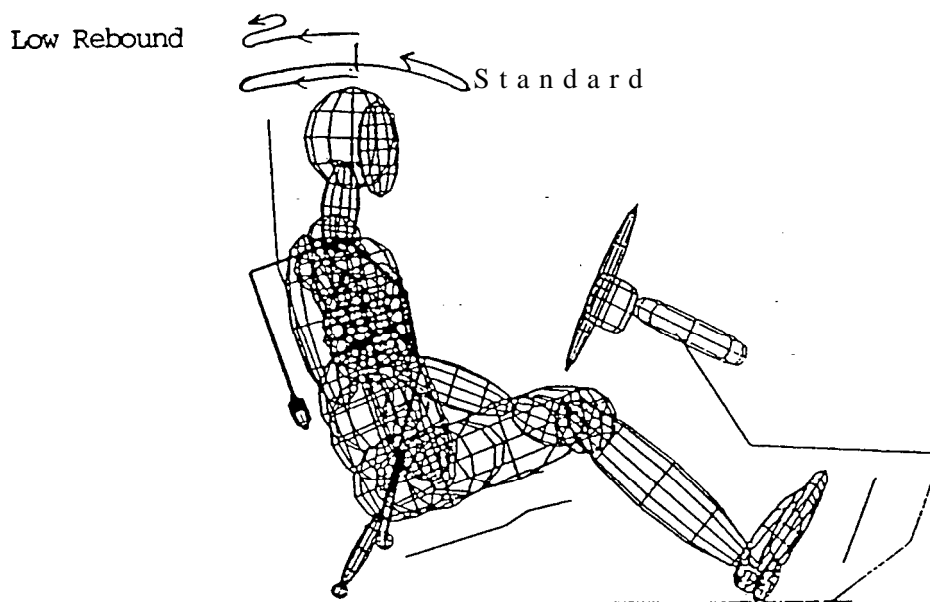
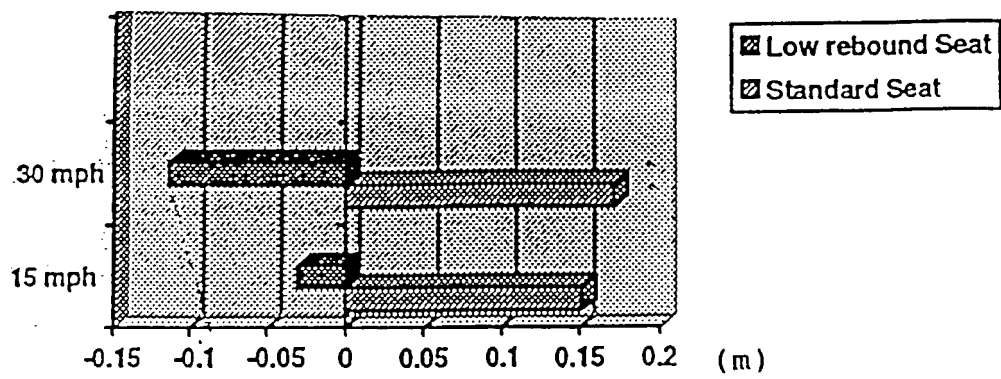


Figure 3.8 Head excursion due to seat back rebound.

3.3.1 Design for Energy Absorber (EA)

This section describes the development of an energy absorbing recliner which serves the purpose of deforming the seat back in a controlled manner. The energy absorber is expected to deform by about 50 mm to produce the desired amount of rotation (maximum of 30°) of the seat back. Design evolved in this study utilizes the support plates of the existing recliner with appropriate modifications. The energy absorption is primarily achieved by the deformation of metal as the recliner pin traverses down a tapered slot created in the supporting metal plates.

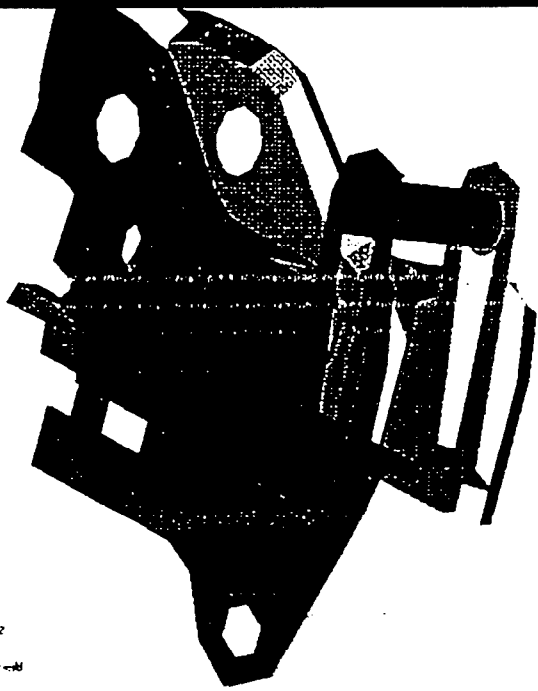
For modeling purposes, a portion of the seat is cut to isolate the recliner and the surrounding area. Tapering slots are created in the recliner support plates. The recliner diameter is 15 mm and it drives down the metal slots which decrease in width from 90% of recliner diameter (at the top) to 40% (at the bottom). About 50 mm of crush space is made available. Since slot width is smaller than the diameter of recliner, resistance is offered by the slot as recliner tries to drive down through it. Metal deformation occurs in the process and energy is absorbed. The recliner is assumed rigid for this purpose. The basic layout of the modified recliner and the existing recliner is shown in Figure 3.9.

A mechanical device is added to the energy absorber to (1) avoid activation of shearing mechanism for low speed crashes and (2) to avoid rattling which would occur if there were no firm support to the recliner. The force-displacement curve for this metal element 1 mm thick is shown in Figure 3.10. A sharp increase in the strength can be noticed during the initial part of the simulation. This would prevent the activation of the energy absorber at low speed crashes.

The energy absorber design is developed and tested using a very refined finite element model of the recliner support plates and the surrounding areas. Due to a very small time step of this refined model, analyzing a full seat model is computationally very expensive. Hence, the seat structure represented by beam elements and the dummy by lumped masses, is attached to the refined recliner model. Once the design for the energy absorber was finalized, it was further tested using a LS-DYNA3D/MADYMO coupling method described below.

3.3.2 Design Verification for Rear Impact

The various design features for rear impact protection were finally tested using a detailed model. A detailed finite element seat model, incorporating the Dual Recliner, Modified Seat Back and the Energy Absorber, is coupled with the MADYMO model of the 50th percentile Hybrid III dummy. The dummy model used had been enhanced by EASi for greater biofidelity. The hip joint had been released. The neck to upper torso joint stiffness had been modified to represent the rearward extension of the neck (Kolita et



2
1-4

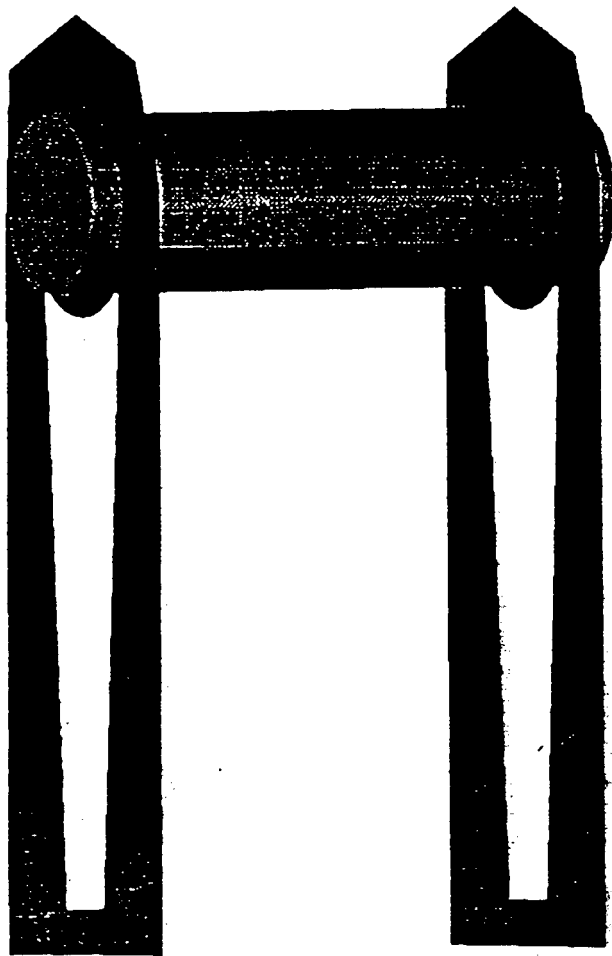


Figure 3.9 Layout of modified recliner.

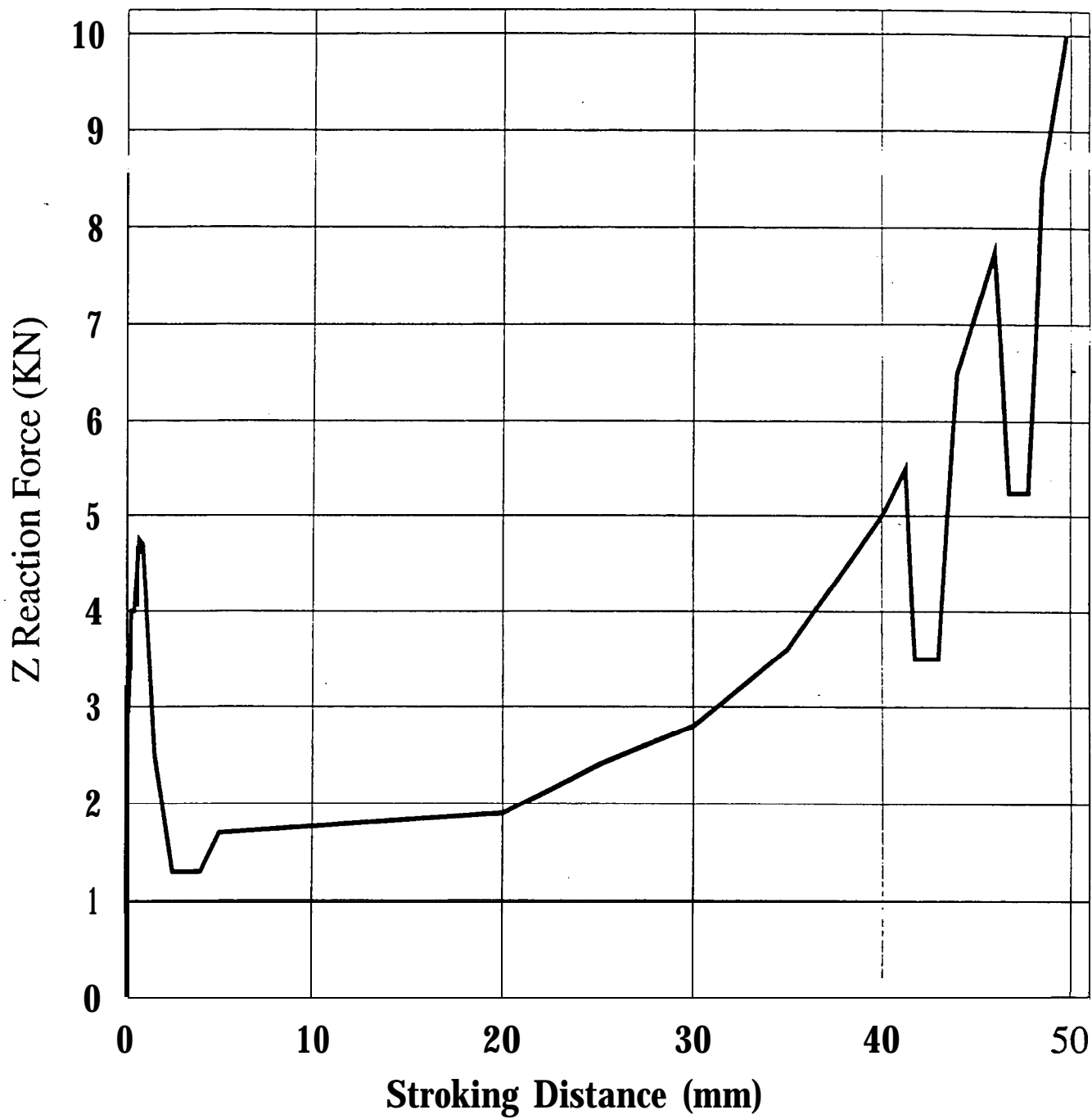


Figure 3.10 Force-displacement curve with the metal element.

al.). The characteristics for the EA are obtained from the detailed EA model and represented in the full seat model as a spring element, in series with the recliner.

The coupled simulation was carried out for 200 msec. with the same rear impact crash pulse as used in the MADYMO study (Figure 3.5). Figure 3.11 shows the set up for the coupled simulation. The results are presented in Table 3.5. Table 3.5 lists the results for the 5th, 50th and 95th percentile dummy obtained from the MADYMO models. The table also lists the results for the 50th percentile dummy obtained using the LSDYNA/MADYMO coupled model. The coupled model has a finite element representation of the seat structure, which is more accurate compared to the rigid body assumptions of the MADYMO model. Table 3.5 also lists the human tolerance values for some of the injury parameters. The injury numbers for the AISS design are well below the human tolerance levels. The injury parameters are compared with the human tolerance values. The final design was also tested for the 5th and the 95th percentile dummies using a MADYMO simulation. These results are reported in Table 3.5 and compared with the human tolerance values.

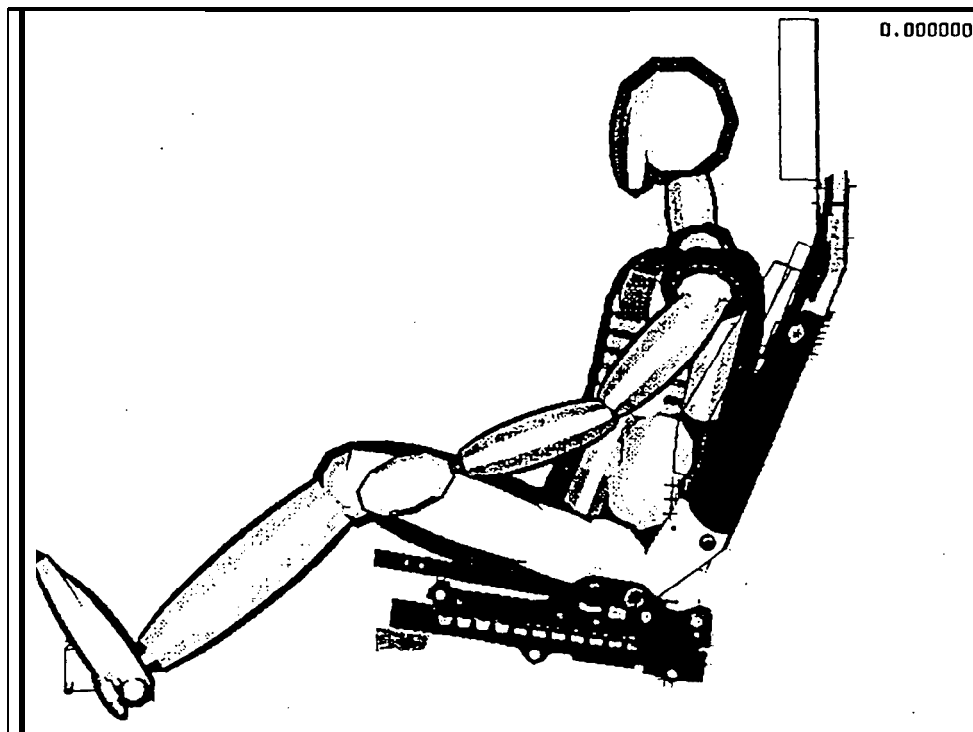


Figure 3.11 Model setup for the coupled simulation.

Table 3.5 Injury numbers for 5th, 50th and 95th percentile dummy models.

	50th %-ile Coupled LSDYNA- MADYMO	Tolerance Levels	5 %-ile MADYMO	50 %-ile MADYMO	95 %-ile MADYMO
DISPLACEMENT (M)					
Chest compression	0.0016	0.0760*	0.0011	0.0087	0.0074
Head excursion			-0.0858	-0.1531	-0.2299
Left shoulder			0.2143	0.2908	0.3409
Left seat corner			0.1506	0.2156	0.2377
ACCELERATION (M/S²)					
Lower Torso	173		289	210	275
Chest	155		175	242	261
Head	248		343	612	620
FORCE (N)					
St. back-lower torso			5648	5863	10824
St. back-left shoulder			444	110	543
St. back-right shoulder			426	115	554
Shoulder belt			891	1352	1330
FLEXION TORQUE (N.M)					
Head-neck	10	60*	27	24	17
CONSTRAINT FORCE (N)					
On head from neck	258		791	1071	1179
On neck from upper torso	338		736	1159	1228
INJURY					
3 MS (m/s ²)	94	588	167	220	223
HIC		1000	43	259	240
ANGLE (DEGREES)					
Seat back angle w.r.t. vertical (initial=23°)	43		37.6	44	46

* Armenia-Cope et al., 1993.

3.4 Inflatable Head Rest

Proper support to the head and neck region during a rear impact can minimize the severity of injury to these regions (Status Report, 1995). Also to be taken into account is the comfort and visibility issues that go with the head-neck support. One of the headrest concepts which helps reduce the severity of injury to the head-neck region is the Catcher's Mitt, which is a reactive system that operates on the pressure **from** the occupants back to force the headrest forward. This system may indeed reduce the whiplash effects by keeping the headrest close to the head, but if the force of the forward motion of the headrest is not substantially controlled, the possibility of an impact to the head is very high. Another concept which was looked at during the course of this project is the use of a non pyrotechnic (compressed gas) inflatable headrest. The idea **is** to inflate a small bag during the heads forward motion, so as to give a pillow effect to the head on its return towards the headrest.

A **MADYMO** model was used to study the inflatable headrest concept. A baseline model was developed based on a Ford Taurus and a JCI seat from the blue prints. The position of the headrest was modeled in accordance with the blueprints provided by JCI, the headrest section of the blueprint and the **MADYMO** headrest section of the model are shown in Figures 3.12 and 3.13. For this study three types of **FE airbags** were used with varying inflator parameters and bag shapes. The three types of bags are shown in Figure 3.14. The response of the occupant with the use of these bags were studied by varying different characteristics of the bag, namely the shape, inflator jet angle, inflator jet diameter and the trigger time of inflation.

Simulations were first performed using a 50th percentile Hybrid III dummy for a 30 mph rear impact. Optimum time of triggering was found to be 25 milliseconds for the cushioning effect of the head. Figures 3.15 through 3.18 show the response of the occupant with the different parametric changes made to the three types of bags. It can be observed that the shape of the bag the gas jet direction and inflator size helps reduce or increase the aggressivity of the bag. From these figures it can be seen that the best inflatable headrest was the type 3 with an inflator jet angle of 45 degrees and a jet diameter of 5 mm. Figures 3.19 through 3.22 show the response of the occupant and the injury numbers with the best parameter for the three types of bags and compared with the baseline case where there was no inflatable headrest. It can be observed that inflatable headrest helps reduce the head excursion and acceleration and reduces the extension torque, which is one of the influencing factors of the whiplash syndrome. Simulation results of the occupant kinematics are shown in Figures 3.23 through 3.26.

Simulations were then performed with the same 50th percentile Hybrid III dummy for a 5 mph rear impact, For this set of simulations based on the 30 mph case, the optimum trigger time was set at 25 ms and the type 3 bag was used. Figures 3.27 and 3.28 show the occupant response, for the baseline and with inflatable headrest simulations, from both the 30 mph and 5 mph rear impact simulations. Figures 3.29 and 3.30 show the trajectory

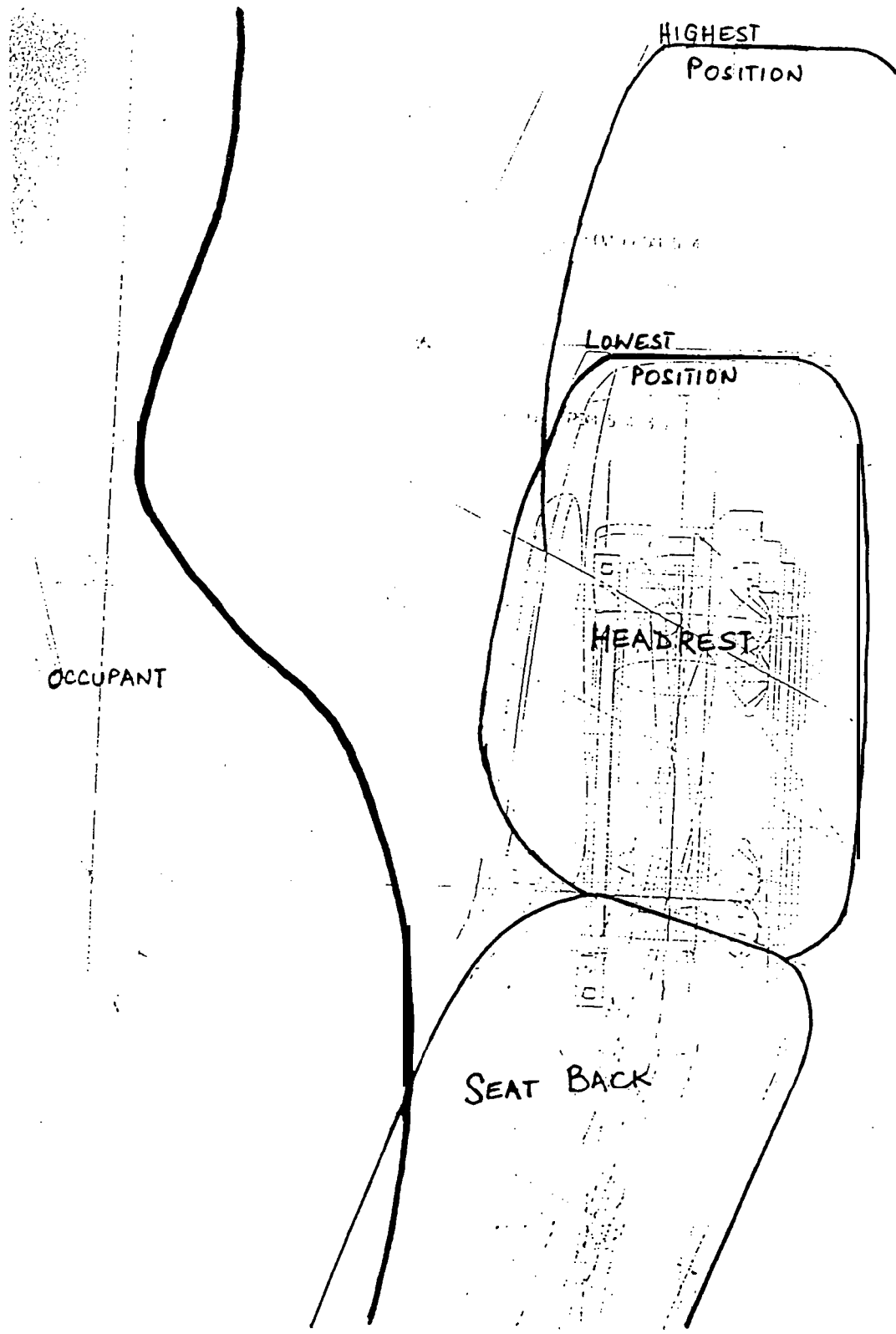


Figure 3.12 Headrest positions from blueprint (courtesy JCI).

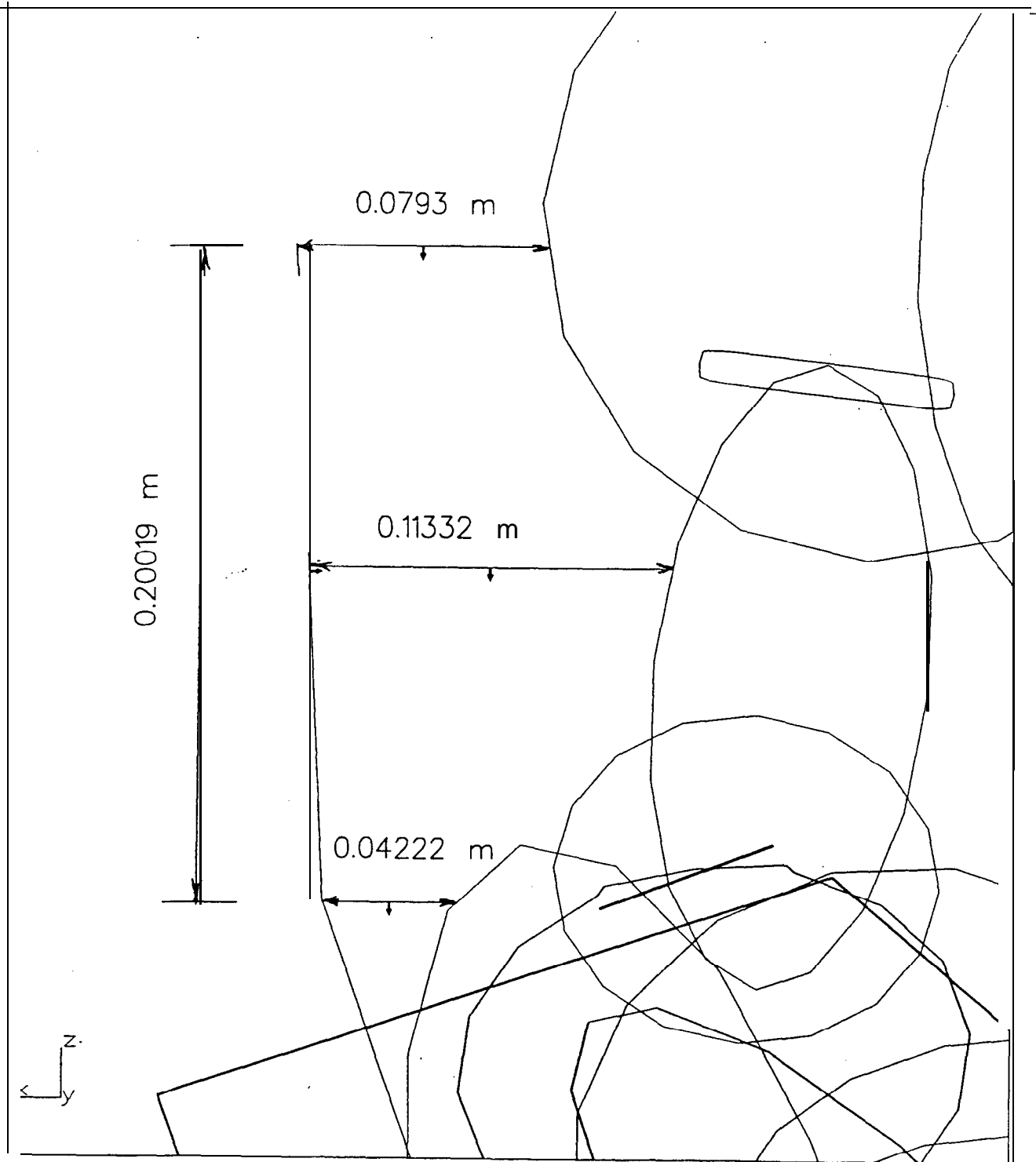


Figure 3.13 MADYMO model setup with headrest.

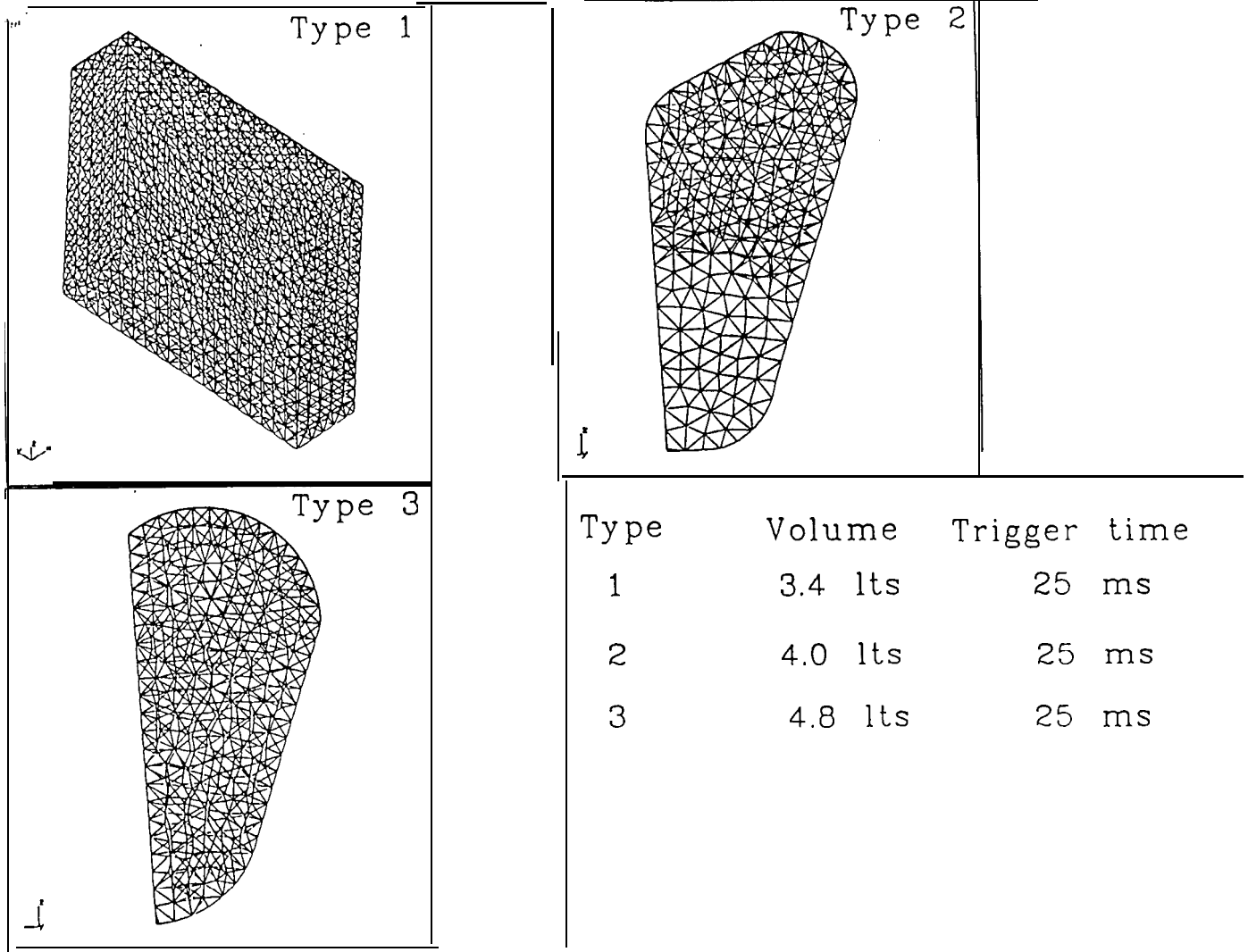


Figure 3.14 Types of inflatable headrest studied.

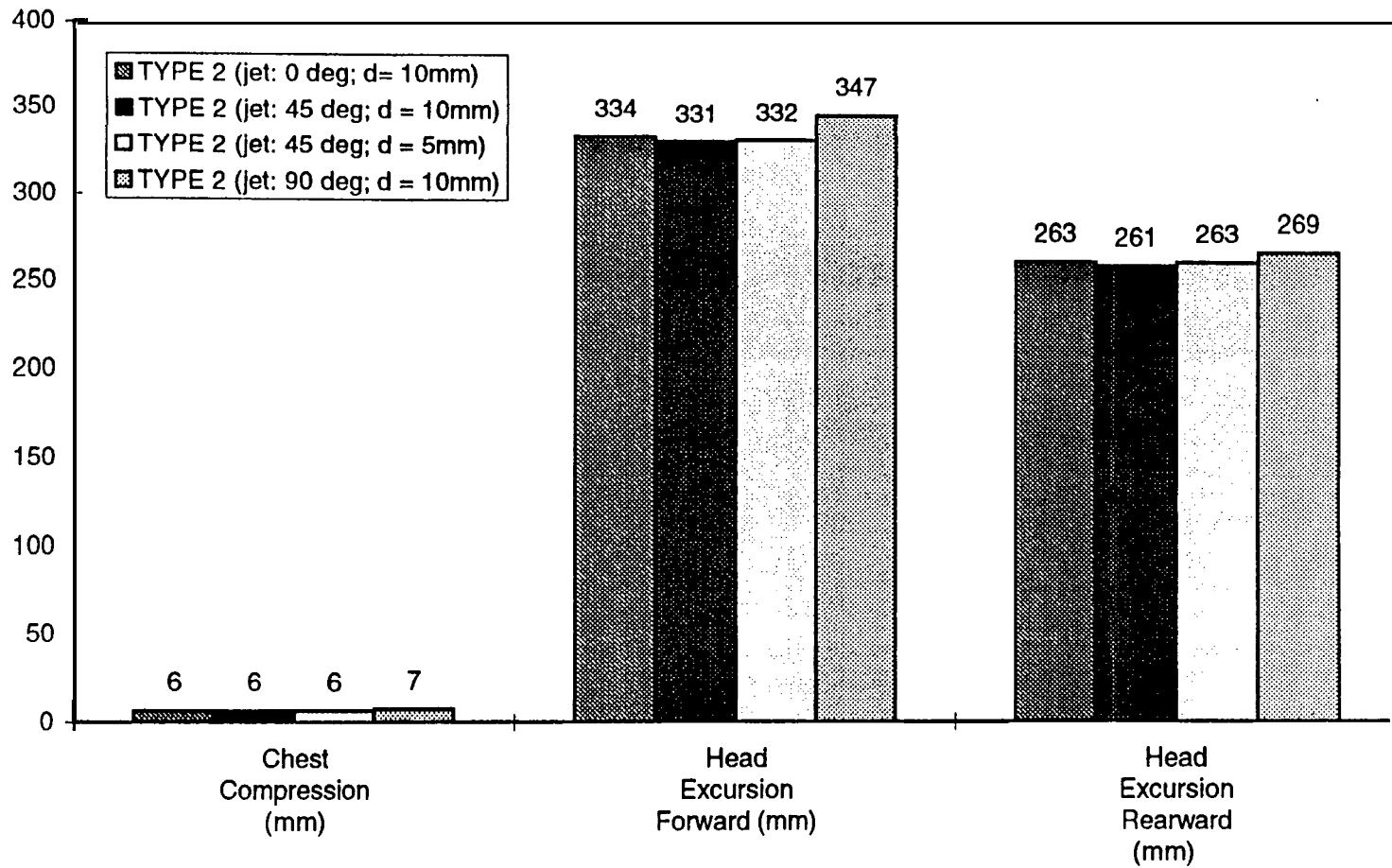


Figure 3.15 Occupant response using Type 2 inflatable headrest (30 mph rear impact).

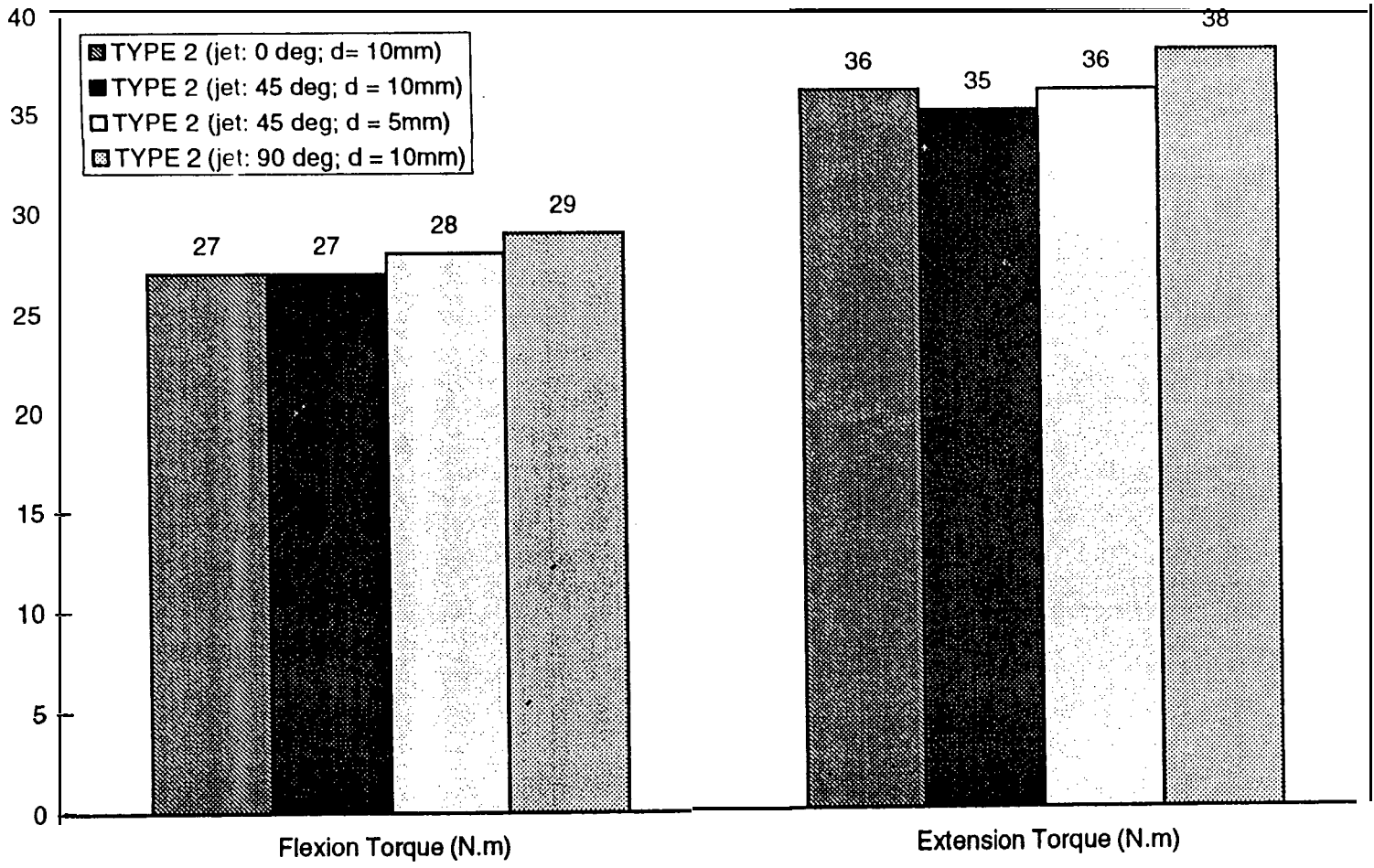


Figure 3.16 Occupant neck response using Type 2 inflatable headrest (30 mph rear impact),

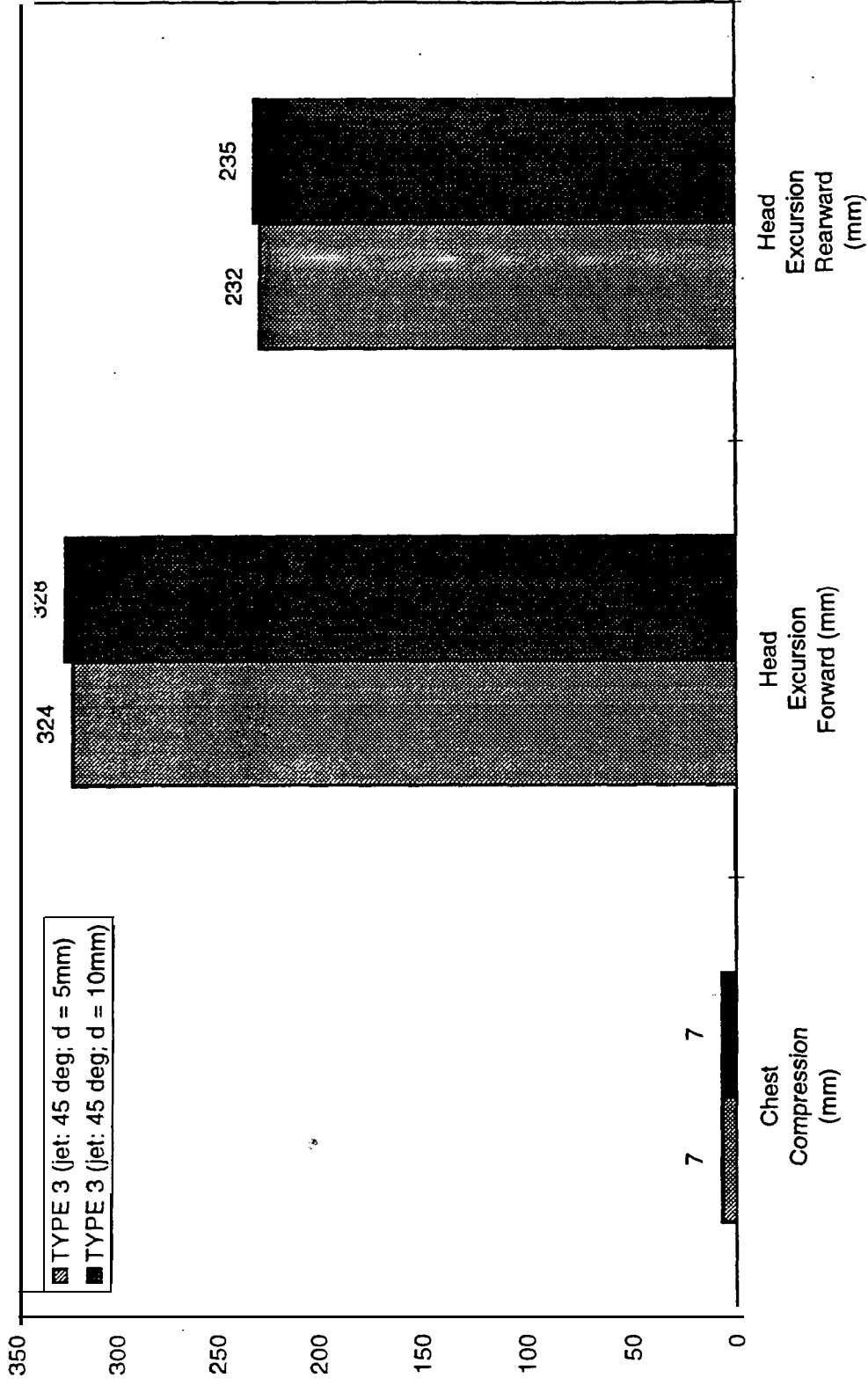


Figure 3.17 Occupant response using Type 3 inflatable headrest (30 mph rear impact).

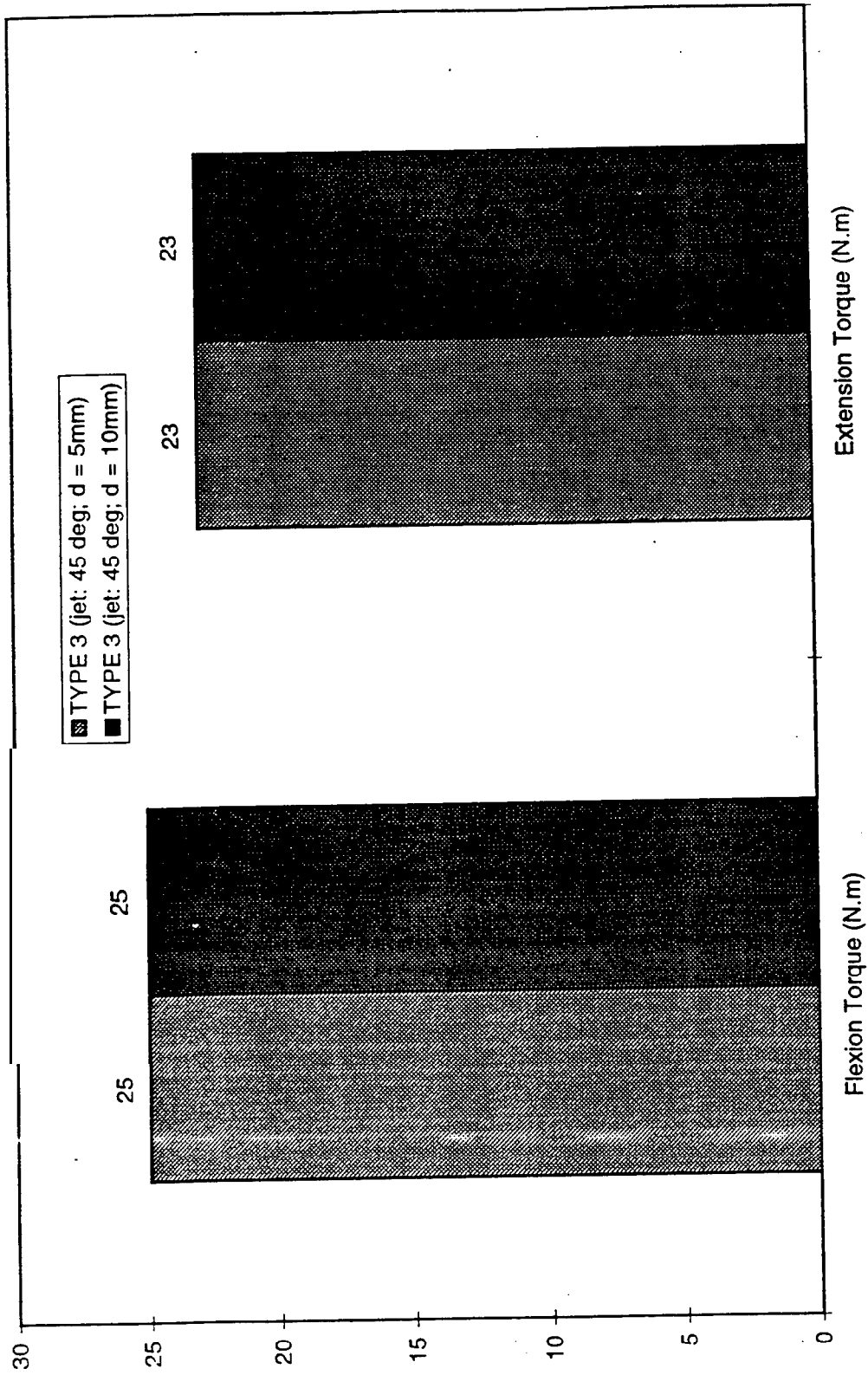


Figure 3.18 Occupant neck response using Type 3 inflatable headrest (30 mph rear impact).

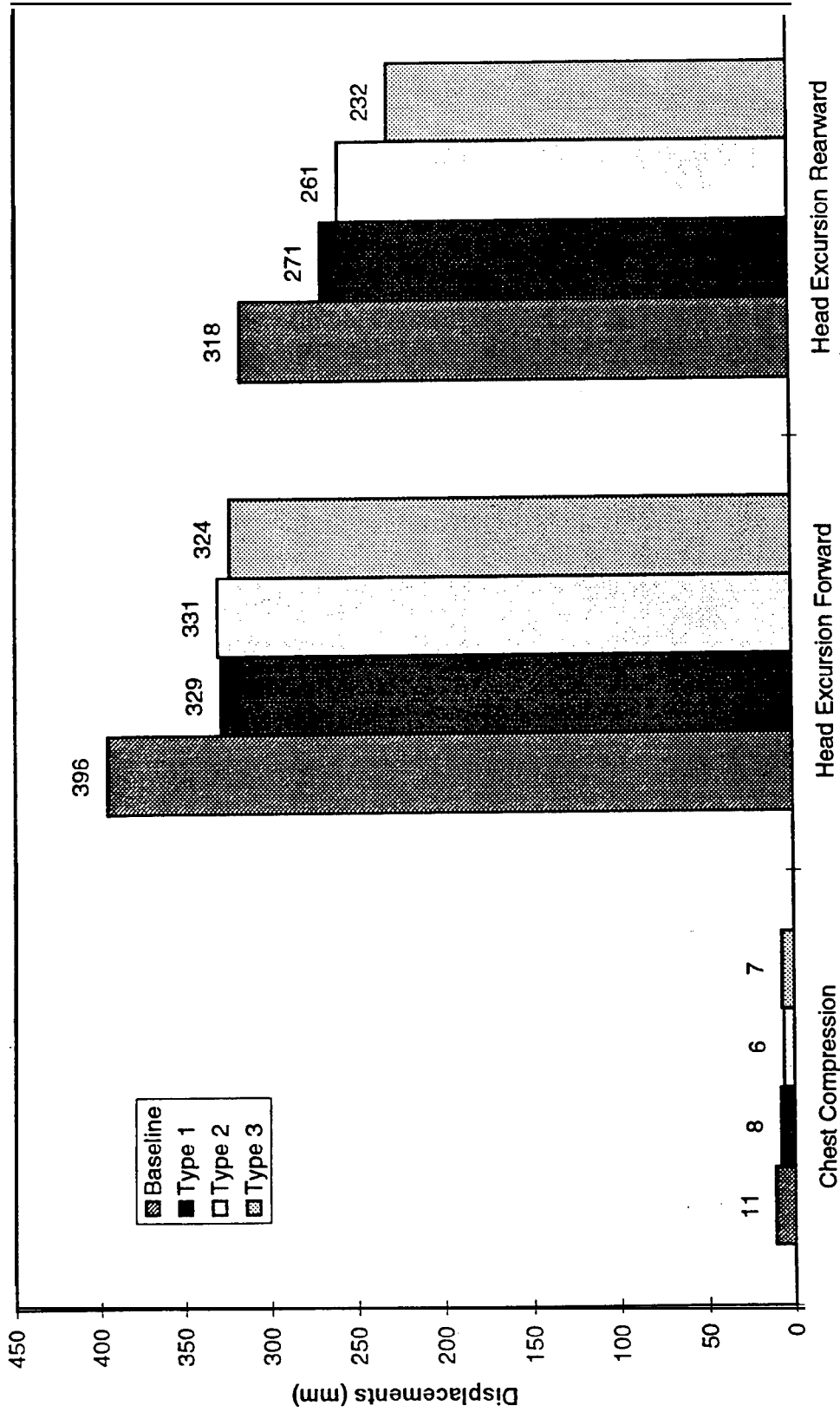


Figure 3.19 Comparison of occupant response using different types of inflatable headrest (30 mph rear impact).

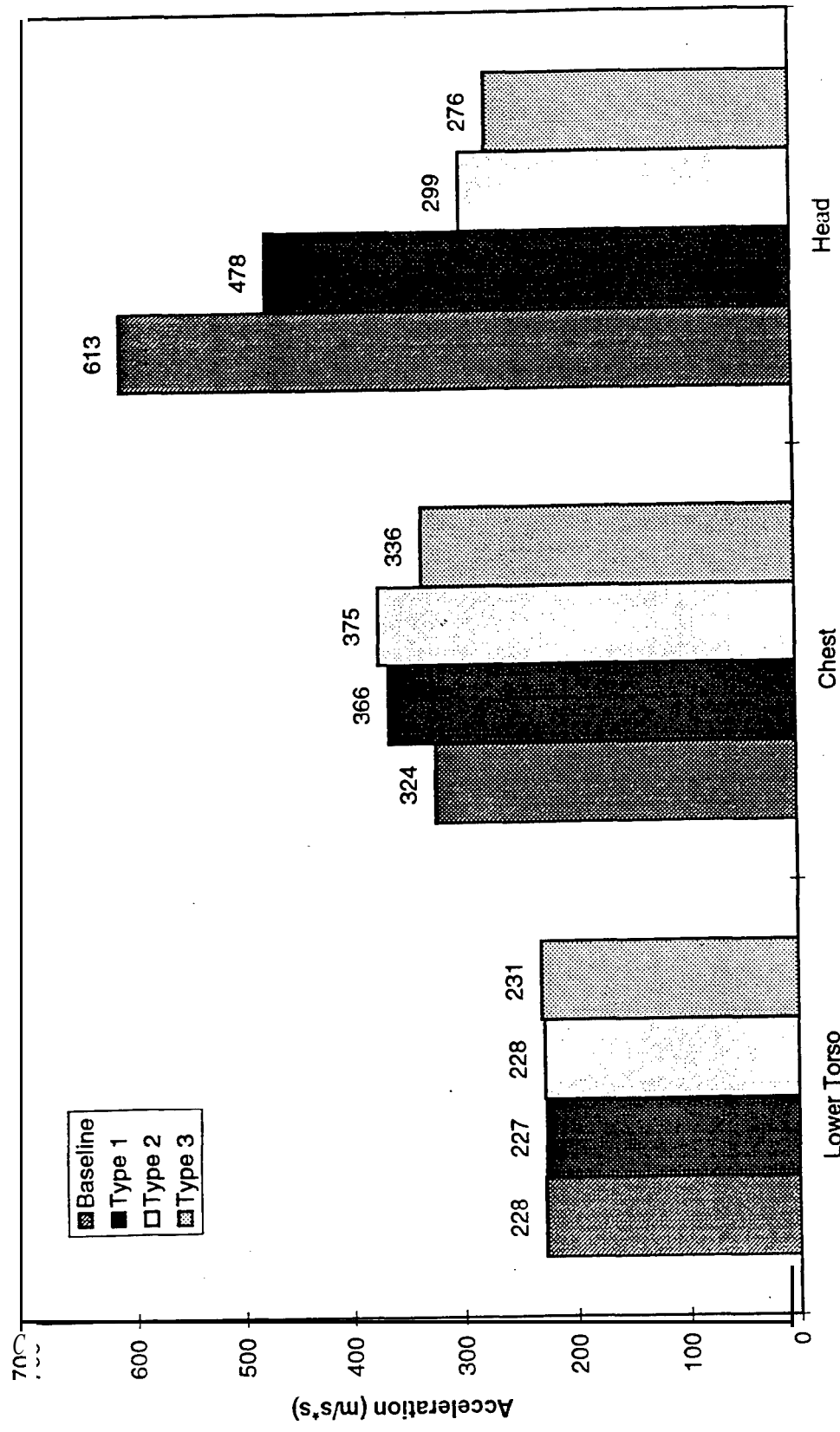


Figure 3.20 Comparison of accelerations using different types of inflatable headrests (30 mph rear impact).

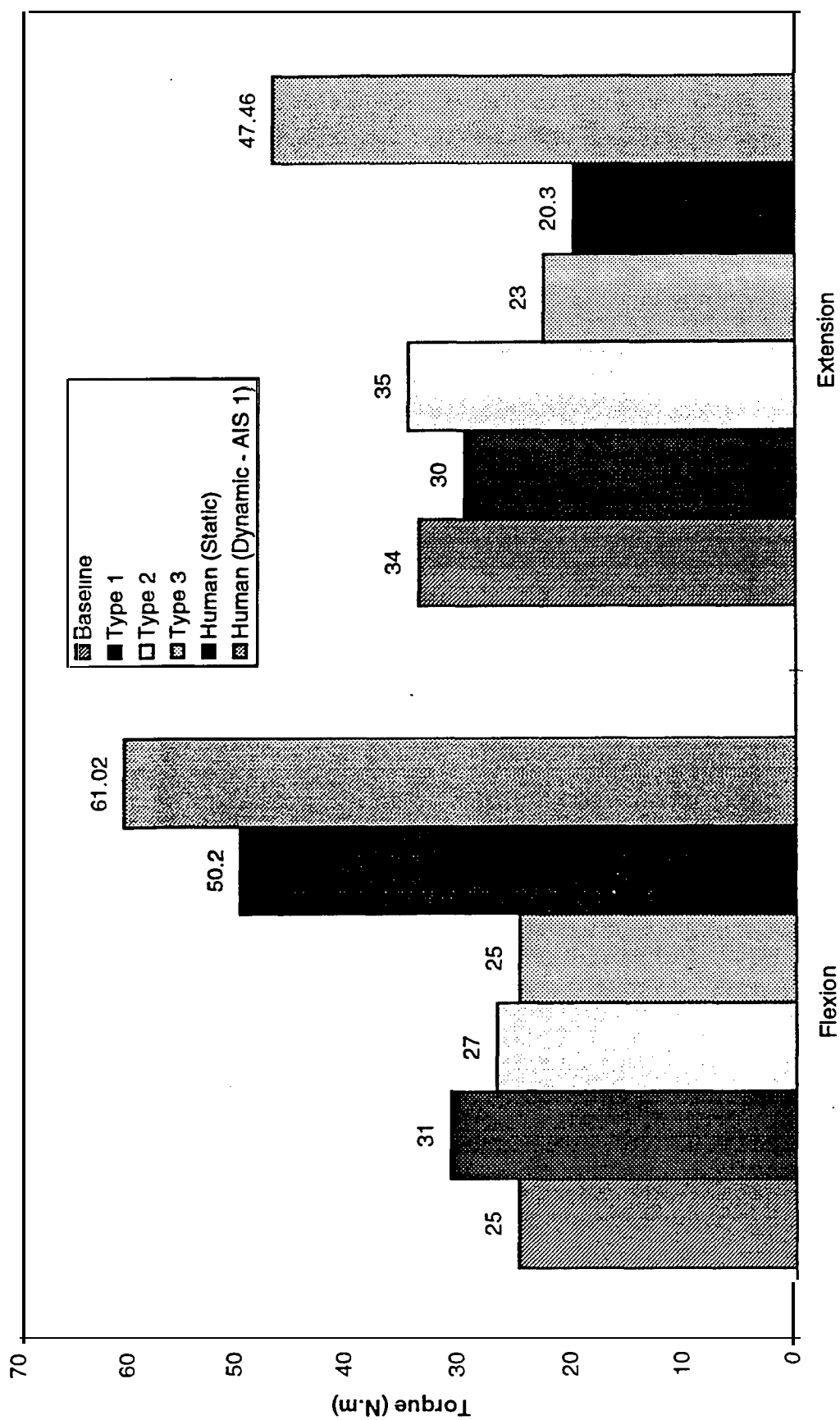


Figure 3.21 Occupant neck response using different types of inflatable headrests (30 mph rear impact).

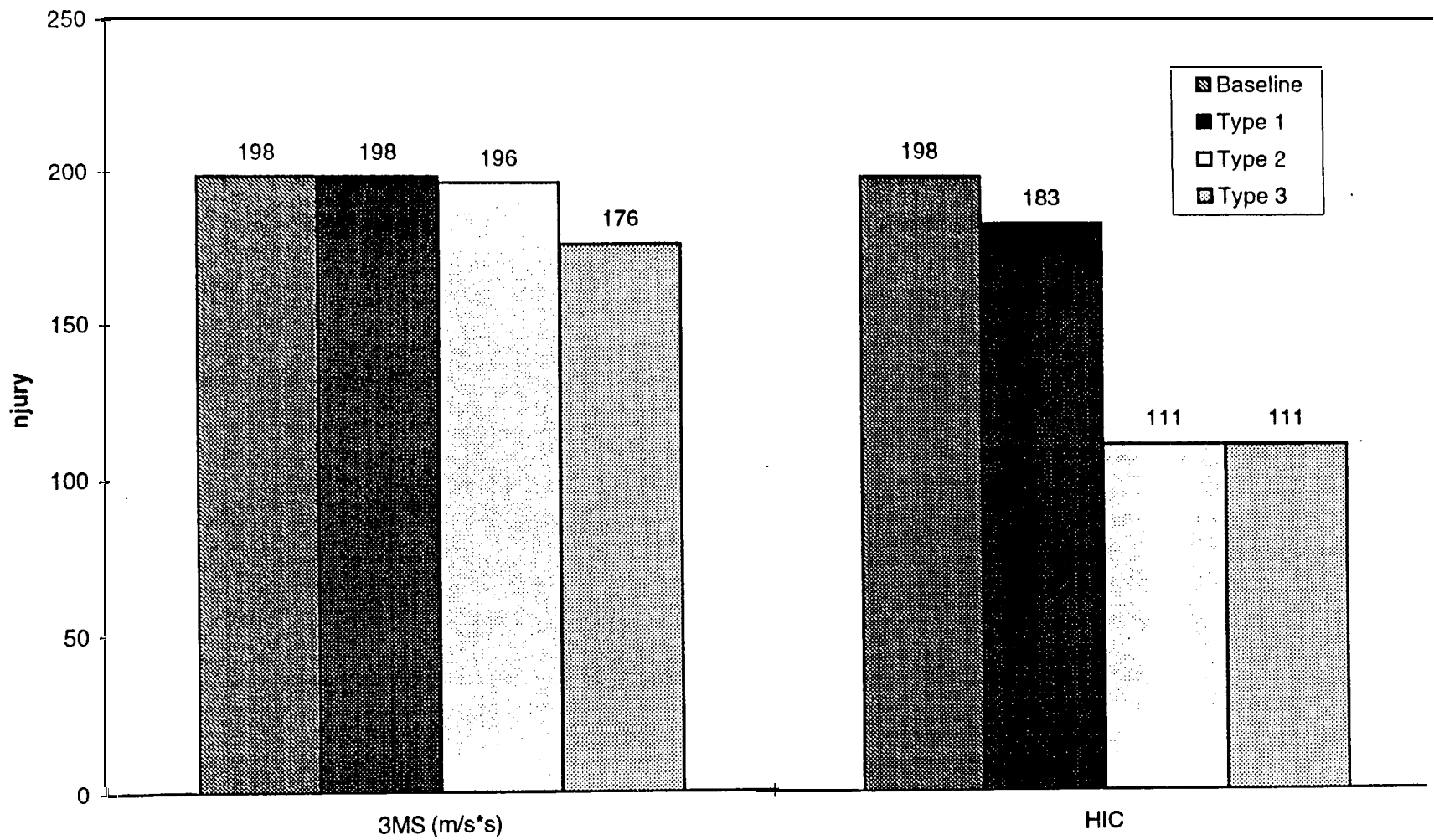


Figure 3.22 Comparison of injury numbers using different inflatable headrests (30 mph rear impact).

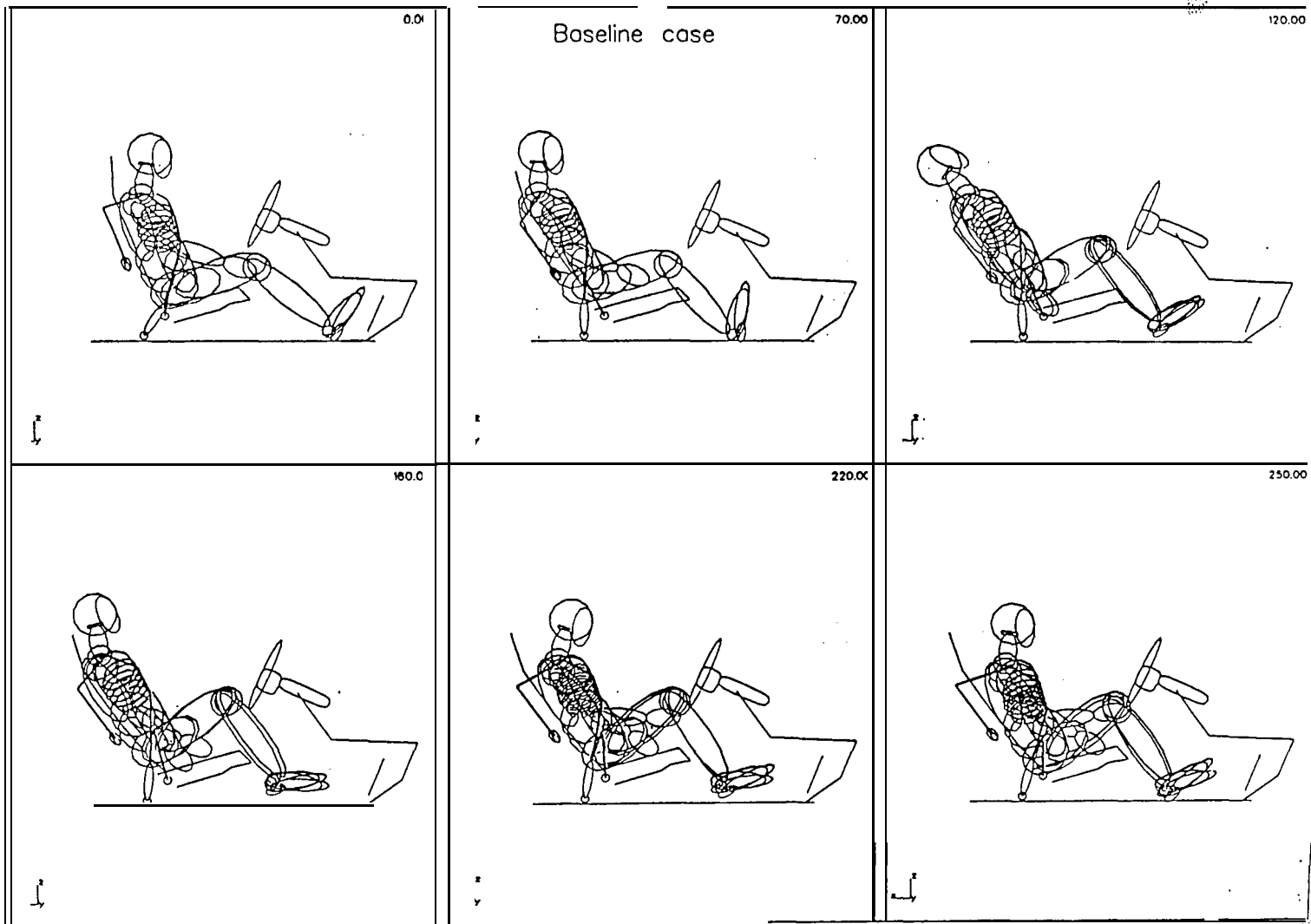


Figure 3.23 Baseline case (without inflatable headrest) simulation (30 mph rear impact).

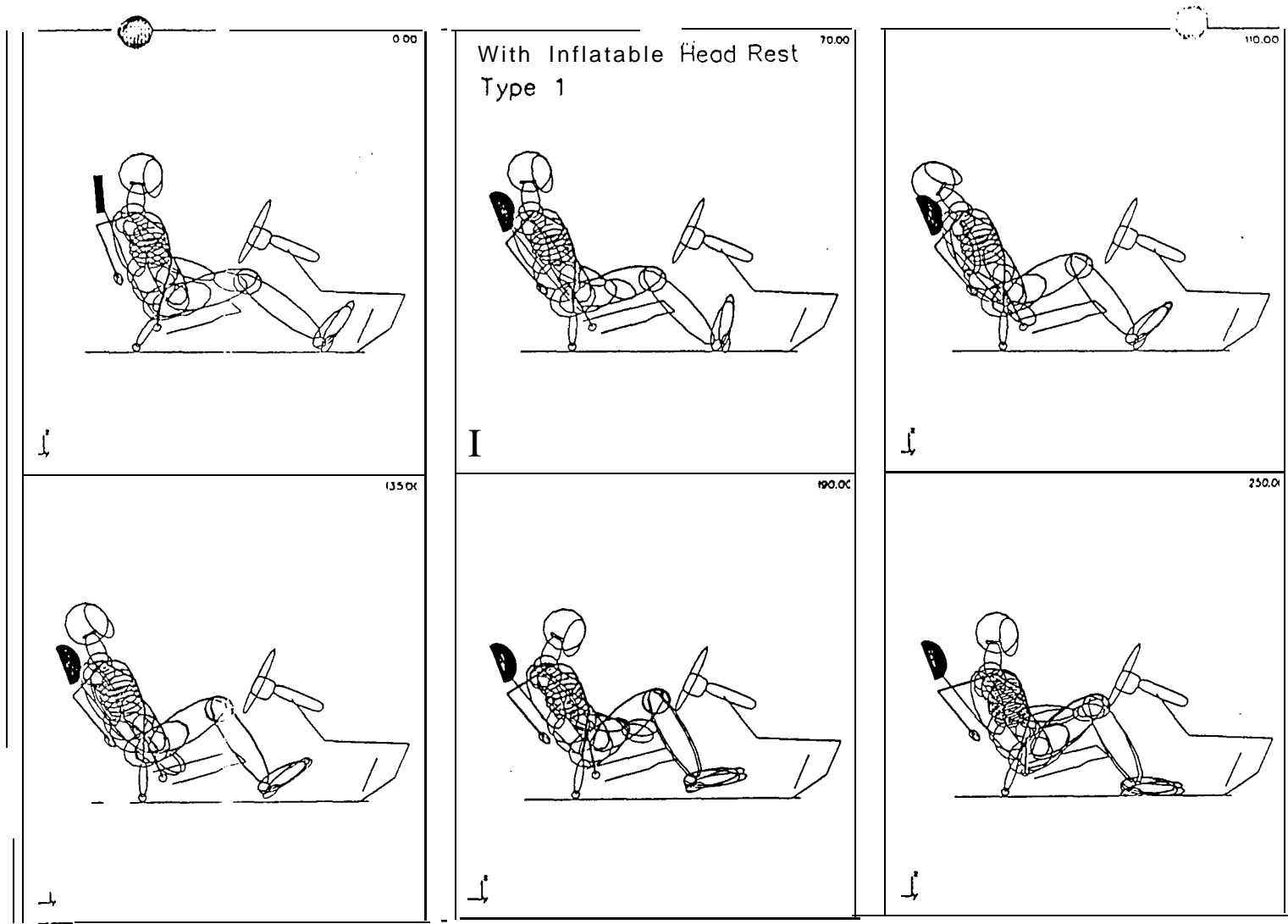


Figure 3.24 Simulation with inflatable headrest Type 1 (30 mph rear impact).

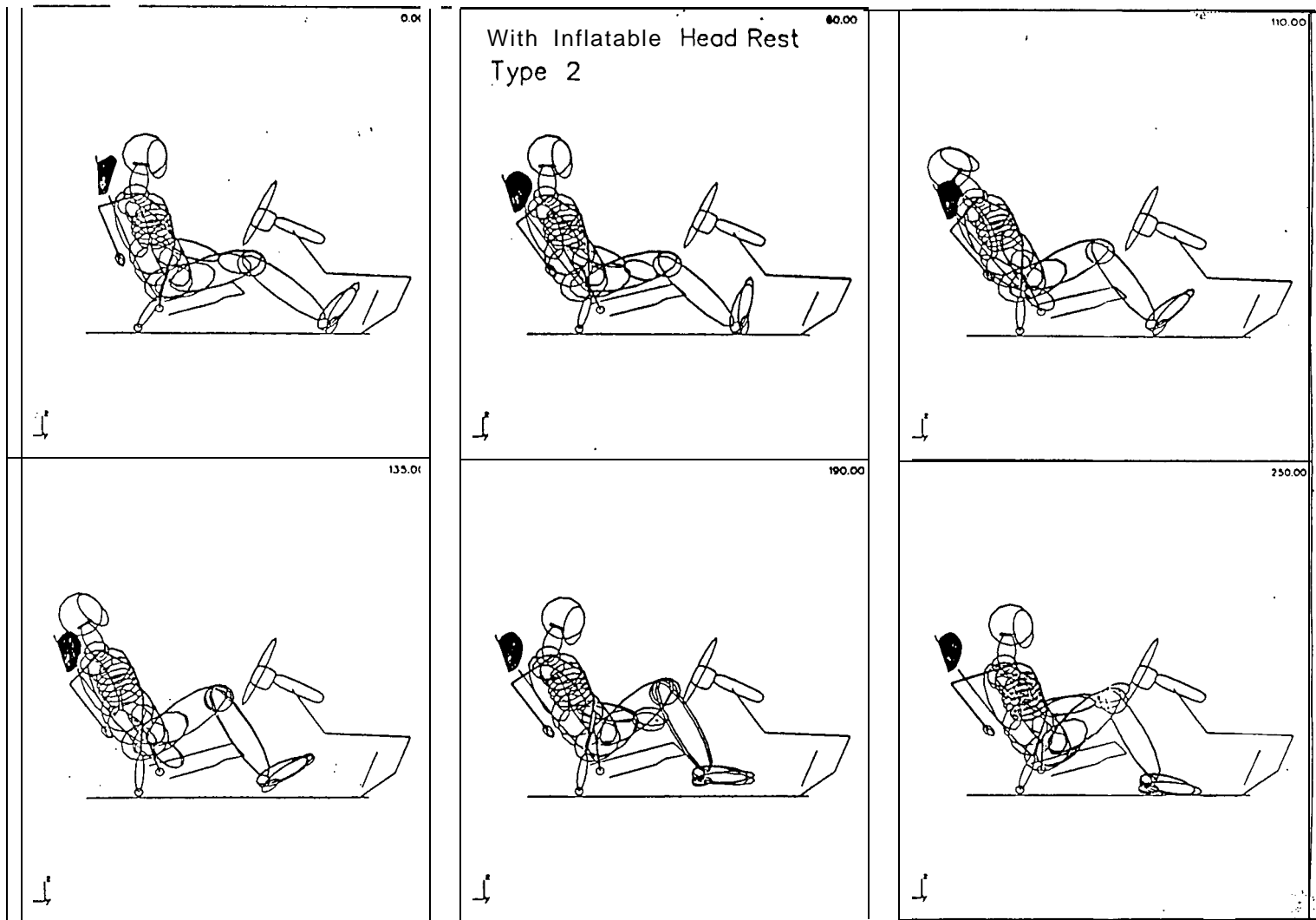


Figure 3.25 Simulation with inflatable headrest Type 2 (30 mph rear impact).

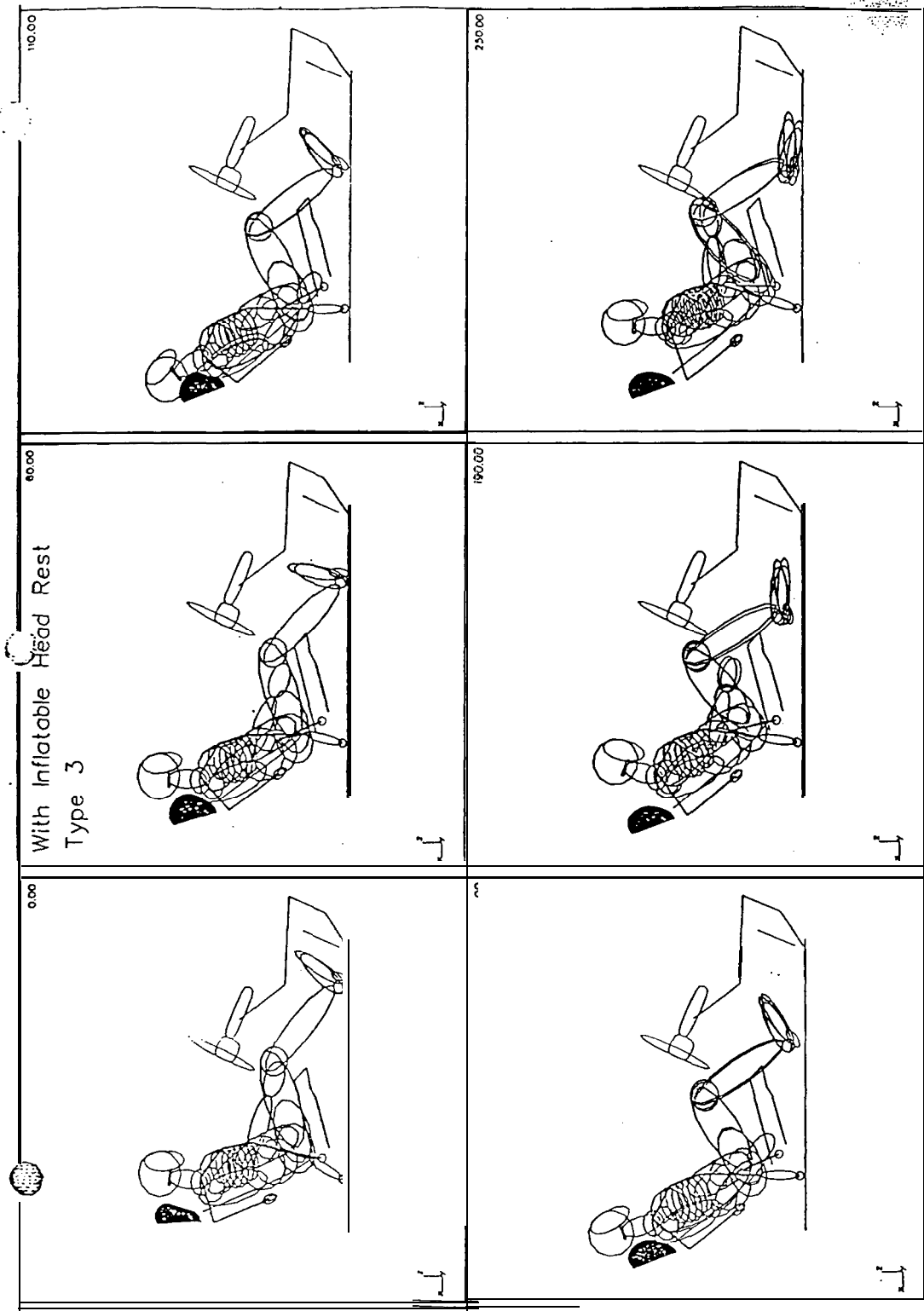


Figure 3.26 Simulation with inflatable headrest Type 3 (30 mph rear impact).

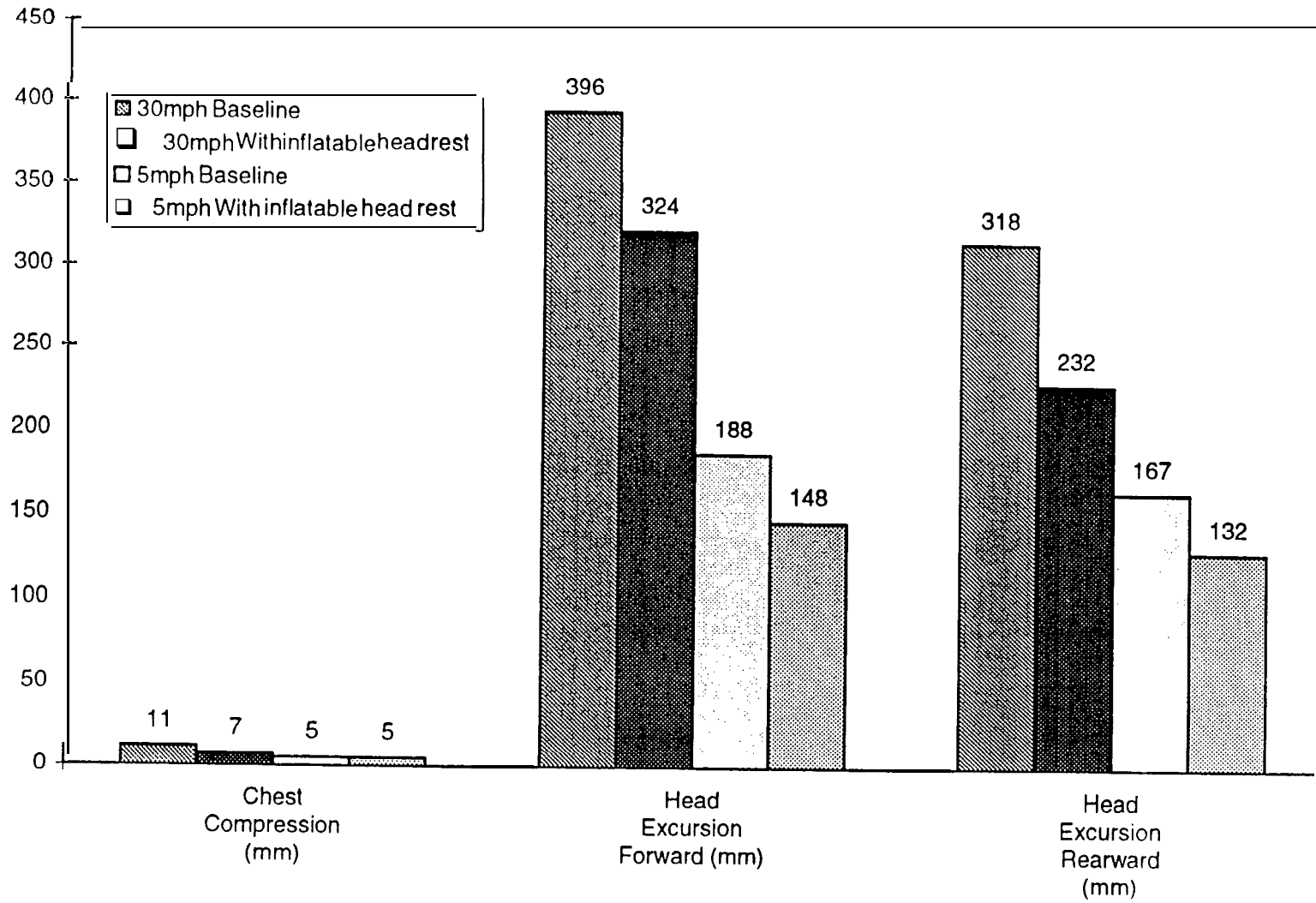


Figure 3.27 Comparison of occupant response at 30 and 5 mph rear impacts.

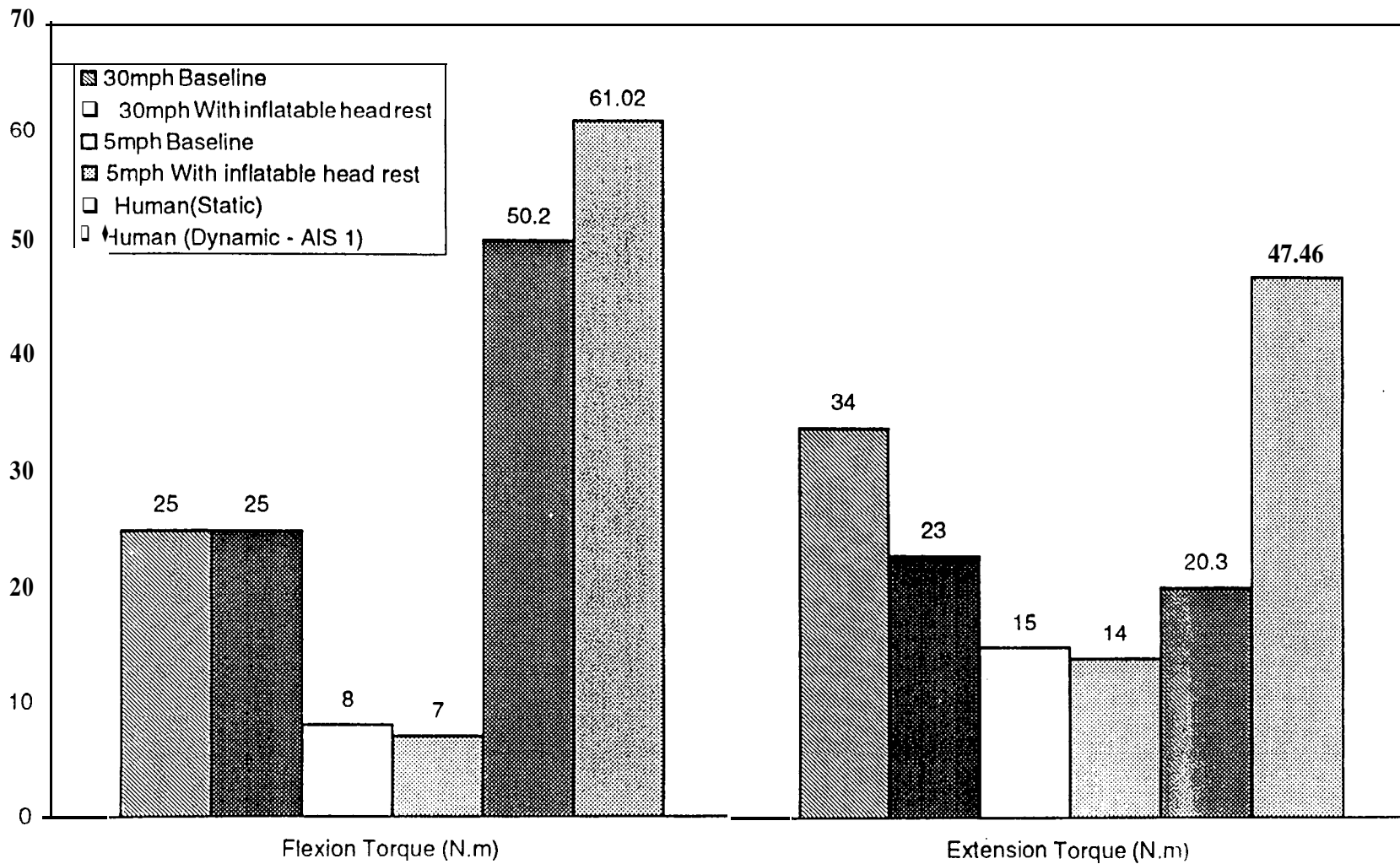


Figure 3.28 Comparison of occupant neck response at 30 and 5 mph rear impacts.

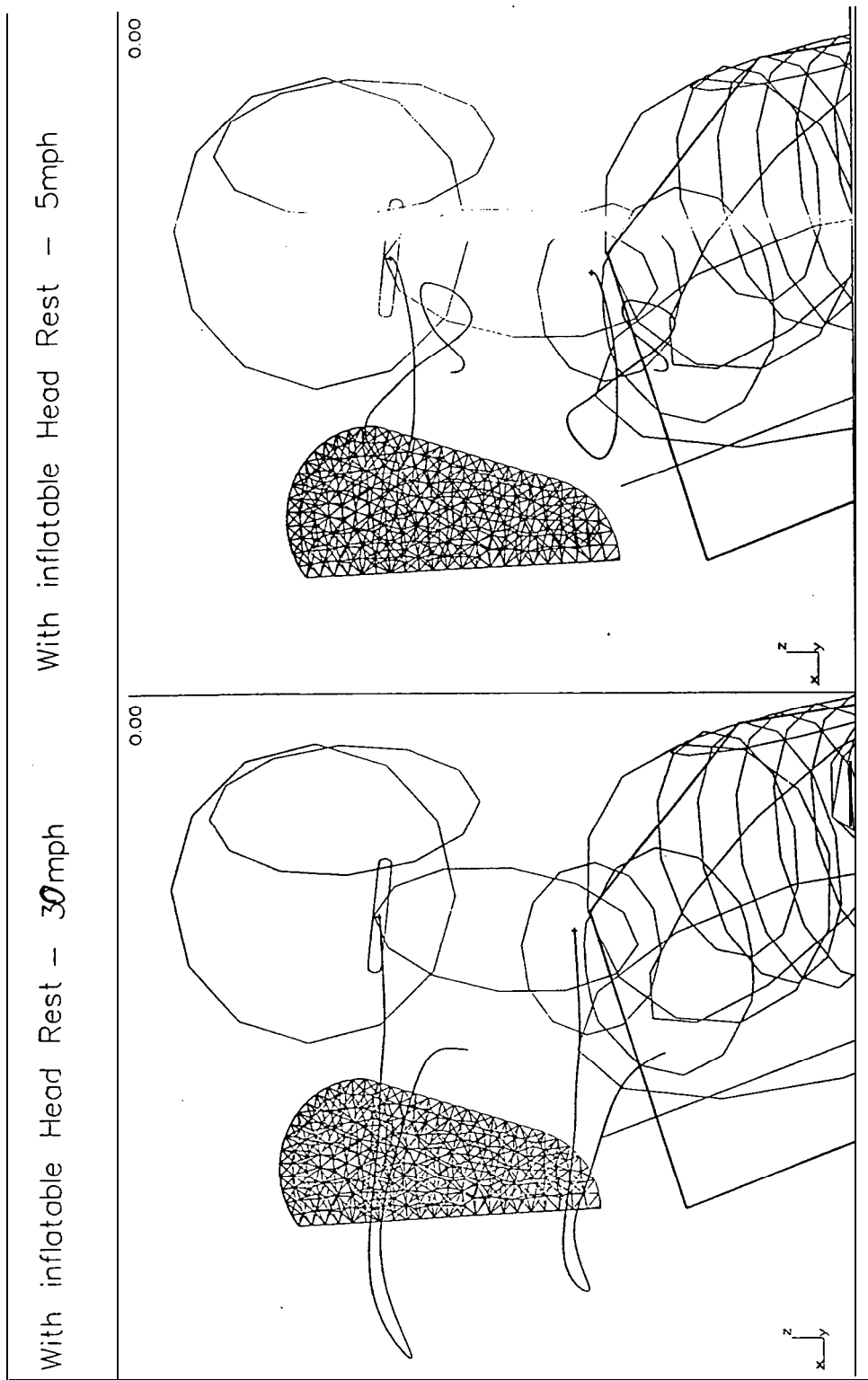


Figure 3.29 Trajectories of the upper and lower neck with inflatable headrest for 30 and 5 mph rear impacts.

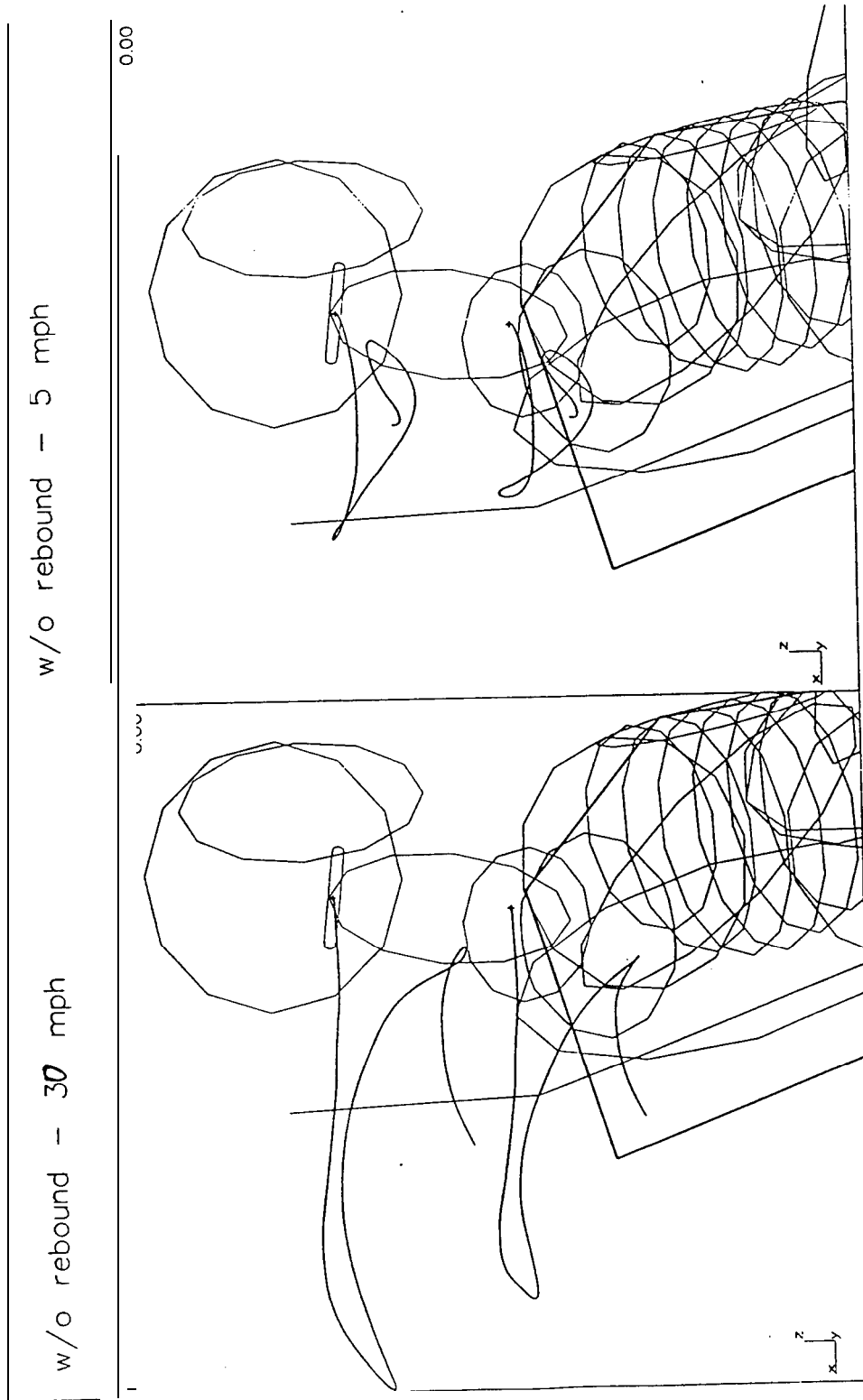


Figure 3.30 Trajectories of the upper and lower neck with standard headrest with a non rebound seat for a 30 and 5 mph rear impact.

of the upper and lower parts of the neck with and without the inflatable headrest for both 30 and 5 mph cases.

Observations:

- High and low speed rear impact (30 mph and 5 mph)
- Helps reduce the head acceleration and head excursion.
- Reduces the extension torque - one of the factors influencing the *whiplash* syndrome.
- Triggering time is very important - optimal trigger observed : 25 msec.
- Shape of the bag, the gas jet direction and inflator size helps reduce or increase the aggressivity of the bag.
- Energy absorbing seat back also reduces the whiplash effect considerably.

4. ROLLOVER

4.1 MADYMO Simulations

Simulations were performed using MADYMO to depict rollover test conditions as per the FMVSS 208 criteria to study the retention of an occupant in the vehicle compartment. A MADYMO model of a Ford Taurus was used (Figure 4.1.). The sled on which the vehicle rests is braked to a stop from 30 mph. The vehicle roll and translation accelerations at the center of gravity were extracted. These were used as inputs in a separate occupant simulation model of the driver (Figure 4.2.). Simulations were conducted using 50th and 95th percentile Hybrid III dummies which were belted down with both the shoulder and lap belts. Two sets of simulations were run with and without a pretensioner. The accelerations **from** the vehicle rollover model was applied to the occupant model. Rolling was simulated about a roll point coincident with the test vehicle center of gravity. Simulations were run for 5 seconds.

The first set of simulations were performed without the use of a belt pretensioner. It was observed that for both dummies the shoulder belt slipped off the occupant shoulder and only the lap belt retained the occupant. In this case the possibility of an ejection was quite high.

The second set of simulations were conducted under very similar conditions as the first except that a belt pretensioner with a pulling distance of 80 mm and pulling time of 9.5 msec, characteristics which are shown in Figure 4.3, was used. The occupant remained restrained through the simulation and there was no head contact with the roof of the vehicle. Results from these simulations are compared in Table 4.1. In this table values for the shoulder belt loads in the case without a pretensioner are not available because the shoulder belt slipped off the dummy shoulder.

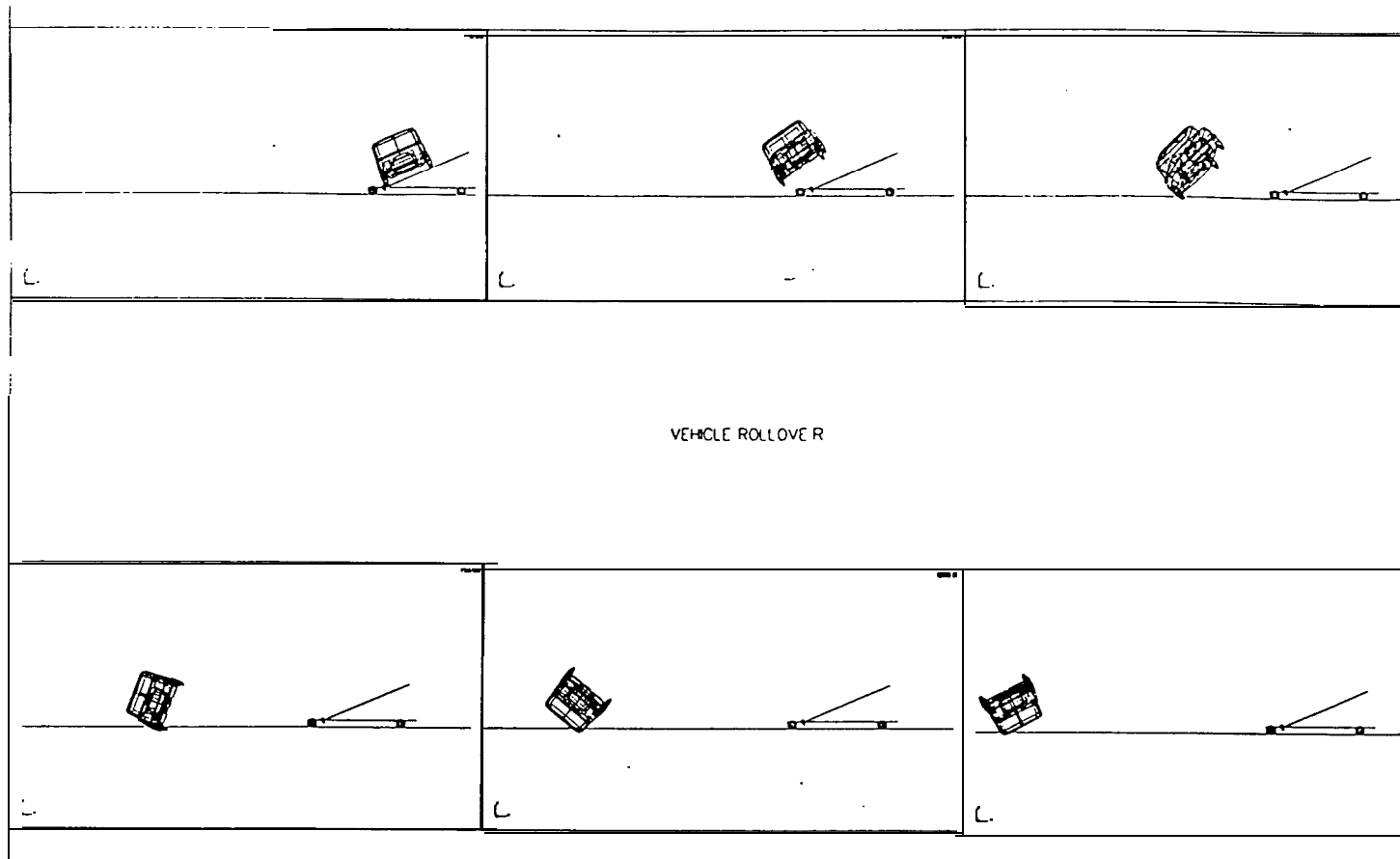


Figure 4.1 Vehicle rollover simulation.

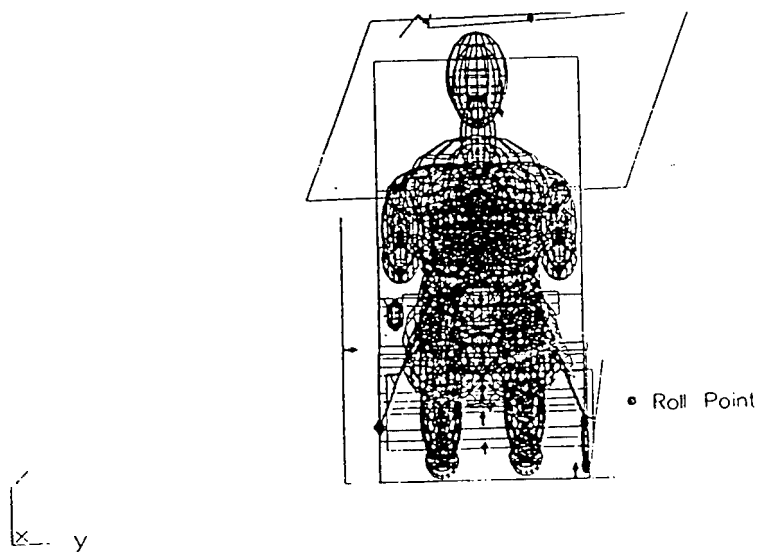


Figure 4.2 Model setup for MADYMO rollover simulations.

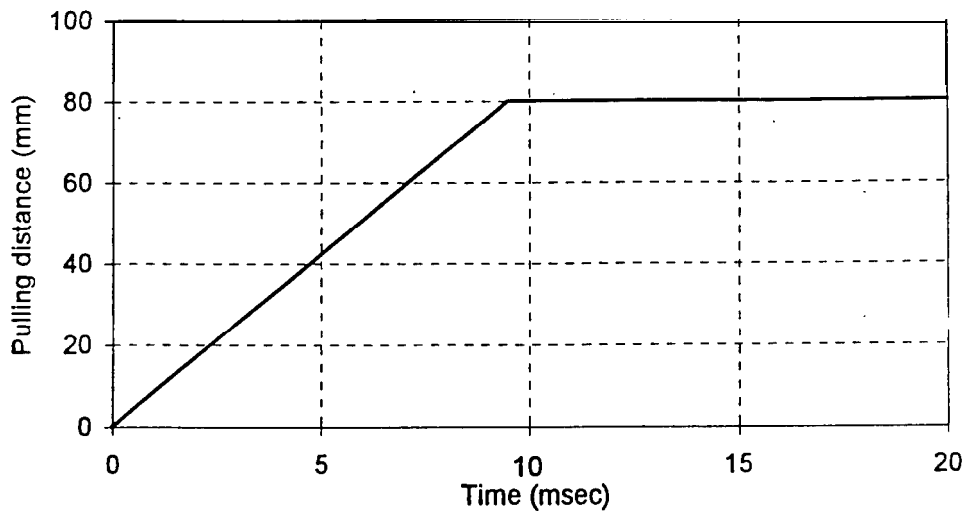


Figure 4.3 Characteristics of the pretensioner.

Table 4.1 Simulation results

		HIC	3MS (m/s ²)	Neck Axial Load, N		Belt Force, N	
				Upper	Lower	Shoulder	Lap
50 th percentile	Without pretensioner	28	34	281	38	-	568
	With pretensioner	27	34.8	118	118	1905.4	516
95 th percentile	Without pretensioner	17	31	318	318	-	792
	With pretensioner	15	43.6	238	332	1383.7	694

Finally a third set of simulations were conducted by inverting the whole vehicle and the occupant as shown in Figure 4.4, to study the head excursion relative to the head rest and roof of the vehicle. For this simulation the occupant was restrained using both belts with and without a pretensioner, and an acceleration field of 1g was applied on the occupant. Results show that both belts held the occupant and there was no contact of the head with the roof of the vehicle.

The layout of the shoulder belt in an integrated restraint seat helps to reduce the vertical drop of the occupant because it loops around the shoulder as seen in Figure 4.4. The shoulder belt would not be able to “catch” the occupant in this manner if it were attached to the B-pillar.

Results of this set of simulations are given in Table 4.2. The head drop of the 95th percentile dummy with a pretensioner was 5.3 cm. This value can be used as guideline to establish the head rest height. Neck loads were small as there was no head contact with the roof and the applied acceleration field was only 1g.

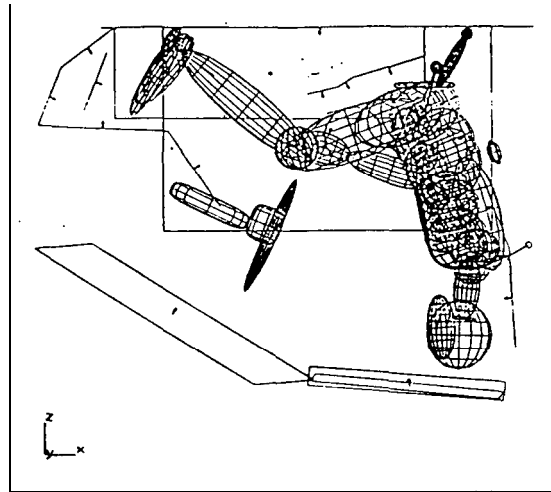


Figure 4.4 Model setup of the inverted simulation.

Table 4.2 Simulation results of the inverted tests.

		HIC	3MS (m/s^2)	Belt Force, N		Head Excursion m
				Shoulder	Lap	
50 th percentile	no pretensioner	1.0	9.8	712	133	0.045
	with pretensioner	0.2	3.4	615	52	0.011
95 th percentile	no pretensioner	0.4	22.1	607	177	0.062
	with pretensioner	0.2	28.5	600	118	0.053

Simulations were also performed with the passenger side shoulder belt anchor position being changed from the right to the left. This change in position was found to be very beneficial for a rollover situation because it reduces the risk of interior body contact. This change in position may hinder visibility and may be of concern from a styling point of view.

4.2 Extended Headrest

To study the behavior of AISS seat in a rollover crash, a full car 20 degree drop test was performed (Bahling et al., 1990). FORD Taurus car model was used for this purpose (Figure 4.5). The objective was to see if an extended head rest could be used to reduce head excursion of the dummy and the potential roof contact due to roof crush. The seat was modeled using beams and springs. Two simulations were made. In the first baseline simulation, the height of the headrest was equivalent to the height of headrest in the current ISS seat. In the second enhanced simulation, the headrest has an additional height. It extends beyond the top of the head of the 95th percentile dummy. This extension equals

the head excursion of a belted dummy which is 62 mm under -1 G. This result was obtained through a simulation in MADYMO.

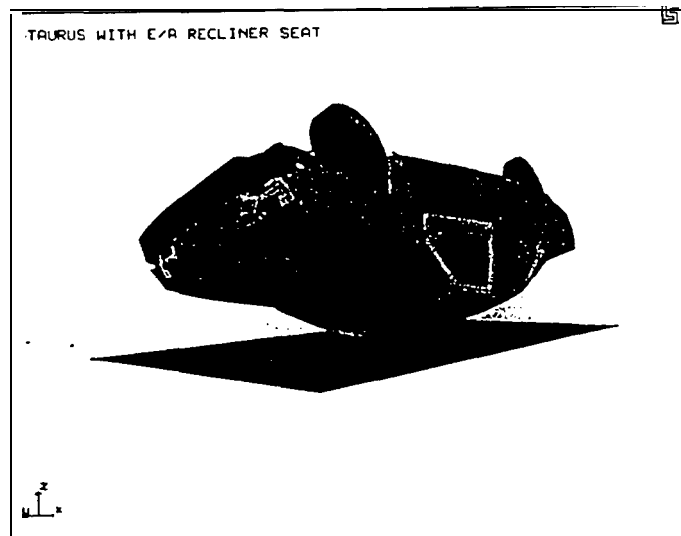


Figure 4.5 Full car rollover drop test.

The deformed shapes for the baseline and enhanced simulations are shown in Figure 4.6. **Overall**, longer headrest has little effect on the deformed shape of the B-pillar. In addition, the headrest does not decrease the roof crush as inertia! **forces** due to the mass of the car are very high.. The headrest and seat structure under either simulation does not provide occupant protection **functionality** similar to an energy absorbing roll bar.

In the Baseline case, head rest remains clear **from** the roof When the contact between headrest and roof occurs, the structure of the car simply pushes the headrest aside and continues to deform. However, in the enhanced case, the headrest is long enough that during roof crush, it strikes the roof This causes the seat-back to deform laterally and **rearwards** by few inches.

The vertical travel of the seat bottom hinge is plotted for these two simulations in Figure 4.7. Very little change in the vertical displacement can be seen between these two cases. This **confirms** that the seat bottom or the floor pan vertical travel is not reduced by the longer headrest.

If we compare the vertical travel of the shoulder point for these two simulations (Figure 4.8), a significant reduction is noticed. For the enhanced case, the displacement reduces from 82 mm to 40 mm. Hence, due to lateral shift in the seat-back, vertical drop in the shoulder point is reduced by almost **50%**. When seat-back deflects laterally, the belted dummy is assumed to move with the seat back. With this assumption, a longer headrest can significantly help in reducing injuries due to head excursion in rollover crashes.

Features relevant to AISS for rollover protection:

1. **Pretensioner**

- The results of these simulations show that the primary **function** of the **AISS** under rollover conditions is to retain the occupant in the seat.
- To this end the firing of the pretensioner is imperative.
- The belt loads under rollover conditions are seen to be **only** a small fraction of the values anticipated under frontal crash conditions.

2. **Extended Headrest**

- The “inverted dummy” simulations have provided an estimate of the height of the headrest which would prevent head to roof contact **from** occurring. For this seat design this distance is 0.98 m **from** the recliner pivot point to the top of the headrest.
- Extended headrest also prevents head to roof contact by altering the trajectory of the head and carrying it away **from** the intruding roof

3. **Load Carrying Capacity of Seat under Roof Crush Loads**

- It is also possible to invoke the seat as a load carrying compression/bending member to reduce roof intrusion in a rollover. This is because the AISS seat-back has been designed to take rear impact loads.
- It was found that the extended headrest does not help in decreasing roof crush.
- Extended headrest **after** contact with the intruding roof modifies the trajectory of the occupant head and moves the head away from the roof, subsequently avoiding any head to roof contact.

4. **Belt Anchor Position**

- Change the position of the passenger side shoulder anchor from right to **left**.
- Helps reduce the interior contact of bodies.

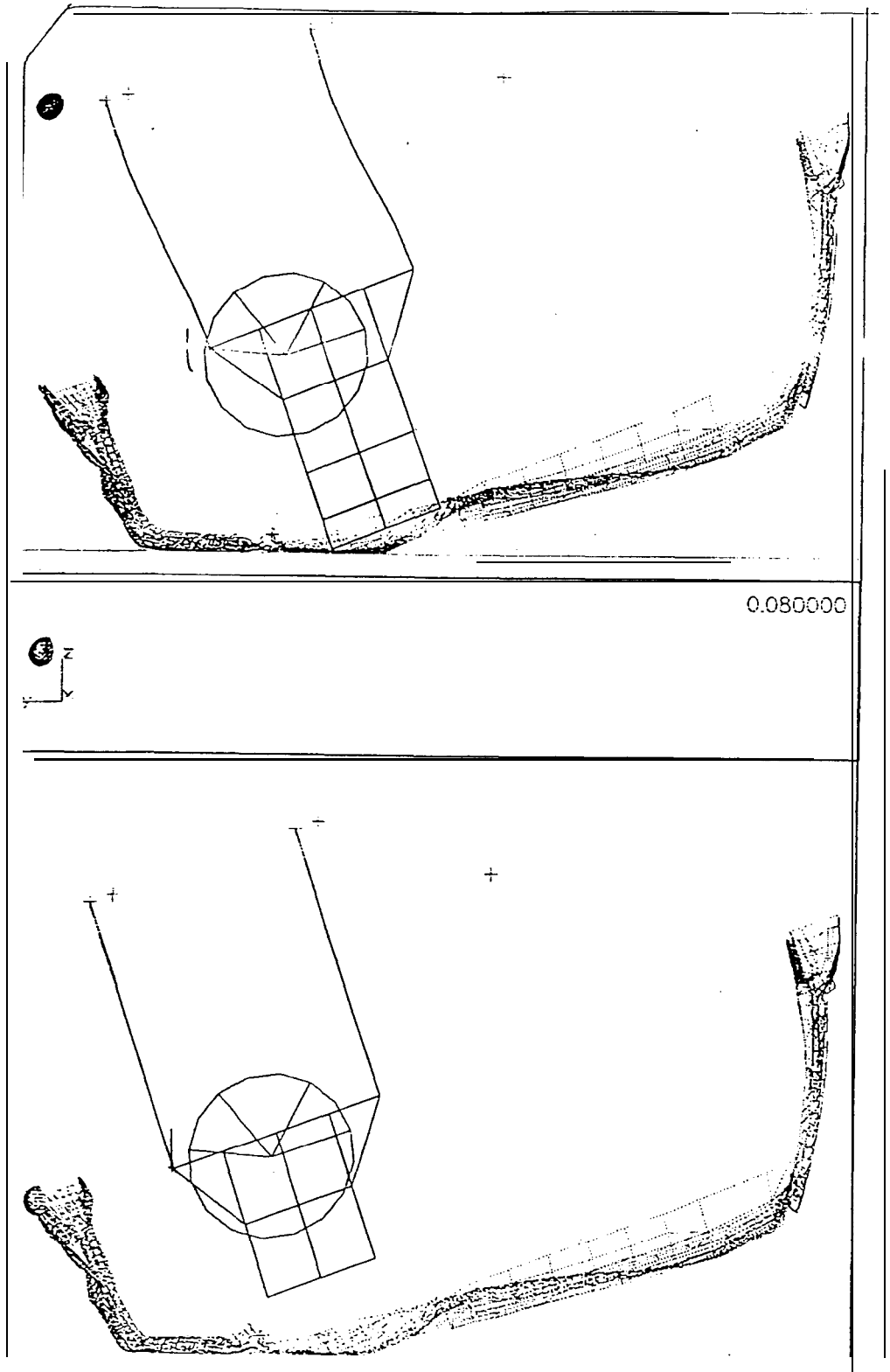


Figure 4.6 Comparison of standard and extended headrest in inverted drop test.

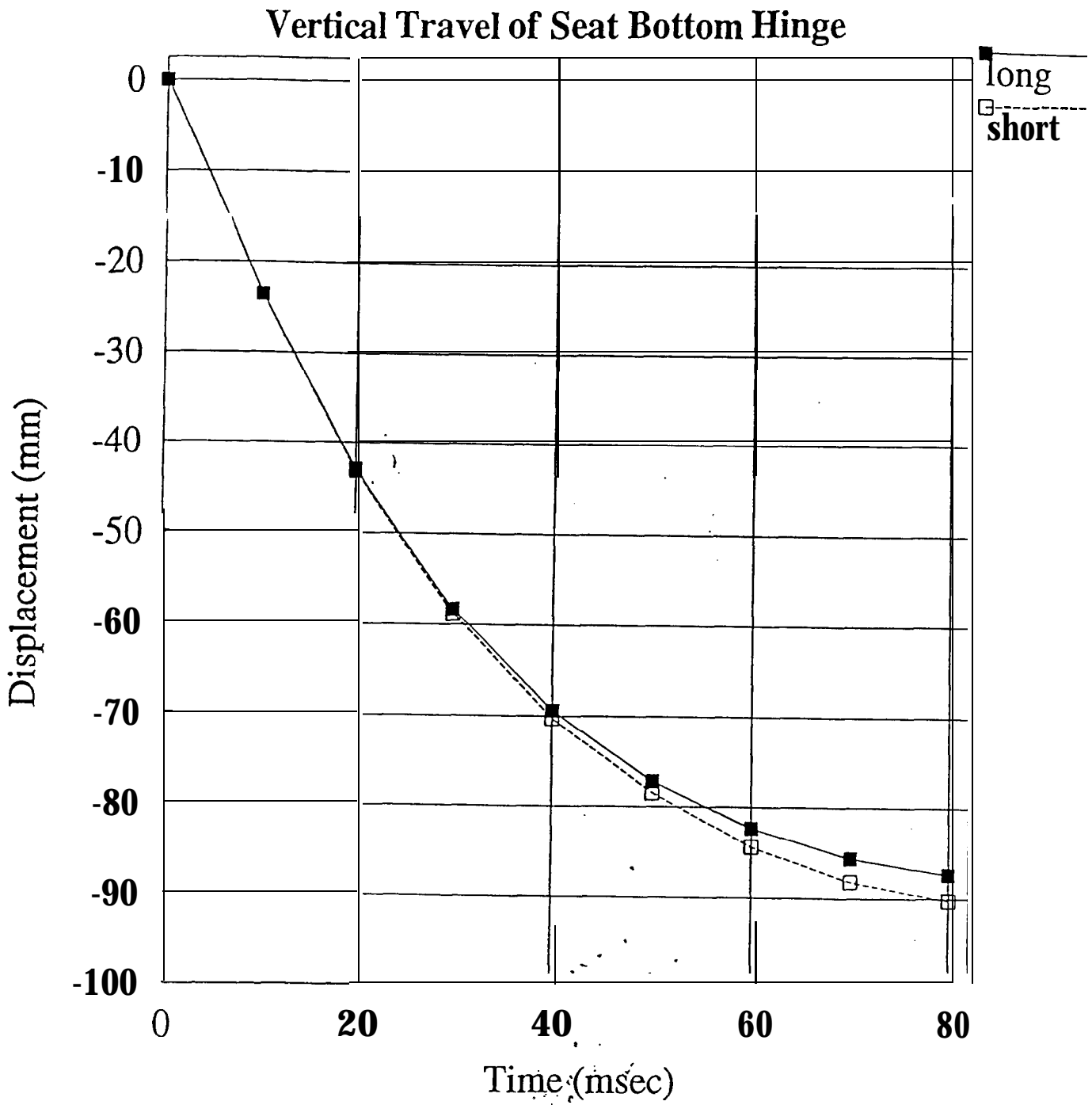


Figure 4.7 Vertical travel of seat bottom hinge.

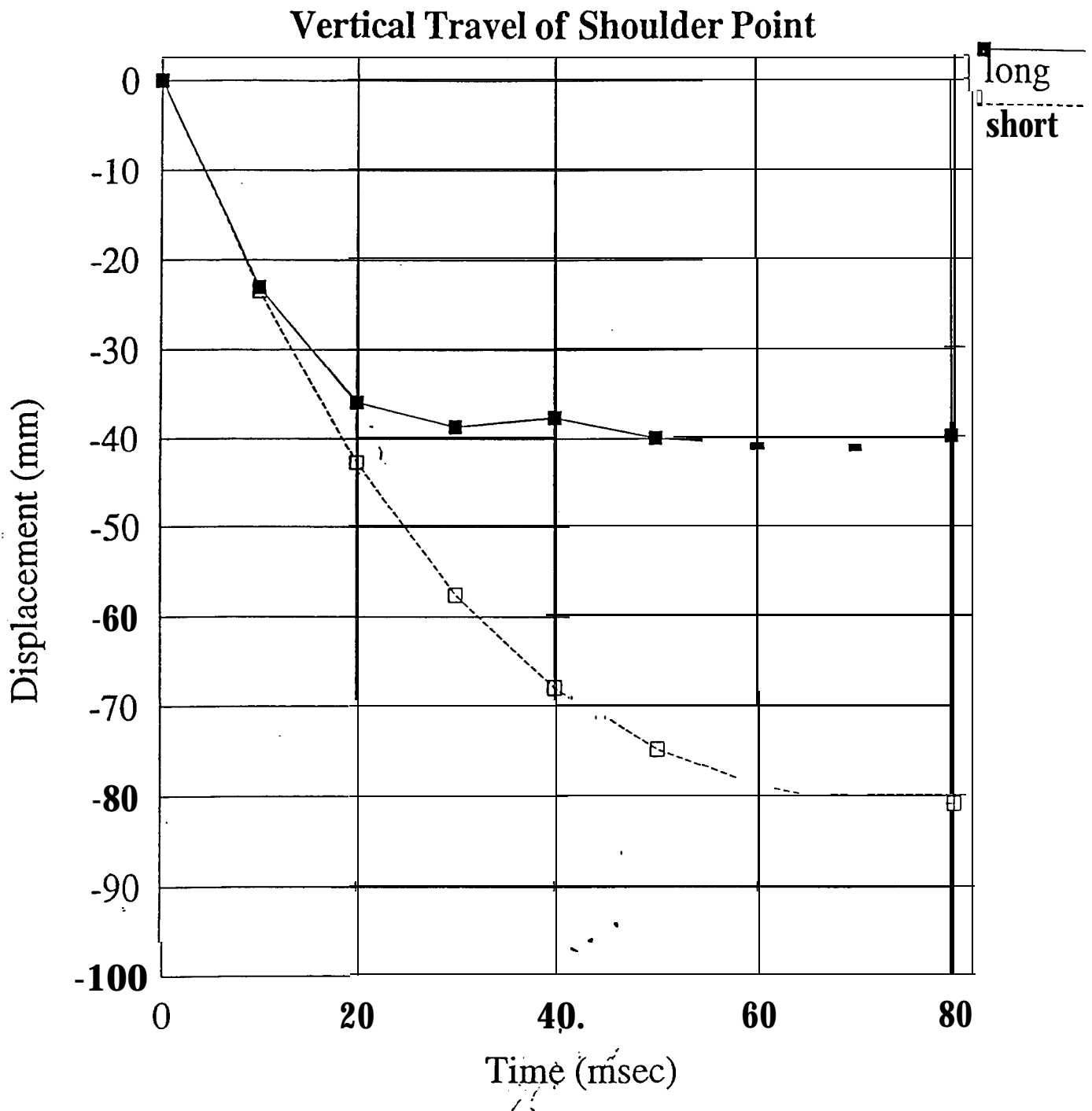


Figure 4.8 Vertical travel of shoulder point.

5. Side Impact Protection

Injuries in side impact collision constitute one fourth of the serious-to-fatal (AIS 3+) injuries sustained by occupants in ordinary passenger cars (Stig Pilhall et al., 1994). On the basis of the review of the accident data during the late 1980's it has been found that that head injuries are the most frequent sources of side impact fatalities followed by chest and abdominal injuries.

Even though researchers have differences of opinion on the mechanisms that produce injury in side crashes, the commonly held belief is that as the striking vehicle or the barrier momentum is transferred to the target vehicle door, the door structure collapses inward with the inner panel striking the stationary occupant. If the occupant comes in contact with the collapsing door as door decelerates, one would expect the door-chest contact velocity to be lower. On the other hand, if the door strikes the occupant as its velocity ramps up, and at or near the peak door velocity, the severity of the impact would be higher. The lower contact velocity can be achieved either by locating the occupant as far away from the door as possible, or by ensuring that the door offers enough resistance to sudden collapse so that the barrier does not "punch" the occupant. This could also be achieved if the seat can be used as move the occupant away from the intruding door. The side impact wing concept evaluated in this study does just that.

To evaluate the concept of improved side impact protection, Ford Taurus full car model is used with AISS seat placed in the car. The model is coupled with a MADYMO 50th percentile side impact dummy in the seat. This dummy model, called EASi-SID was developed and calibrated at EASi Engineering.

A shield is provided for the dummy using a 1 mm thick plate near the shoulder. A wing is also provided near the bottom of the seat-back so that it gets the hit from the door and starts deforming the seat-back (Figure 5.1). The wing is provided slightly above the pivot point of the seat-back such that maximum deformation can be achieved near shoulder point. The concept explored in this model is that when the almost rigid wing near the pivot point takes the hit, it will move the shoulder point laterally at an even higher rate. This will cause the dummy's upper body to move due to the shield. The shield is placed at 45 degrees with respect to the seat-back plane. If the seat-back starts slipping behind the dummy, then the shield will catch the dummy and impart velocity to the upper body. A deformable shield is modeled because a rigid shield would have the same effect as if the impact occurs right next to the dummy. As the shield gets loaded, it will start deforming, thereby passing less force or acceleration to the upper body. This will of course bring the door profile closer to the upper body. Deformed shape of the door and seat is shown in Figure 5.2. Although, there is contact between the door and the wing, lateral displacement of the wing causes local buckling in the seat pillar and does not induce significant movement in the seat-back.

Since placement of wing at the bottom of the pillar does not produce desired lateral movement in the seat-back, in the next iteration the wing was placed at the middle of the

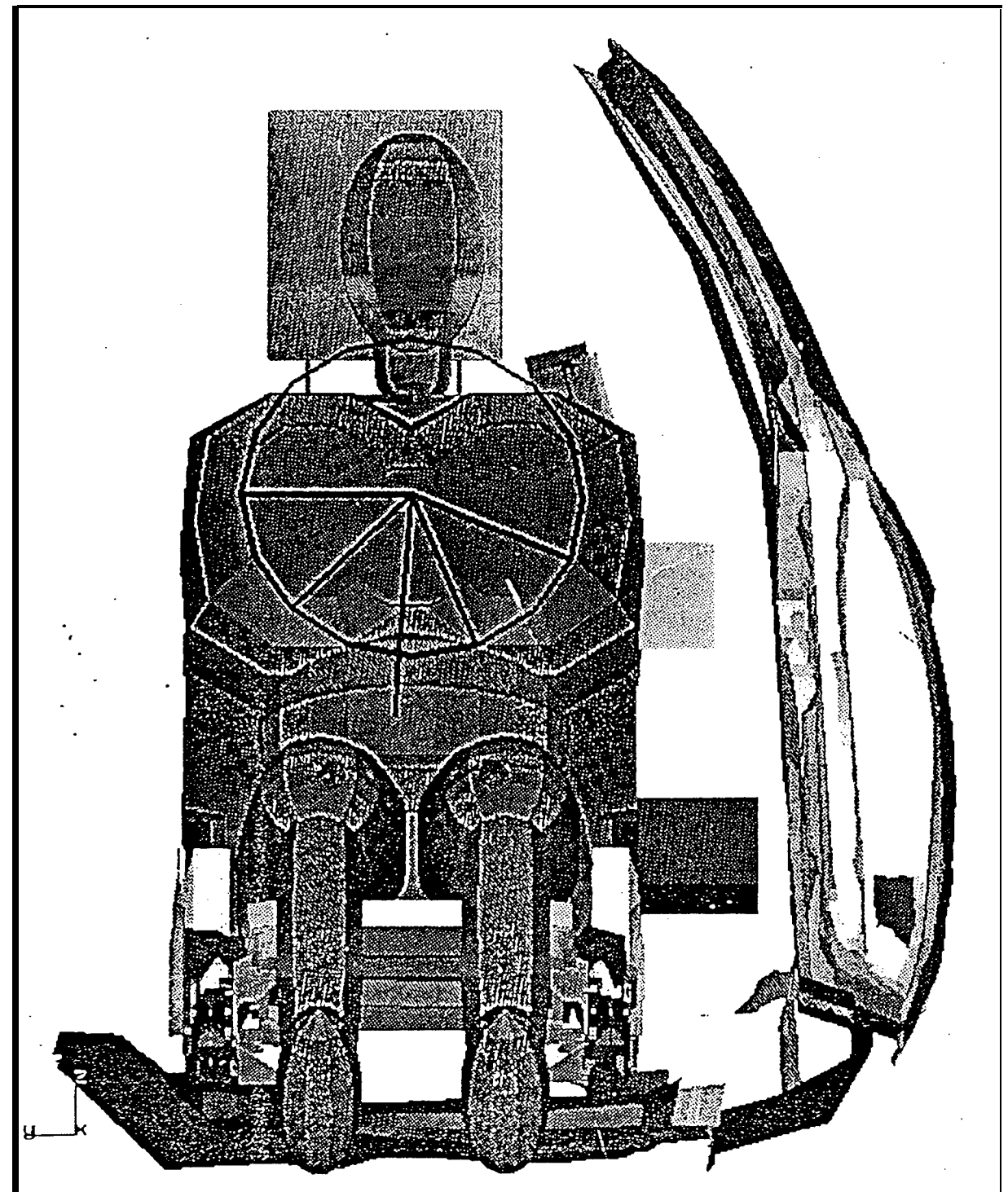


Figure 5.1 Model setup for side impact test with wing and shield.

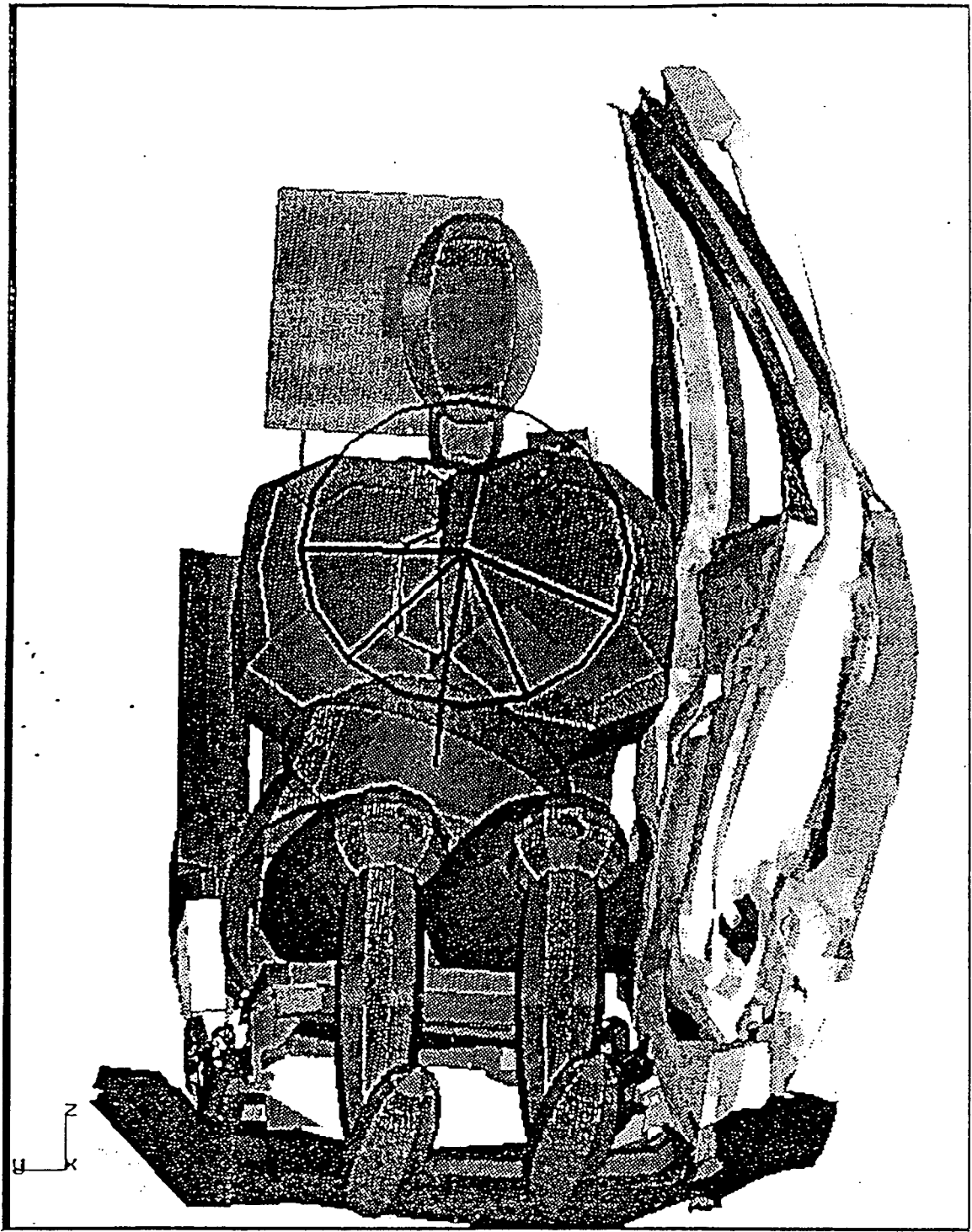


Figure 5.2 Simulation for side impact test with wing and shield.

left pillar. For faster turn-around time the model was simplified, where only the seat was modeled in detail and the door was modeled by a rigid wall. The seat was constrained by rigidly fixing the mounting brackets. Although, in a full car simulation, seat mounting brackets move with the floor pan, not very significant movement occurs in such simulation: Hence, we believed this assumption to be quite reasonable at least for the first few milliseconds. Velocity of the rigid wall was approximated by the velocity of the face of the wing in the above simulation. It increased from 0 to 10 m/sec in the first 12 msec and then remained constant. However, in this case excessive bending of the left pillar also occurs without significant movement of the seat-back as a whole. Hence, in the next iteration, the wing was placed at the top of the left pillar. This iteration showed that by placing the wing at the top, local buckling of the left pillar was avoided. When the door comes in contact with the wing, it starts pushing the seat back laterally. As the seat moves, the shield attached to the left pillar comes in contact with the dummy's upper body. The upper body of dummy starts picking up the velocity and moving away from the door. However, in this simulation it was noticed that hard contact between the metal of the shield and upper body of dummy caused some numerical problems. To get around this problem and also to enhance the effectiveness of the shield, a foam padding is provided in the front of the shield. Foam is provided such that, the outside angle of shield is maintained at 45 degrees while the inside angle of the front face of the foam is increased to 60 degrees with respect to the seat-back.

Further, in order to quantify the improvements, if any, due to the introduction of wing and shield concept, a baseline simulation was also made. The AISS seat without wing or shield was simulated under the same conditions as the seat with these improvements. The rigid wall comes in contact with the seat at 17 msec.

For the enhanced case, a point at the top of right pillar had a displacement of 139.8 mm at 22.33 msec (Figure 5.3). The same point in the baseline case covered the same distance in 33.95 msec. Since, the seat is fixed at the brackets, going beyond this point started causing distortion problems. Hence, we restricted ourselves to this range. As the rigid wall or door hit the seat, because of the seat-back foam and shield, the lower torso starts attaining velocity. Comparison of the lower torso velocity is shown in Figure 5.4. In the baseline case, its velocity increased to about 10 m/s at 28 msec. Since the hit occurred at 17 msec, this increase happened in 11 msec only causing high acceleration in the lower torso. On the other hand, in the enhanced case, maximum velocity attained by lower torso was only about 5 m/s and the increase occurred over a period of 22 msec. This significantly reduced the accelerations seen by the lower torso. At about 20 msec when the lower torso started picking up velocity in the baseline run, it had already moved away from the door by 42 mm (Figure 5.5) in the enhanced run while in the baseline run it had hardly moved at all. This places the lower torso very much closer to the rigid wall and so more vulnerable to a stronger hit. In the enhanced case, the lower torso starts going away early in the simulation when rigid wall is at a distance. While in the baseline case, the lower torso moves when rigid wall is much closer and imparts a much higher force.

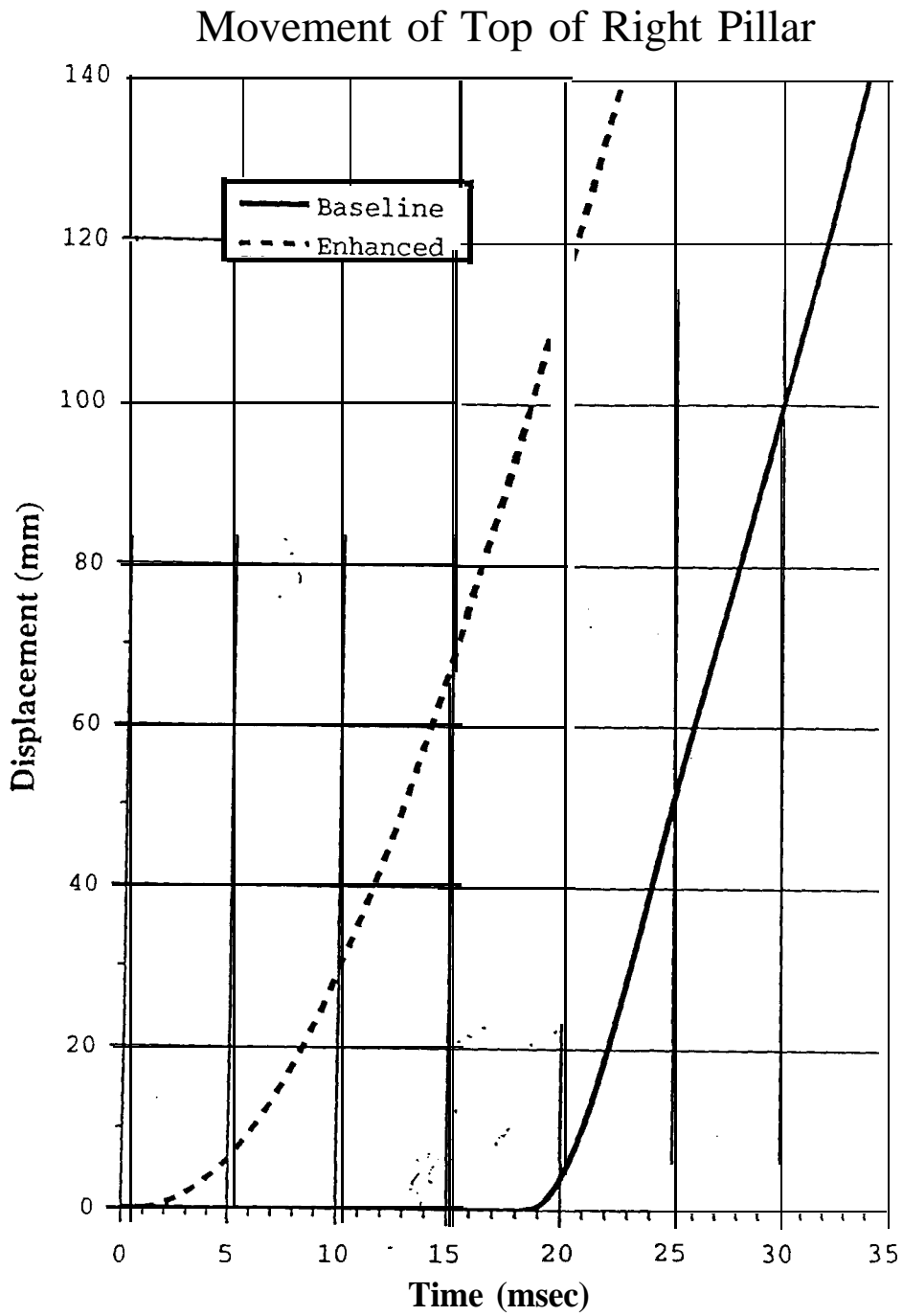


Figure 5.3 Comparison of displacement of the top right pillar with standard and enhanced seat.

Velocity of Lower Torso

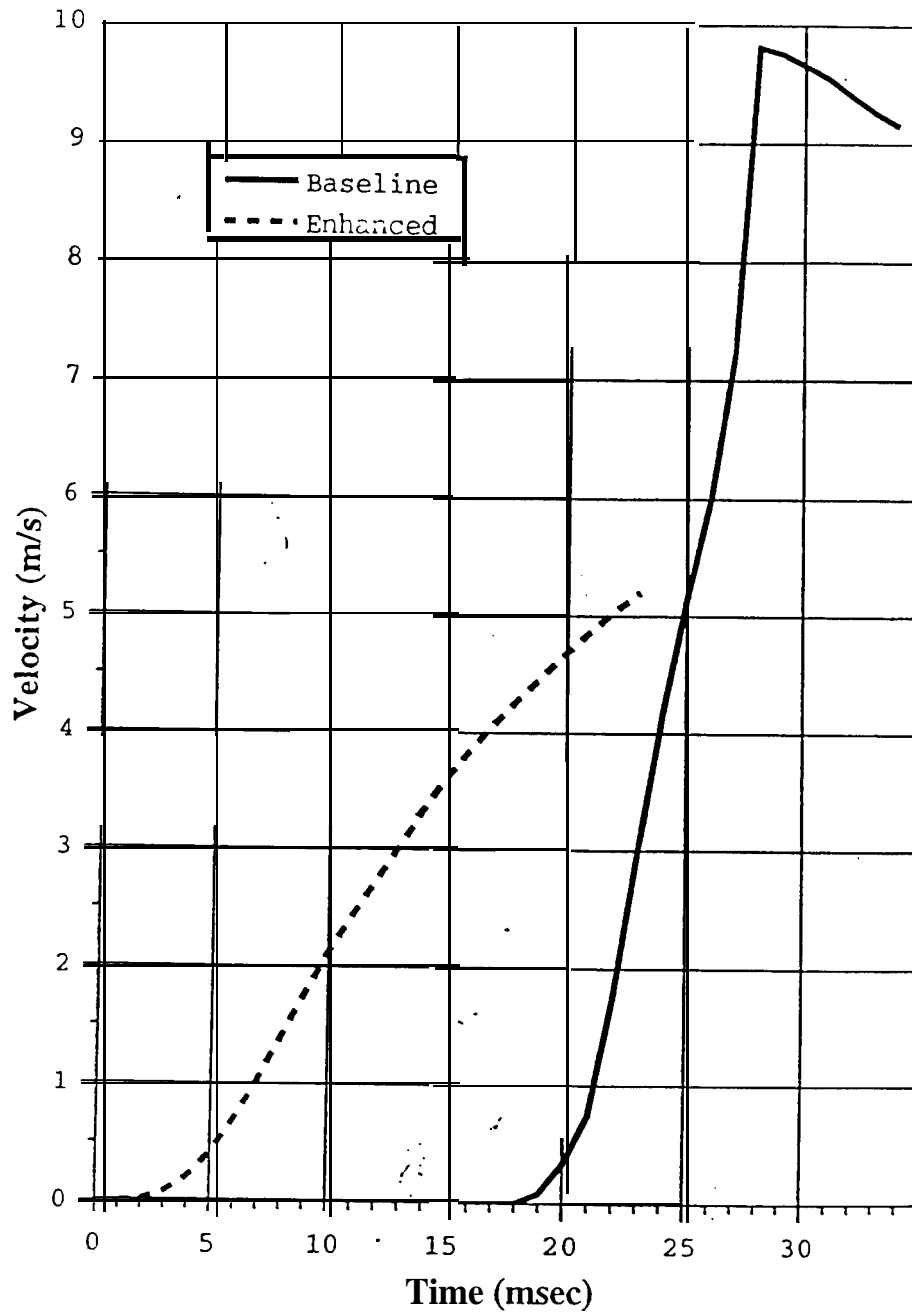


Figure 5.4 Comparison of lower torso velocity with standard and enhanced seat.

Movement of Lower Torso

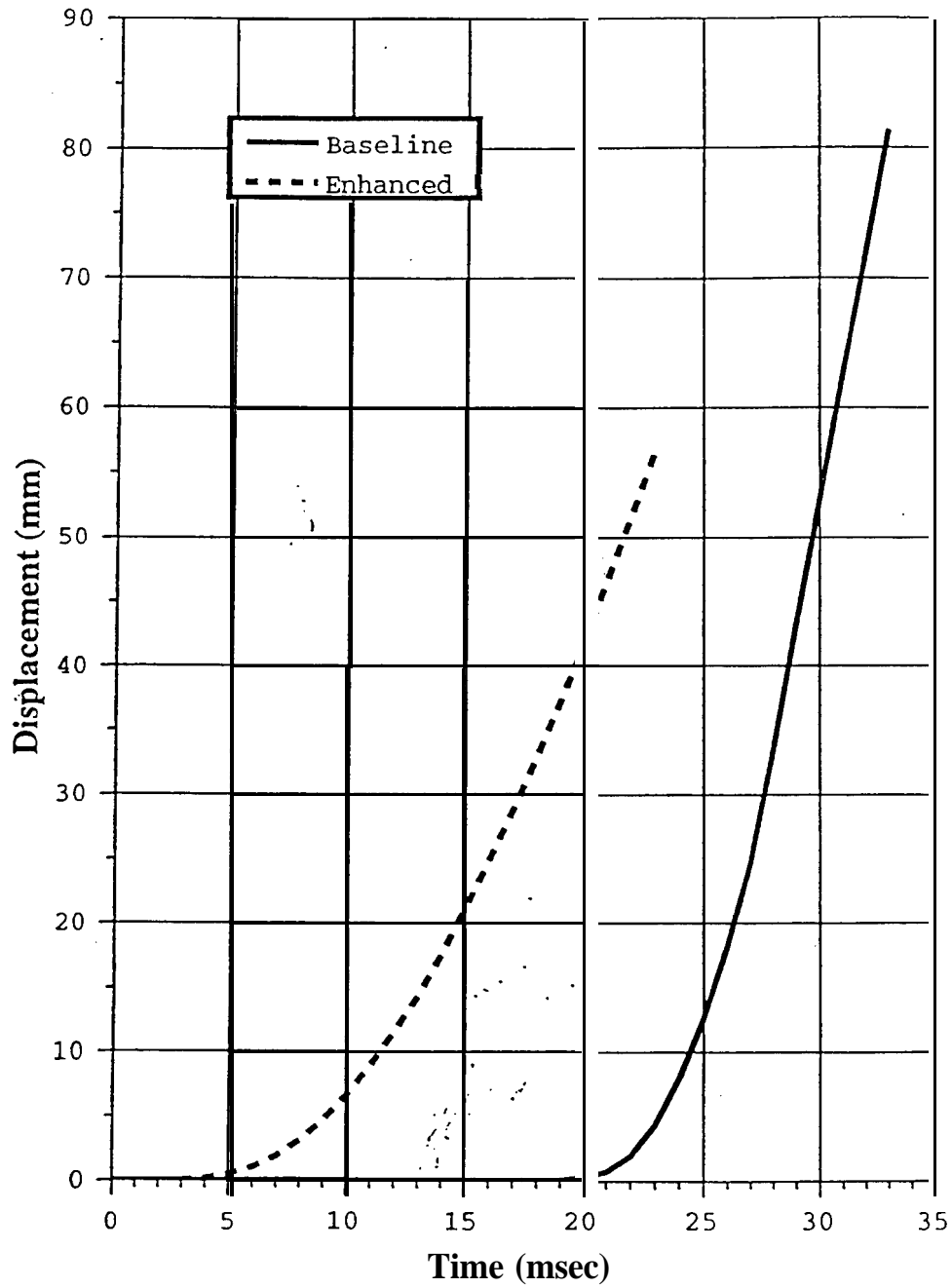


Figure 5.5 Comparison of lower torso movement with standard and enhanced seat.

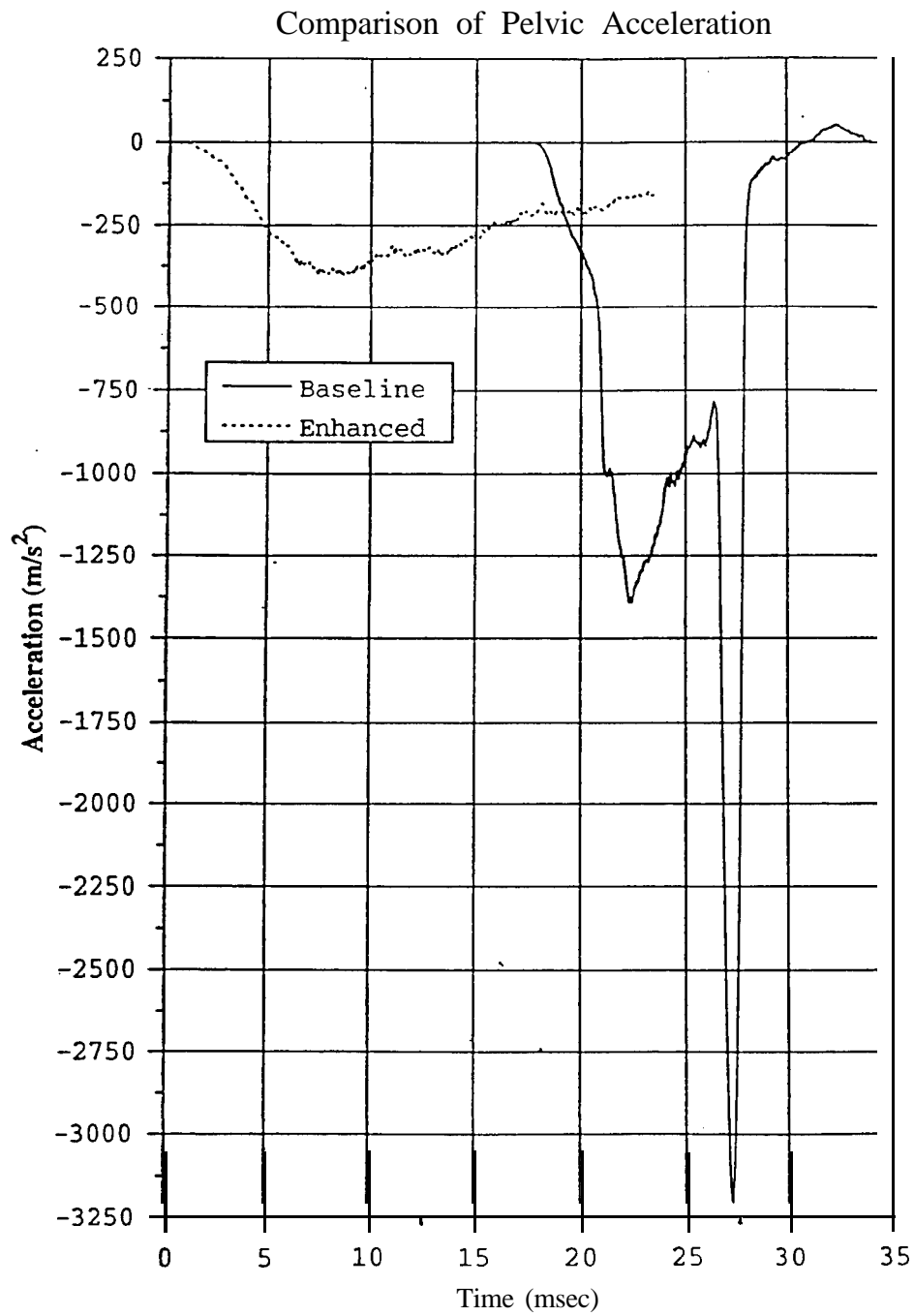


Figure 5.6 Comparison of the pelvic acceleration with standard and enhanced seat.

Comparison of T12

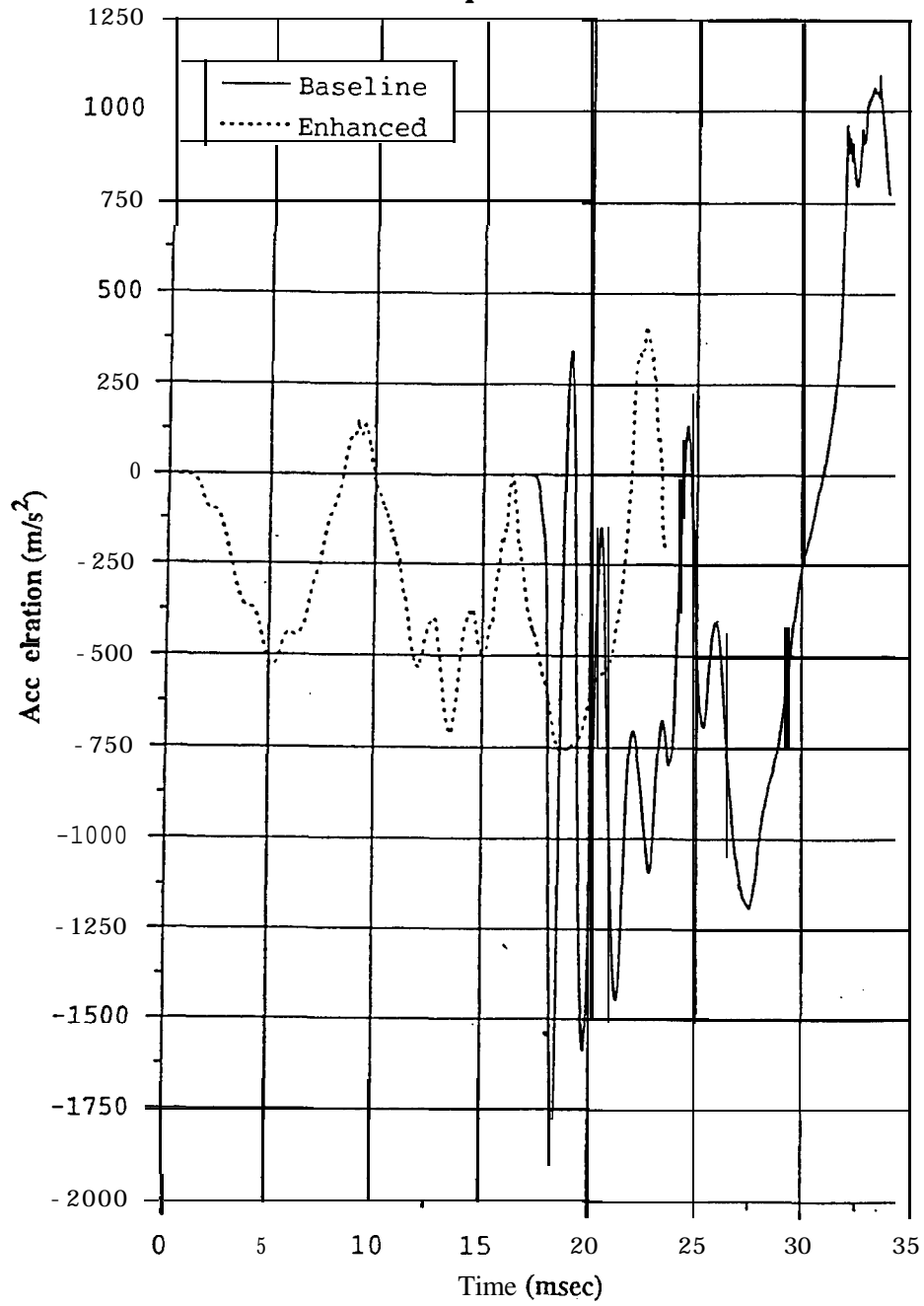


Figure 5.7 Comparison of the T12 acceleration with standard and enhanced seat.

In Figure 5.6 the pelvic acceleration is compared for the two cases. Pelvic acceleration was obtained from the MADYMO database. As expected, a significant reduction can be noted in the pelvic acceleration for the enhanced run. For the baseline case, maximum pelvic acceleration is about 320 G while for the enhanced case, it is only about 40 G. Similar reduction can be noted for T12 also (Figure 5.7). T12 is about 190 G for the baseline case and is reduced to about 75 G for the enhanced case. Overall TTI injury criterion is reduced from a significantly high value for the baseline case to 88 for the enhanced case.

FUTURE WORK

- The analytical results presented here are to be verified with prototyping and testing in the future.
- Incorporating the design concepts proposed here into production will be based on cost versus benefit analysis.
- Investigate the inflatable tubular (ITC) for side impact protection.

SUMMARY

- 4000 N load limit is found to be favorable for 30 mph frontal impact for a 50th percentile Hybrid III dummy. A 30 percent reduction in the risk of AIS \geq 4 thoracic injury is seen.
- Belt pretensioner increases the effectiveness of shoulder belt load limiter in frontal impact. 50 percent reduction in linear chest acceleration 3MS is seen with the use of a pretensioner. Belt pretensioner is also found to be very effective in rollover crashes by reducing head excursion.
- A design concept for a energy absorber in series with a linear recliner has been explored and shows promise as a basis for further development.
- The energy absorber meets the maximum seat back rotation guideline for the 5th, 50th and the 95th percentile dummies.
- The occupant kinematics and injury parameters are very favorable for the 50th percentile dummy, calculated using a LS-DYNA/MADYMO coupled simulation.

REFERENCES

- Bahling, G. S., Bundorf, R. T., Kaspzyk, G. S., Moffatt, E. A., Orłowski, K. F. and Stocke, J. E., "Rollover and Drop Tests - The Influence of Roof Strength on Injury Mechanics Using Belted Dummies", SAE Paper # 9023 14, 1990.
- Haland, Y., Nilson, G., "Seat Belt Pretensioners to Avoid the Risk of Submarining - A Study of Lap-Belt Slippage Factors", 13th International Technical Conference on Experimental Safety Vehicles", 1993, pp. 1060- 1068.
- Kallieris, D., Rizzetti, A., Mattem, R., Morgan, R., Eppinger, R., Keenan, L., "On the Synergism of the Driver Air Bag and the 3-Point Belt in Frontal Collisions", 39th Stapp Car Crash Conference Proceedings, 1995.
- Langweider K., Hummel T., Sagerer F., "Characteristics of Neck Injuries of Car Occupants", Proc. International IRCOBI Conference on the Biomechanics of Impacts, 198 1, pp. 78-79.
- Lowne R., Gloyns P., Roy P., "Fatal Injuries to Restrained Children Aged 0-4 Years in Great Britain 1972- 1986", Eleventh International Conference on Experimental Safety Vehicles, 1987.
- Mendis, K., Ridella, A, and Mani, A., "Dummy Neck Design Support," Contract No. DTNH-22-92-D-07323, Project No. NRD-0 1-3-07227, EASi Engineering, Dec, 1994.
- Mertz, H.J., Williamson, J.E., Vander Lugt, D., "The Effect of Limiting Shoulder Belt Load with Air Bag Restraint", SAE paper # 950886,
- Partyka, S., " Office of Vehicle Safety Standards, Rulemaking, NHTSA, 1992.
- Pilhall, S., Komer, J., Ouchterlony, B., "SIPSBAG - A New, Seat-Mounted Side Impact Airbag System", Volvo Car Corporation, 14th ESV Conference paper # 94-S6-O-13, 1994.
- Pilkey W.D. and Sieveka, E., "Analytical Modeling of Occupant Seating/Restraint Systems", NHTSA Report for DTRS-57-90-C-00092, 1994.
- Renouf, M.A., "A Car Accident Injury Database: Overview and Analyses of Entrapment and Ejection. TRRL Research Report 320. Transport and Road Research Laboratory, Crawthorne, 199 1.
- Status Report, Insurance Institute for Highway Safety, Vol. 30, No. 8, September 16, 1995.

Svensson, M.Y., Lovsund, P., Haland, Y., and Larsson, S., "Rear End Collisions - A Study of the Influence of Backrest Properties on Head-Neck Motion using a new Dummy Neck, SAE Paper # 930343, 1993.

Thomas C.' et al., "Protection Against Rear-End Accidents", Proc. International IRCOBI Conference on the Biomechanics of Impacts, 1982, pp. 17-29.

Viano, D.C., "Influence of Seat Back Angle on Occupant Dynamics in Simulated Rear End Impacts", SAE Paper # 922521, 1992.